The nucleotide binding domains of multidrug resistance p-glycoproteins

by

Heidi de Wet
B.Sc., B.Sc.(Hons)

This thesis is presented in fulfilment of the requirement of the degree of

DOCTOR OF PHILOSOPHY
in the
Department of Chemical Pathology
UNIVERSITY OF CAPE TOWN

March 2000

DECLARATION

I, Heidi de Wet, hereby declare that the work on which this thesis is based is my original work (except where acknowledgements indicate otherwise), and that neither the whole work nor any part of it has been, is being, or is to be submitted for another degree in this or any other university.

I empower the University of Cape Town to reproduce for the purpose of research either the whole or any portion of the contents in any manner whatsoever.

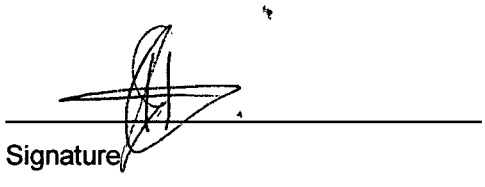

Signature

31/8/00

Date

Dedicated to my father, William Charles Griffith
(1/2/1945-26/5/1992)

SUMMARY

Multidrug resistance (MDR) – the phenomena where cancer cells become resistant to previously effective drugs – is a common obstacle in successful treatment of cancer. There are several causative factors of MDR. The active extrusion of drugs mediated by a family of membrane transporters, the p-glycoproteins, is one of the major factors resulting in treatment failure. If these drug transporters could be inhibited it would mean that lower doses of chemotherapeutic drugs could be used, making treatment more bearable and effective. Among many promising inhibitors is a large family of plant metabolites known as flavonoids. They have the advantage of huge diversity and a basic scaffold containing several hydroxyl groups suitable for derivatization and adding extensions.

The mechanism of the p-gps is also of considerable interest. How can a single protein transport such a diversity of substrates? The structure of p-gps consist of a tandem of transmembrane domain (TMD) and a nucleotide binding domain (NBD), to yield a protein constructed as [TMD-NBD][TMD-NBD]. There is a great interest in how the NBDs cooperate to hydrolyse ATP and effect the translocation of drugs.

In this study, we explore the use of a photoactivatable ATP analogue, 2',3',4'-O-(2,4,6, trinitrophenyl)8-azido-adenosine triphosphate (TNP-8N_3-ATP) as a probe of the ATP site. Specific derivatization of one or both ATP sites would allow elucidation of active site residues, possibly yield insights into site-site cooperativity and coupling, and provide a valuable means of measuring drug binding to the ATP site through competitive inhibition of photolabeling. There is evidence that the TNP moiety increases the affinity for the ATP site of p-gps 1000-fold over ATP. This could make TNP-8N_3-ATP a valuable probe of these sites.

The first p-gps investigated were the yeast proteins Pdr5p and Yor1p. Pdr5p is implicated in pleiotropic drug resistance, while Yor1p confers oligomycin resistance to yeasts in which it is over expressed. It is of interest to note that Pdr5p maintains a membrane topology of [NBD-TMD][NBD-TMD], the opposite of human and mouse p-gp, while Yor1p (a member of the drug resistance conferring MRP family) has a similar membrane topology to that of human and mouse p-gp - [TMD-NBD][TND][NBD]. We found that the yeast pumps, Pdr5p and Yor1p, are well photolabeled at acidic pH with pKa(Pdr5p) = 7.3. Pdr5p and Yor1p bind TNP-8N_3-ATP with a fairly modest affinity (Kd = 16 – 40 μM), and efficiency of labeling is approximately 80 % for Pdr5p. Photolabeling is dependent on Mg^{2+} and is inhibited up to 90 % by ATP - Ki(ATP) = 0.44 mM and 0.322 mM for Pdr5p and Yor1p respectively.

Photolabeling of the NBDs was also studied by using soluble recombinantly expressed mouse NBD2. Two polypeptides of different lengths were investigated – sNBD2 from Thr^{1044} - Thr^{1224}

and LNBD2 from Lys^{1025} – Ser^{1276}. Both TNP-$8N_3$-ATP and $8N_3$-ATP photoprobes were used. Both sNBD2 and LNBD2 behaved very similarly. Photolabeling of both proteins was characterised by tight nucleotide binding (Kd(TNP$8N_3$-ATP) = 0.8 – 2.6 μM and Kd($8N_3$-ATP) = 37 μM), with efficient derivatization, close to mol/mol, at acidic pH (pKa = 6.8 and 7.8 for sNBD2 and LNBD2 respectively). Labeling of both proteins with both probes at acidic pH was completely inhibited by ATP, yielding a Ki(ATP) = 0.5 – 2.7 mM. Interestingly, we find that both sNBD2 and LNBD2 are labeled extremely well even in the absence of Mg^{2+}. Since the specificity is excellent, as judged from the complete inhibition of photolabeling by various nucleotides, it suggests that both isolated domains are largely folded correctly. This was somewhat unexpected since sNBD2 appears to lack essential β-strands in two β-sheets flanking the ATP binding site according to the crystal structure of the histidine transporter nucleotide binding domain, HisP. Yet, there may be important differences in site architecture of the isolated domains and the whole protein, especially in relation to the Mg^{2+} site. An exciting possibility is that the differences reflect the lack of the *trans* membrane domain in the isolated NBD2. It could mean that the three fairly large extra membranous loops of the transmembrane domain are required for proper constitution of the ATP site.

Considerable effort was expended in trying to identify the amino acids(s) derivatised by photolabeling with TNP-$8N_3$-ATP, but unfortunately it was unsuccessful. The main problems were: the hydrophobic nature of the NBDs which necessitated manipulation in 4-8 M urea; the need to use thermolysin as a proteolytic enzyme, both because of its stability in 4 M urea and because most other proteases catalytically hydrolyse the TNP moiety from the TNP-peptide adduct; the fact that, in general, many TNP-peptide were produced and the yield and range were variable, and the limited availability of p-gp protein.

Thirty one flavonoids from the classes of flavonols, chalcones and chrysins were investigated for binding to the ATP site of mouse NBDs. Many contained prenylated extensions that had previously been shown to bind tightly to the isolated NBDs. However, our work showed that such extensions prevented binding to the ATP site. The only direction for elaboration was in ring B, seen in the tight binding of kaempheride and even the greatly extended dehydrosilybin. The 3-OH group was shown to be essential for binding to the ATP site, as none of the chrysins, which lack this group, were able to bind. An exception to this 3-OH rule and blockage by prenylated extensions to ring A, was broussochalcone A, which has an open ring C. Its ability to bind to the ATP site is obviously related in some way to this increase flexibility between the A and B rings. Identification of these structural requirements for binding to the ATP site is important for the future design of more powerful flavonoid reversers of multidrug resistance. Perhaps as important is the finding that hydrophobic flavonoids that previously have been shown to bind to the isolated NBDs and to reverse drug pumping do not bind at the ATP site and therefore must be binding at another site.

A new photoprobe of ATP sites, namely (4-azido-2-nitrophenyl)AMP, where the phenyl ring is linked to the phosphonyl group, was synthesised. This ATP analogue may be useful for labeling amino acid residues adjacent to the γ-phosphate of ATP. The probe was shown to be photoactive and to bind to LNBD2 with an affinity similar to ATP. Addition of the TNP-moiety onto the ribose increase the binding affinity approximately 100-fold, making it's binding similar to TNP-$8N_3$-ATP. However, irradiation of ANP-TNP-AMP did not appear to yield a covalent nucleotide–protein adduct as judged from the lack of subsequent inhibition of photolabeling by $8N_3$-ATP.

ACKNOWLEDGEMENTS

I would like to thank everyone that had, in any way, contributed to this thesis. Special thanks to my supervisor, David McIntosh, for many hours of fruitful discussion and for teaching me the rigors and enchantment of science. Thanks also to Dave Woolley (whose years of experience shaved a year or two off my PhD) and to my collaborators, Attilio Di Pietro, for supplying me with recombinant mouse p-gp (and the numerous students involved in preparing my samples), to Dennis Barron for the flavonoids and to Andre Goffeau and Annabelle Decottignies for the yeast proteins.

I would also like to acknowledge the various institutions involved in the financial support of my studies: UCT, the Ernst and Ethel Erickson Trust and the Paul and Stella Loewenstein Trust. The financial assistance of the National Research Foundation towards this research is hereby acknowledged. Opinions expressed in this work, or conclusions arrived at, are those of the author and are not necessarily to be attributed to the National Research Foundation. Deserving a special mention is our post-graduate bursary officer, Sandy Dewberry.

Many thanks to Ben.

TABLE OF CONTENTS

ABBREVIATIONS

AF	ammonium formate	
ANP-AMP	4-azido-2-nitrophenyl adenosine mono phosphate	
ANP-TNP-AMP	4-azido-2-nitrophenyl-2',3'-O-(2,4,6-trinitrophenyl) monophosphate	adenosine
DTNB	5,5' – dithiobis(2-nitrobenzioc acid)	
EGTA	bis-(β-aminoethyl ether) N.N.N',N', - tetraacetic acid	
G3PDH	glyceraldehyde 3-phosphate dehydrogenase	
MDR	multidrug resistance	
MRP	Multidrug-Resistance-Associated Protein	
NBD	nucleotide binding domain	
NBD-Cl	7-chloro-4-nitrobenzo-2-oxa-1,3-diazole	
NEM	N-ethylmaleimide	
PGA	phosphoglyceric acid	
PGK	phosphoglycerate kinase	
PKA	protein kinase A	
PTH	phenylthiohydantoin	
p-gp	p-glycoprotein	
SDS	sodium dodecyl sulphate	
TCA	trichloroacetic acid	
TM	membrane spanning region	
TMD	transmembrane domain	
TNBS	2,4,6 – trinitrobenzenesulfonic acid	
SDS	sodium dodecyl sulphate	

CHAPTER 1: LITERATURE OVERVIEW

Introduction

Emerging drug resistance to previously effective treatment is a common theme in many diseases today (Neu, 1992). The malarial parasite, *Plasmodium falciparum,* first reported to be resistant to the anti-malarial drug Chloroquine in the 1960's (Newbold, 1990), is one of many organisms that developed means of escaping the damaging effects of drugs. At present, drug resistance to anticancer therapy is the primary reason for treatment failure in cancer. (Chan *et al.*, 1991; Ling, 1992)

Successful treatment of tumors during chemotherapy involves several steps. These include delivery of anticancer drugs to the tumor, transport into the tumor cells (passive or active), possible metabolism to an active form and interaction with the target molecules. Interference in any of these steps could contribute to drug resistance in tumors. Decreased drug uptake may result from changes in the physiochemical properties of the cellular membrane; increased drug efflux can be mediated by energy dependent drug efflux pumps; there could be reduced metabolic activation of the drug or increased deactivation of the drug; increased expression of target sites; structural changes in the target site due to point mutations; or increased repair mechanisms for damaged target sites (Hayes and Wolf, 1990; Bradshaw and Arceci, 1998). Drug resistance may be the result of a combination of the above mentioned mechanisms.

Tumor cells can be either intrinsically resistant, being unresponsive to treatment from the outset, or acquire resistance after repeated exposure to anticancer drugs (Gerlach *et al.*, 1987; Hayes and Wolf, 1990). Classical Multi Drug Resistance (MDR) is the phenomenon whereby cancer cells become resistant to a wide variety of structurally unrelated compounds with different subcellular targets, after prolonged exposure to a single compound. The protein responsible for MDR was identified as a 150 –170 kDa membrane protein, called the P-glycoprotein (p-gp) (Kartner *et al.*, 1983; Cornwell *et al.*, 1986).

ATP binding cassette superfamily

The first human p-gp was cloned and purified and it was demonstrated that transfection of full-length cDNA for the human MDR1 into wild type cells rendered the cells resistant to a variety of chemotherapeutics (Hamada and Tsuruo, 1988; Pastan *et al.*, 1988). The sequencing of the human p-gp revealed homologies with many other transport proteins and this was the birth of a new major superfamily of proteins, called the ATP Binding Cassette Family (ABC type transporters). Over the years the family expanded to include proteins of various origins, ranging from man to micro-organisms, binding and transporting a large number of structurally diverse substrates. By 1998 more than 200 prokaryotic and eukaryotic

ABC proteins had been cloned and characterized, while presently some 1 500 ABC genes have been sequenced (Cole *et al.*, 1998., A. Goffeau, personnel communication).

At the time of writing this thesis, 30 human ABC full length sequences are known (Reviewed by Klein *et al.*, 1999). These ABC proteins can be grouped into 8 subfamilies, most of which are involved in the translocation of various substrates. The White subfamily transporters are involved with the transport of eye pigment precursors into pigment cells, while the members of the ANZA subfamily (ANZAI and ANSAII) are multi component arsenite transport systems. The 4 ALD subfamily transporters (ALDP, PMP70, ALCPR and PMP69) are all localized to the peroxisomal membrane and mutations in these proteins lead to peroxisomal disorders. The functions of the members of the ABC1 subfamily - the largest of the human ABC proteins - are currently being elucidated and there is evidence supporting the involvement of these proteins in the engulfment of apoptotic cells by macrophages. The function of ABC50, the only member of the GCN20 subfamily, is unknown. Not fulfilling a transport function, the OABP (or RNAse L inhibitor) subfamily acts as regulatory proteins whose co-expression inhibits activation of RNase L. The proteins implicated in multi drug resistance are part of the subfamilies MDR1/TAP and MRP/CFTR and are discussed in more detail below.

The sequencing of several microorganisms' genomes revealed that the ABC family is very well represented and appears to be involved in the transport of a wide variety of substrates. *Thermogata maritima*, a thermophilic bacterium belonging to the order Thermotogales, possesses a large number of carbohydrates and amino acid transporters. Of these, 84 % are members of the ABC super family – with 9 sugar ABC transporters, 11 oligopeptide ABC transporters and several miscellaneous transporters: one ribose transporter, two maltose transporters, one glycerol transporter, two amino acid transporters, a phosphate transporter and a spermidine transporter (Nelson *et al.*, 1999). The genome of *Mycobacterium tuberculosis*, responsible for the chronic infectious disease tuberculosis, revealed 10 ABC transporters. The roles of these transporters again proved to be diverse and were postulated to be involved in electron transport (cydC and cydD), sugar uptake (sugC), molybdate uptake (modC), phosphate transport and uptake (phoT and pstB), osmoprotection (proV) and, of course, drug resistance (drrA giving rise to daunorubicin resistance) (Cole *et al.*, 1998).

The yeast genome yielded 29 putative ABC proteins. Of these, 19 are predicted to be localised in the plasma membrane, 2 are localised either in the endoplasmic reticulum or plasma membrane, 5 are predicted to be soluble and 3 are localised in the mitochondria (Decottignies *et al.*, 1997). Of the 29 proteins, biochemical or physiological information is available for only 10 proteins (STE6, Pdr5p, SNQ2, Yor1p, YCF1, GCN20, YEF3, PXA1, YKL88, and ATM1). Six families could be distinguished according to amino acid sequence homologies and these could be further divided into 10 subclusters. The majority of these proteins are typical membrane spanning ABC transporters, with 16 being expressed as a

single peptide [TMD-NBD-TMD-NBD] (cluster I) or [NBD-TMD-NBD-TMD] (cluster II) and another 6 as "halfe proteins", [TMD-NBD][TMD-NBD] or [NBD-TMD][NBD-TMD (cluster II). The five proteins allocated to cluster IV are unique in displaying two NBDs but no transmembrane domains and are postulated to interact with tRNAs, while the smallest yeast ABC protein is the YFL028 (cluster VI) with only one NBD – resembling a soluble ATP-binding subunit.

In the future, by comparing sequences of ABC proteins found in microorganisms, the human equivalents could be identified and knowledge of these related proteins utilized in functional studies - shedding light on mechanisms of human disease. Analysis of human genes expressed in yeast cells can also be very powerful in elucidating the function of unknown human ABC transporters.

The MDR/TAP subfamily

Well known members of this family are the mammalian p-glycoproteins: the human MDR1, 2 and 3, the rat and murine Mdr1a, Mdr1b (also called Mdr3 and Mdr1) and Mdr2 and the hamster Pgp1, 2 and 3 (Borst, 1997). Of these the human MDR1, the rat and murine Mdr1a and Mdr1b and the hamster Pgp1 and Pgp2 are responsible for the MDR phenotype observed in the cells in which they are over expressed. There is also evidence that these proteins act as broad specificity translocases for short chain phospholipids *in vivo* (Bosch *et al.*, 1997). The human MDR2 and 3, the rat and murine Mdr2 and the hamster Pgp3 are phosphatidylcholine translocators responsible for phosphatidylcholine transport into bile (Ruetz and Gros, 1994, Borst, 1997, Dekkers *et al.*, 1998, Smith *et al.*, 1998,).

P-gp typically consists of two homologous-membrane associated halves. Each half is made up of a transmembrane domain (TMD) - postulated by hydropathy amino acid analysis to span the membrane 6 times – and a nucleotide binding domain (NBD) on the cytoplasmic face of the membrane (Yoshima *et al.*, 1989, Liu *et al.*, 1998, van Veen *et al.*, 1998). The mammalian protein is arranged in a [TMD-NBD-TMD-NBD] configuration and is expressed as a single polypeptide (Fig 1.1).

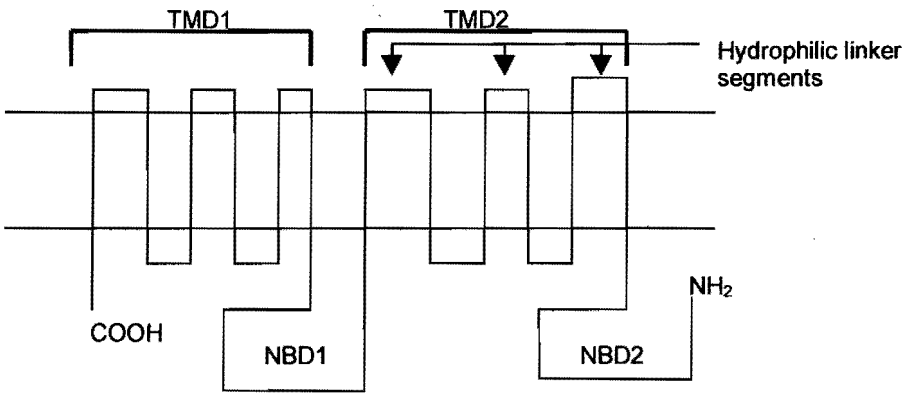

Figure 1.1. Mammalian p-gp is expressed as a single polypeptide and is arranged in a [TMD-NBD-TMD-NBD] configuration.

Other members of this subfamily, TAP1 and TAP2, exist as half transporters - [TMD-NBD]. By forming a heterodimer the TAP1/TAP2 complex acts as a peptide transporter carrying peptides across the endoplasmic reticulum membrane, making the peptides available for immunorecognition by the major histocompatibility complex. Although different membrane topologies for p-gp have been suggested, present data favour the "six-plus-six" model (Reviewed Higgins *et al.*, 1997, Kast *et al.*, 1996, Loo and Clarke, 1995).

The NBDs have 3 sequence signatures characteristic of ABC transporters and other ATP binding proteins: the consensus Walker A [$G(X)_4$GKS/T] and Walker B [$R/K(X)_{6-8}L(Hyd)_4D$] motifs and a short linker peptide –LSGG$(X)_3$RHydXHydA- between the Walker A and Walker B motifs (where Hyd indicates a hydrophobic amino acid) (Walker *et al.*, 1982, Ames *et al.*, 1992). The conserved lysine residue in the walker A motif (**K**) proved to be essential for drug transport and ATPase activity in all ABC transporters characterized to date; the yeast Pdr5p being the exception to this rule as it lacks this lysine residue in NBD1(Cole *et al.* 1998). Intron/exon analysis of the MDR1 gene suggests that p-gp arose by a gene fusion event of two related but independently evolved proteins, rather than by gene duplication as previously suggested (Chen *et al.*, 1986, Gros *et al.*, 1986, Chen *et al.*, 1990). Again a subject of debate, the oligomeric state of p-gp appears to be a monomer (Loo and Clarke, 1996). This is supported by a recent low resolution structure (2.5 nm) of hamster p-gp where the crystal structure exhibits a single protein consisting out of two mirror images, each made up from 6 TMD units (Rosenberg *et al.*, 1997).

The MRP/CFTR subfamily

An additional protein, the Multidrug-Resistance-Associated Protein (MRP1), was also found to confer a multi drug resistance phenotype *in vitro* (Berger *et al.*, 1997, Deeley and Cole, 1997. Norris *et al.*, 1996; Grant *et al.*, 1994; Kruh *et al.*, 1994; Cole *et al.*, 1992). This new member of the ABC family has a molecular weight of 190 kDa and shared a 15 % amino acid identity with p-gp. MRP is able to transport glutathione (GSH) conjugates of drugs, explaining how MRP1 can provide resistance to small hydrophilic oxyanions like arsenite and antimonite (Borst *et al.*, 1997). Arsenite can form trivalent complexes with GSH and there is proof that this is the form in which arsenite is extruded from cells by MRP1. The human canacular Multispecific Organic Anion Transporter (cMOAT) (also called MRP2) functions as an anionic conjugate transporter and absence of this protein results in the Dubin-Hohnson syndrome –a condition characterized by conjugated hyperbilirubinemia and impaired secretion of anionic conjugates from hepatocytes into bile.

Not long after the identification of the first MRP, several other structurally similar transport proteins were identified which now constitute the MRP branch of the ABC superfamily. Other proteins belonging to the MPR branch are the sulfonylurea receptor and K+ channel regulator SUR1 - involved in modulating insulin secretion in the pancreas (Bryan and Afuilar -Bryan,

1997). ATP sensitive potassium channels, K(ATP), are made up from heteromultimers – 4 pore forming, inwardly rectifying K^+ channel subunits, Kir6.x, complexed with 4 regulatory sulfonylurea receptor (SUR) subunits (Reviewed by Babenko *et al.*, 1998). Typically, SUR1/Kir6.2 complexes are found in neuronal and pancreatic beta-cells, SUR2A/Kir6.2 in the heart and SUR2B/Kir6.1 in vascular smooth muscle (Dorschner *et al.*, 1999). Inwardly rectifying K^+ channels are affected by nucleotide levels and therefore couple membrane conductance to metabolism by regulating electrical activity of cells through controlling membrane potential or modulation of action potential (Schwanstecher *et al.*, 1998). In β-cells of the pancreas, opening of Kir6.2 sets a resting potential while closing depolarizes the plasma membrane, causing Ca^{2+} influx through a voltage sensitive L-type Ca^{2+} channel and insulin release. Mutations in channel subunits that prevent closure, cause Familial Hyperinsulinism. Hypoglycemic sulfonylureas like glipizide and tolbutamide, close the ATP-sensitive potassium channels of β-cells(Ashfield *et al.*, 1999).

Cystic Fibrosis Transmembrane Conductance Regulator (CFTR) is a Cl^- channel in lung epithelial. Defects in this protein are responsible for Cystic Fibrosis – one of the most common lethal genetic diseases among Caucasians today (Riordan *et al.*,1989). CFTR is a Cl^- channel and also possibly regulates other channels in lung epithelial. Being structurally similar to p-gp, CFTR also contains the duplicated [TMD-NBD-TMD-NBD] motif, but differs by the presence of a large cytoplasmic "R-domain" found between the two halves of the protein. Phosphorylation of this R-domain by protein kinase A is essential for channel function. Although the 2 NBDs of CFTR function cooperatively in catalysis the NBDs are not structurally and functionally as similar as seen with p-gp (Senior and Gadsby, 1997, Cotten and Welsh., 1998, Gadsby *et al.*, 1998, Ramjeesingh *et al.*, 1999, Szabo *et al.*, 1999). This is one of the major differences between these 2 groups -the NBDs of p-gps are very similar and performs the same function while the NBDs of MRP proteins are markedly less similar and are postulated to act in a functionally distinct manner. Hydrolysis of ATP at the N-terminal NBD is the rate-limiting step for opening a phosphorylated CFTR channel, while hydrolysis at the C-terminal NBD triggers channel closing. Channel regulation is, however, not yet completely understood and is complicated by phosphorylation of multiple sites in the R-domain and by ATP hydrolysis at the NBD's.

MRPs differ structurally from p-gps by the presence of a third N-terminal transmembrane spanning region, where the protein crosses the membrane 5 times with the N-terminus extracellular, joined to the rest of the protein by a intracellular linker region (Kast and Gros, 1998). Intron/exon analysis of MRP coding genes suggests a fusion event between a gene encoding the additional N-terminal membrane-spanning region and the gene encoding a common 4-domain ancestor, resulting in a [TMD-TMD-NBD-TMD-NBD] polypeptide configuration (Grant *et al.* 1997, Tusnady *et al.* 1997). The function of this additional transmembrane domain – called TMD0 – is speculative since truncated MRP1 lacking TMD0

behaves like wild-type MRP1 in both transport function and regulation of membrane targeting (Bakos *et al.* 1998). There are no three dimensional structures available on this branch of the ABC family.

MDR/TAP and MRP/CFTR subfamilies of micro organisms

The ABC transporters of microorganisms linked to drug resistance, have also been divided into two groups according to their mammalian family members (van Veen and Konings, 1998, Klein *et al.*, 1999). The MDR group consists of, among others, the Pdr5p and Snq2p proteins from *Saccharomyces cerevisiae,* responsible for pleiotropic drug resistance in yeasts (Balzi *et al.*, 1994; Decottignies *et al.*, 1995) the Cdr1p protein expressed by *Candida albicans*, conferring antifungal resistance (Prasad *et al.*, 1995) and the pfMDR1 protein from *Plasmodium falciparum*, implicated in drug resistance in malarial parasites (Foote *et al.*, 1989; Wilson *et al.*, 1989). The mechanism of pfMDR1 mediated drug resistance is uncertain however, as previous evidence of resistance to quinoline-containing antimalarial drugs by active extrusion in yeast overexpressing pfMDR1, proved not to be reproducible (Ruetz *et al.*, 1996b; Ruetz *et al.* 1999). Examples of the MRP group are the Ycf1p and Yor1p proteins from *Saccharomyces cerevisiae*, conferring cadmium and pleiotropic drug resistance respectively and 1tPgpA from *Leishmania tarentolae*, giving rise to heavy metal resistance (Callaghan *et al.*, 1991,Szczypka *et al.*, 1994; Cui *et al.*, 1996, Decottignies *et al.*, 1998.).

Similar to their mammalian relatives, the p-glycoproteins of microorganisms are also expressed in a "six-plus-six" membrane topology with variations on the [TMD-NBD-TMD-NBD] theme. Yeast proteins Pdr5p and Snq2p are typically expressed as a single polypeptide with a membrane topology of [NBD-TMD-NBD-TMD] – the reverse of the mammalian protein topology - while pfMDR1 retains the topology seen for p-gp. Other ABC proteins of microorganisms, such as LmrA of *Lactococcus lactis* and ADP1p of *S.Cerevisiae*, are expressed as half p-gps with a single TMD domain and NBD in a [TMD-NBD] configuration. There is evidence that these two halves associate in the membrane to form a single active transporter – [TMD-NBD][TMD-NBD] (Berkower and Michaelis, 1991, Berkower *et al.*, 1996, Gao *et al.*, 1996). As another variation on the theme, the DrrAB transporter of *Streptomyces* expresses its TMDs as a single polypeptide which associates with a second NBD containing polypeptide to form an active transporter – [TMD-TMD][NBD-NBD].

Functional Similarities of p-gp and MRP

Not surprisingly, proteins of the ABC family demonstrate functional similarities and can successfully swop the roles under challenge. With conservative replacements, such as the mouse Mdr2 protein with its human homolog MDR3, the introduced protein completely restores the excretion of phospholipids into the bile (Smith *et al.*, 1998). Both mouse mdr3 and pfMdr1 are able to restore mating and a-factor export in sterile Ste6 mutants (Raymond

et al., 1992. Volkman *et al.*, 1995). Human MRP1 also partially restores mating in yeast lacking Ste6p and completely regenerates resistance to cadmium completely in cadmium-sensitive, Ycf1p lacking, yeast (Tommasins *et al.*, 1996, Ruetz *et al.*, 1996a). Surprisingly, when the bacterial antibiotic-resistance protein, LmrA, was expressed in human lung fibroblast cells, it proved to be completely functionally interchangeable with human MDR1 – showing similar pharmacological characteristics and affinities for vinblastine and Mg-ATP (van Veen and Konings, 1998). Even MRP, that shows low levels of structural homology to Ste6p, restores mating in sterile Ste6 mutants (Ruetz *et al.*, 1996a). When MDR1 residues Q330, V331 and L332 of membrane spanning domain 6 were introduced into human MDR2 (a phosphatidylcholine transporter), it was sufficient to allow MDR2 to transport several MDR1 substrates, again indicating close functional relationships between proteins of the ABC family (Zhou *et al.*, 1999).

Nucleotide Binding Domains of p-gp

P-gp shows a characteristic drug-stimulated, vanadate-inhibited, ATPase activity with a K_m for MgATP of 1 mM and a V_{max} of 0.3 – 2 μmol per min per mg of protein. The 2 nucleotide binding domains of p-gp share over 80 % sequence identity and almost all of the sequence of NBD1 can be exchanged with the corresponding NBD2 fragments with no significant loss of function (Al-Shawi *et al.*, 1994, Beaudet *et al.*, 1998). Vanadate trapping of ATP (Fig 1.2) – where vanadate trapping requires hydrolysis of the nucleotide - in one NBD completely inhibits ATP hydrolysis in the other site showing that the amino- and carboxy- terminal nucleotide-binding domains (NBD1 and NBD2) cannot function independently as catalytic sites (Urbatsch *et al.*, 1995).

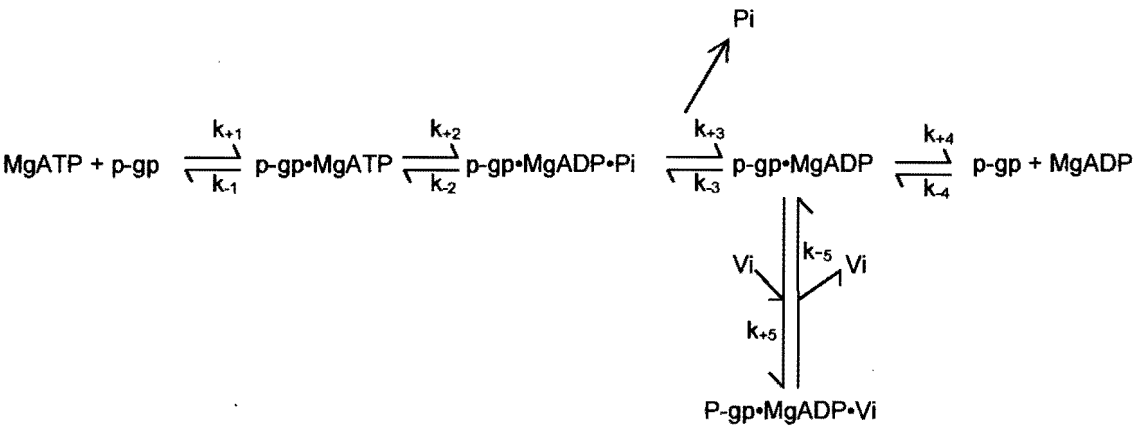

Figure 1.2. The mechanism for vanadate trapping of ATP, adapted from Senior *et al.*, 1995

Vanadate trapping of Mg – or Co-8N_3-ATP – followed by photo-attachment of the nucleotides to the NBDs revealed that both NBDs are derivatised in equal proportion, non-selectively, and

that hydrolysis is possible at both nucleotide binding domains (Urbatsch *et al.*, 1995). Vanadate trapping of ATP is completely abolished in mouse Mdr3 mutants showing no ATPase activity (point mutations in the Walker A – K429R, K1072R - or Walker B motifs – D551N, D1196N - in each of the two NBDs). Mutations in one NBD site prevents a single turnover and trapping in the nonmutated site, again showing that the NBDs cannot function independently as catalytic sites (Urbatsch *et al.*, 1998). NBD1 and NBD2 can both bind and hydrolyze ATP, but apparently ATP is not hydrolyzed simultaneously by both sites. Reconstituted p-gp incubated with ATP or $8N_3$-ATP and subjected to photochemical peptide bond cleavage with orthovanadate and ultraviolet light yielded cleavage products representative of either of the ATP sites, suggesting that ATP hydrolysis is limited to one binding site at a time (Hrycyna *et al.*, 1998). Mutations in one NBD (lysine to methionine and cysteine to alanine in the Walker A motif), completely inhibit ATP hydrolysis even when the nonmutated NBD contains a bound nucleotide (Takada *et al.*, 1998).

N-ethylmaleimide (NEM) inactivation of ATPase activity is another powerful tool to dissect events taking place at either NBD. NEM reacts with cysteine residues (Cys^{431} and Cys^{1074} in the human sequences or Cys^{430} and Cys^{1072} in the mouse sequence) within the Walker A motif and inactivates ATPase activity (Loo and Clarke, 1995a). The cysteine itself in each NBD is not essential as p-gp devoid of cysteine residues retains it's ability to confer resistance similar to wildtype, indicating that the ethyl succinimide moiety of NEM is probably positioned close to the catalytic site of p-gp (Loo and Clarke, 1995a., Liu and Sharom, 1996). In the latter study, where a single cysteine was re-introduced into a cysteine-less p-gp mutant, it was shown that covalent modification of a single cysteine residue by NEM within either of the nucleotide binding domains was adequate for complete inhibition of ATPase activity (Loo and Clarke, 1995b). Similar results were obtained when p-gp was allowed to react with 7-chloro-4-nitrobenzo-2-oxa-1,3-diazole (NBD-Cl) that modifies the same cysteine residues as NEM, Cys^{431} and Cys^{1074} in the human and hamster sequence or Cys^{430} and Cys^{1072} in the mouse sequence (Senior *et al.*, 1998). The nucleotide binding domains are labeled in a non-selective fashion, and reaction of one site with NBD-Cl prevents reaction with the other site and completely inhibitions ATPase activity (Senior *et al.*, 1998). This supports the vanadate-induced ATP trapping experiments showing that NBD1 and NBD2 interact strongly and that catalytic cooperativity between NBD1 and NBD2 is mandatory for ATPase activity.

Analysis of the drug and nucleotide binding sites has relied heavily on the use of radiolabeled photoactive substrates, reversers and nucleotides (Kotzybe-Hilbert *et al*, 1995, Greenberger, 1998). The majority of these analogs contain either tritiated or iodinated phenyl-substituted arylazide groups. Aromatic azides are some of the most widely used photoaffinity probes, but this common use is more related to the chemical stability in the dark and ease of synthesis than it's general suitability for the task. On ultraviolet irradiation of a phenyl azide, the azide is promoted to a singlet excited state which could a) loose a nitrogen to form a singlet nitrene or

b) undergo intersystem crossing to a triplet azide, which can also loose a nitrogen to form a triplet nitrene. The different intermediates lead to different reactions in photoaffinity labelling experiments. In the case of the singlet nitrene an ideal, seemingly non-discrimative, reaction with any amino acid residue or medium constituents is expected. Triplet azides react with nucleophiles such as cysteinyl and histidinyl residues, while triplet nitrenes lead to less predictable radical chemistry. The latter two species are not ideal labelling reagents as they react slowly and preferably with nucleophiles. Inherently, photoactive ligands also present certain limitations. The addition of a photoactive moiety changes the structure of the ligand, possibly perturbing receptor-ligand interaction. The reactive domain of the ligand may be some distance away from the actual site of interaction and the reactive intermediate could have a long half-life, allowing it to diffuse from the binding site at the time of irradiation giving rise to non-specific labeling (Greenberger, 1998).

P-gp has been shown be derivatised by the photoactive nucleotide derivatives 8-azido-ATP, 2-azido-ATP and 2',3'–O-(2,4,6–trinitrophenyl)8-azido-ATP (TNP-8N_3-ATP) (Cornwell *et al.*, 1986, al-Shawi *et al.*, 1994, Sankaran *et al.*, 1997b, Decottignies *et al.*, 1998). The recombinant mouse C-terminal nucleotide binding domain and N-terminal nucleotide binding domain, overexpressed in *Escherichia coli,* bound the TNP derivatives of ADP and ATP - TNP-ADP and TNP-ATP – and MANT ATP (2'(3')-N-methylanthraniloyl-ATP) with high affinity (Baubichon-Cortay *et al.*, 1994, Dayan *et al.*, 1997). Vanadate-assisted trapping of Mg-8-azido-ADP in the catalytic site of p-gp, followed by photoactivation, led to the identification of Tyr^{398} and Tyr^{1041} as the labeled amino acids (Sankaran *et al.*, 1997b).

Drug Binding Sites

The p-gp's ability to bind a wide range of structurally diverse compounds suggests the existence of either many different binding sites or a non-specific promiscuous site. Several mutagenesis and photolabeling studies placed the drug binding sites of p-gp in the membrane spanning regions (TM) of the protein. In a site-directed mutagenesis study, the transmembrane segment 6 (TM6) of human p-gp proved to play an important role in drug-protein interaction and coupling of drug binding to ATPase activity (Loo and Clarke., 1994a). Further studies showed that TM6 and TM12, possibly situated close to each other in the tertiary structure, form part of a drug binding pocket (Zhang *et al.*, 1995, Loo and Clarke, 1997a). Mutations located within TM4-6 reduced the inhibitory effect of various steroids, suggesting poor binding of these steroids to a disrupted binding site (Quang and Gruol, 1999). Other transmembrane helixes may also be involved: mutations to His^{61} in TM1 of human p-gp to influences substrate specificity while mutations in TM3 (Gly185Val) result in a decrease in drug transport (not due to a decrease in drug binding, but in bound drug released from the protein) and mutations in TM11 led to decreased drug binding to p-gp (Safa *et al.*, 1990, Kajiji *et al.*, 1993, Taguchi *et al.*, 1997). When hamster p-gp was photolabeled with a diazirine-cyclosporin A analog, the binding site of cyclosporin A was located between the end

of TM11 and the end of TM12 (Demeule *et al.*, 1998). The binding sites of prazosin and forskolin were also placed at TM6 and TM12 according to photolabeling studies with azide derivatives (Greenberger *et al.*, 1991, Greenberger *et al.*, 1993, Zhang *et al.*, 1995). Photolabeling of hamster p-gp with [^{125}I]iodomycin showed the binding site to be formed by the last segment of TM4, the beginning of TM5 (Demmer, *et al.*, 1997). In summary, using both mutagenesis and photolabeling studies, drug binding sites had been allocated to TM 4,5,6,11 and 12, while mutations in TM1 and 3 was also demonstrated to be involved in drug binding and translocation.

Evidence of multiple drug binding sites is mounting. The p-gp substrate, vinblastine and the p-gp reverser, verapamil (discussed below), compete for the same or overlapping sites, while nicardipine binds on a distinct but interacting site (Pascaud *et al.*, 1998). Azidopine, a photoactive compound, labels p-gp in two distinct locations – one within the amino half of the protein and one in the carboxy half of the protein (Bruggemann *et al.*, 1992). Using [^{125}I]iodoarylazidoprazosin, a photoactive analog of prazosin, two nonidentical drug-interaction sites were located on p-gp, again one on each halve of the protein (Dey *et al.*, 1997). Verapamil and progesterone derivatives are also shown to bind in a noncompetitive fashion, pointing to distinct binding sites for these compounds on p-gp (Orlowski *et al.*, 1996). Two photoreactive analogs of taxol, 3' and 7'-p-benzoyldihydrocinnamoyl (BzDC), specifically photolabeled murine mdr1b at two distinct sites – 3'-BzDC identifying a region that includes half of transmembrane domain 12, terminating just after the Walker A motif of NBD2 and 7'-BzDC identifying a region including all of TM7 and half of TM8 (Wu *et al.*, 1998). An overlapping site for steroids and anthracyclines within the first half of the protein and a taxzane site within the second half of the protein has also been proposed (Quang *et al.*, 1999).

It is clear that the interaction of drugs with the TM domains and drug binding sites of p-gp are complex. In a feasible proposal explaining the non-specificity of the drug binding site/s, Shapiro and Ling argued that substrates and reversers bind to the drug binding site/s of p-gp from of the lipid bilayer (Shapiro and Ling., 1998b). An idea previously proposed by Raviv *et al.* (1990) using 5-[125I]iodonaphthalene-1-azide ([125I]INA) and confirmed by Homolya *et al.* (1993); that demonstrated that the hydrophilic free acid from of an acetoxymethyl ester was not exported by MDR1. The high local substrate concentration in the restricted bilayer volume could lead to the binding to low affinity, low specificity site/s. Shapiro and Ling also propose the presence of at least two sites, each interacting with the other in a positive co-operative manner. Following Hoechst 33342 and/or Rhodamine 123 movement after ATP addition by monitoring the initial rate of decrease in fluorescence as the compounds are transported into the inside-out vesicle interior, several conclusions were drawn (Shapiro and Ling, 1997b). The fluorescent dyes, Hoechst 33342, and Rhodamine 123 both bind to separate sites, where the presence of one stimulates the transport of the other. Colchicine

inhibited Hoechst transport while stimulating Rhodamine 123 transport. On the other hand, Daunorubicin and other anthracyclines had the opposite effect – they stimulated Hoecht 33342 transport, while inhibiting transport of Rhodamine 123. Other p-gp modulators like vinblastine, actinomycin D, and etoposide inhibited both Hoechst 33342 and Rhodamine 123 transport, indicating that these drugs are binding to both sites.

In an extensive overview of current photolabeling data by Greenberger (1998) and Safa (1998) photolabeling studies points to the presence of four overlapping but distinct modulator binding sites – one for vinblastine, verapamil, cyclosporin A and phenothiazines, a second for dihydropyridine calcium channel blockers, a third site for megestrol acetate and the calcium channel blockers bepridil and prenylamine; and a fourth for [125I]arylazidoprazosin ([125I]AAP). Using equilibrium and kinetic radioligand binding assays Martin *et al.* (2000) identified the presence of at least 4 distinct binding sites on p-gp - 3 of which are drug binding sites. The current literature supports the presence of more than one drug binding site, but the complex allosteric interactions between these various sites and the modulator binding sites discussed further in the next section, remain to be elucidated.

Modulator Binding Sites

Several compounds, called p-gp modulators, also interact with p-gp, having various effects on ATPase activity, drug binding and extrusion. Reversers are a group of hydrophobic, structurally diverse p-gp modulators responsible for decreased drug extrusion and the reversal of multi drug resistance. The mechanism of inhibition of drug extrusion can be diverse. Some may act as substrates of p-gp and competitively inhibit efflux of the cytotoxic agents from the cell. Others may bind at the substrate site, but not be transported. Binding at a second substrate binding site or to a separate allosteric inhibitory sites – either in the membrane domain or in the NBD – can also lead to p-gp inhibition. Compounds that inhibit ATP binding and hydrolysis have also received attention as potential p-gp reversers.

Examples of classical reversers are the calcium channel blockers verapamil and SR33557, antiarrhythmic agents such as quinidine, the immunosuppressant cyclosporin A, vinca alkaloid analogs and the anticancer drug, tamoxifen (Tsuro *et al.*, 1981, Slater *et al.*, 1986, Zamora *et al.*, 1988, Solary *et al.*, 1991, Callaghan *et al.*, 1995, Jaffrezou *et al.*, 1995 and Nayfield *et al.*, 1995). Different reversers bind to p-gp at different sites and the resulting effect is often complex with respect to ATPase activity as well as the modulation of drug binding and transport. Martin *et al.* (2000) demonstrated the existence of 4 binding sites on p-gp - 3 drug binding sites and 1 regulatory site. The 4 binding sites were shown to display complex allosteric interactions, where binding at one site switches the other sites between high and low affinity conformations. Not all modulators tested seemed to interact with p-gp at the regulatory site and some bound to the drug binding sites.

Studies using various reversers further demonstrate regulatory complexity. Reversers verapamil and progesterone both increase basal ATPase activity, reversing drug resistance by competing with the transported substrate vinblastine (Garrigos *et al.*, 1997, Callaghan *et al.*, 1997). Verapamil inhibits vinblastine binding in a competitive manner, but since these two compounds have different effects on both basal p-gp activity and on MgATP concentration dependence of p-gp ATPase activity, it suggests that they bind p-gp either on different and overlapping sites or on distant but interacting sites. Typically, vinblastine has little or no stimulatory effect on ATPase activity, while verapamil activates. Also, lower concentrations of MgATP are needed for half maximal ATPase activity in the presence of verapamil than in the presence of vinblastine. Progesterone inhibits vinblastine binding in a non-competitive manner, suggesting a separate site for this reverser (Garrigos *et al.*, 1997). A photoreactive dihydropyridine, (2,6-dimethyl-4-(2-(trifluoromethyl)-phenyl)-1,4-dihydropyridine-3,5-dicarboxylic acid {2-[3-(4-benzoylphenyl)propionylamino]ethyl} ester ethyl ester) labels multiple reverser binding sites – as was demonstrated by the noncompetitive nature of inhibition by various compounds - distinct from the vinblastine binding site on p-gp in membranes of multidrug-resistant CCRF-ADR5000 cells (Boer *et al.*, 1996).

Depending on steroid hydrophobicity and the phosphorylated state of p-gp, steroids can act as either substrates or reversers (Barnes *et al.*, 1996). There is evidence of multiple steroid binding sites on p-gp as shown by the mutually non-exclusive inhibition of ATPase activity by four progesterone derivatives (Orlowski *et al.* 1996). This apparent lack of specificity could, alternatively, reflect the ability of the steroids to accumulate within the p-glycoprotein containing membranes – where greater accumulation of a specific steroid will be reflected in higher concentrations of steroid available for interaction with p-gp (Quang and Gruol, 1999). Photoaffinity labeling of human p-gp with tritiated progesterone, [^{3}H]progesterone, placed the progesterone binding site in the membranous domain of p-gp, since photolabeling of the p-gp is overcome by a 200 fold molar excess of vinblastine (Qian and Beck, 1990). The more recent results contradict the earlier, placing the progesterone binding site separate from the vinblastine binding site (Garrigos *et al.* 1997). In a study where tryptophan fluorescence was used to report modulator binding to a mouse recombinant NBD1 (corresponding to segment 371-705, where Trp^{696} fluorescence is monitored) the steroid RU 486 and Δ^6-progesterone bound to a site distinct form the nucleotide binding site on the NBD (Dayan *et al.* 1997). Monitoring the effect that various peptides, drugs and reversers (including progesterone, verapamil and vinblastine) had on ATPase activity, the existence of a common drug and modulator binding site is also argued (Borgnia *et al.*, 1996).

Of particular importance to this study, another class of reversers called flavonoids, was shown to bind at the nucleotide binding domains of p-gp. Again using tryptophan fluorescence, the binding site of various flavonoids was placed next to the ATP binding site and overlapping with the steroid binding site on a recombinantly expressed hexa-histidine tagged C-terminal

nucleotide binding domain (H6-NBD2) of mouse p-gp (Conseil *et al.*, 1998). Binding of a flavone to recombinantly expressed C-terminal NBD2 of ltrmdr1 of *Leishmania tropica* was directly correlated with flavone inhibition of daunomycin efflux and parasite growth inhibition in the presence of flavone – the first study to demonstrate the relationship between reverser binding to NBD and reversal of drug resistance of p-gp (Perez-Victoria *et al.*, 1999). Recently, several contradictory findings were reported on the naturally occurring flavonoids quercetin, kaempferol and genistein (Ferte *et al.*, 1999). For example, quercetin was demonstrated to activate p-gp, resulting in an increase in doxorubicin resistance, while other groups demonstrated that quercetin inhibited p-gp mediated transport of rhodamine 123 and Hoechst 33342 (Critchfield *et al.*, 1994, Scambia *et al.*, 1994, Shapiro and Ling, 1997a). Since flavonoids are found in abundance in plants, fruit and vegetables, it should be considered as a contributing factor during chemotherapy treatment (Perez-Victoria *et al.*, 1999).

Drug design and structure activity relationships

First generation reversers, mainly verapamil, cyclosporin A and structurally related analogues had mediocre benefits in clinical trails – the benefit of mdr reversal overshadowed by the added toxicity of the reverser (Dhainaut *et al.*, 1996). A common theme in many MDR reversers are that these structurally diverse compounds are generally hydrophobic or amphipathic, mostly protonated, contain a cyclic tertiary amine and several aromatic ring systems (Zamora *et al.*, 1988, Gottesman and Pastan, 1993, Pajeva and Wiese, 1998, Berger *et al.*, 1999). Rational drug design is aimed at providing a new generation of reversers with a higher affinity for p-gp with more potent inhibitory effects at lower concentrations of drug with fewer side effects or added toxicity. In drawing conclusions about the efficiency of reversers of multidrug resistance, both immediate effects of the reverser on the p-gp – like drug extrusion inhibition – and the long term effects on the cell system *in vivo* - like cell toxicity must be considered (Ferte *et al.*, 1999). In order to give a short overview of recent developments in this field, especially novel flavonoid derivatives, 3 representative studies are briefly discussed below.

In one study, 28 flavonoid derivatives (from parent compound diosmentin, Fig 1.3) containing a N-benzylpiperazine chain (Fig 1.4) were evaluated for MDR-modulating activity (Ferte *et al.*, 1999).

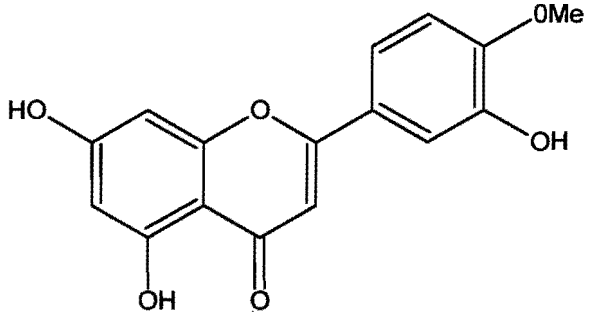

Figure 1.3. The chemical structure of diosmetin

The rationale behind these new derivatives was to increase it's lipophilic properties (by mono or diacetylation of the phenol groups at various positions) and to introduce a basic nitrogen (by adding a N-benzyl group). Previous studies looking at structure-activity relationships of p-gp interacting drugs and their effects on ATPase activity showed that p-gp affinity for drugs was highly correlated with the surface area of the drug while ATPase stimulation was dependent on the partition coefficient of the drug into the plasma membrane (Litman *et al.*, 1997). In the Ferte et al. study a variety of factors influenced reverser characteristics, but lipophilic compounds containing several ring systems and a tertiary amine are good candidates for MDR modulation. Importantly, the nature of substituents on the flavonoid phenols and on the benzyl ring were critical in determining the potency of the molecule. Replacement of the flavone ring by flavanone (the double bond at position 2,3 on ring C is reduced, see Fig 1.7 for labeling) did not alter the MDR-modulating efficiency of the molecule, but did prove to be less toxic *in vivo*. Substitution of flavone hydroxyl groups showed a direct correlation between the position of substitution and mdr-modulation activity, while there was a more complex relationship between the benzyl substitution pattern and modulation potency of p-gp. Quaternization of the basic nitrogen proved to be detrimental to activity and suggests a critical requirement of reversers to display a basic nitrogen. This probably reflects the charged compound's inability to cross the lipid membrane, rather than it's inability to interact with the drug binding site. It appears that lipophilicity is not the sole determinant of the degree of MDR-modulating activity of a reverser, but can be regarded as a favourable parameter within a homologous series. The most active compounds were either a flavone or a flavanone moiety with a 2,3,4-trimethoxybenzylpiperazine chain (Fig 1.4) and were more potent than the classical reverser, verapamil.

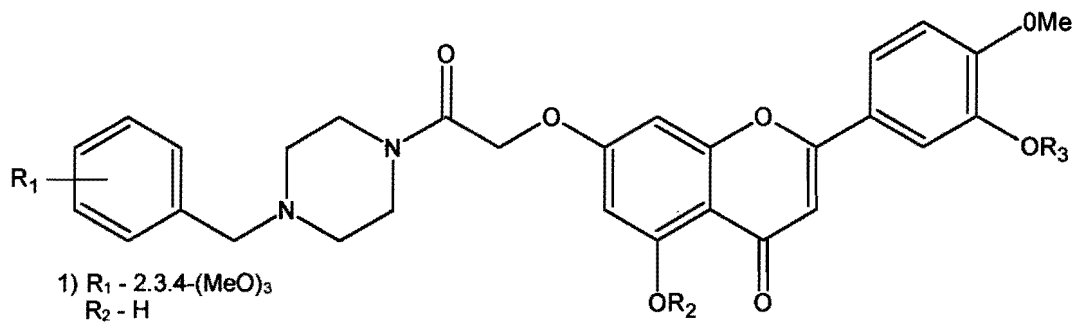

1) R_1 - 2.3.4-$(MeO)_3$
R_2 - H
R_3 - H

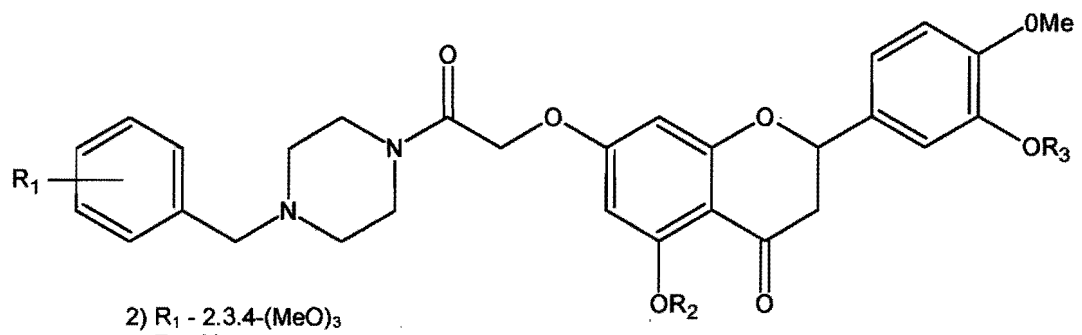

2) R_1 - 2.3.4-$(MeO)_3$
R_2 - H
R_3 - H
3) R_1 - 2,3,4-$(MeO)_3$
R_2 - $COC(CH_3)_3$
R_3 - $COC(CH_3)_3$

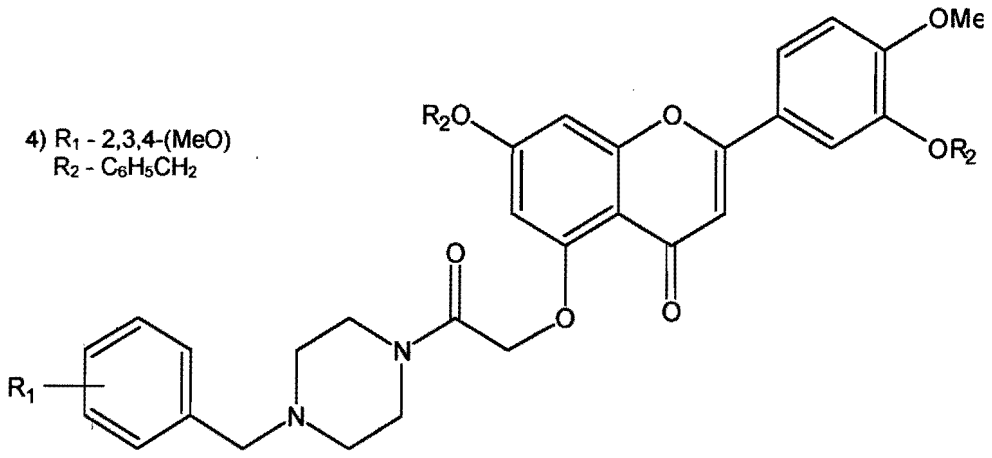

Figure 1.4. The chemical structures of diosmetin derivatives identified to be potent MDR reversers

Using verapamil as the parent compound (Fig 1.5), 59 α-aryl-α-thioether-alkyl, -alkanenitrile, and –alkanecarboxylic acid methyl ester tetrahydroisoquinoline and isoindoline derivatives were synthesised in the quest to find tight binding, low toxicity p-gp reversers (Berger *et al.*, 1999). Several of these compounds restored sensitivity to vincristine in mice and proved not to be cytotoxic at doses needed for mdr reversal.

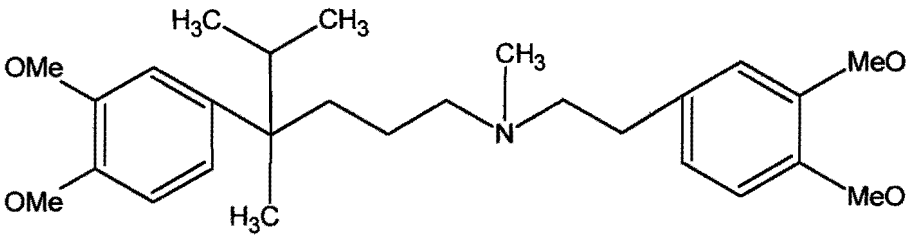

Figure 1.5. The chemical structure of Verapamil

This effect was believed to be the result of direct interaction with p-gp. Compound 15h (Fig 1.6), the most potent of this series of reversers, was demonstrated to bind directly to p-gp through its' prevention of p-gp photolabeling with [^{125}I]iodoarylazidoprazosin – a reporter of the vinblastine binding site. Compound 15h is not extruded by p-gp like verapamil and cyclosporin A, which would argue for either tighter binding to the same site as vinblastine or binding to a second distinct site. It appears from their work that electron donating alkoxy substituents on the aromatic rings provided greater inhibition than halogens in the same position. Altering the steric bulk of R5 and R6 groups affected binding to p-gp strongly. Changes to linker chain length, n, and larger substituents at R1-R4 were well tolerated. Thus, although the p-gps bind a wide variety of structurally unrelated substrates and reversers, they are very sensitive to variations on a specific structural theme. The value of this study is that

the effective compounds were shown to be nontoxic, reverse drug resistance in vivo, and to directly interact with the p-gp.

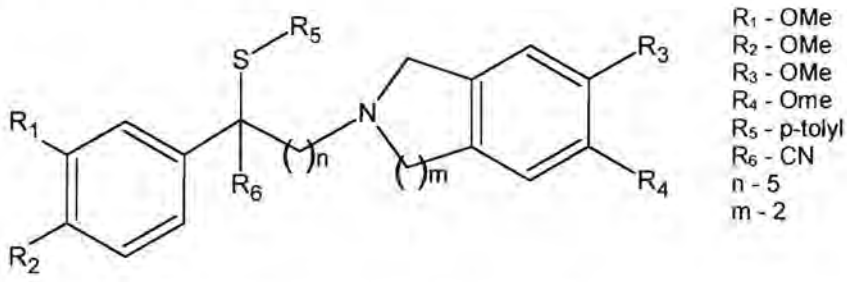

Figure 1.6. The chemical structure of compound 15h

Tight binding halogenated chalcones are also promising candidates for MDR reversers (Bois *et al.*, 1998). Variations on naturally occurring chalcones, flavones, and isoflavones (Fig 1.7) showed that flavones generally have a higher affinity for recombinantly expressed mouse C-terminal NBD than isoflavones. A hydroxy group at position 5 (or position 2 in chalcones) on ring A proved to be essential for tight binding to the NBD, while substitutions at position 7 (or position 4 in chalcone) were well tolerated. Reducing the double bond at position 2,3 on ring C in flavones had a detrimental effect on binding to the NBD.

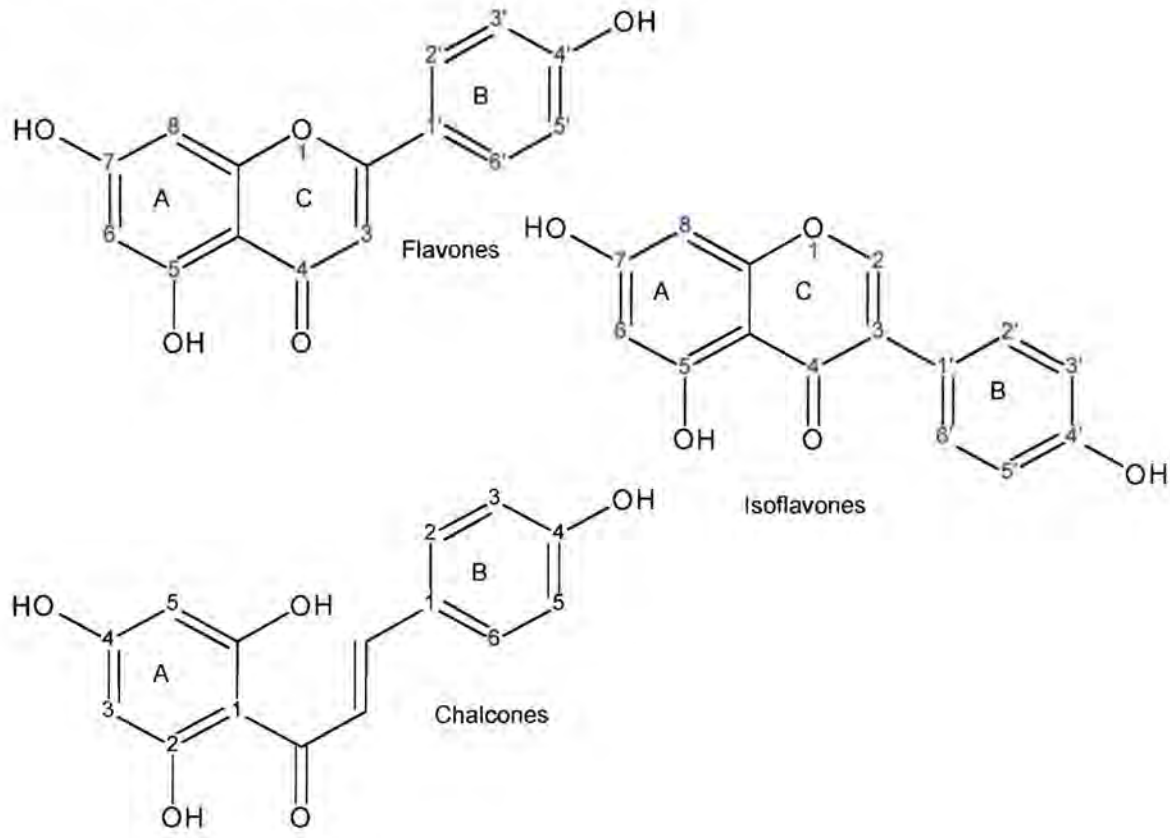

Figure 1.7. The chemical structures of flavones, isoflavones and chalcones

Site-Site interaction

Not only do the two nucleotide binding domains of p-gp interact strongly with each other, but interaction between the transmembrane domains and the nucleotide binding domains is mandatory for drug binding and translocation. When the NH_2- and COOH- terminal halves of human p-gp were expressed separately in HEK 293 cells, each half molecule exhibited basal ATPase activity, but no drug stimulated ATPase activity was detected (Loo *et al.*, 1994). When the half molecules were expressed together, full drug-stimulated ATPase activity was restored showing coupling of ATPase activity with drug binding. Stoichiometric coupling of drug transport with ATP hydrolysis is shown in several studies with coupling ratios from 0.35 – 1 molecules of drug transported per molecule of ATP hydrolyzed (Eytan *et al.*, 1996, Ambudkar *et al.*, 1997, Shapiro *et al.*, 1998). On the other hand, keeping in mind the high basal ATPase activity displayed by p-gp, ATP hydrolysis cannot be viewed as rigidly associated with drug transport.

By following the change in fluorescence of 2-(4-maleimidoanilino)naphthalene-6-sulfonic acid (MIANS) labeled p-gp - labeling the same cysteine as NEM and NBD-Cl - quenching by ATP and drugs were shown to be different, pointing to different conformational changes upon either nucleotide or drug binding (Liu and Sharom, 1996). These results were confirmed by a number of subsequent studies. Conformational changes in p-gp upon nucleotide binding was shown by changes in the proteolysis profile of trypsin-treated p-gp (Wang *et al.*, 1997). Binding of vinblastine or verapamil alone produced a unique conformational change. The conformation adopted by p-gp was different depending on the presence of either both nucleotide and drug or nucleotide or drug alone, indicating different conformations associated with different stages of transport (Mechetner *et al.* 1997, Wang *et al.*, 1998). Tryptophan quenching experiments showed distinct conformational changes in p-gp upon ATP binding and ATP hydrolysis and another two conformational changes were detected upon the addition of anthracycline derivatives in the presence and absence of MgATP (Sonveaux *et al*, 1999).

Utilizing vanadate trapping of MgADP to report on conformational changes in the nucleotide binding domain upon nucleotide or drug binding, several insights were gained into the interaction between nucleotide binding sites and drug binding sites. Vanadate trapping prevented labeling of p-gp by photoreactive substrate analogs, indicating that ATP hydrolysis results in conformational change with a reduced affinity for substrates – a change that could reflect drug being released from a low affinity site after transport across the cell membrane (Ramachandra *et al.*, 1998). The rate of vanadate dependent nucleotide trapping was directly related to drug concentration, indicating the direct relationship between ATPase activity and drug binding (Szabo *et al.*, 1998). In human p-gp, where drug extrusion and ATPase activity appear to be more tightly coupled than hamster p-gp, vanadate trapping of MgADP is dependent on the presence of drug, since no inhibition of ATPase activity by vanadate is seen

in the absence of drugs (Rao, 1998). This suggests a different catalytic cycle for basal ATPase activity and drug stimulated ATPase activity.

In a p-gp containing mutations in NBD1 Walker B motif residues [ERGA – DKGT] (522-525) and T578C, the affinity for ATP was similar to wild type – as reflected by the Km(ATP) measured at increasing concentrations of MgATP under conditions of optimal drug stimulation - while drug-stimulated ATPase activity (V_{max}) was severely affected. Both the mutants showed complete loss of verapamil-induced ATPase activity while retaining a degree of valinomycin-induced ATPase activity. Binding of these drugs to p-gp was not affected as shown by photolabeling studies with [125I]iodoarylazidoprazosin, suggesting that these residues are involved in a signal pathway between the drug and ATP binding sites (Beaudet *et al.*, 1998). Introducing cysteine residues into TM6 and TM12, which are directly connected to NBD1 and NBD2, and monitoring the effect of substrate and ATP binding on crosslinking between these two helices, it was shown that TM6 and TM12 undergo different conformational changes upon drug binding or during ATP hydrolysis. Cross-linking was inhibited by cyclosporin A, verapamil, vinblastine and colchicine, showing that movement between TM6 and TM12 is also essential for drug-stimulated ATPase activity (Loo and Clarke, 1997a). Structural flexibility of the linker region, connecting the first [TMD-NBD] of the protein with the second [TMD-NBD], also appears to be a prerequisite for ATP hydrolysis and drug transport. A 17 amino acid insertion of a predicted flexible structure between amino acids 681 and 682 yielded a functional p-gp capable of conferring drug resistance. In contrast, a 34 amino acid deletion from the middle of the linker region eliminated ATP hydrolysis and drug transport activities, indicating the importance of this peptide in communication between drug binding and ATP hydrolysis (Hrycyna *et al.*, 1998a).

The role of phosphorylation of p-gp remains to be elucidated. P-gp is phosphorylated at several sites in the linker region of the protein. Mutating serines 661, 667, 675 and 683 in human MDR1 proved that phosphorylation by protein kinase C does not effect the rate of drug transport and does not play a role in the establishment of the multi drug resistance phenotype (Germann *et al.*, 1996, Goodfellow *et al.*, 1996). Phosphorylation of the linker region does, however, modulate the interaction of certain drugs with MDR1 and had been shown to play a role in the ability of p-gp to modulate volume activated chloride channels (Barnes *et al.*, 1996, Szabo *et al.*, 1997, Bond *et al.*, 1998).

Catalytic Mechanisms

Several catalytic mechanisms have been suggested by various authors, all of them trying to reconcile drug binding to more than one site coupled to ATP hydrolysis at the two interacting nucleotide binding domains.

The model proposed by Senior, Fig 1.8, shows alternating ATP hydrolysis, where if one site enters a transition state conformation, the other cannot do so (Senior and Gadsby, 1997). Drug transport is coupled to ATP hydrolysis through the relaxation of the high energy catalytic site conformation generated by ATP hydrolysis. This is different from other transport ATPases, since p-gp does not utilize a covalent E~P catalytic intermediate, suggesting that ATP hydrolysis itself generates a high chemical potential conformation. The relaxation of this intermediate is most likely coupled to drug transport – from a high affinity, inside-facing drug binding site to a low affinity, outside-facing drug binding site.

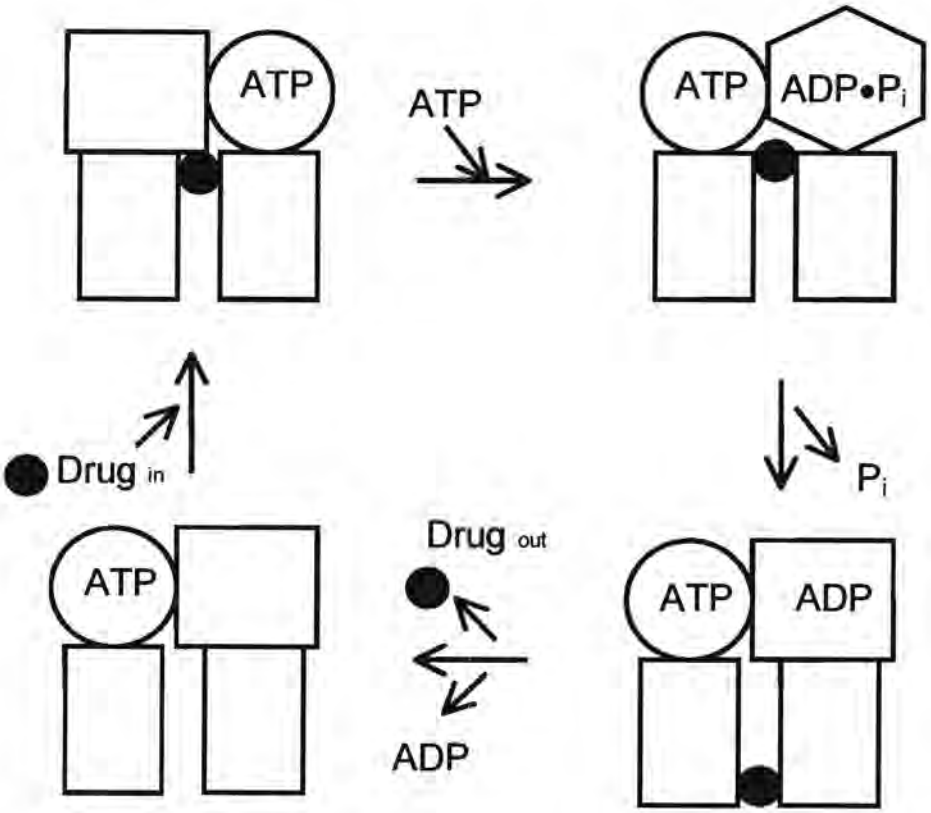

Figure 1.8. Catalytic mechanism of p-gp as proposed by Senior *et al.*, 1997.

In Fig 1.8, the circles, squares and hexagon represent the different conformations of the two NBDs, while the rectangles represent the two TMDs. In this scenario (top left), ATP is bound to the C-terminal (NBD2), but not to the N-terminal (NBD1), with the drug bound to the inside-facing, high affinity drug binding site. Binding of ATP at NBD1 allows ATP hydrolysis at NBD2, resulting in a conformational change that prevents hydrolysis of ATP bound NBD1. This high chemical potential conformation (p-gp•Mg-ADP•P_i) couples drug extrusion with conformation relaxation in the next step when Pi is released and the drug binding site changed into an outside facing, low affinity site. When ADP is released, the protein is ready for another cycle, this time using ATP hydrolysis at the NBD1 to drive the formation of the high chemical potential conformation.

Considering the possibility of two drug binding sites together with two sequential ATP binding sites, with a coupling ratio of one substrate molecule transported per ATP hydrolyzed, Shapiro postulated six step catalytic cycle (Fig 1.9) (Shapiro and Ling, 1998b). In the Shapiro model, only one ATP binding site is occupied at a time – the binding of ATP to one of the two sites prevents binding of a second ATP to the other site. Hydrolysis of the bound ATP is coupled to the transport of one of the two drugs bound to the two drug binding sites. $ADP \bullet P_i$ release allows occupation of the alternating ATP binding site by ATP. Both drug binding sites need to be occupied in this model, in agreement with the experimental evidence that the binding of one drug stimulates the transport of the other (Shapiro and Ling, 1997b).

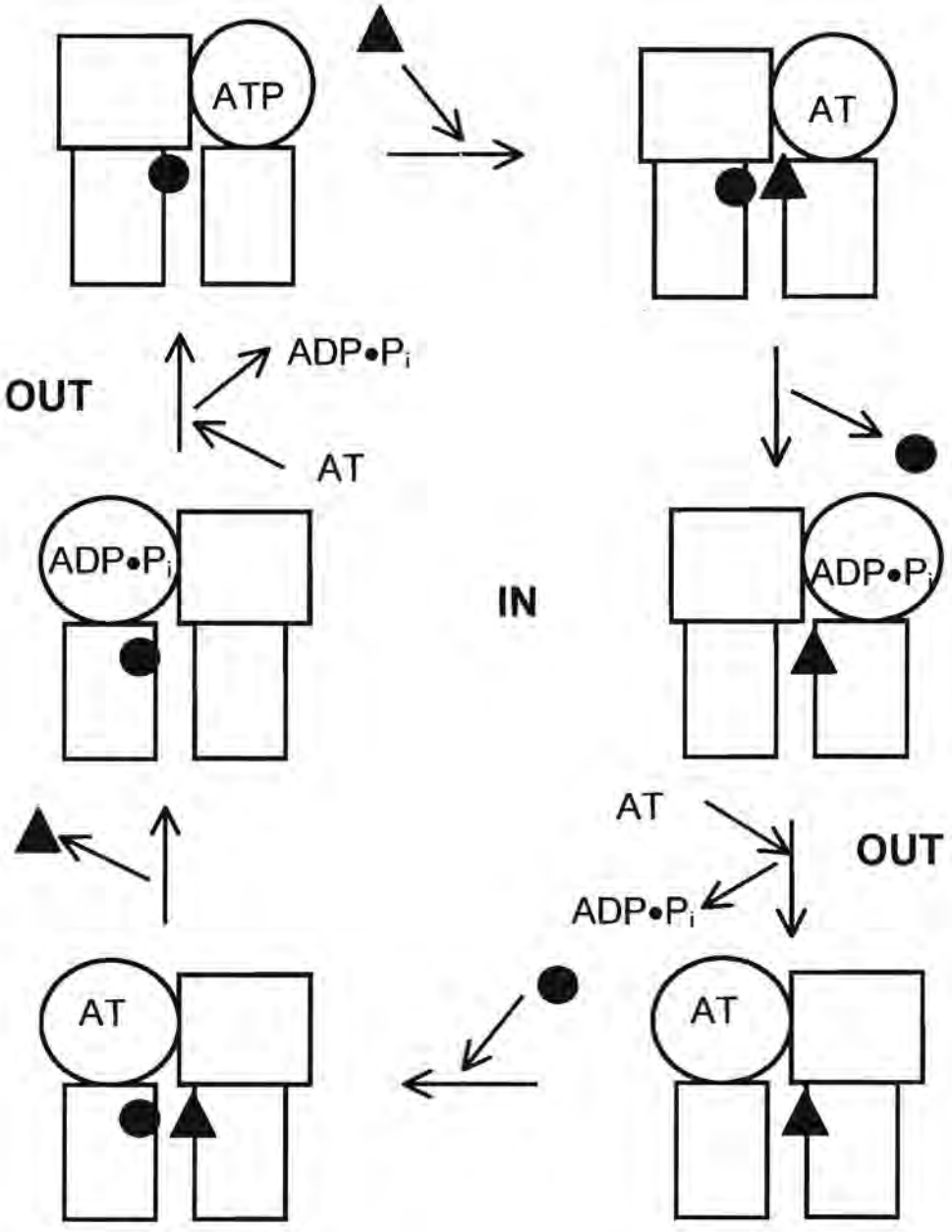

Figure 1.9. Catalytic mechanism of p-gp as proposed by Shapiro *et al.*, 1998.

A third model proposed by Stein (Fig 1.10) incorporates the "vacuum cleaner model", where drugs are mopped up from the lipid bilayer and extruded (Stein, 1997). It is in agreement with alternating ATP binding sites and a conformational change from a high affinity drug binding site to a low affinity drug binding site, responsible for drug movement upon ATP hydrolysis. It also takes into account the three dimensional structure of the protein – proposing that drugs are preferentially scavenged from the membrane, transported into the aqueous cavity of p-gp from which it is expelled upon binding of the second ATP to the alternating site (Rosenberg *et al.*, 1997). This model also includes two interacting drug binding sites, where the binding of the second drug from within the lipid bilayer (together with the second ATP binding to the alternating ATP binding site) plays a role in the conformational change needed to expel the first drug from within the aqueous cavity.

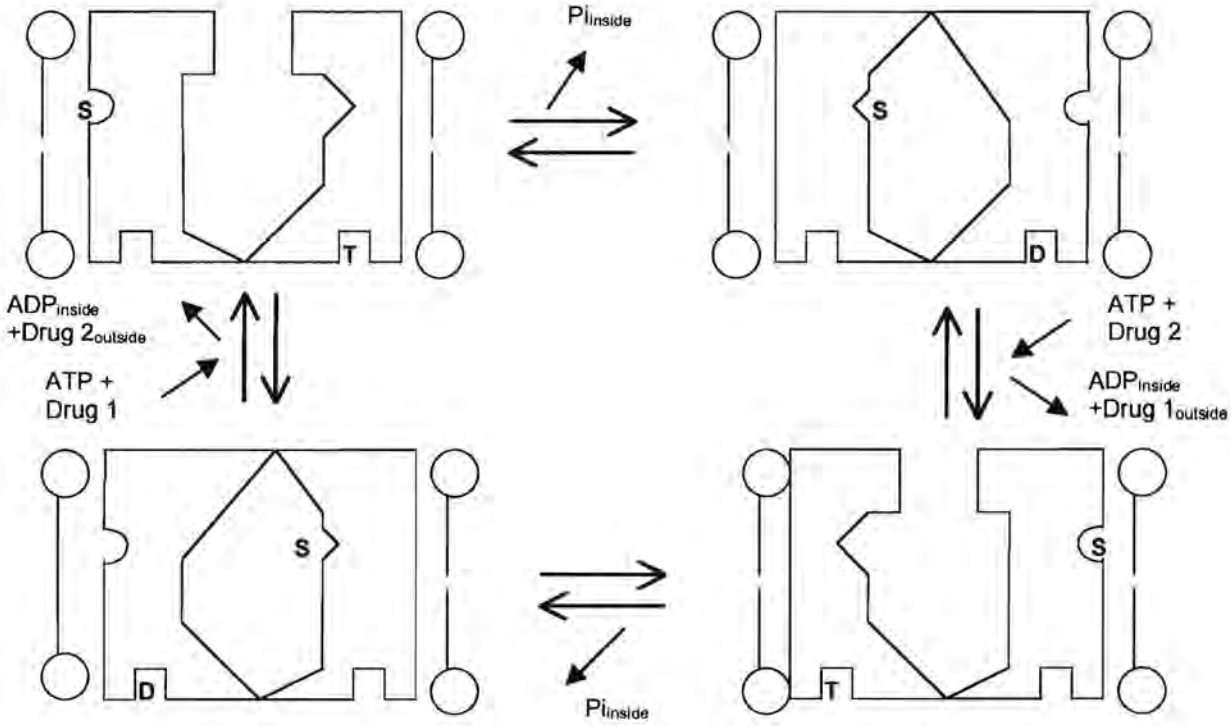

Figure 1.10. Catalytic mechanism of p-gp as proposed by Stein, 1997.

Three dimensional structures of ATP Binding Cassette Proteins

A three dimensional reconstruction of p-gp purified from Chinese hamster ovary CH'B30 cells has been made using single particle images and Fourier projection maps of two-dimensional crystalline arrays (Rosenberg *et al.*, 1997). When viewed from above (Fig 1.11), the extracellular face of the membrane, the projection map of the protein shows a protein ring surrounding a large central aqueous pore of 5 nm in diameter - the protein ring made up from the proposed 12 membrane spanning helixes.

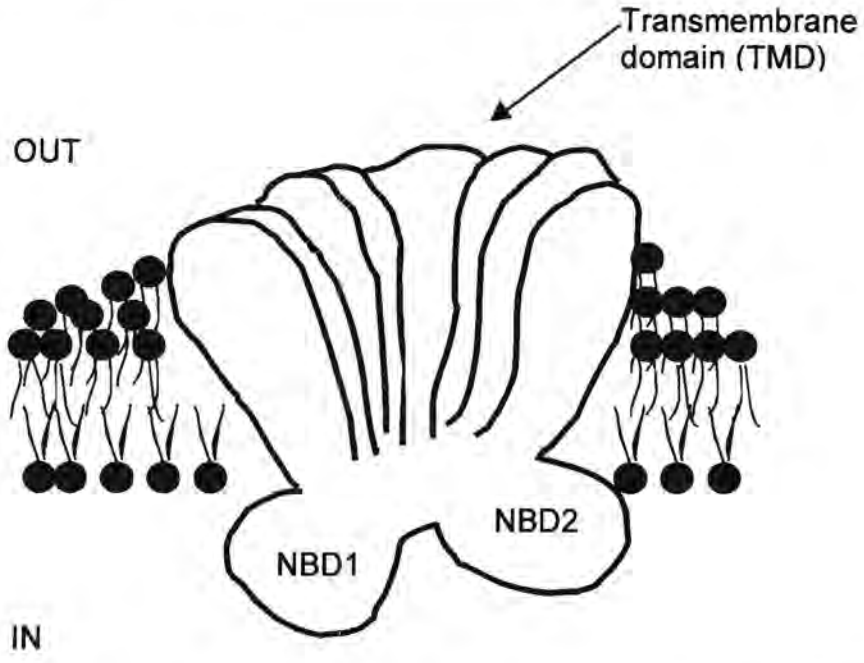

Figure 1.11. A three dimensional reconstitution of p-gp, adapted from Higgins *et al.*, 1997, based on 3 dimensional studies done by Rosenberg *et al.*, 1997.

The protein ring is divided into two halves – the two transmembrane domains (TMD) - each made up from the three extracellular loops connecting pairs of membrane spanning helixes. The two membrane spanning domains can be orientated with respect to each other in two ways (Fig 1.12). The first possibility being true twofold symmetry, where helixes 1 and 6 of the first TMD neighbors helixes 12 and 7 of the second TMD respectively. The second possibility is mirror symmetry where helix 1 and 6 of the first TMD neighbors helix 7 and 12 of the second TMD respectively. Cross-linking studies showed that helix 6 and 12 are in close proximity, suggesting that mirror symmetry were most likely for the two TMD (Loo *et al.*, 1996).

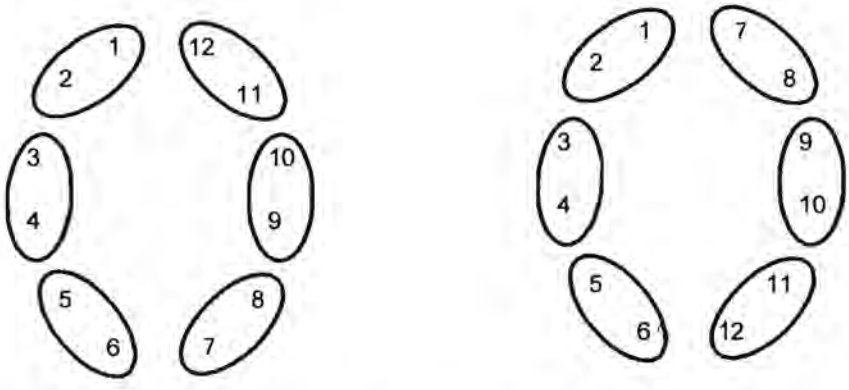

Figure 1.12. Two possible orientations of the membrane spanning regions of p-gp, adapted from Higgins *et al.*, 1997.

Viewed from the side, the cone shaped pore spans the membrane and is closed at the cytoplasmic face of the membrane, presumably by the NBDs and the cytoplasmic loops connecting the membrane spanning helixes. The central pore is open to the lipid phase within the plane of the membrane, potentially providing access between the central pore and the lipid phase. It is here that the substrates are postulated to bind to the drug binding sites of p-gp from within the lipid bilayer, to be transported into the aqueous pore and extruded. The two nucleotide binding domains at the cytoplasmic face of the membrane are snuggled against the TMDs in the membrane, appearing to be more closely associated with its corresponding TMD than with each other. The two NBDs are also asymmetrically organized. Since structural determination was done in the absence of both ATP and substrates, it is possible that direct interaction between the two NBDs only occur in the presence of the above mentioned ligands. Indirect coupling between the two NBDs can also be mediated through transmembrane domain interaction.

The crystal structure of a NBD of the periplasmic histidine permease of *Salmonella typhimurium* became available in late 1998 (Hung *et al.*, 1998). This protein is expressed as four separate subunits that assemble in the membrane as a functional unit. It typically consists of two transmembrane domains, HisQ and HisM, with two nucleotide binding domains, HisP, to form a membrane bound complex $HisQMP_2$. This membrane bound complex also interacts with a ligand presenting subunit, HisJ, that induces ATP hydrolysis upon binding to the membrane bound complex at the periplasmic surface of the protein. The HisP protein was crystallized as a dimer. As seen in Fig 1.13, the HisP subunit is L shaped, with the dimer interface consisting of a β-sheet of 6 strands (β3 and β8-β12). ATP binds near the bottom of this β-sheet in the figure shown. The middle section of each subunit is a mixture of α-helixes and β-sheets (β1, β2, β4-β7, α1 and α2), while the free end consists mainly of α-helices (α3-α9).

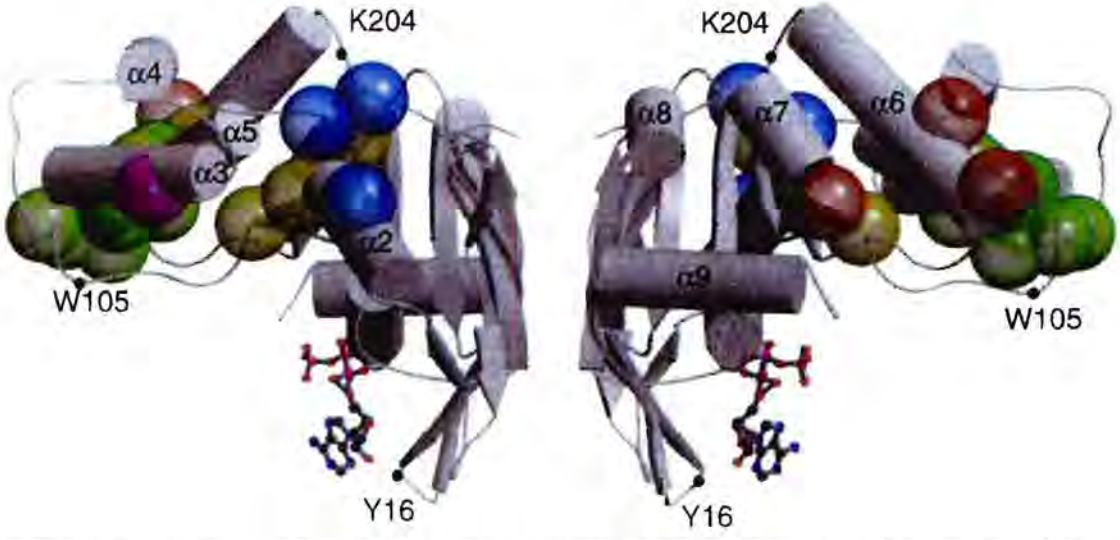

Figure 1.13. The 3 dimensional structure of the HisP protein dimer as determined by Hung *et al.*, 1998.

The amino acids interacting with ATP and possibly with Mg^{2+} are indicated in Fig 1.14. As expected, ATP interacts directly with the Walker A sequence motif, also called the phosphate binding loop, residues Gly^{39} to Lys^{45}, linking β3 to α1. This phosphate binding loop wraps around the phosphates of ATP, allowing hydrogen bonding between the β-phosphate and the main chain nitrogens of Ser^{41} to Lys^{45} and the γ-phosphate and Ser^{41}. Tyr^{16} is also involved in stabilizing ATP binding, this being the tyrosine previously placed at the ATP binding site through $8N_3$-ATP photolabeling (Senior *et al.*, 1996). A bit further away, Asp^{178} (on the end of β9) also interacts with the γ-phosphate of ATP through a water molecule. This water molecule most likely takes the place of Mg^{2+} that was absent from the crystal. Asp^{178} is highly conserved in all ABC transporters and is predicted to be the residue that interacts with the divalent cation during ATP hydrolysis. Glu^{179} and Gln^{100} also form hydrogen bonds with a second water molecule interacting with the γ-phosphate – this water molecule could play a catalytic role during γ-phosphate hydrolysis.

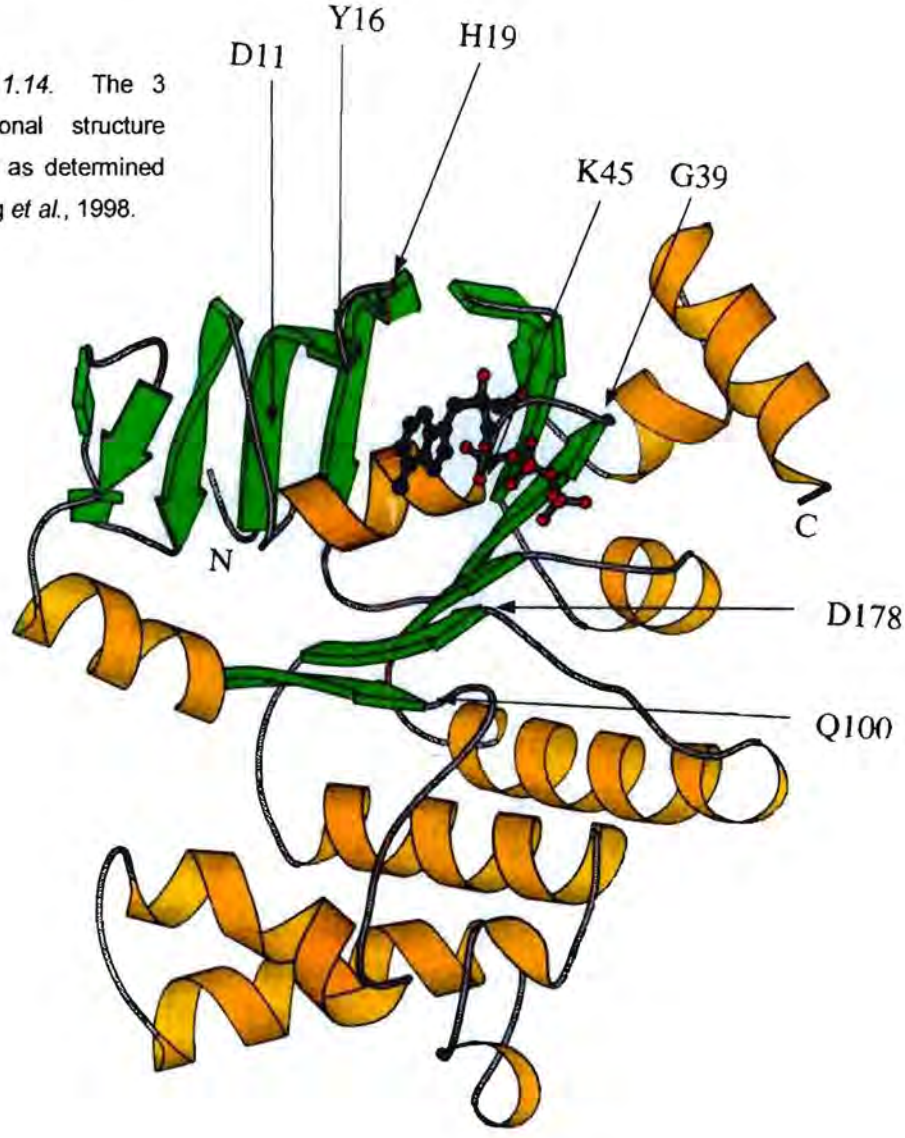

Figure 1.14. The 3 dimensional structure of HisP as determined by Hung *et al.*, 1998.

Interaction between the NBD and TMD takes place at the top face of the dimer, opposite from the ATP binding site. Mutations in these interacting domains uncouples HisP from regulatory control by HisQ and HisM or disrupts the tertiary structure of the top part of the NBD, perturbing communication between the ATP binding site and the rest of the protein (Petronelli *et al.*, 1991). ATP hydrolysis is induced by the presentation of ligand by HisJ at the periplasmic surface of the protein, resulting in cross-membrane signaling between the liganded periplasmic receptor and the cytoplasmic ATP-binding sites. This could occur in two ways. Firstly, conformational changes at HisQ and HisM can result in conformational changes in the top part of HisP that contain residues that is important for ATP hydrolysis (Gln^{100}, Asp^{178} and Glu^{179}) and can lead directly to hydrolysis of ATP at the bottom part of HisP. Alternatively, ATP hydrolysis can also be the direct result of a change in orientation between the bottom ATP binding domain of HisP and the top interacting part of HisP induced by direct movement between the six-stranded β-sheet shared by the two regions.

In summary, the three dimensional data seem well supported by previously found experimental data. The ATP binding domains interact strongly, as seen with the dimer structure in HisP. ATP hydrolysis is directly coupled to ligand/substrate binding and is accompanied by a conformational change in the protein. Substrates appear to have access to the protein from within the lipid bilayer from where they can be transported into the aqueous pore.

In this study

Proteins of particular interest to this study are the yeast proteins Pdr5p and Yor1p as well as the recombinant NBDs of the mouse p-gp, mdr1 (Decottignies *et al.*, 1994, Decottignies *et al.*, 1998, Boubichon-Cortay *et al.*, 1994). The yeast p-gp protein Pdr5p is typically expressed as a single polypeptide with a membrane topology of [NBD-TMD-NBD-TMD] – the reverse of the mammalian protein topology - while the yeast MRP protein Yor1p's membrane topology is similar to the mammalian p-gp. Being under the control of the PDR1 and PDR3 transcription factor genes, Pdr5p gives rise to pleiotropic drug resistance in the cells in which it is overexpressed. Pdr5p ATPase activity is optimal over a broad pH range, extending from 5.5 to 8.0. Typically, a plasma membrane bound Pdr5p exhibits a Km(ATP) = 0.5 mM and a Vmax = 2.5 μmol of Pi/ min/ mg of protein and can also hydrolyze CTP, GTP, UTP and ADP but not AMP. The purified enzyme yields a Km(ATP) = 0.25 mM and a Vmax = 0.25 μmol Pi/ min/ mg of protein. Pdr5p ATPase activity was inhibited by known MDR substrates and reversers such as vanadate, oligomycin and actinomycin D and the UTPase activity stimulated on the addition of verapamil. The Yor1p yeast MRP protein is responsible for oligomycin and reveromycin A resistance on overexpression (Katzmann *et al.*, 1995).

The recombinant NBD2 of mouse mdr1 p-gp (sNBD2 and LNBD2) were initially designed to assess ATP binding to a single NBD, as could be reported by tryptophan fluorescence.

These recombinant NBDs, expressed as either a fusion proteins to GST or a histidine tagged protein, bound ATP in the mM concentration range, as well as the ATP derivatives, TNP-ATP and TNP-ADP, in the micromolar range. Little or no ATPase activity was measured for these recombinant NBDs. In the absence of membrane located substrate or modulator binding sites, it was established that not only does NBD2 bind nucleotide, but also steroids and flavonoids at sites close to and partially overlapping the ATP binding site (Conseil *et al.*, 1998).

Aims of this research programme

The overall theme of the project was to apply TNP-$8N_3$-ATP as a photoaffinity probe of the ATP binding sites of p-gps. There was evidence that TNP-ATP bound much more tightly than ATP to the ATP binding site of p-gp (Baubichon-Cortay *et al.*, 1994, Senior *et al.*, 1995). Specific photolabeling is a good measure of the integrity of the ATP binding site, active site amino acids can be identified and inhibitors of nucleotide binding can be identified and characterised.

1) To test whether TNP-$8N_3$-ATP could be used as a photoaffinity probe of yeast protein Pdr5p. P-gps are expressed in small amounts in mammalian cell plasma membrane and it is difficult to obtain amounts of protein suitable for identifying active site residues and for kinetic studies. The laboratory of Prof. A. Goffeau, University of Louvain-la-Neuve, Belgium was able to overexpress several yeast pumps, including Pdr5p, Snq2p and Yor1p, by selective elimination of transcription factors and unwanted pumps. Large amounts of protein can be prepared from yeast culture in this way.

2) To characterise the nucleotide binding properties of Yor1p by photolabeling with TNP-$8N_3$-ATP. While Pdr5p and Snq2p had been well characterised at the start of the programme, Yor1p was in the process of being investigated by A. Decottignies in Prof. Goffeau's laboratory. Preliminary work suggested that the pump had very low or zero ATPase activity. This study set out to ascertain whether Yor1p could bind nucleotides

3) To characterise the nucleotide binding site of soluble recombinant NBD2 of mouse p-gp and identify amino acid residues ligating ATP. Many bacterial ABC transporters are of modular construction and the laboratory of Dr A. Di Pietro was engaged in producing the nucleotide binding domain (NBDs) of mouse p-gp. The aim of this study was to understand the nucleotide binding properties of individual domains and also to investigate whether drugs / reversers binding sites existed on the NBDs. We undertook to establish whether TNP-$8N_3$-ATP could be used as a probe of mouse NBD2.

4) *To investigate the interaction of flavonoids with the ATP binding site of mouse NBD2 using TNP-$8N_3$-ATP and $8N_3$-ATP as photoprobes.* Efficient and specific photolabeling of mouse

NBD2 with TNP-$8N_3$-ATP and $8N_3$-ATP suggested that they could be used to monitor binding of drugs / reversers / flavonoids to the ATP binding site. Using tryptophan fluorescence, Dr. A. Di Pietro's laboratory had established that several flavonoids bind to the recombinant mouse NBD with high affinity. The question was whether these flavonoids bind to the ATP binding site or to a separate binding site as was proposed (Conseil *et al.*, 1998).

5) Synthesis of new derivatives of TNP-$8N_3$-ATP and $8N_3$-ATP, designed to photolabel the phosphate binding region of the ATP site in addition to the adenine region. Bifunctional crosslinkers offer the possibility of derivatization providing measurement of the distance between residues and preventing domain movements. We looked into placing an aryl azido moiety onto the monophosphate of the 8-azido probes.

CHAPTER 2: METHODS

Materials

All the buffers used, the tri-n-octylamine and tri-butylamine salt of pyrophosphoric acid, 5,5'-dithiobis(2-nitrobenzoic acid) (DTNB), ethyleneglycol–bis-(β-aminoethyl ether) N.N.N',N',-tetraacetic acid (EGTA), trypsin, dialysis tubing, Triton X-100 and phospho(enol)pyruvate were from Sigma. Dioxan, ether, DC plastikfolien PEI Cellulose F and molecular sieve 4A were from Merck. Dimethyl formamide, tri-n-butylamine, sodium dodecyl sulphate (SDS), acetonitrile, urea, $MgCl_2$, CH_3COOCH_4 and potassium phosphate was from BDH Laboratory Supplies. The diphenylphosphochloridate and imidazole were from Aldrich and the methanol from Baxter Healthcare Corporation. The pyridine and glycerol were from Analar, the TEAD and 2,4,6-trinitrobenzenesulphonic acid (TNBS) from Fluka. The AG1-X4 resin was from Bio-RAD, the DE52 resin from Whatman, the PD-10 sephadex columns from Pharmacia Biotech, the Sep-Pak C18 cartridges from Waters and the Ni^{2+}His•Bind metal chelation resin from Novagen. The NADH, pyruvate kinase, lactate dehydrogenase and thermolysin were from Boehringer Mannheim. Glycerol and trichloroacetic acid were from Merck and the QuickSave Scintillant from Zinsser Analytic. Peptide sequence analysis was performed using a gas phase sequenator similar to commercial machines. The amino acids were converted to the phenylthiohydantoin derivatives (PTH) and analysed by HPLC using standard procedures. MALDITOF analyses were performed on a Voyager Perseptive Biosystems DE-PRO with α-hydroxy cynammic acid as matrix. The transmembrane predictions were done by TMPred at ExPASy Tools: http://www.ch.embnet.org/software/TMPRED_form.html, and the sequence alignments with DNAMAN ver 4.13, Lynnon BioSoft, USA.

Chemical Syntheses

Synthesis of 4-azido-2-nitrophenyl adenosine mono phosphate (ANP-AMP).

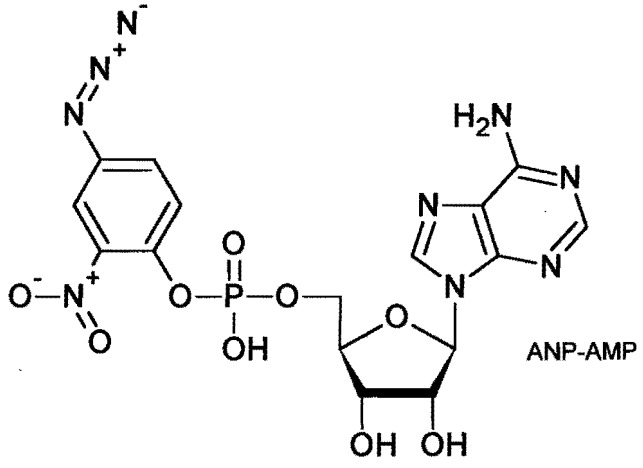

ANP-AMP

4-Azido-2-nitrophenol (ANP) was synthesised from 4-amino-2-nitrophenol according to the method of Lauquin (Lauquin *et al.*, 1980). ANP-AMP was synthesised according to the general method of Michelson for the synthesis of nucleotide anhydrides (Michelson, 1964). AMP, 100 μmol, (free acid) was suspended in 700 μl methanol; 100 μmol tri-n-octylamine was added and the nucleotide dissolved at 60 °C in a water bath. Methanol was removed under reduced pressure. The residue was redissolved in 150 μl DMF and solvent removed under reduced pressure (1-2 h) to remove traces of moisture. The tri-n-octylammonium salt of AMP was dissolved in 700 μl dioxan, and if insoluble, a further 300 μl DMF was added. These steps were all carried out under a nitrogen atmosphere and in the dark. The solution was vortexed vigorously.

To make the P'-nucleoside-5'-P^2-diphenyl pyrophosphate, 30 μl of diphenylphosphochloridate and 45 μl tri-n-butylamine was added and the solution kept at room temperature for 1 h. Solvent was removed under reduced pressure overnight. The P'-nucleoside-5'-P^2-diphenyl pyrophosphate was redissolved in 100 μl dioxan and 200 μmol ANP, dissolved in 200 μl pyridine, was added to the solution and left at room temperature for 3 h. Solvents were removed under reduced pressure and the ANP-AMP precipitated by the addition of 2 ml ether, washed three times with 1 ml ether and dried under reduced pressure. The precipitated material was dissolved in 1 ml water and passed through a C18 Sep-Pak cartridge to remove contaminating AMP. The nucleotide was eluted with 60 % acetonitrile. ANP-AMP was purified on a strong anion exchange column, AG1X4, and eluted with discontinuous increasing concentrations of HCl. Typically, 100 μmol ANP-AMP eluted in 50 ml 60 mM HCl from a 5.5 ml bed volume of AG1X4 column. The final yield of ANP-AMP was ~ 20 %, but yields did vary between syntheses. The purity was checked by analytical HPLC, which showed essentially a single peak, eluting at 17 % (v/v) acetonitrile off a C18 column.

The reaction was followed throughout by means of TLC (PEI-Cellulose F sheets from MERC, using 1 m LiCl as running buffer). The formation of AMP-ANP could be clearly observed as a new major spot, migrating just below AMP that increased over time concurrent with AMP decline.

Synthesis of 4-azido-2-nitrophenyl-2',3'-o-(2,4,6-trinitrophenyl) adenosine monophosphate (ANP-TNP-AMP).

Addition of the TNP moiety was carried out using the method described by Seebregts (Seebregts *et al.*, 1989). 5,5'–dithiobis(2-nitrobenzioc acid) (DTNB), 25 μmol, and 17 μmol of 2,4,6-trinitrobenzenesulfonic acid (TNBS) was dissolved in 1 ml 0.8 M Na_2CO_3/$NaHCO_3$ mixture. This was added to 1 μmol ANP-AMP dissolved in 1 ml water and stirred in the dark at room temperature for 16 h. The reaction mix was passed through a Sep-Pak cartridge, the cartridge washed with 2.5 ml 15 % (v/v) acetonitrile, and the nucleotide eluted with 1 ml 60 % (v/v) acetonitrile. The 60 % (v/v) acetonitrile fraction was retained and the acetonitrile

evaporated by a nitrogen stream. Preparative purifications of nucleotide were carried out on a Waters reverse phase radially compressed PAD-C18 cartridge where solvent A was 10 % (v/v) acetonitrile, 10 mM KPi, pH 6.0 and solvent B was 50 % (v/v) acetonitrile, 10 mM KPi, pH 6.0. A Spectra-Physics 8700XR pump delivered the solvent. A Bromma 2151 variable wavelength monitor monitored effluent at a wavelength of 210 nm. Analytical HPLC was carried out on a Vydac reverse phase C18 or C4 column with a Beckman System Gold solvent module 126 and diode array detector module 168, with standard solvent A as 10 mM KPi, pH 6.0 and solvent B as 60 % (v/v) acetonitrile, 10 mM KPi, pH 6.0. ANP-TNP-AMP eluted at ~30 % B. The final yield of ANP-TNP-AMP was from 11% to 20%, and the purity as judged by HPLC was greater than 98 %.

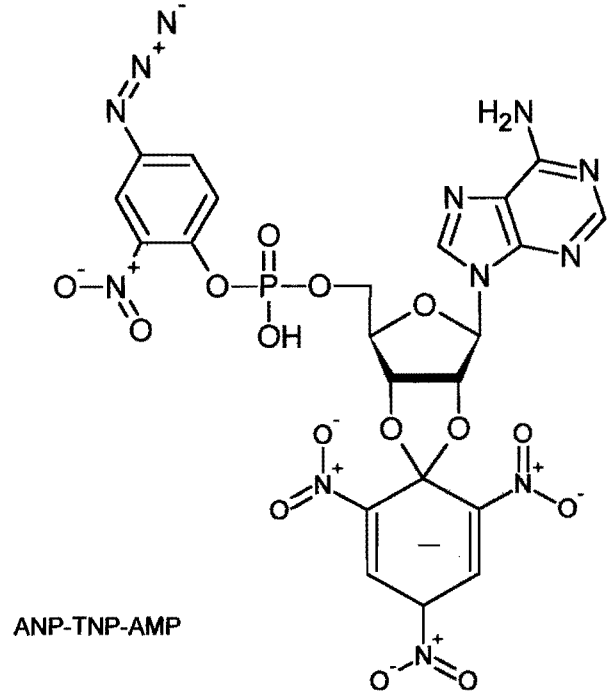

ANP-TNP-AMP

Synthesis of 4-azido-2-nitrophenyl-8N_3-adenosine mono phosphate (ANP-8N_3-AMP) and 4-azido-2-nitrophenyl-2',3'-O-(2,4,6-trinitrophenyl)-8-azido-adenosine monophosphate (ANP-TNP-8N_3-AMP)

For making the 8N_3-derivatives of ANP-AMP and ANP-TNP-AMP, the same experimental procedures were followed as described above for the azido-less nucleotides. 8N_3-nucleotides were available in the laboratory and were originally synthesised according to the method of Seebregts (Seebregts *et al.*, 1989).

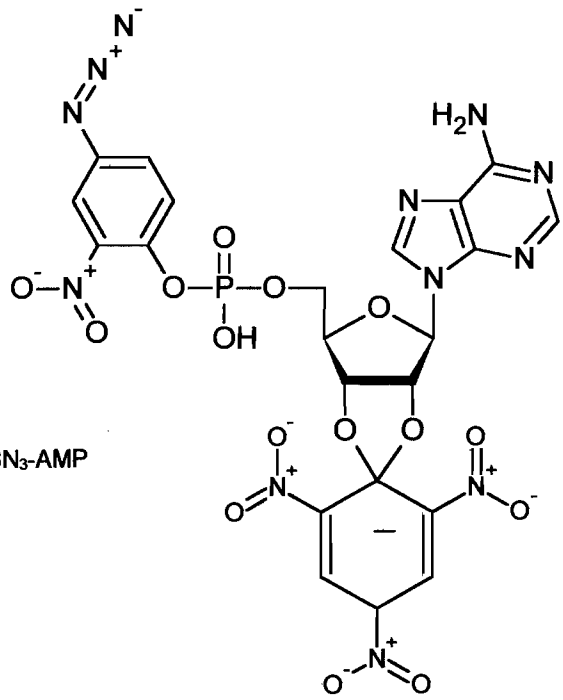

ANP-TNP-8N_3-AMP

Synthesis of [γ-^{32}P]8N_3-ATP and [γ-^{32}P]TNP-8N_3-ATP

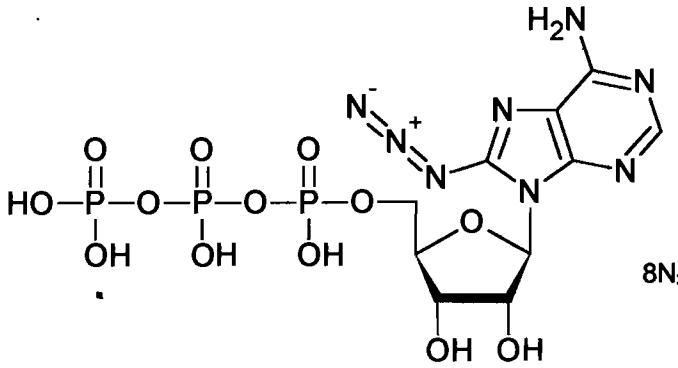

8N_3-ATP

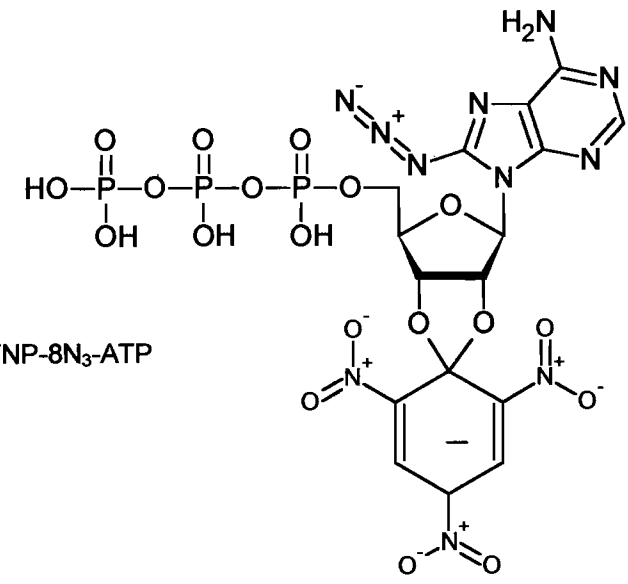

TNP-8N_3-ATP

High specific activity [γ-^{32}P]8N_3-ATP was synthesised essentially according to the exchange method of Glynn and Chappell (1964). TRIS.HCl, 250 µl 200 mM,/12 mM $MgCl_2$, pH 8.0 stock solution was added to a thick walled glass bottle with 51 µl 100 mM NaOH, 2 µl 500 mM cysteine, 15 µl 15 mM 8N_3-ATP, 5 µl 100 mM phosphoglyceric acid, 8 µl 0.1 mg/ml glyceraldehyde 3-phosphate dehydrogenase, 6 µl 0.01mg/ml phosphoglycerate kinase and 2 mCi [^{32}Pi]. The mixture was kept at room temperature for 1 h in the dark with occasional mixing. Adequate exchange of [^{32}Pi] to [γ-^{32}P]8N_3-ATP was checked after 1 h by thin layer chromatography (TLC) – a minimum amount of the reaction mix was spotted on PEI-Cellulose F paper and developed in 1 M LiCl. The reaction mix was applied to a 2cm x 0.5cm DE52 weak anion exchange column with 1/8" ID outlet tubing (1 ml dead volume). All fractions were collected in thick-walled glass bottles. The reaction bottle was washed out with 0.5 ml H_2O that was also applied to the column. The column was washed with 5 ml H_2O and acidified with 5 ml 1 mM HCl. The [^{32}Pi] and 8N_3-ADP were eluted with 7 ml 10 mM HCl and a further 1 ml of 30 mM HCl (outlet tubing dead volume). The [γ-^{32}P]8N_3-ATP was eluted with 7 ml 30 mM HCl and collected in a freeze-drying flask. The fraction was neutralised with 120 µl 0.8 M Na_2CO_3/$NaHCO_3$ to ~ pH 7.0 and freeze-dried overnight.

For the addition of the TNP moiety, the [γ-^{32}P]8N_3-ATP was dissolved in a minimum amount of H_2O and 83 µl of 5,5'–dithiobis(2-nitrobenzioc acid) (TNBS) and 2,4,6-trinitrobenzenesulfonic acid (DTNB) stock solution added (6 mg TNBS and 12 mg DTNB dissolved in 500 µl 0.8 M Na_2CO_3/$NaHCO_3$). The reaction was left at room temperature for 4 h in the dark, stirring continuously. Conversion to [γ-^{32}P]TNP-8N_3-ATP was monitored as before on TLC. The reaction mix was diluted with 5 ml H_2O to reduce the salt concentration and applied to a 4 cm x 0.5 cm (ID) DE52 weak anion exchange column with 3/8"ID outlet tubing (2.5 ml dead volume). The column was washed with 5 ml H_2O, 10 ml 0.2 mM ammonium formate (AF) pH 8.2, 15 ml 0.5 mM AF pH 8.2 and 4 ml 1 mM AF pH 8.2. These fractions were discarded. The [γ-^{32}P]TNP-8N_3-ATP was eluted in 21 ml 1 mM AF pH 8.2. The eluate was applied to a C18 Sep-Pak cartridge and washed with 2 ml 10 mM KPi, pH 7.0 and an additional 0.8 ml H_2O to remove the salt. The [γ-^{32}P]TNP-8N_3-ATP was eluted with 2 ml 60 % CH_3CN and the CH_3CN evaporated under a stream of nitrogen. The purity was checked by analytical HPLC (over 95 %) and the activity of the 8N_3-group confirmed by monitoring the disappearance of the 280 nm absorbance peak, characteristic of the azido adenine moiety, on a diode array spectrophotometer after irradiation of [γ-^{32}P]TNP-8N_3-ATP for 60 s. Diode array scans were performed on a Hewlett Packard Diode Array spectrophotometer (8450A). The final 2 ml sample was aliquoted and stored at -20°C. The synthesis are generally performed with 2-3 mCi [^{32}P]Pi and the final specific activity of the two nucleotides was approximately 2 X 10^7 cpm/nmol.

Proteins

The two recombinant carboxyl-terminal nucleotide binding domains from mouse p-gp (sNBD2 and LNBD2) used in this study were expressed in *E.coli* as described by Boubichon-Cortay *et al.* (1994) and Conseil *et al.* (1998) in the laboratory of Dr. Attilio Di Pietro. In this study two polypeptides of different lengths were investigated – sNBD2 from Thr^{1044} to Thr^{1224} and a longer polypeptide, LNBD2, from Lys^{1025} to Ser^{1276}. The proteins were either expressed as recombinant fusion proteins attached to the N-terminal end of glutathione *S*-transferase (GST) or as hexahistidine-tagged recombinant proteins (Fig 2.1).

For the GST fusion proteins, the cDNA encoding the relevant protein was produced and amplified by reverse transcription PCR from mouse adrenal cell mRNA, inserted into a pGEX-KT vector and used to transform JM105 *E.coli* cells. Induced cells containing expressed fusion proteins were lysed using a SLM-Aminco French pressure cell press. Lysed cells were centrifuged at 30 000 x g for 30 min and the supernatant mixed with glutathione-Sepharose 2B gel equilibrated with PBS buffer containing 1 % Triton X-100 at 4 °C. The GST-NBD2 fusion protein was eluted with 10 mM reduced glutathione in 50 mM Tris-HCl, pH 8.0, and stored in liquid nitrogen in the presence of 15 % glycerol. The recombinant proteins were cleaved from the GST fusion protein using freshly prepared thrombin with a thrombin to fusion protein ration of 1:200, leaving two amino acids, G and S before the start of the relevant mouse sequence. Released sNBD2 or LNBD2 was purified as an unretained fraction from a Fractogel EMD-DMAE-650(M) column equilibrated with 50 mM Tris-HCl, 10 % glycerol, pH 7.5 and 1 mM dithiothreitol.

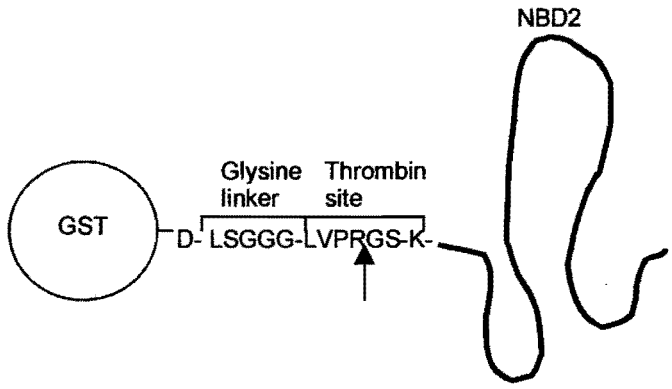

Figure 2.1. Mouse NBD GST fusion protein

For the hexahistidine-tagged proteins (H_6-tagged in this case) the cDNA encoding domain was amplified by PCR from the recombinant plasmid encoding the GST-NBD2, restriction digested, ligated into the corresponding sites of linearized pQE-30 vector and used to transform JM109 *E.coli* cells. Again, induced cells expressing the recombinant protein were lysed by French press treatment and recombinant H6-NBD2 purified from the soluble fraction by using nickel-nitrilotriacetic acid affinity column. The protein of interest was eluted from the column with 250 mM imidazole and dialysed against 20 mM potassium phosphate, 0.5 M

NaCl, 20 % glycerol and 0.01 % HECAMEG at pH 6.8. The full amino acid sequence of sNBD2 and LNBD2 is shown in supplement 1 and 2 at the end of this chapter.

The yeast proteins Pdr5p, Yor1p and SNQ2 were overexpressed in yeast and plasma membrane fractions were prepared as described by Decottignies *et al.* (1998) in the laboratory of Prof. Andre Goffeau. Overexpression of the yeast proteins was accomplished by performing multiple deletions sequentially in the US50-18C PDR1-3 strain by repeated use of the *hisG-URA3-hisG* casette followed by selection of the *ura3* auxotrophic marker with 5-fluoroorotic acid. The gene promoters and ORF ends were cloned into a pSK vector and the linearized fragments of the plasmids used to transform the yeast strain. Plasma membranes were isolated from the pellet sedimented at 15 000 x g for 40 min. This step was preceded by selective precipitation of the mitochondria at pH 5.2. Plasma membrane proteins (5mg/ml) were solubilized with 0.2 % (w/v) n-dodecyl-β-D-maltoside and 8 mM Tris-HCl, pH 7.5 and the solubilized proteins separated on a 33.3 ml linear sucrose gradient. The full amino acid sequence of Pdr5p and Yor1p is shown in supplement 3 and 4 at the end of this chapter.

Photolabeling and SDS-PAGE

The standard irradiation medium for LNBD2 and sNBD2 was 25 mM buffer, 20% (w/v) glycerol, 0.01% (w/v) Triton X-100, 1 mM $MgCl_2$ and a) 5 mM EGTA at < pH 7.0, 0.5 mM EGTA at >pH 7.0 or b) 10 mM EDTA in a volume of 75 µl. The standard photolabeling conditions came about as a result of initial experiments shown in chapter 4, where the influence of salt, Triton X-100, buffer, pH and glycerol on photolabeling, were investigated. The standard irradiation medium for the yeast proteins Pdr5p and Yor1p was similar except that Triton X-100 was omitted. The irradiation time was chosen as 1 min, since irradiation for longer times did not increase the amount of photolabeling observed. The buffer and pH, as well as conditions deviating from the standard, are specified in the legends to the figures.

Samples were irradiated using a 100 Watt Xenon lamp (Hi-Teck) with quartz cuvettes of fresh toluene positioned at either side of the central quartz cuvette to protect the protein form U.V damage (cut off at 290 nm). Irradiated samples were transferred to Eppendorf tubes on ice and 8 µl 20% (w/v) SDS, containing bromophenol blue, was added. LNBD2/sNBD2 samples were separated in 15% (w/v) polyacrylamide gels prepared according to Laemmli (Laemmli *et al.*, 1970) and run for 3 h at 4 °C at 35 mA. Yeast proteins were separated in a similar manner in 7.5 % (w/v) polyacrylamide gels. Gels were dried and the radioactivity quantified using an Instant Imager (Packard Instrument Company). Graphs were drawn using Sigma Plot 3.0 (Jandel Scientific Software) and nonlinear regression were used for fittings.

The data obtained from concentration dependent photolabeling of proteins with [γ-^{32}P]TNP-8N_3-ATP or [γ-^{32}P]8N_3-ATP were fitted to the binding equation

$$Y = (Y_{max} \cdot S)/(Kd + S)$$

Where Y = relative counts, Y_{max} - relative maximum counts, [S] = nucleotide probe concentration and Kd = concentration of probe at which half maximal labelling is obtained.

Data obtained from ATP (or inhibitor) inhibition of either [γ-^{32}P]TNP-8N_3-ATP or [γ-^{32}P]8N_3-ATP photolabeling was fitted to the binding algorithm

$$Y = \{100 \cdot K_{0.5(ATP)}/(K_{0.5(ATP)} + [ATP]\} + F$$

where Y = percentage photolabeling, F = offset, Kd = concentration of ATP at half maximal inhibition.

The "true" dissociation constant for ATP (or inhibitor) binding was obtained from the equation

$$Ki_{(ATP)} = Kd_{(ATP)} /\{1 + ([TNP\text{-}8N_3\text{-}ATP]/Kd_{[TNP\text{-}8N3\text{-}ATP]})\}$$

where TNP-8N_3-ATP could also be 8N_3-ATP, depending on the identity of the radiolabel.

This equation was deduced from the standard binding equation

$$Y = [L]/K_D + [L]$$

which can be rewritten for competitive inhibition as

$$1 - Y = 1 - ([L]/K_{0.5} + [L]) = K_{0.5}/(K_{0.5} + [L])$$

where $K_{0.5} = K_D\{1 + ([L]/Ki)\}$ and K_D = Ki(ATP), $K_{0.5}$ = Kd(ATP) and Ki = Kd(radiolabel)

The pKa values for pH dependent photolabeling of various proteins with [γ-^{32}P]TNP-8N_3-ATP or [γ-^{32}P]8N_3-ATP were obtained from the equation

$$Y = \{(A \cdot 10^{pKa-x})/(10^{pKa-x} + 1)\} + F$$

where Y = percentage photolabeling, x = pH and F = offset

This equation was deduced from the standard binding equation

$$pH = pKa + \log Y/(Y_{max} - 1)$$

Preparative LNBD2 photolabeling, dialysis and processing of peptides by HPLC

Samples were irradiated for 5 min to compensate for inner-filter effects, in 2.5 ml standard medium (25 mM MES, pH 6.0, 20% (w/v) glycerol, 0.01% (w/v) Triton X-100 and 1 mM

$MgCl_2$), transferred to dialysis bags (Sigma D-9277, size cut off 12 000 Da) and dialyzed for 6 h against 2 ℓ 25 mM NH_4HCO_3, pH 7.4, with buffer changes every 2 h. The protein precipitated during dialysis and the contents of the dialysis bag was transferred to a centrifuge tube and pelleted at 3000 rpm for 15 min. The protein was washed twice by re-pelleting in 2.5 ml 100 mM NH_4HCO_3, pH 7.5. The final pellet was dissolved in 600 µl 8 M urea with the help of a Potter Elevehjem homogenizer. The urea concentration was lowered to 6 or 4 M (thermolysin) and 4 M (trypsin, V8 protease, and clostripain) with 300 ul 100 mM NH_4HCO_3 and the pH adjusted to pH 7 – 8. Digestion with thermolysin was always carried out in the presence of 5 mM MgCl. Digestion was performed at various times, protease concentrations and temperatures as indicated in the legend to the figure. The digest was separated by HPLC (Beckman System Gold 319, Diode Array Detector Module 168) using a C4 reverse phase column (4.5 mm X 250 mm, Vydac) Solvent A: 10 mM KPi, pH 6.0; Solvent B: 10 mM KPi, pH 6.0, 60% (v/v) acetonitrile. Selected peaks were further purified on a C18 reverse phase column (4.5 mm X 250 mm, Vydac) - Solvent A: 10 mM CH_3COONH_4 pH 6.4; Solvent B: 10 mM CH_3COONH_4, 60 % (v/v) acetonitrile.

Preparative LNBD2 photolabeling, Ni^{2+} column purification and processing of peptides by HPLC

Samples were irradiated for 5 min in 2.5 ml standard medium (25 mM MES, pH 6.0, 20% (w/v) glycerol, 0.01% (w/v) Triton X-100 and 1 mM $MgCl_2$). Irradiated samples were pooled and placed on ice. Solid urea was added to a final concentration of 8 M. The sample was applied to a nickel column (0.5 cm X 1cm, equilibrated in 5 mM imidazole, 0.5 M NaCl and 20 mM Tris.HCl, pH 7.9), washed with 4 ml of wash buffer (8 M urea, 0.5 M NaCl and 20 mM Tris.HCl, pH 7.9) and eluted in 900 ul elution buffer (8 M urea, 1 M imidazole, 0.5 M NaCl and 20 mM Tris.HCl pH 7.9). The eluate was diluted two fold and digested with 20 % thermolysin (w/w assuming 100% protein yield) for 2.5 h at 30 °C in the presence of 5 mM MgCl. The digest was analyzed on a C4 reverse phase column, as above.

Preparative Pdr5p photolabeling, size exclusion column purification and processing of peptides by HPLC

Samples were irradiated for 5 min in 2.5 ml medium (25 mM MES, pH 6.0, 20% (w/v) glycerol and 11 mM $MgCl_2$). Irradiated samples were kept on ice. Samples were applied to a PD10 size exclusion column (Sephadex G-25 M) and the protein eluted in 3.5 ml 25 mM NH_4HCO_3, pH 7.6. The eluate pH was adjusted to pH 7.5, $CaCl_2$ added to a final concentration of 5 mM and digested with 4 % (w/w) thermolysin at 37 °C for 2 h. TNP-peptides were separated on a C18 Sep-Pak cartridge and eluted with 60 % CH_3CN, 10 mM KPi, pH 5.5. The CH_3CN was evaporated under a stream on nitrogen and the digest was analyzed on a C18 reverse phase column with 10 mM KPi, pH 6.0 as solvent A and 60 % CH_3CN, 10 mM KPi, pH 6.0 as solvent B.

Quantification of photolabeling by filtration

Various concentrations of sNBD2 (0.25, 0.5, 1 and 1 μM) and PDR5 (0.2, 0.4, 0.8 and 1.37 μM) were irradiated for 5 min in 1 ml 25 mM MES, pH 6.0, 20% (w/v) glycerol, 0.01% (w/v) Triton X-100 and 1 mM $MgCl_2$ (for sNBD2) and in 1.23 ml 25 mM MES, pH 6.0, 20% (w/v) glycerol and 1 mM $MgCl_2$ (for Pdr5p). The [γ-^{32}P]TNP-8N_3-ATP concentration was 30 μM for sNBD2 and 50 μM for PDR5. The protein was precipitated by the addition of 1 ml 10% (w/v) trichloro acetic acid (TCA) and collected on a GF/F 2.5 cm Whatman filter with a mild vacuum. The filters were washed twice with 5 ml of 5% (w/v) TCA and assayed for radioactivity on a Beckman liquid scintillation system, LS6000IC.

Supplement

Amino acid sequence of sNBD2

```
1044 trpnipv lqglslevkk gqtlalvgss gcgkstvvql
1081 lerfydpmag svfldgkeik qlnvqwlrah
     lgivsqepil fdcsiaenia ygdnsravsh
1141 eeivraakea nihqfidslp dkyntrvgdk gtqlsggqkq
     riaiaralvr qphilllldea
1201 tsaldtesek vvqealdkar egrt
```

Amino acid sequence of LNBD2

```
1276 kptlle
     gnvkfngvqf nyptrpnipv lqglslevkk gqtlalvgss gcgkstvvql
1081 lerfydpmag svfldgkeik qlnvqwlrah lgivsqepil
     fdcsiaenia ygdnsravsh
1141 eeivraakea nihqfidslp dkyntrvgdk gtqlsggqkq
     riaiaralvr qphilllldea
1201 tsaldtesek vvqealdkar egrtciviah rlstiqnadl
      ivviengkvk ehgthqqlla
1261 qkgiyfsmvq agakrs
```

Amino acid sequence of Pdr5p

```
1    mpeaklnnnv ndvtsyssas sstenaadlh nyngfdehte ariqklartl
     aqsmqnstq
61   sapnksdaqs ifssgvegvn pifsdpeapg ydpkldpnse nfssaawvkn
     mahlsaadpd
121  fykpyslgca wknlsasgas advayqstvv nipykilksg lrkfqrsket
     ntfqilkpmd
181  gclnpgellv vlgrpgsgct tllksissnt hgfdlgadtk isysgysgdd
     ikkhfrgevv
241  ynaeadvhlp hltvfetlvt varlktpqnr ikgvdresya nhlaevamat
     yglshtrntk
301  vgndivrgvs ggerkrvsia evsicgskfq cwdnatrgld satalefira
     lktqadisnt
361  satvaiyqcs qdaydlfnkv cvlddgyqiy ygpadkakky fedmgyvcps
     rqttadflts
421  vtspsertln kdmlkkgihi pqtpkemndy wvkspnykel mkevdqrlln
     ddeasreaik
481  eahiakqskr arpsspytvs ymmqvkylli rnmwrlrnni gftlfmilgn
     csmalilqsm
541  ffkimkkgdt stfyfrgsam ffailfnafs slleifslye arpitekhrt
     yslyhpsada
601  fasvlseips kliiavcfni ifyflvdfrr nggvfffyll inivavfsms
     hlfrcvgslt
661  ktlseamvpa smlllalsmy tgfaipkkki lrwskwiwyi nplaylfesl
     linefhgikf
721  pcaeyvprgp ayanisstes vctvvgavpg qdyvlgddfi rgtyqyyhkd
     kwrgfgigma
781  yvvffffvyl flceynegak qkgeilvfpr sivkrmkkrg vlteknandp
     envgersdls
841  sdrkmlqess eeesdtygei glskseaifh wrnlcyevqi kaetrrilnn
     vdgwvkpgtl
901  talmgasgag ktlldclae rvtmgvitgd ilvngiprdk sfprsigycq
     qqdlhlktat
961  vreslrfsay lrqpaevsie eknryveevi kilemekyad avvgvagegl
     nveqrkrlti
```

```
1021  gveltakpkl lvfldeptsg ldsqtawsic qlmkklanhg qailctihqp
      sailmqefdr
1081  llfmqrggkt vyfgdlgegc ktmidyfesh gahkcpadan paewmlevvg
      aapgshanqd
1141  yyevwrnsee yravqseldw merelpkkgs itaaedkhef sqsiiyqtkl
      vsirlfqqyw
1201  rspdylwskf iltifnqlfi gftffkagts lqglqngmla vfmftvifnp
      ilqqylpsfv
1261  qqrdlyeare rpsrtfswis fifaqifvev pwnilagtia yfiyyypigf
      ysnasaagql
1321  hergalfwlf scafyvyvgs mgllvisfnq vaesaanlas llftmslsfc
      gvmttpsamp
1381  rfwifmyrvs pltyfiqall avgvanvdvk cadyelleft ppsgmtcgqy
      mepylqlakt
1441  gyltdenatd tcsfcqistt ndylanvnsf yserwrnygi ficyiafnyi
      agvffywlar
1501  vpkkngklsk k
//
```

Amino acid sequence of Yor1p

```
1     mtitvgdavs etelenksqn vvlspkasas sdistdvdkd tssswddksl
      lptgeyivdr
61    nkpqtylnsd diekvtesdi fpqkrlfsfl hskkipevpq tdderkiypl
      fhtniisnmf
121   fwwvlpilrv gykrtiqpnd lfkmdprmsi etlyddfekn miyyfektrk
      kyrkrhpeat
181   eeevmenakl pkhtvlrall ftfkkqyfms ivfailanct sgfnpmitkr
      liefveekai
241   fhsmhvnkgi gyaigaclmm fvngltfnhf fhtsqltgvq aksiltkaam
      kkmfnasnya
301   rhcfpngkvt sfvttdlari efalsfqpfl agfpailaic ivllivnlgp
      ialvgigiff
361   ggffislfaf klilgfriaa niftdarvtm mrevlnnikm ikyytweday
      ekniqdirtk
421   eiskvrkmql srnfliamam slpsiaslvt flamykvnkg grqpgnifas
      lslfqvlslq
481   mfflpiaigt gidmiiglgr lqslleaped dpnqmiemkp spgfdpklal
      kmthcsfewe
541   dyelndaiee akgeakdegk knkkkrkdtw gkpsastnka krldnmlkdr
      dgpedlekts
601   frgfkdlnfd ikkgefimit gpigtgkssl lnamagsmrk tdgkvevngd
      llmcgypwiq
661   nasvrdniif gspfnkekyd evvrvcslka dldilpagdm teigergitl
      sggqkarinl
721   arsvykkkdi ylfddvlsav dsrvgkhimd ecltgmlank trilathqls
      lierasrviv
781   lgtdgqvdig tvdelkarnq tlinllqfss qnsekedeeq eavvagelgq
      lkyesevkel
841   telkkkatem sqtansgkiv adghtsskee ravnsislki yreyikaavg
      kwgfialply
901   ailvvgttfc slfssvwlsy wtenkfknrp psfymglysf fvfaafifmn
      ggftilcamg
961   imaskwlnlr avkrilhtpm syidttplgr ilnrftkdtd sldneltesl
      rlmtsqfani
1021  vgvcvmcivy lpwfaiaipf llvifvliad hyqssgreik rleavqrsfv
      ynnlnevlgg
1081  mdtikayrsq erflaksdfl inkmneagyl vvvlqrwvgi fldmvaiafa
      liitllcvtr
```

1141 afpisaasvg vlltyvlqlp gllntilram tqtendmnsa erlvtyatel
pleasyrkpe
1201 mtppeswpsm geiifenvdf ayrpglpivl knlnlniksg ekigicgrt**g**
agkstimsal
1261 yrlneltagk ilidnvdisq lglfdlrrkl aiipqdpvlf rgtirknldp
fnertddelw
1321 dalvrggaia kddlpevklq kpdengthgk mhkfhldqav eeegsnfslg
erqllaltra
1381 lvrqsk**ilil de**atssvdye tdgkiqtriv eefgdctilc iahrlktivn
ydrilvlekg
1441 evaefdtpwt lfsqedsifr smcsrsgive ndfenrs

The Walker A and Walker B sequences are shown in bold and underlined. The predicted transmembrane spanning regions (TM) are underlined.

CHAPTER 3: CHARACTERISATION OF YEAST PROTEINS PDR5P AND YOR1P BY PHOTOLABELING WITH [γ-^{32}P]TNP-8N_3-ATP.

Pdr5p

Genome sequencing has shown that the yeast possesses 19 p-gps predicted to be located in the membrane (Decottignies *et al.*, 1997). Of these, only Pdr5p, Yor1p and Snq2p appear to be expressed in significant amounts (Baubichon-Cortay *et al.*, 1994). Deletion of any two of these genes, as well as some of the other p-gps, allows isolation of a preparation enriched in the desired protein. Mutation of the regulator genes PDR3 and PDR10 also results in enhanced expression (Decottignies *et al.*, 1994). The well-characterised yeast p-gp, Pdr5p, was investigated as a preliminary study leading into the characterisation of the newly discovered yeast protein, Yor1p. Pdr5p was previously shown to exhibit a robust ATPase activity and also interacted with several other nucleotides, while at the commencement of this study, no ATPase activity could be detected for Yor1p.

The protein composition of plasma membrane preparations containing the p-gps enriched either in Pdr5p, Snq2p or Yor1p are shown in Fig 3.1. Conveniently, the 100-kDa yeast H^+/K^+-ATPase pump, PMA1, migrates just below the p-gps - that are of molecular size in the region of 160 kDa - and can be used to obtain relative expression levels of the yeast pumps. In the negative control the genes of six p-gps, including Pdr5p, Snq2p and Yor1p, have been deleted (lane 1). Overexpression of Pdr5p yields an amount of protein nearly equivalent to the plasma membrane H^+/K^+-ATPase, usually the most plentiful membrane protein (lane 2). Expression of Snq2p appears to be less (lane 3). Yor1p is well expressed and has a higher apparent molecular weight (lane 4). Lane 5 shows a yeast strain expressing both Yor1p and Snq2p, while lane 6 shows the unmodified parental strain expressing all of the p-gps.

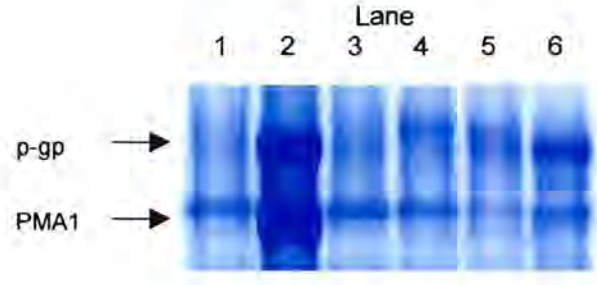

Figure 3.1. Coomassie blue stained polyacrylamide gel of membrane enriched fractions of various yeast proteins. Lane 1: negative control, lane 2: Pdrp5p, lane 3: Snq2p, lane 4: Yor1p, lane 5: Yor1p (top) and Snq2 (bottom), lane 6: positive control containing all the proteins.

Initially, photolabeling of Pdr5p was carried out at pH 8.5 as Pdr5p and Yor1p displayed a maximal ATPase activity at alkaline pH (Decottignies *et al.*, 1995., Decottignies *et al.*, 1998). Photolabeling was carried out in 25 mM EPPS and 20 % (v/v) glycerol with ATP binding site concentration (one for PMA1 and two for Pdr5p) estimated to be below 1 μM. The protein preparations used in the following experiments were membrane fractions containing both

PMA1 and the relevant yeast protein (Fig 3.1). According to Coomassie blue stained polyacrylamide gels, PMA1 and p-gp proteins constitutes about 80 % of the total protein fraction. Using the total amount of protein as determined by Bradford analysis (Bradford, 1976), the relative protein concentration was calculated and the samples diluted to an estimated concentration of below 1 μM for the p-gps.

The divalent cation requirements of Pdr5p photolabeling with [γ-^{32}P]TNP-8N$_3$-ATP was ascertained in the presence of either 1 mM $MgCl_2$ or 2 mM EDTA (Fig 3.2). This experiment was carried out in the presence of 20 % (v/v) glycerol, as glycerol functions as a scavenger of free nitrenes, promoting specific labeling as well as stabilising protein structure.

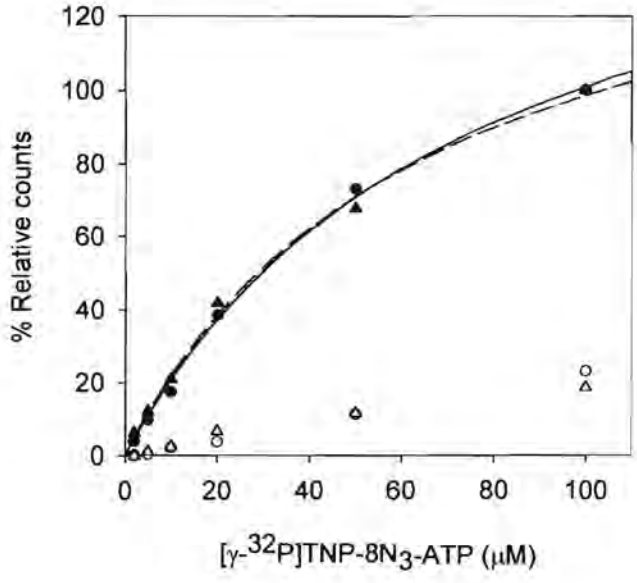

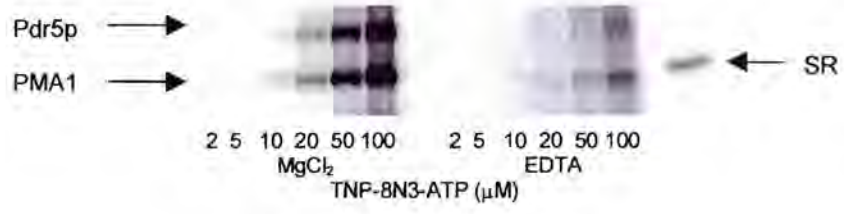

Figure 3.2. Concentration dependent photolabeling of Pdr5p (circles) and PMA1 (triangles), in the presence of 25 mM EPPS, pH 8.5 and 20 % (v/v) glycerol, with increasing concentrations of [γ-^{32}P]TNP-8N$_3$-ATP in the presence of 1 mM $MgCl_2$ (filled symbols) and absence (open symbols) of $MgCl_2$. The lower figure shows an autorad of the SDS-PAGE of this experiment. The band on the far right is the sarcoplasmic reticulum Ca^{2+} ATPase (110 kDa), included as a positive control for [γ-^{32}P]TNP-8N$_3$-ATP photolabeling.

In the presence of 1 mM $MgCl_2$, [γ-^{32}P]TNP-8N$_3$-ATP photolabeled both Pdr5p and PMA1 successfully and displayed a binding constant for PDR5 (Kd) of 46 μM and PMA1 of 74 μM. In the absence of the divalent cation little labeling was observed.

When this experiment was repeated in the absence of glycerol, similar results were obtained with Kd (Pdr5p) = 40.1 μM and Kd(PMA1) = 44.7 μM (Fig 3.3), showing that glycerol does not play an important role in [γ-^{32}P]TNP-8N$_3$-ATP interaction with the protein or in maintaining

protein integrity. $MgCl_2$ was again important for [γ-^{32}P]TNP-8N$_3$-ATP photolabeling of both proteins.

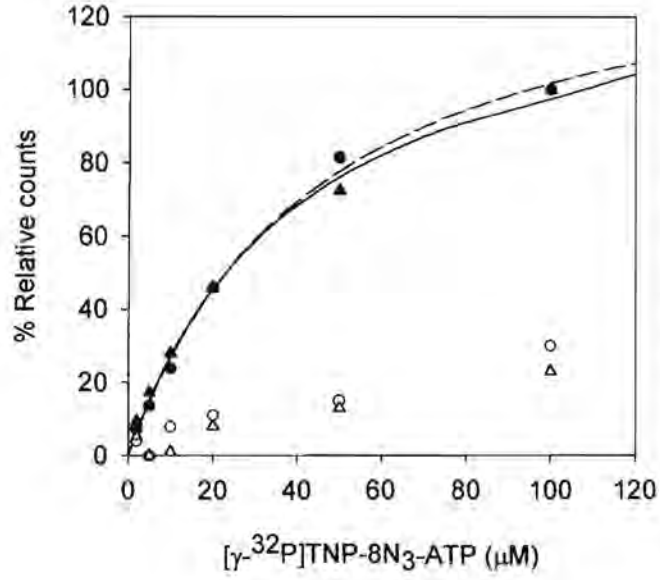

Figure 3.3. Concentration dependent photolabeling of Pdr5p (circles) and PMA1 (triangles) in 25 mM EPPS, pH 8.5, in the absence of glycerol, with increasing concentrations of [γ-^{32}P]TNP-8N$_3$-ATP in the presence (filled symbols) and absence (open symbols) of 1 mM $MgCl_2$.

To determine if [γ-^{32}P]TNP-8N$_3$-ATP is binding to the nucleotide binding sites of Pdr5p (and PMA1) and to ascertain the degree of specificity of this interaction - the effect of increasing concentrations of ATP (in the presence and absence of 20 % (v/v) glycerol) on photolabeling with [γ-^{32}P]TNP-8N$_3$-ATP, was tested (Fig 3.4).

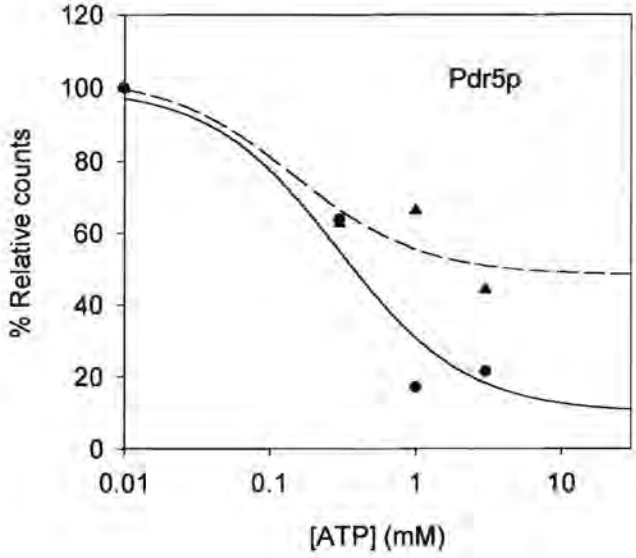

Figure 3.4. ATP inhibition of [γ-^{32}P]TNP-8N$_3$-ATP photolabeling of Pdr5p (top graph) and PMA1 (bottom graph) in 25 mM EPPS, pH 8.5, with 20 % (v/v) glycerol (circles, solid lines) or in the absence (triangles, dashed lines) of glycerol. The [γ-^{32}P]TNP-8N$_3$-ATP concentration was 50 μM and the irradiation done in the presence of 1mM $MgCl_2$.

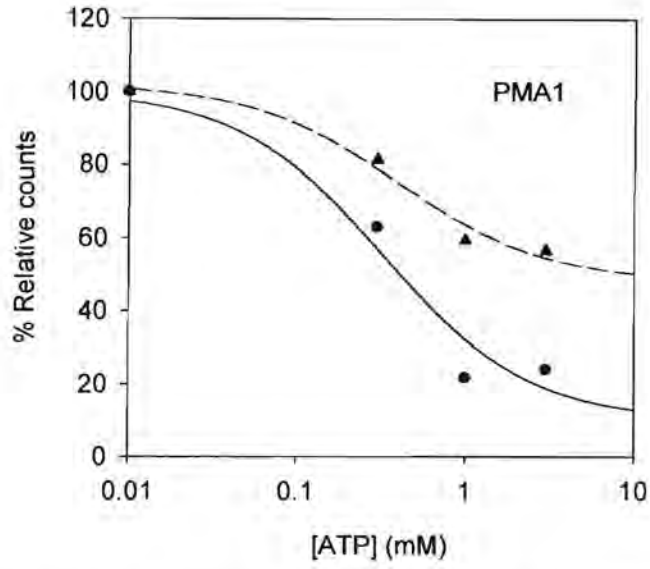

For both Pdr5p and PMA1, increasing concentrations of ATP, in the presence of glycerol, shows significant inhibition of [γ-^{32}P]TNP-8N$_3$-ATP photolabeling (circles, solid lines), with ~ 80 % inhibition of photolabeling at 3 mM ATP. In this preliminary experiment, the Ki(ATP) is calculated to be ~ 0.2 mM for both PDR5 and PMA1, but more data is needed for an accurate value. ATP inhibition of photolabeling is less in the absence of glycerol (triangles, dashed lines) with only approximately 50 % inhibition seen at 3 mM ATP. This suggests that there may be some non-specific labeling of the protein in the absence of glycerol, outside the ATP binding site. This is in agreement with studies on the Ca^{2+} ATPase of sarcoplasmic reticulum (Seebregts and McIntosh, 1989). Consequently, glycerol was included in all future experiments.

The pH dependence of Pdr5p and PMA1 photolabeling with [γ-^{32}P]TNP-8N$_3$-ATP is shown in (Fig 3.5).

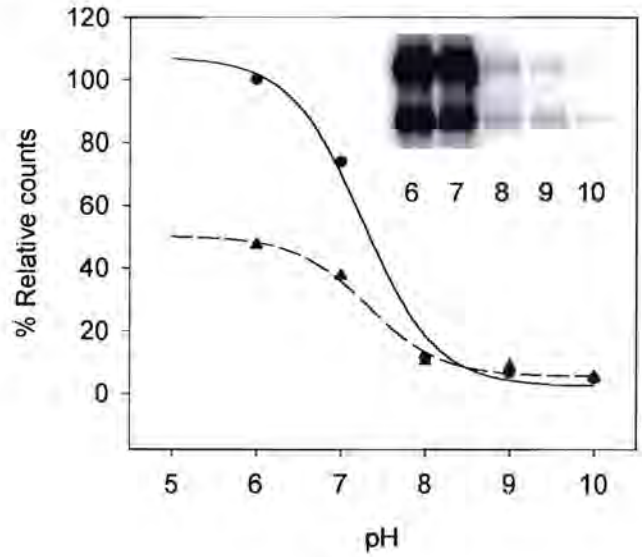

Figure 3.5. pH dependent photolabeling of Pdr5p (circles, solid line) and PMA1 (triangles, dashed line) with [γ-^{32}P]TNP-8N$_3$-ATP. The [γ-^{32}P]TNP-8N$_3$-ATP concentration was 50 μM and irradiations done in 25 mM buffer, 20 % (v/v) glycerol and 1 mM $MgCl_2$. MES was used for pH 6.0, HEPES for pH 7.0, EPPS for pH 8.0 and CHES for pH 9.0 and 10. The insert shows an autorad of a SDS-PAGE of this experiment.

Photolabeling was significantly enhanced at lower pH for both Pdr5p (circles) and PMA1 (triangles) with a pKa of 7.3 for Pdr5p and 7.5 for PMA1. Noticeably, the ratio of Pdr5p to PMA1 photolabeling is also pH dependent, with approximately equal photolabeling of both proteins at alkaline pH (see Fig 3.2, bottom figure) while Pdr5p is labeled twice as much as PMA1 at acid pH (see Fig 3.5 gel insert).

The photolabeling performed at pH 8.5 in the previous figures was clearly not under optimal conditions. Therefore the concentration dependent photolabeling of Pdr5p and PMA1 was repeated at pH 6.0 and is shown in Fig 3.6.

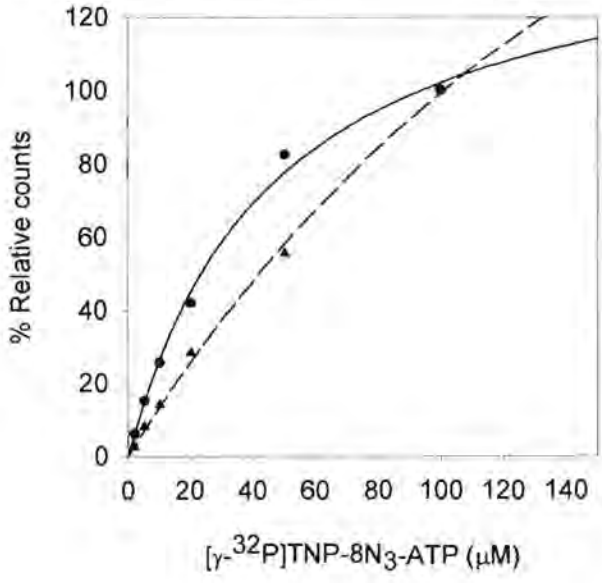

Figure 3.6. Concentration dependent photolabeling of Pdr5p (circles, solid lines) and PMA1 (triangles, dashed lines) in 25 mM MES, pH 6.0, in the presence of 20 % (v/v) glycerol and 1 mM $MgCl_2$.

Pdr5p is photolabeled by [γ-^{32}P]TNP-8N$_3$-ATP with a Kd at pH 6.0 of 46.2 μM. PMA1 is not saturated at 100 μM [γ-^{32}P]TNP-8N$_3$-ATP and the estimated Kd for PMA1 for this experiment is 245 μM. The average Kd of PMA1 for [γ-^{32}P]TNP-8N$_3$-ATP at pH 6.0, taken over 6 experiments with various protein preparations, is 146 μM (data not shown).

Different Pdr5p preparations were also tested for ATP site integrity. Pdr5p enriched membrane fractions kept frozen at – 80 °C and purified, freeze dried Pdr5p (re-suspended in H_2O prior to experiments) were both labeled with [γ-^{32}P]TNP-8N$_3$-ATP and displayed affinities of Kd = 61.4 μM and Kd = 16.2 μM respectively at pH 6.0 (Fig 3.7). The Pdr5p mutant Sc31, with the amino acid mutation G1004A in the N terminal NBD displayed a Kd of 30 μM, indicating that the ATP site was intact. The results suggest that the purified freeze dried preparation may be best (Fig 3.7).

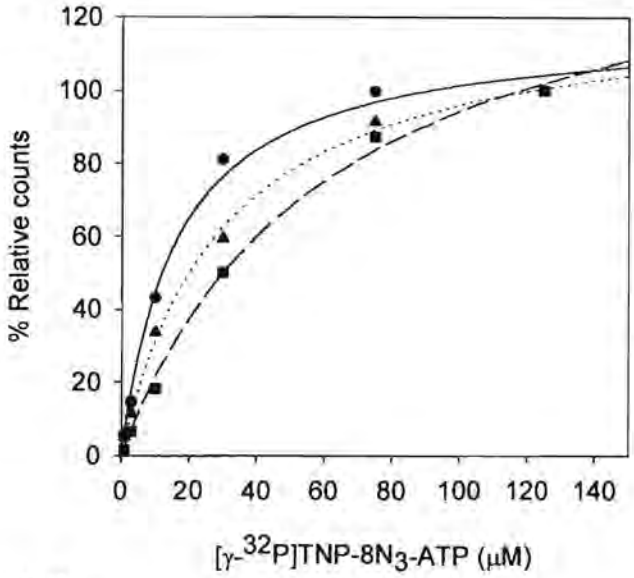

Figure 3.7. Concentration dependent photolabeling of various Pdr5p preparations in 25 mM MES, pH 6.0 with [γ-^{32}P]TNP-8N$_3$-ATP in the presence of 20 % (v/v) glycerol and 11 mM $MgCl_2$. Circles – purified, freeze dried Pdr5p. Triangles – Pdr5p mutant, Sc31, freeze dried. Squares – membrane enriched Pdr5p, in solution stored at – 80 °C.

Yor1p

Having established optimal TNP-8N$_3$-ATP photolabeling conditions for Pdr5p, Yor1p was also investigated. Initially, no ATPase activity could be detected for Yor1p and the integrity of the nucleotide binding domains came under suspicion. To determine if Yor1p had intact NBDs that was able to bind ATP, the interaction of Yor1p with TNP-8N$_3$-ATP was investigated. Photolabeling of Yor1p was carried out in standard medium - 25 mM MES, pH 6.0, 20% (w/v) glycerol - with a protein concentration of < 1 μM. The divalent cation requirements of Yor1p photolabeling were tested (Fig 3.8). Two concentrations of $MgCl_2$ (1 and 11 mM) were compared to that in 2 mM EDTA.

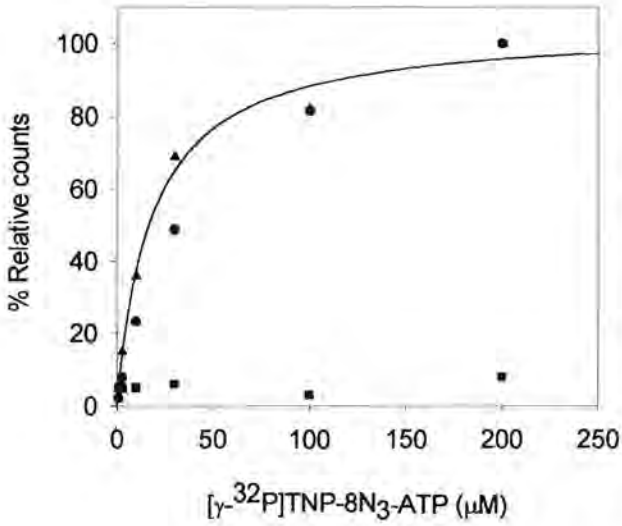

Figure 3.8. Concentration dependent photolabeling of Yor1p in 25 mM MES, pH 6.0 and 20 % (v/v) glycerol with increasing concentrations of [γ-^{32}P]TNP-8N$_3$-ATP in the presence of $MgCl_2$ (circles, 1 mM $MgCl_2$ and triangles, 11 mM $MgCl_2$) or in 2 mM EDTA (squares). The curve through the 11 mM $MgCl_2$ data points was fitted to the average of the two experiments. The lower figure shows an autorad of the SDS-PAGE of this experiment

Yor1p is labeled with [γ-^{32}P]TNP-8N$_3$-ATP in the presence of both 1 and 11mM $MgCl_2$ (triangles and circles), with a Kd of 31.4 μM – the average dissociation constant as calculated from two experiments. This yeast protein too is dependent on the presence of $MgCl_2$ for little [γ-^{32}P]TNP-8N$_3$-ATP labeling is seen in the presence of EDTA (squares).

The effect of ATP on PMA1, Pdr5p and Yor1p [γ-^{32}P]TNP-8N$_3$-ATP photolabeling.

To determine if [γ-^{32}P]TNP-8N$_3$-ATP is also interacting with the ATP binding site of these proteins with a degree of specificity at pH 6.0 - as was case at pH 8.5, in the presence of glycerol, for Pdr5p and PMA1 – photolabeling of these proteins were done in the presence of increasing concentrations of ATP (Fig 3.9).

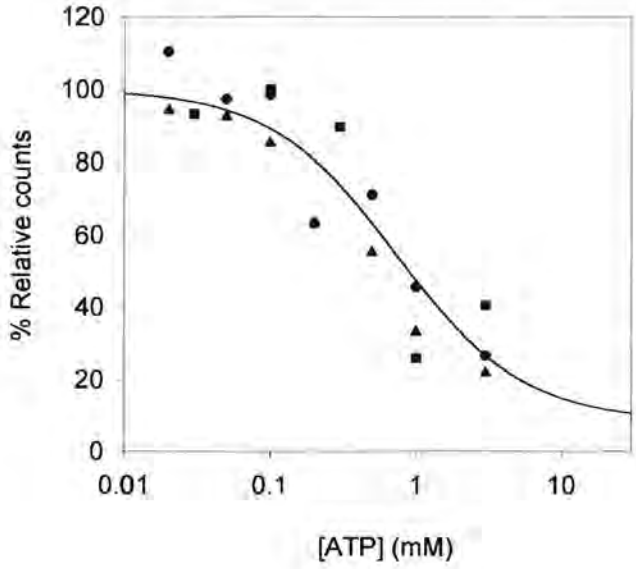

Figure 3.9. Effect of increasing concentrations of ATP on [γ-^{32}P]TNP-8N$_3$-ATP photolabeling of Yor1p (squares), Pdr5p (circles) and PMA1 (triangles) in 25 mM MES, pH 6.0, 1 mM $MgCl_2$ and 20 % (v/v) glycerol. The [γ-^{32}P]TNP-8N$_3$-ATP concentration was at the Kd for Pdr5p or Yor1p respectively. The line is drawn as fitted for Pdr5p.

The Ki(ATP) are 0.322 mM, 0.44 mM and 0.495 mM for Yor1p, Pdr5p and PMA1 respectively. The PMA1 data is the average of two experiments.

In summary, photolabeling of Pdr5p and Yor1p indicates a fair affinity for TNP-8N$_3$-ATP (Kd 10-40 μM), with a dependence on $MgCl_2$, and is optimal at acidic pH with a pKa of 7.3 for

Pdr5p. The specificity seems reasonable in the presence of glycerol as judged by the strong inhibition by ATP in the milli molar concentration range.

Preparative photolabeling of Pdr5p with [γ-^{32}P]TNP-8N_3-ATP

In order to identify the amino acids derivatised by photolabeling of Pdr5p, a 210 μg sample of yeast membrane enriched with Pdr5p (but still containing PMA1 and other minor proteins) was photolabeled with 50 μM of TNP-8N_3-ATP in 2.5 ml standard medium – 25 mM MES, pH 6.0, 20% (w/v) glycerol – and 11 mM $MgCl_2$. A negative control, where irradiation of TNP-8N_3-ATP was carried out prior to the addition of protein, was also performed to identify any tight binding photolysis products. The samples were applied to PD10 size exclusion columns and were eluted with 3.5 ml of 25 mM NH_4HCO_3, followed by digestion with 4 % (w/w) thermolysin for 2 h at 37 °C. The digests were applied to primed C18 Sep-pak cartridges and peptides eluted with 60 % (v/v) CH_3CN. These samples were analysed on a C4 reverse phase column by HPLC.

The HPLC profile of the negative control (Fig 3.10) shows most of the peptides eluting between 11 and 25 min (blue, 210 nm) with a very small amount of tight binding TNP photolysis products eluting at 15.5',18.6' and 26.6'(green, 408 nm).

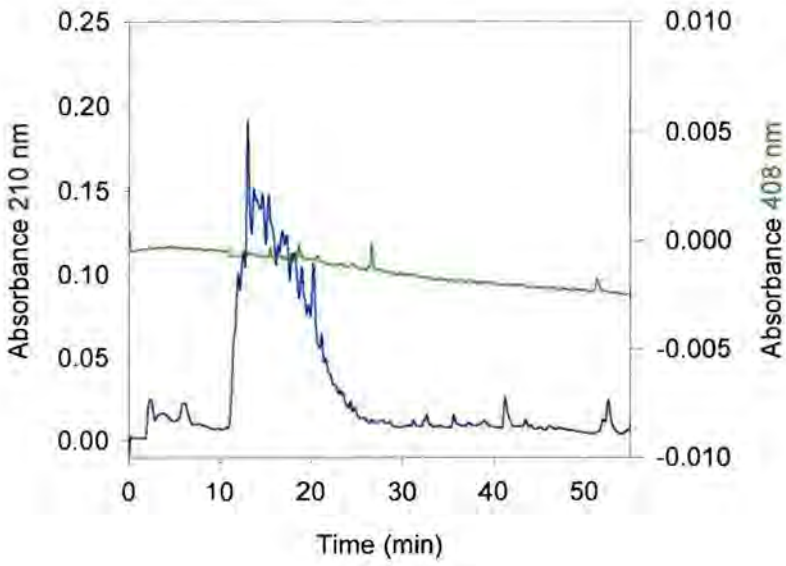

Figure 3.10. Negative control - HPLC profile of 210 μg yeast membrane enriched with Pdr5p (containing PMA1), added to 50 μM of [γ-^{32}P]TNP-8N_3-ATP pre-irradiated for 5 min in 25 mM MES, pH 6.0, 20% (w/v) glycerol, 11 mM $MgCl_2$. Purified sample was digested with 4 % (w/w) thermolysin. The peptide profile is shown in blue, 210 nm. The TNP profile is shown in green, 408 nm. Tight binding photolysis products can be seen at 15.5',18.6' and 26.6'.

The HPLC profile of the sample irradiated in the presence of protein (Fig 3.11) displays a similar peptide profile at 210 nm absorbance (dark blue) as seen with the negative control,

showing reproducible digestion of the protein. The 408 nm trace exhibits two large (16.5' – 17.5' and 18.5' – 19.5') and six smaller TNP peaks.

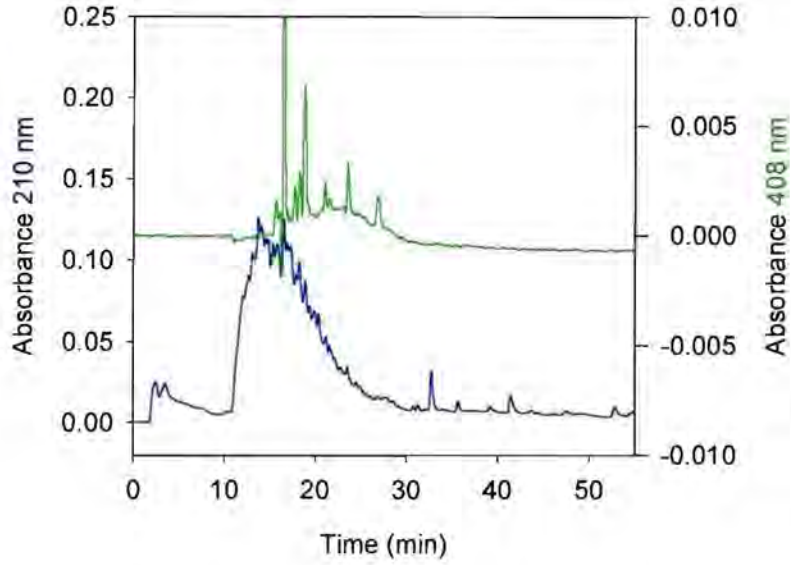

Figure 3.11. HPLC profile of 210 µg of yeast plasma membrane enriched with Pdr5p and PMA1, irradiated for 5 min in the presence of 50 µM of [γ-^{32}P]TNP-8N$_3$-ATP in 25 mM MES, pH 6.0, 20% (w/v) glycerol, 11 mM $MgCl_2$, and digested with 4 %(w/w) thermolysin .

When superimposing the two 408 nm traces of the two experiments (Fig 3.12), the later eluting large peak (18.5' – 19.5') overlaps with a peak of similar elution time in the negative control, suggesting that this peak is a photolysis product rather than a TNP-peptide. The remaining prominent peak (16.5' – 17.5) is consequently the main candidate for a TNP-peptide. Unfortunately, this peak is co-eluted with a large amount of peptides, making further purification of this peak difficult. And, since the samples did not consist of pure Pdr5p, this TNP-peptide could also be from PMA1. When this experiment was repeated in the presence of 1 mM $MgCl_2$, similar results were obtained for 3 different experiments (Fig not shown).

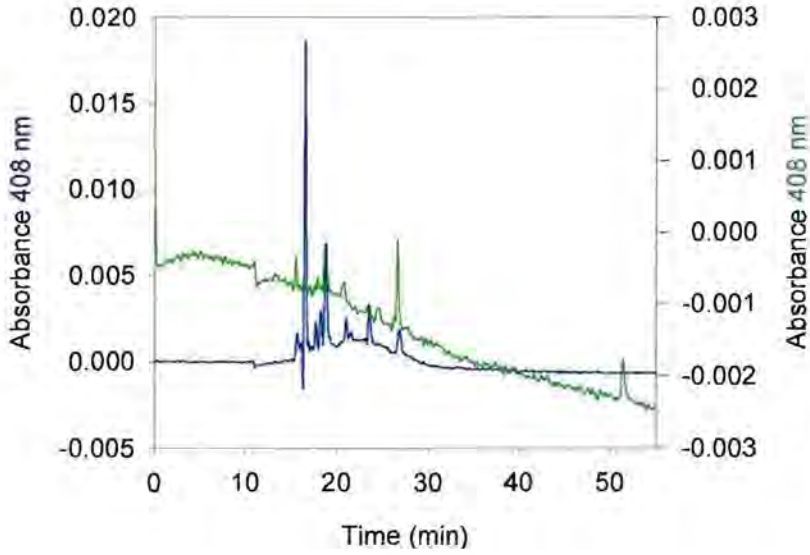

Figure 3.12. Superimposed 408 nm traces of digested Pdrp5/PMA1 protein. Green – protein added after irradiation of [^{32}P]TNP-8N$_3$-ATP - negative control. Blue – protein photolabeled in the presence of 50 µM [^{32}P]TNP-8N$_3$-ATP.

Using 1.05 mg pure, freeze dried Pdr5p (containing no PMA1) photolabeling, digestion and purification were repeated as before (data not shown). Again, two large peaks and several smaller TNP-peaks were present at 408 nm. The later eluting peak coincided with a peak present in the negative control, in agreement with previous experiments. Efforts to purify the major peak away from contaminating peptides were unsuccessful.

Although photolabeling of Pdr5p appears to be specific according to successful inhibition of [γ-^{32}P]TNP-8N$_3$-ATP photolabeling with ATP, a single major peak could not be identified on HPLC after photolabeling and digestion. This could be due to several reasons. Firstly, there is evidence of the presence of tight binding photolysis products that complicate the 408 nm profile. If both of the NBDs of Pdr5p are photolabeled, more than one photolabeled peptide is expected. Thermolysin cleaves at hydrophobic amino acids, and lack of specificity could lead to several different length TNP peptides.

CHAPTER 4: CHARACTERISATION OF SNBD2 BY PHOTOLABELING WITH [γ-^{32}P]8N_3-ATP AND [γ-^{32}P]TNP-8N_3-ATP.

In order to gain a better understanding of the nucleotide binding properties of individual domains of the p-gp, we investigated the recombinant carboxyl-terminal nucleotide binding domain from mouse p-gp. Two recombinant carboxyl-terminal nucleotide binding domains from mouse p-gp (sNBD2 and LNBD2) were used in this study. The shorter mouse NBD discussed in this chapter, sNBD2, constitutes Thr^{1044} to Thr^{1224}. To determine if TNP-8N_3-ATP would be a good photoprobe for monitoring interaction at the ATP binding site of sNBD2 and to establish if this recombinant sNBD had an intact ATP binding site, interaction of sNBD2 with 8N_3-ATP and TNP-8N_3-ATP was investigated. Optimal conditions for the photolabeling of sNBD2, with [γ-^{32}P]8N_3-ATP and [γ-^{32}P]TNP-8N_3-ATP was determined by examining various parameters, such as pH dependence, divalent cation requirements, influence of different buffers, salt concentrations and the presence of glycerol or sucrose in the irradiation medium.

The pH dependence of sNBD2 photolabeling with [γ-^{32}P]8N_3-ATP and [γ-^{32}P]TNP-8N_3-ATP was assayed in 25 mM buffer, pH 6.0, 20 % (v/v) glycerol and 1 mM $MgCl_2$ (Fig 4.1).

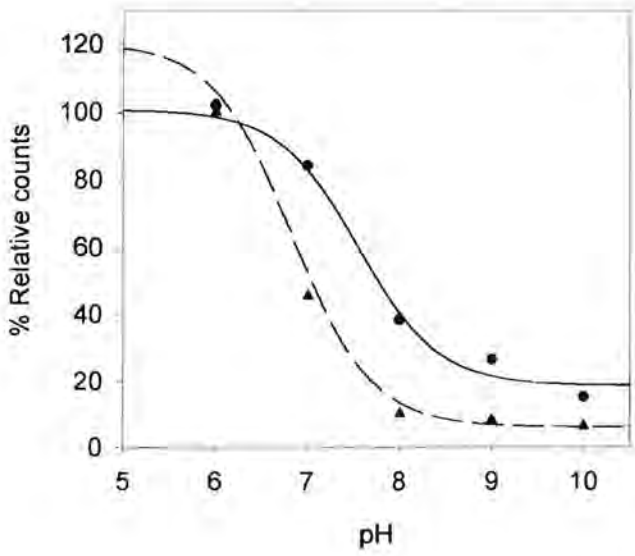

Figure 4.1. pH dependent photolabeling of sNBD2 with [γ-^{32}P]8N_3-ATP (triangles, dashed line) and [γ-^{32}P]TNP-8N_3-ATP (circles, solid line) in 25 mM buffer, 20 % (v/v) glycerol and 1 mM $MgCl_2$. The sNBD2 concentration was 0.5 μM and 0.1 μM respectively. The [γ-^{32}P]TNP-8N_3-ATP concentration was 50 μM and [γ-^{32}P]8N_3-ATP 25 μM. MES was used as buffer for pH 6.0, HEPES for pH 7.0, EPPS for pH 8.0 and CHES for pH 9.0 and 10.0 The lower figure shows autorads of the SDS-PAGE of these experiments.

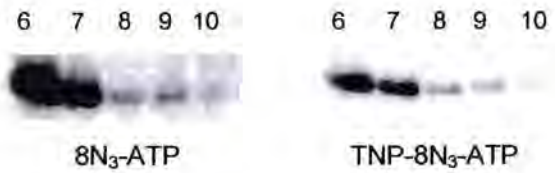

The pH dependent photolabeling of sNBD2 was maximal at acidic pH for both probes, with pKa for [γ-^{32}P]8N_3-ATP = 6.8 and [γ-^{32}P]TNP-8N_3-ATP = 7.5 (the values being the average of two experiments).

Optimal photolabeling conditions were further investigated for [γ-^{32}P]TNP-8N$_3$-ATP by ascertaining the effect of potassium phosphate buffer, pH 6.0, at high and low concentrations as compared to MES buffer – in the presence of glycerol (Fig 4.2, lane 1-4). The influence of sodium chloride (lanes 5 and 6), Triton X-100 (lanes 7 and 8) and sucrose instead of glycerol (lanes 9 and 10) were also investigated.

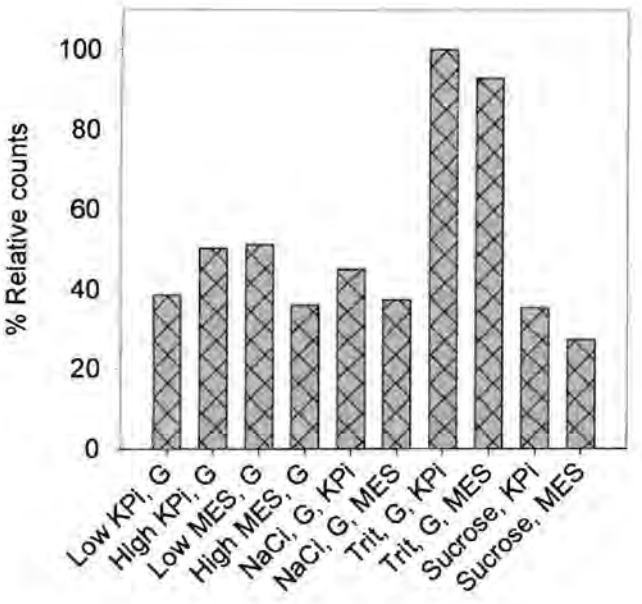

Figure 4.2. Photolabeling of 1 μM sNBD2 with 50 μM [γ-^{32}P]TNP-8N$_3$-ATP under various conditions. Standard irradiation medium contained 25 mM buffer, pH 6.0, 1 mM $MgCl_2$, 5 mM EGTA and 20 % (v/v) glycerol. Lane 1: 40 mM KPi. Lane 2: 100 mM KPi. Lane 3: 25 mM MES. Lane 4: 100 mM MES. Lane 5: 40 mM KPi and 500 mM NaCl. Lane 6: 25 mM MES and 500 mM NaCl. Lane 7: 20 mM KPi and 0.1 % (v/v) Triton X-100. Lane 8: 25 mM MES and 0.1 % (v/v) Triton X-100. Lane 9: 100 mM KPi and 20 % (w/v) sucrose. Lane 10: 100 mM MES and 20 % (w/v) sucrose.

Labeling of sNBD2 with [γ-^{32}P]TNP-8N$_3$-ATP (in the absence of Triton X-100) was optimal at either high KPi concentrations in the presence of glycerol, or at low MES concentrations in the presence of glycerol. However, the effects of buffer type and concentration as well as salt concentration are rather small. Triton X-100 showed the most pronounced effect with a 2 fold increase of photolabeling in the presence of 0.1 (v/v) triton X-100.

Photolabeling of sNBD2 with [γ-^{32}P]TNP-8N$_3$-ATP in the presence of increasing concentrations of Triton X-100 (Fig 4.3) revealed that very low concentrations of Triton X-100 (> 0.003 %) is adequate to facilitate maximal photolabeling and that high concentrations of Triton X-100 (> 0.1 % v/v) is detrimental to photolabeling. Subsequently, 0.01 % (v/v) Triton X-100 was used in all experiments.

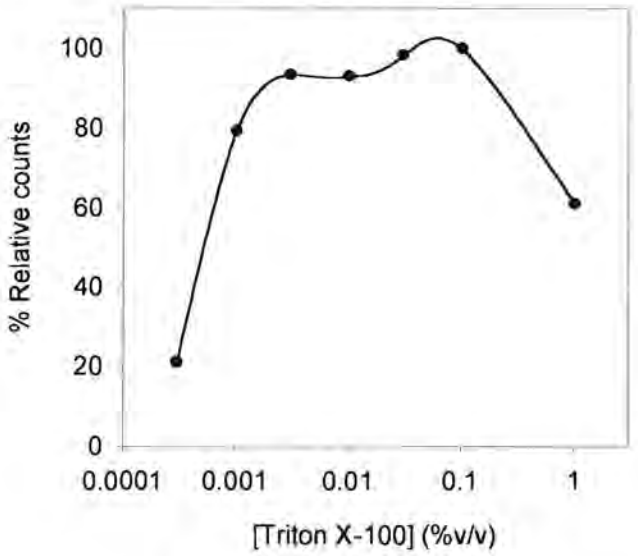

Figure 4.3. Photolabeling of 1 μM sNBD2 with 50 μM [γ-^{32}P]TNP-8N$_3$-ATP in the presence of increasing concentrations of Triton X-100. Irradiation was done in 25 mM MES, pH 6.0 and 20 % (v/v) glycerol in 1mM $MgCl_2$.

The divalent cation requirements for sNBD2 photolabeling with [γ-^{32}P]TNP-8N$_3$-ATP was determined in the presence (open circles, solid line) and absence (filled circles, dashed line) of $MgCl_2$ under standard conditions – 25mM MES, pH 6.0, 20 % (v/v) glycerol and 0.01 % (v/v) Triton X-100 (Fig 4.4).

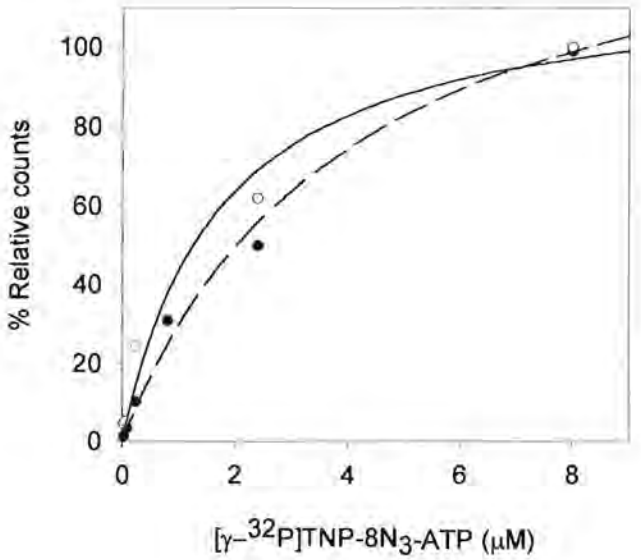

Figure 4.4. Concentration dependent photolabeling of 0.5 μM sNBD2 with [γ-^{32}P]TNP-8N$_3$-ATP in the presence of 1 mM $MgCl_2$ (filled circles, dashed line) and absence of $MgCl_2$ – 2 mM EDTA (open circles, solid line). Irradiation was done in 25mM MES, pH 6.0, 20 % (v/v) glycerol and 0.01 % (v/v) Triton X-100. The lower figure shows an autorad of the SDS-PAGE of this experiment.

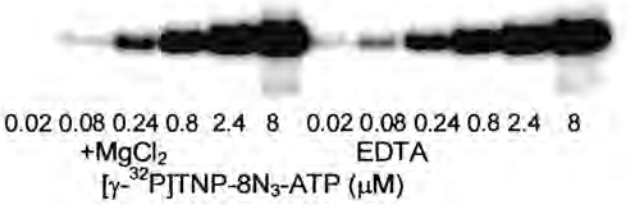

Unlike the intact yeast proteins Pdr5p and Yor1p, photolabeling of sNBD2 is not dependent on the presence of $MgCl_2$ and sNBD2 binds [γ-^{32}P]TNP-8N$_3$-ATP with an affinity (Kd) of 4 μM in the presence of 1 mM $MgCl_2$ or a Kd of 1.7 μM in EDTA. Binding appeared to be less tight in the presence of $MgCl_2$.

To determine if the two ATP probes display similar divalent cation requirements, this experiment was repeated with [γ-^{32}P]8N$_3$-ATP (Fig 4.5).

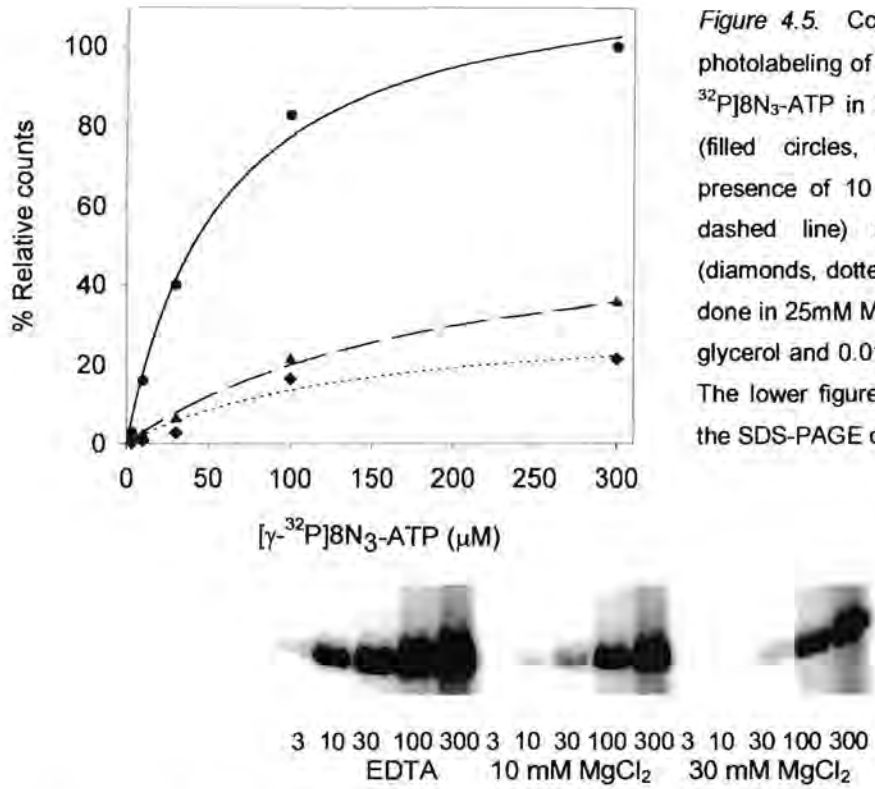

Figure 4.5. Concentration dependent photolabeling of 0.5 μM sNBD2 with [γ-^{32}P]8N$_3$-ATP in the absence of $MgCl_2$ (filled circles, solid line), in the presence of 10 mM $MgCl_2$ (triangles, dashed line) and 30 mM $MgCl_2$ (diamonds, dotted line). Irradiation was done in 25mM MES, pH 6.0, 20 % (v/v) glycerol and 0.01 % (v/v) Triton X-100. The lower figure shows an autorad of the SDS-PAGE of this experiment.

As for [γ-^{32}P]TNP-8N$_3$-ATP, sNBD2 photolabeling with [γ-^{32}P]8N$_3$-ATP was not dependent on the presence of Mg^{2+} - on the contrary, photolabeling is inhibited at high concentrations of $MgCl_2$. The affinity of sNBD2 for [γ-^{32}P]8N$_3$-ATP, as reflected in the Kd, is 57, 196 and 143 μM at 0, 10 and 30 mM $MgCl_2$ respectively. It is not only the affinity for [γ-^{32}P]8N$_3$-ATP that decreases at higher $MgCl_2$ concentration, but also maximal labeling – reflecting a decrease in labeling efficiency at higher $MgCl_2$ concentrations.

A more extensive concentration range of [γ-^{32}P]TNP-8N$_3$-ATP and greater number of data points produced a Kd value in EDTA of 0.8 μM. (Fig 4.6).

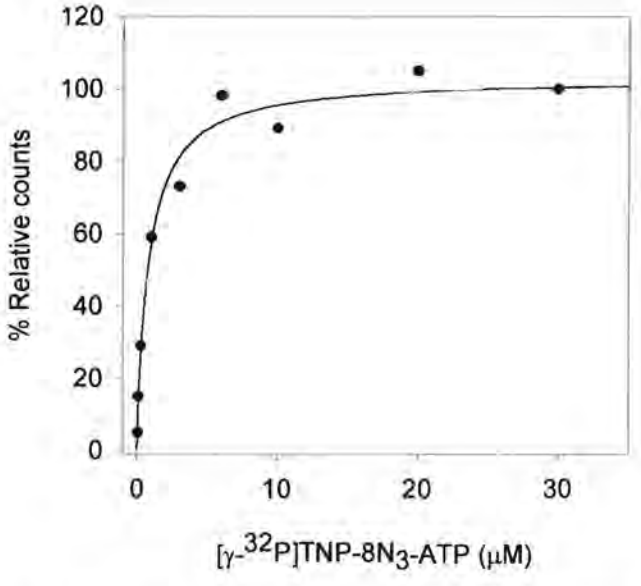

Figure 4.6. Concentration dependent photolabeling of 0.5 μM sNBD2 with [γ-^{32}P]TNP-8N$_3$-ATP in 2 mM EDTA. Irradiation was done in 25mM MES, pH 6.0, 20 % (v/v) glycerol and 0.01 % (v/v) Triton X-100.

A similar experiment using [γ-^{32}P]8N$_3$-ATP in EDTA produced a Kd of 37.2 μM (Fig 4.7).

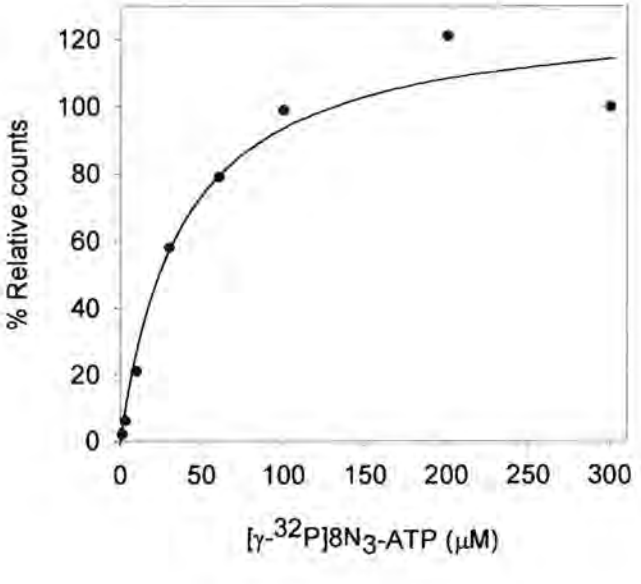

Figure 4.7. Concentration dependent photolabeling of 0.5 μM sNBD2 with [γ-^{32}P]8N$_3$-ATP in 2 mM EDTA. Irradiation was done in 25mM MES, pH 6.0, 20 % (v/v) glycerol and 0.01 % (v/v) Triton X-100.

The effect of increasing ATP concentrations on [γ-^{32}P]8N$_3$-ATP photolabeling is shown in Fig 4.8.

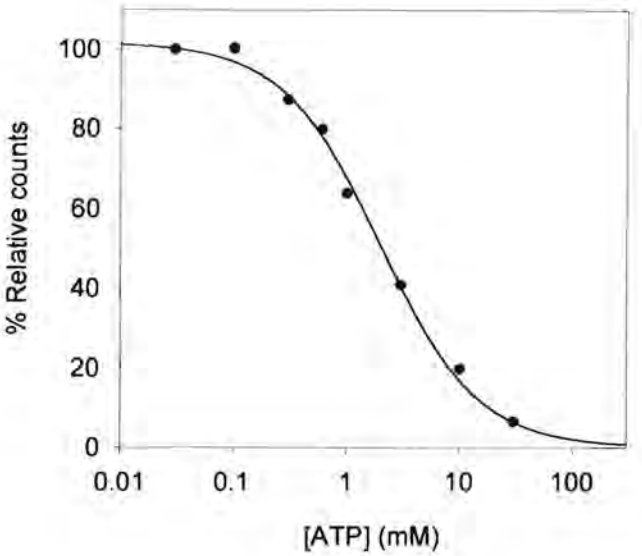

Figure 4.8. Inhibition of [γ-^{32}P]8N_3-ATP photolabeling of 0.5 μM sNBD2 with increasing concentrations of ATP. The concentration of [γ-^{32}P]8N_3-ATP was at the Kd for this probe – 36 μM. Irradiation was done in 25mM MES, pH 6.0, 20 % (v/v) glycerol, 0.01 % (v/v) Triton X-100 and 2 mM EDTA

ATP completely blocked photolabeling with half maximal inhibition at 2 mM ATP. This translates to a Ki(ATP) of 1 mM. This value is similar to the Km value for the whole protein (reviewed by Senior and Gadsby, 1997). The results strongly suggest that the photolabeling is specific and the recombinant protein is correctly folded at the ATP binding site.

The recombinantly expressed mouse C-terminal sNBD consequently binds both [γ-^{32}P]8N_3-ATP and [γ-^{32}P]TNP-8N_3-ATP with an affinity of 37.2 μM and 0.8 μM respectively. The binding of both photoaffinity ATP probes is not dependent on the presence of Mg^{2+} and labeling is, on the contrary, perturbed by high concentrations of $MgCl_2$. Maximal labeling takes place at acidic pH, 0.1 % (v/v) Triton X-100 and in the absence of $MgCl_2$. Under these conditions, [γ-^{32}P]8N_3-ATP photolabeling of sNBD2 is completely inhibited by ATP, with a Ki(ATP) = 1 mM.

CHAPTER 5: CHARACTERISATION OF LNBD2 BY PHOTOLABELING WITH [γ-^{32}P]8N_3-ATP AND [γ-^{32}P]TNP-8N_3-ATP.

While working on the shorter mouse NBD2 (sNBD2 -Thr^{1044} to Thr^{1224}), a paper published by Sankaran demonstrated that Tyr^{1041} (Tyr^{1042} in the mouse sequence) of full length p-gp, isolated from hamster CHO cells, is the primary reaction target of 8N_3-ATP (Sankaran *et al.*, 1997b). Since this amino acid is absent from the sequence of sNBD2, a longer polypeptide, LNBD2, from Lys^{1025} to Ser^{1276} was investigated. It was of interest to see if the longer recombinant NBD of the mouse p-gp interacted with the two ATP photoprobes in a similar fashion as was the shorter recombinant NBD. As for sNBD2, optimal labeling conditions for LNBD2 with [γ-^{32}P]8N_3-ATP and [γ-^{32}P]TNP-8N_3-ATP was assessed. The pH dependence of LNBD2 photolabeling with [γ-^{32}P]8N_3-ATP and [γ-^{32}P]TNP-8N_3-ATP was assayed under standard conditions – 25 mM buffer, 20 % (v/v) glycerol and 0.1 % (v/v) Triton X-100 (Fig 5.1).

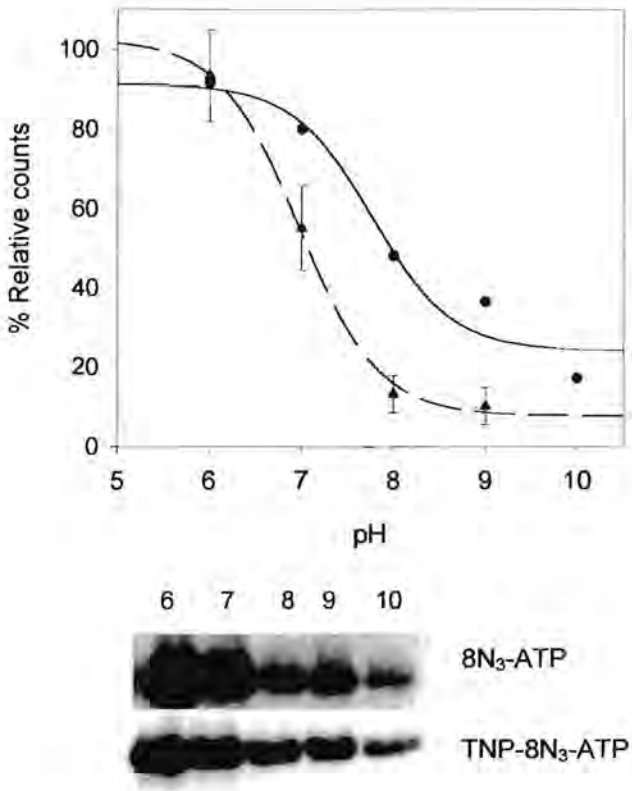

Figure 5.1. pH dependent photolabeling of LNBD2 with [γ-^{32}P]8N_3-ATP (triangles, dashed line) and [γ-^{32}P]TNP-8N_3-ATP (circles, solid line). LNBD2 concentrations were 0.5 and 0.1 μM respectively. Irradiation was done in 25 mM buffer, pH 6.0, 1 mM $MgCl_2$, 20 % (v/v) glycerol and 0.1 % (v/v) Triton X-100. The [γ-^{32}P]TNP-8N_3-ATP concentration was 11.1 μM and the [γ-^{32}P]8N_3-ATP concentration 25 μM. MES was used as buffer for pH 6.0, HEPES for pH 7.0, EPPS for pH 8.0 and CHES for pH 9.0 and 10.0. The figure below shows autorads of the SDS-PAGE of these experiments. The error bars show the standard deviation over 3 experiments.

The pH dependent photolabeling of LNBD2 in 1 mM $MgCl_2$ was also maximal at acidic pH for both probes, with pKa for [γ-^{32}P]8N_3-ATP = 6.8 and [γ-^{32}P]TNP-8N_3-ATP = 7.8 (the pKa values for [γ-^{32}P]TNP-8N_3-ATP photolabeling is the average of two experiments and for [γ-^{32}P]8N_3-ATP the average of three experiments).

Photolabeling LNBD2 with [γ-^{32}P]TNP-8N_3-ATP with Triton X-100 - 0.01 % (v/v) and 0.1 % (v/v) - and without Triton X-100, in the absence of glycerol, in increasing concentrations of

sucrose (10 % (w/v) and 20 % (w/v)), in increasing concentrations of NaCl (10, 100, 1000 mM) and in the presence of 10 % (v/v) DMSO is shown in Fig 5.2.

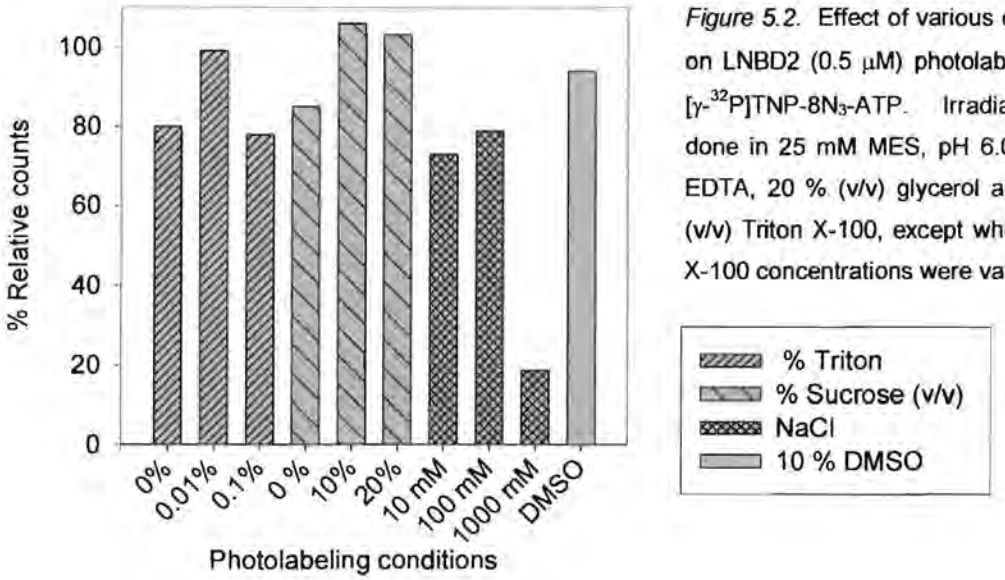

Figure 5.2. Effect of various conditions on LNBD2 (0.5 μM) photolabeling with [γ-^{32}P]TNP-8N$_3$-ATP. Irradiation was done in 25 mM MES, pH 6.0, 10 mM EDTA, 20 % (v/v) glycerol and 0.1 % (v/v) Triton X-100, except where Triton X-100 concentrations were varied. .

Photolabeling of LNBD2 appears comparable under all these conditions, except at very high salt concentrations (1000 mM NaCl), reflecting a more stable protein less influenced by the irradiation medium composition than sNBD2.

The divalent cation requirements for LNBD2 photolabeling with [γ-^{32}P]TNP-8N$_3$-ATP was determined in the absence of $MgCl_2$ (in 10 mM EDTA) and in the presence of 10 and 30 mM $MgCl_2$, pH 6.0 (Fig 5.3).

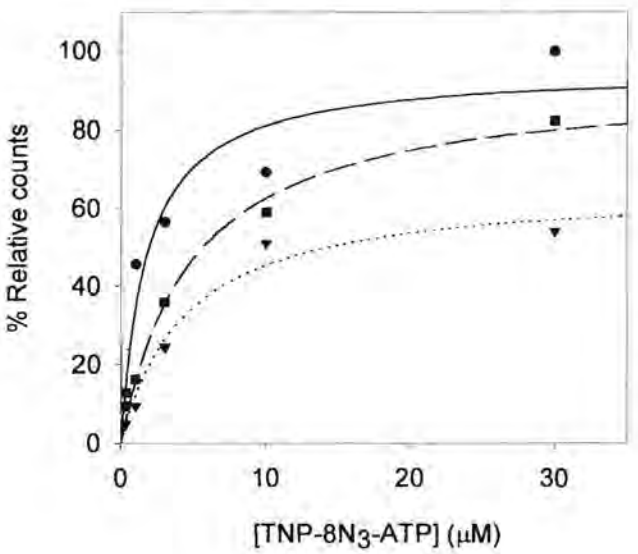

Figure 5.3. Concentration dependent photolabeling of LNBD2 (0.5 μM) with [γ-^{32}P]TNP-8N$_3$-ATP in 10 mM EDTA (circles, solid line), in the presence of 10 mM $MgCl_2$ (squares, dashed line) and 30 mM $MgCl_2$ (triangles, dotted line). Irradiation was done in 25 mM MES, pH 6.0, 20 % (v/v) glycerol and 0.1 % (v/v) Triton X-100. The figure below shows an autorad of the SDS-PAGE of this experiment

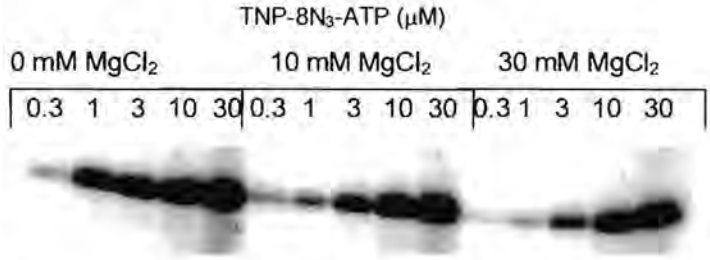

As for sNBD2, photolabeling of LNBD2 with [γ-^{32}P]TNP-8N_3-ATP is not dependent on the presence of divalent cations and is inhibited by high concentrations of $MgCl_2$. The Kd of LNBD2 for [γ-^{32}P]TNP-8N_3-ATP is 1.75 μM in EDTA, 4.88 μM in 10 mM $MgCl_2$ and 4.39 μM in 30 mM $MgCl_2$. Maximal labeling is also affected with 50% inhibition at approximately 30 mM $MgCl_2$.

Photolabeling with [γ-^{32}P]8N_3-ATP displayed similar divalent cation inhibition (Fig 5.4). The Kd for [γ-^{32}P]8N_3-ATP in EDTA is 17.4 μM, in 1 mM $MgCl_2$ 59 μM, in 10 mM $MgCl_2$ 68.7 μM and in 30 mM $MgCl_2$ 100.9 μM. The maximal photolabeling for [γ-^{32}P]8N_3-ATP is , however, much more effected at high concentrations of $MgCl_2$ than [γ-^{32}P]TNP-8N_3-ATP, with 50% inhibition at approximately 3 mM $MgCl_2$.

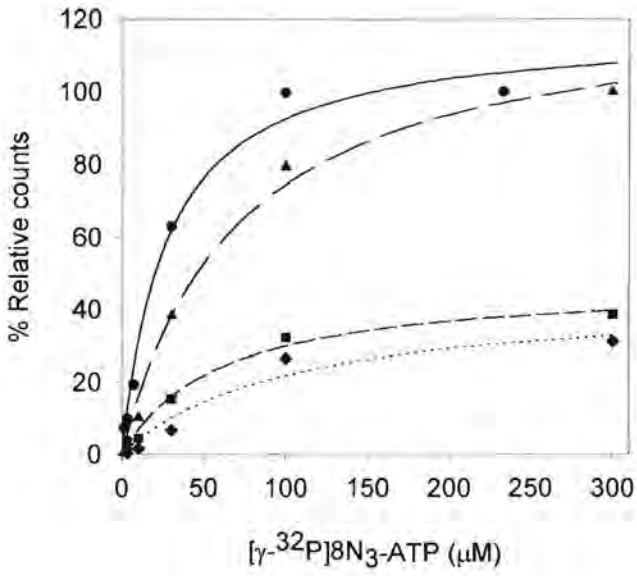

Figure 5.4. Concentration dependent photolabeling of LNBD2 (0.5 μM) with [γ-^{32}P]8N_3-ATP in 10 mM EDTA (circles, solid line), in the presence of 1 mM $MgCl_2$ (triangles, dashed line), 10 mM $MgCl_2$ (squares, short dashed line) and 30 mM $MgCl_2$ (diamonds, dotted line) Irradiation was done in 25 mM MES, pH 6.0, 20 % (v/v) glycerol and 0.1 % (v/v) Triton X-100. The lower figure is an autorad of the SDS-PAGE of this experiment

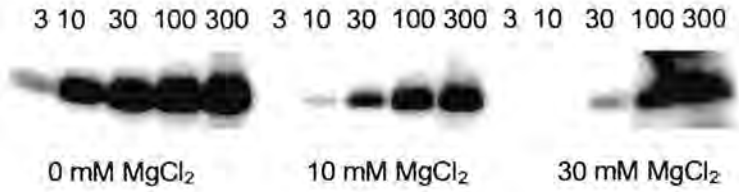

Using a more extensive concentration range of [γ-^{32}P]TNP-8N$_3$-ATP and more data points, photolabeling of LNBD2 in 25 mM MES, pH 6.0, 20 % (v/v) glycerol, 0.01 % Triton X-100 and 10 mM EDTA, yielded a Kd for [γ-^{32}P]TNP-8N$_3$-ATP of 2.6 μM (Fig 5.5).

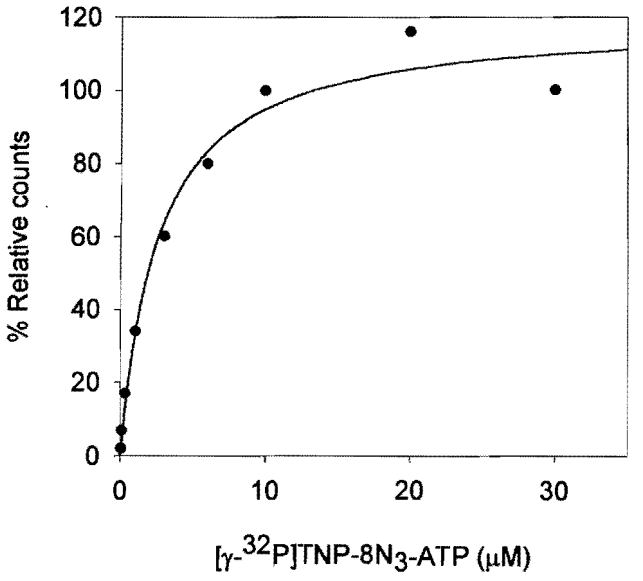

Figure 5.5. Concentration dependent photolabeling of 0.1 μM LNBD2 with [γ-^{32}P]TNP-8N$_3$-ATP in 10 mM EDTA, Irradiation was done in 25 mM MES, pH 6.0, 20 % (v/v) glycerol and 0.1 % (v/v) Triton X-100.

For similar [γ-^{32}P]8N$_3$-ATP photolabeling of LNBD2 the Kd = 35.6 μM (Fig 5.6).

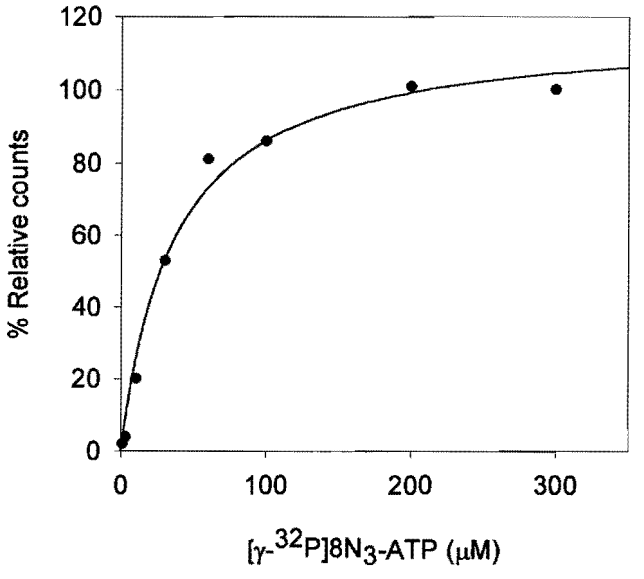

Figure 5.6. Concentration dependent photolabeling of 0.5 μM LNBD2 with [γ-^{32}P]8N$_3$-ATP in 10 mM EDTA. Irradiation was done in 25 mM MES, pH 6.0, 20 % (v/v) glycerol and 0.1 % (v/v) Triton X-100.

As the previous experiments on the pH dependence of photolabeling were conducted in the presence of 1 mM $MgCl_2$, it was of interest to see if it is changed by excluding $MgCl_2$ (Fig 5.7).

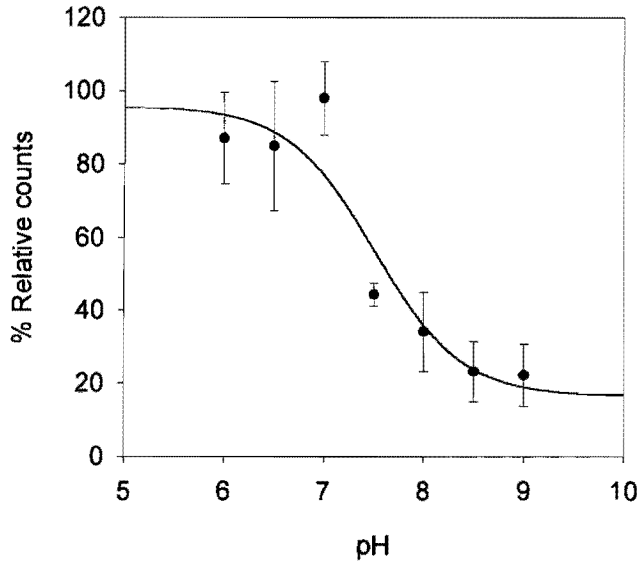

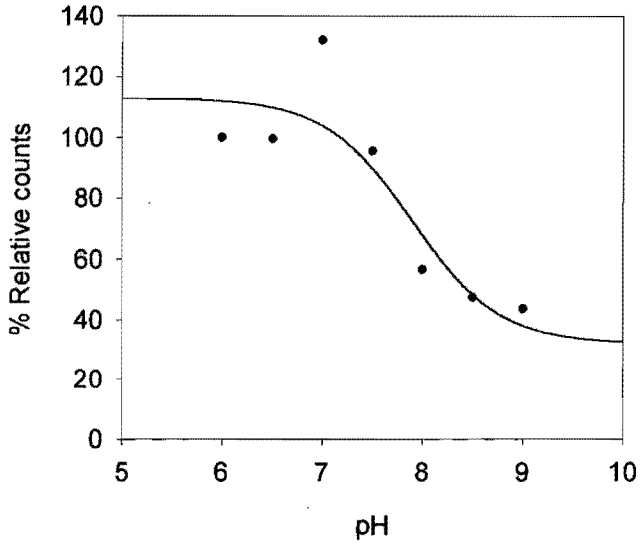

Figure 5.7. pH dependent photolabeling of LNBD2 with [γ-^{32}P]8N_3-ATP (top) and [γ-^{32}P]TNP-8N_3-ATP (bottom) in 10 mM EDTA. The LNBD2 concentration was 0.5 and 0.1 μM respectively. The [γ-^{32}P]TNP-8N_3-ATP concentration was 2.6 μM and the [γ-^{32}P]8N_3-ATP concentration 25 μM. MES was used for pH 6.0, HEPES for pH 7.0, EPPS for pH 8.0 and CHES for pH 9.0 and 10.0.

Photolabeling of LNBD2 with [γ-^{32}P]8N_3-ATP and [γ-^{32}P]TNP-8N_3-ATP in EDTA, is similar to that seen in the presence of 1mM $MgCl_2$, with a pKa = 7.5 and 7.9 respectively.

The effect of increasing concentrations of ATP on photolabeling of LNBD2 with both probes in the absence of $MgCl_2$ is shown in Fig 5.8.

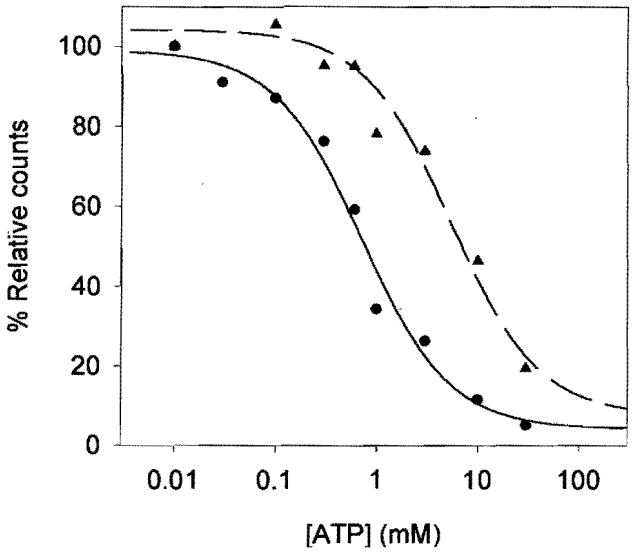

Figure 5.8. Inhibition of [γ-^{32}P]8N_3-ATP (circles, solid lines) and [γ-^{32}P]TNP-8N_3-ATP (triangles, dashed line) photolabeling of LNBD2 with increasing concentrations of ATP. The LNBD2 concentration was 0.5 and 0.1 μM respectively. The concentration of [γ-^{32}P]TNP-8N_3-ATP (2.6 μM) and [γ-^{32}P]8N_3-ATP (35.6 μM) was at the Kd of the probes. Irradiation was done in 25 mM MES, pH 6.0, 20 % (v/v) glycerol, 0.1 % (v/v) Triton X-100 and 10 mM EDTA.

Increasing concentrations inhibited photolabeling. The Ki(ATP) for [γ-^{32}P]TNP-8N_3-ATP and [γ-^{32}P]8N_3-ATP was calculated to be 2.7 mM and 0.5 mM respectively. It is not clear why there should be a difference in Ki(ATP) for the two probes, but it is possible that photolabeling of one probe is on equivalent to an equilibrium situation. As for sNBD2, inhibition of photolabeling approaches completion at 30 mM ATP, indicating that for LNBD2, photolabeling is also specific and that the ATP binding site of this recombinant protein is intact.

TNP-ATP was also effective in blocking LNBD2 photolabeling with [γ-^{32}P]TNP-8N_3-ATP and [γ-^{32}P]8N_3-ATP (Fig 5.9).

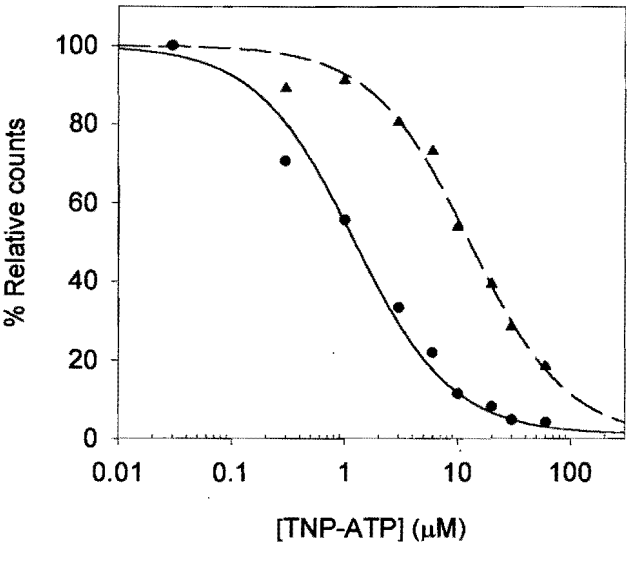

Figure 5.9. Inhibition of [γ-^{32}P]8N_3-ATP (circles, solid lines) and [γ-^{32}P]TNP-8N_3-ATP (triangles, dashed line) photolabeling of LNBD2 with increasing concentrations of TNP-ATP. The LNBD2 concentration was 0.5 and 0.1 μM respectively. The concentration of [γ-^{32}P]TNP-8N_3-ATP and [γ-^{32}P]8N_3-ATP was at the Kd of the probes. Irradiation was done in 25 mM MES, pH 6.0, 20 % (v/v) glycerol, 0.1 % (v/v) Triton X-100 and 10 mM EDTA.

The Ki(TNP-ATP) for [γ-^{32}P]TNP-8N_3-ATP and [γ-^{32}P]8N_3-ATP was calculated to be 7.0 μM and 0.6 μM respectively.

The high affinity of LNBD2 for [γ-^{32}P]8N_3-ATP was unexpected as the affinity for ATP itself is in the mM range. ATP and 8N_3-ATP differ in the adenine orientation about the glycoside bond – ATP being in the *anti* and 8N_3-ATP in the *syn* conformation (Czarnecki, 1984, Suhadolnik *et al.*, 1988). The different orientation of the adenine ring could explain the difference in Kd for these two ligands. In order to test this hypothesis, the *syn* nucleotide, 8Br-ATP was tested as an inhibitor and the results are shown in Fig 5.10 (Tavale and Sobell, 1970).

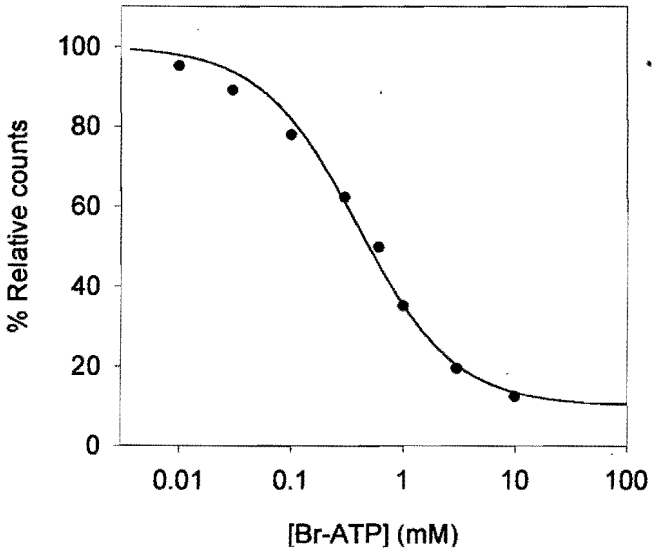

Figure 5.10. Inhibition of [γ-^{32}P]8N_3-ATP photolabeling of 0.5 μM LNBD2 with increasing concentrations of 8Br-ATP. The concentration of [γ-^{32}P]8N_3-ATP was 36 μM. Irradiation was done in 25 mM MES, pH 6.0, 20 % (v/v) glycerol, 0.1 % (v/v) Triton X-100 and 10 mM EDTA.

The Ki(Br-ATP) = 0.194 mM - 2.5 times tighter than the Ki(ATP) of 0.5 mM. Although Br-ATP binding is tighter than ATP, it is not in the concentration range of 35.6 μM, obtained for 8N_3-ATP,suggesting that there may be a special interaction of the azido group with a side chain of the protein, in addition to it being in the *syn* conformation.

In summary, the long recombinant mouse C-terminal nucleotide binding domain, LNBD2, interacts with the ATP photoactive probes, [γ-^{32}P]8N_3-ATP and [γ-^{32}P]TNP-8N_3-ATP, in a very similar fashion to the shorter NBD2. Photolabeling is pH dependent in the presence of Mg^{2+} with maximal labeling at pH 6.0. Photolabeling is inhibited by $MgCl_2$ with the TNP probe being less sensitive to the effects of the divalent cation. In the absence of $MgCl_2$, [γ-^{32}P]8N_3-ATP photolabeling is similar to that found in the presence of $MgCl_2$, while [γ-^{32}P]TNP-8N_3-ATP photolabeling is not much influenced by pH. Photolabeling is inhibited by increasing concentrations of ATP, TNP-ATP and Br-ATP. This provides evidence that the ATP binding pockets of LNBD2 and sNBD2 are intact and that the labeling is at the ATP site.

CHAPTER 6: STABILITY OF THE γ-PHOSPHATE OF COVALENTLY ATTACHED NUCLEOTIDE

One possible explanation for the pH dependence of photolabeling in $MgCl_2$ is hydrolysis of the γ-phosphate at alkaline pH. This possibility was tested by labeling sNBD2 with [γ-^{32}P]TNP-8N_3-ATP and the monitoring the stability of the ^{32}P with time at 25 °C.

Samples of sNBD2 were photolabeled under standard conditions – 25 mM MES, pH 6.0, 20 % (v/v) glycerol and 0.01 % (v/v) Triton X-100 - incubated at both pH 6.0 and pH 8.5 in the presence and absence of $MgCl_2$ and analysed on a 15 % (w/v) polyacrylamide gel (Fig 6.1).

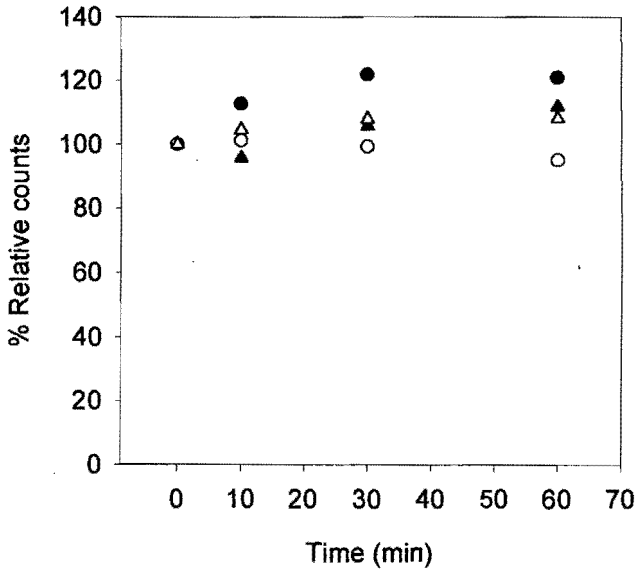

Figure 6.1. Stability control of the γ-phosphate. sNBD2 (0.1 μM) was photolabeled at pH 6.0 with [γ-^{32}P]TNP-8N_3-ATP and incubated at pH 6.0 (circles) and pH 8.5 (triangles) in the presence (filled symbols) and absence (open symbols) of 1 mM $MgCl_2$, 25 °C. Irradiation was done in standard medium - 25 mM buffer, 20 % (v/v) glycerol and 0.01 % (v/v) Triton X-100 - with a final EDTA concentration of 10 mM for the samples containing no $MgCl_2$. MES was used for pH 6.0 and EPPS for pH 8.0.

No change in the amount of γ-^{32}P is observed over a period of one hour of incubation at both pH 6.0 and pH 8.5. A similar experiment carried out for LNBD2 also showed no hydrolysis (data not shown).

Quantification of [γ-^{32}P]TNP-8N_3-ATP photolabeling of sNBD2 and Pdr5p

To determine the [γ-^{32}P]TNP-8N_3-ATP labeling efficiency of sNBD2 and Pdr5p, increasing concentration of protein (sNBD2: 0.25, 0.5, 1 and 2 μM and Pdr5p: 0.2, 0.4, 0.8 and 1.37 μM) photolabeled in the presence of saturating concentrations of [γ-^{32}P]TNP-8N_3-ATP, were precipitated with 10 % (w/v) trichloroacetic acid, washed and the radioactivity assayed (Fig 6.2). Controls were unirradiated samples treated in the same manner.

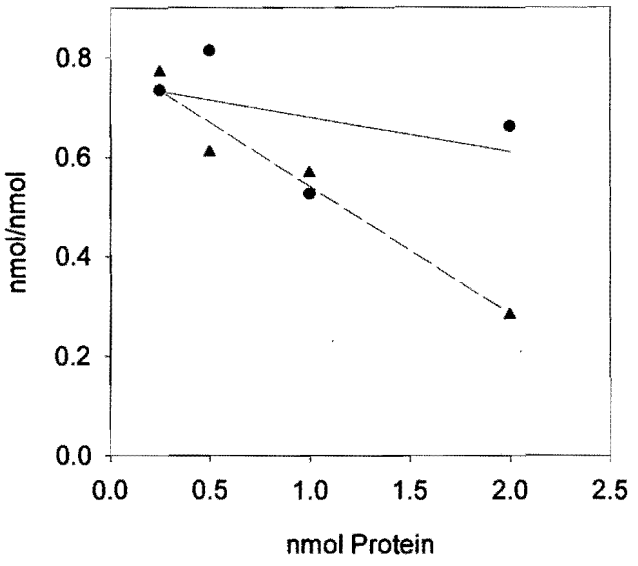

Figure 6.2. Labeling efficiency of sNBD2 (circles, solid line) and purified Pdr5p (triangles, dashed line) at different amounts of protein - NBD2: 0.25, 0.5, 1 and 2 μM and Pdr5p: 0.2, 0.4, 0.8 and 1.37 μM) with [γ-^{32}P]TNP-8N$_3$-ATP. The [γ-^{32}P]TNP-8N$_3$-ATP concentration was 50 μM for Pdr5p and 30 μM for sNBD2. Labeling was done in 25 mM MES, pH 6.0, 20 % (v/v) glycerol and 0.01 % (v/v) Triton X-100 with the Triton X-100 omitted from Pdr5p experiments.

High labeling efficiencies of close to 0.8 nmol/nmol were obtained for both proteins at dilute concentrations of protein. Pdr5p appeared to be less efficiently photolabeled at higher concentrations compared to sNBD2.

Reaction of N-ethylmaleimide with sNBD2 and LNBD2

Several sulfhydryl modification agents have been shown to react with cysteine residues of the p-gps. In particular Cys^{1074} in the human and hamster sequence (Cys^{1072} in the mouse sequence) in the second nucleotide binding domain, located in the Walker A motif of the ATP binding site, seems highly reactive. Both *N*-ethylmaleimide (NEM) and 7-chloro-4-nitrobenzo-2-oxa-1,3-diazole (NBD-Cl) reacted with Cys^{1074} (Loo and Clarke, 1995b, Senior *et al.*, 1998). NEM and 2-(4-maleimidoanilino)naphthalene-6-sulfonic acid (MIANS) also compete for the same site on p-gp (Liu *et al.*, 1996). It was demonstrated for both NBD-Cl and MIANS that although ATP protects against reaction with these sulfhydryl modification agents, reaction prior to the addition of ATP does not inhibit the binding of ATP itself – indicating that the inhibition of ATPase activity by the reagents is not a result of competitive inhibition with ATP at the nucleotide binding site.

The effect of NEM derivatization on [γ-^{32}P]TNP-8N$_3$-ATP photolabeling of sNBD2 is shown in Fig 6.3. The experiments were done in such way that the protein was preincubated for various times with NEM at pH 8.5. Then, at timed intervals, the pH was either kept at pH 8.5 or lowered to pH 6.0 and the samples photolabeled.

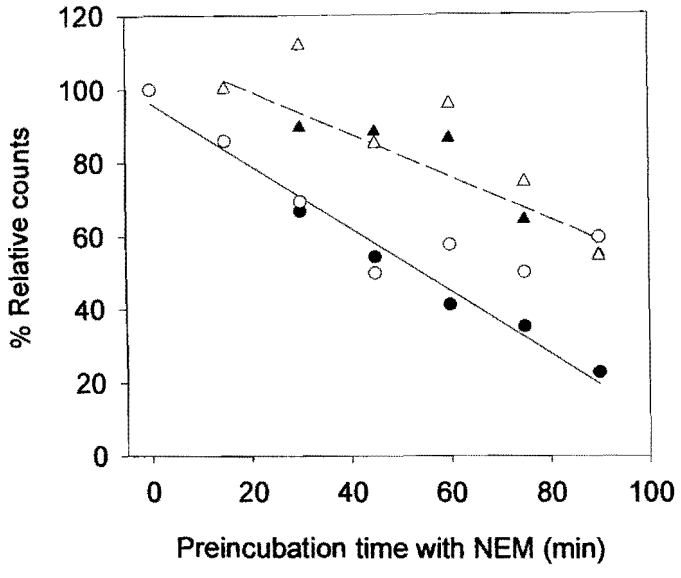

Figure 6.3. The effect of NEM derivatization on [γ-^{32}P]TNP-8N$_3$-ATP photolabeling. sNBD2 (0.1 μM) was preincubated with (filled symbols) or without (open symbols) 20 mM NEM, 25 mM EPPS, pH 8.5 at 23 °C. At timed intervals aliquots were removed and the protein photolabeled with [γ-^{32}P]TNP-8N$_3$-ATP (3 μM) in 25 mM MES, pH 6.0, 20 % (v/v) glycerol and 0.01 % (v/v) Triton X-100 (circles) or 25 mM EPPS, pH 8.5, 20 % (v/v) glycerol and 0.01 % (v/v) Triton X-100 (triangles) in the presence of 1 mM $MgCl_2$.

Both control and NEM derivatised sNBD2 show a similar extent of photolabeling over time. This indicates that NEM derivatization does not inhibit nucleotide binding. The fall off in photolabeling over the hour also indicates that the protein is unstable and shows that denatured sNBD does not photolabel.

Similar results were obtained with LNBD2 using [γ-^{32}P]TNP-8N$_3$-ATP or [γ-^{32}P]8N$_3$-ATP as photoprobes (data not shown). The results are compatible with the previously mentioned work that indicated NEM derivatization does not inhibit nucleotide binding.

CHAPTER 7: FLAVONOID BINDING TO THE ATP BINDING SITE OF SNBD2 AND LNBD2.

Flavonoids are a family of inducible metabolites often synthesised in plants as a reaction to fungal attack or challenge with biotic or abiotic elicitors (Reviewed by Barron and Ibrahm, 1996). Interaction of several flavonoids with the recombinantly expressed mouse NBDs has been detected using tryptophan fluorescence (Bois *et al.*, 1998, Conseil *et al.* 1998, Perez-Victoria *et al.*, 1999). In order to screen potential reversers binding to the ATP binding site of p-gp and identify positions on the flavonoid nucleus where elaboration may be possible, the effects of a variety of flavonoids on photolabeling of sNBD2 and LNBD2 with [γ-^{32}P]TNP-8N_3-ATP and [γ-^{32}P]8N_3-ATP, were tested.

Flavonoids are divided into several classes and the ones investigated in this study are shown in Fig 7.1.

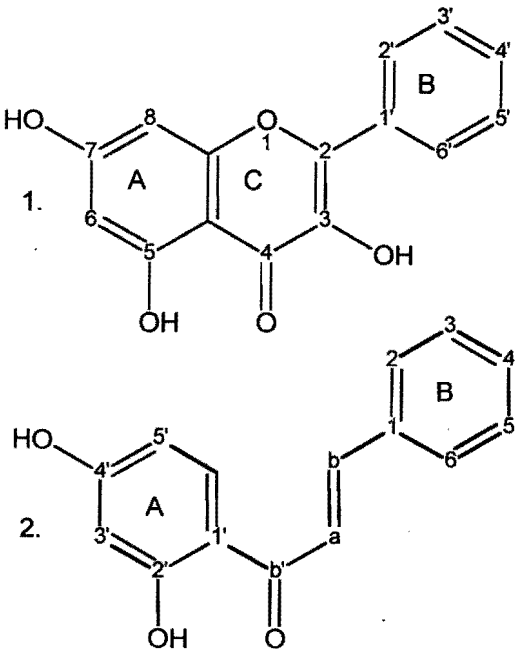

Figure 7.1. Structures of the different classes of flavonoids: flavonols (1), chalcones (2) and chrysins (3)

Initially, four compounds were investigated for inhibition of [γ-^{32}P]TNP-8N_3-ATP photolabeling of sNBD2 and LNBD2, namely 8(1,1-DMA)3-Me-kaemferide, 8(1,1-DMA)kaemferide, kaemferide and broussochalcone A (Fig 7.2).

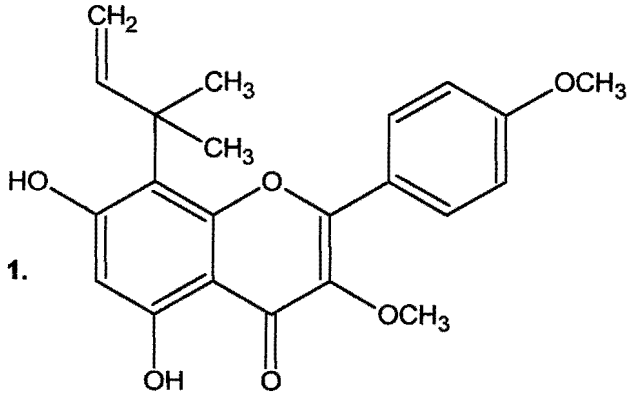

Figure 7.2. Structures of the flavones 8(1,1-DMA) 3-Me-kaemferide (1), 8(1,1-DMA) kaemferide (2), kaemferide (3) and the chalcone broussochalcone A (4).

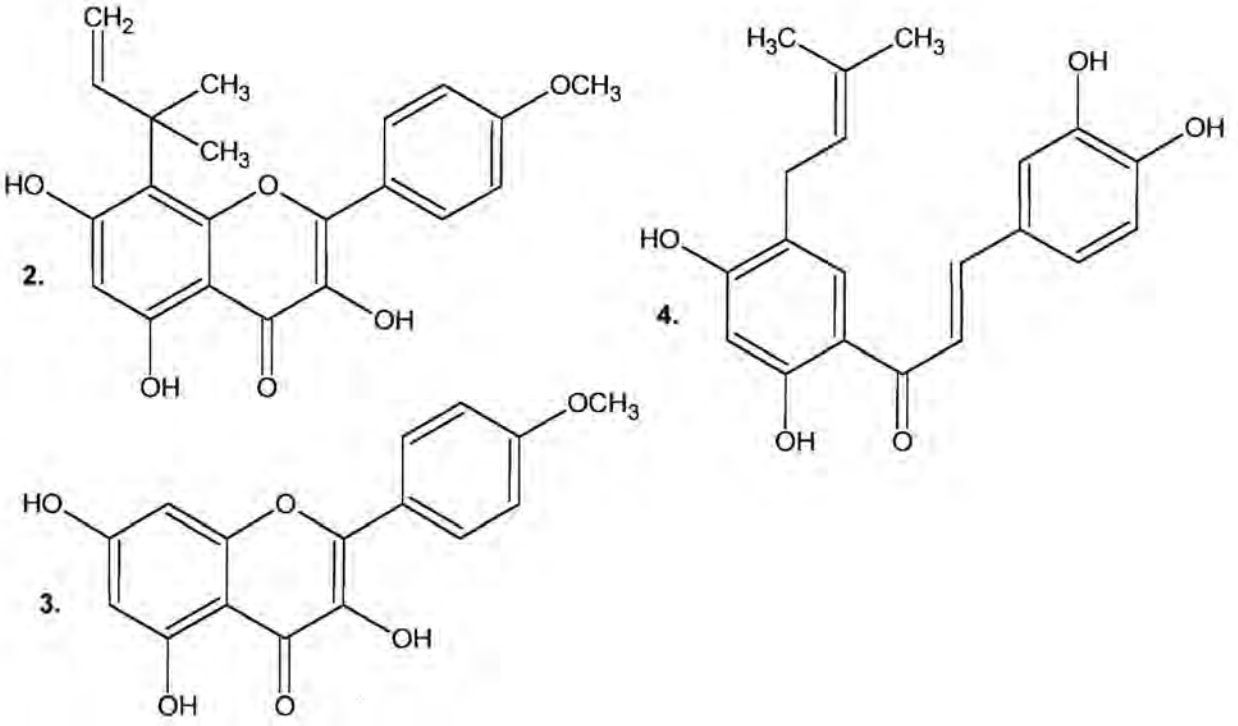

Testing the effects of 1 and 10 μM of these 4 compounds on photolabeling of sNBD2 in standard medium - 25 mM MES, pH 6.0, 20 % (v/v) glycerol and 0.01 % (v/v) Triton X-100, in 1mM $MgCl_2$ - with [γ-^{32}P]TNP-8N_3-ATP, kaemferide and broussochalcone A showed some promise as inhibitors (Fig 7.3). These two compounds were consequently studied in more detail.

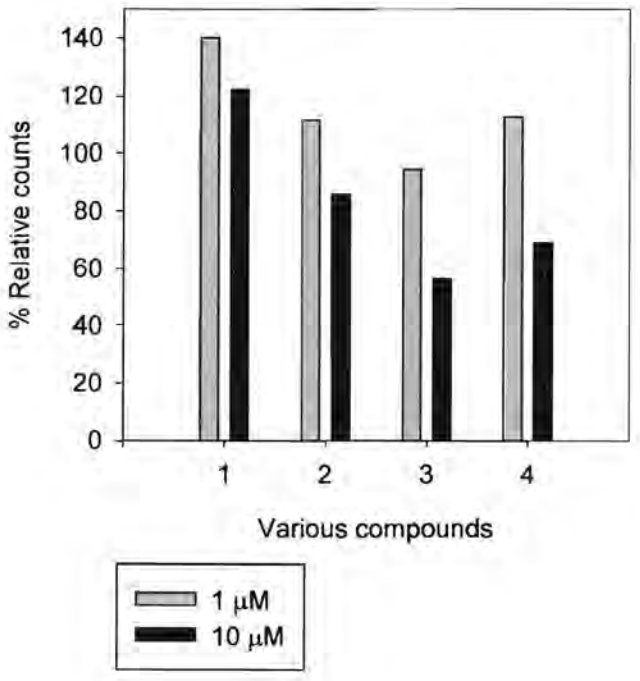

Figure 7.3. Effect of 1 and 10 μM of the flavones 8(1,1-DMA) 3-Me-kaemferide (1) 8(1,1-DMA) kaemferide (2), kaemferide (3) and the chalcone broussochalcone A (4) on [γ-^{32}P]TNP-8N_3-ATP photolabeling of sNBD2. Photolabeling was done in standard medium -25 mM MES, pH 6.0, 20 % (v/v) glycerol and 0.01 % (v/v) Triton X-100 and 1 mM $MgCl_2$. The concentration of NBD2 and [γ-^{32}P]TNP-8N_3-ATP was 0.1 μM and 3 μM respectively.

Firstly, the effects of increasing concentrations of kaemferide and broussochalcone A on sNBD2 photolabeling with [γ-^{32}P]TNP-8N$_3$-ATP were monitored at pH 6.0 (Fig 7.4).

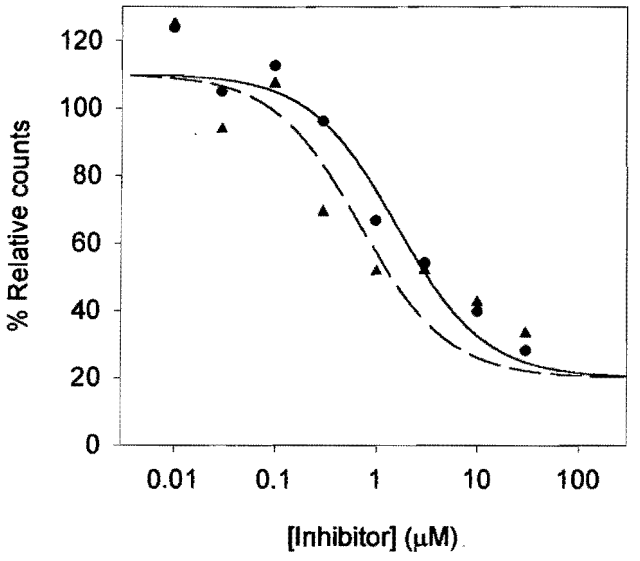

Figure 7.4. Effect of increasing concentrations of kaemferide (circles, solid line) and broussochalcone A (triangles, dashed line) on sNBD2 photolabeling with [γ-^{32}P]TNP-8N$_3$-ATP. Photolabeling was done in standard medium. The concentration of sNBD2 and [γ-^{32}P]TNP-8N$_3$-ATP was 0.1 μM and 3 μM respectively.

Under these conditions, photolabeling of sNBD2 by [γ-^{32}P]TNP-8N$_3$-ATP is inhibited by increasing concentrations of both of these flavonoids with a Ki(kaemferide) = 1 μM and Ki(broussochalcone A) = 0.4 μM.

This experiment was repeated at alkaline pH to determine if pH plays a role in flavonoid binding to sNBD (Fig 7.5).

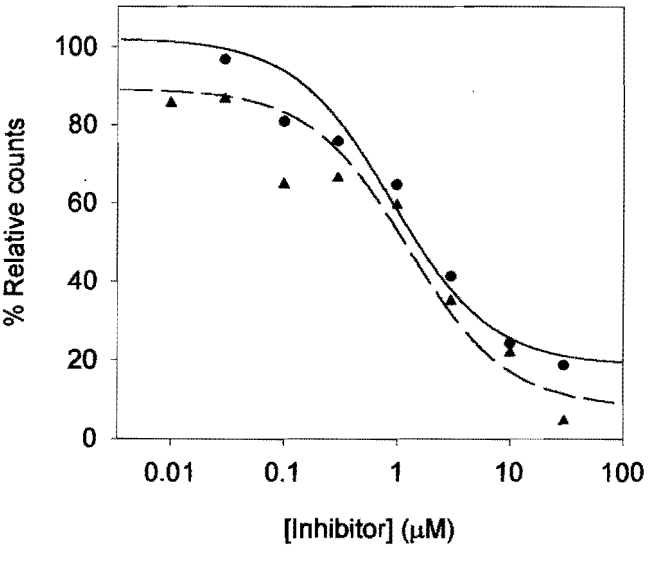

Figure 7.5. Effect of increasing concentrations of kaemferide (circles, solid line) and broussochalcone A (triangles, dashed line) on sNBD2 photolabeling with [γ-^{32}P]TNP-8N$_3$-ATP. Photolabeling was done in standard medium, using EPPS buffer, pH 8.5. The concentration of sNBD2 and [γ-^{32}P]TNP-8N$_3$-ATP was 0.1 μM and 3 μM respectively.

Photolabeling of sNBD2 by [γ-^{32}P]TNP-8N_3-ATP at alkaline pH is also inhibited by increasing concentrations of both of these flavonoids with similar Ki values to those calculated at pH 6.0- Ki(kaemferide) = 0.5 μM and Ki(broussochalcone A) = 0.71 μM, assuming pH does not affect the affinity of the protein for TNP-8N_3-ATP.

Turning to the LNBD2, the effect of increasing concentrations of these two compounds in the absence of $MgCl_2$ was investigated using [γ-^{32}P]TNP-8N_3-ATP (Fig 7.6).

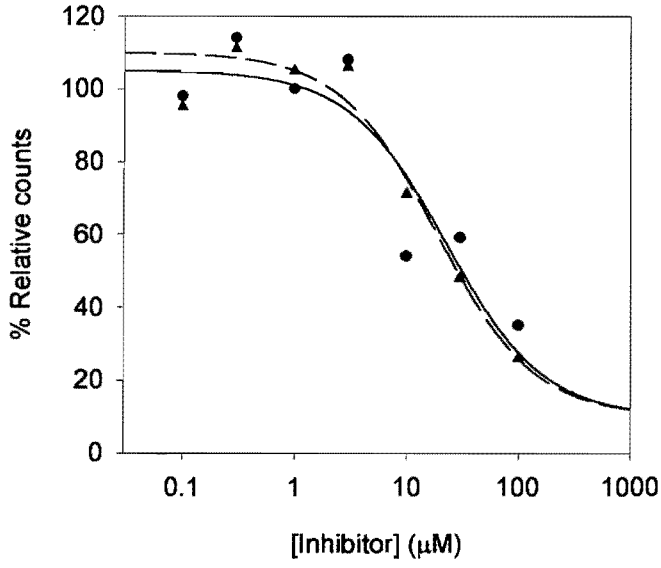

Figure 7.6. Effect of increasing concentrations of kaemferide (circles, solid line) and broussochalcone A (triangles, dashed line) on LNBD2 photolabeling with [γ-^{32}P]TNP-8N_3-ATP. Photolabeling was done in standard medium - 25 mM MES, pH 6.0, 20 % (v/v) glycerol and 0.01 % (v/v) Triton X-100 - in 10 mM EDTA. The concentration of LNBD2 and [γ-^{32}P]TNP-8N_3-ATP was 0.1 μM and 8 μM respectively.

Inhibition of [γ-^{32}P]TNP-8N_3-ATP photolabeling of LNBD2 is seen in the absence of $MgCl_2$ with Ki(kaemferide) = 5.6 μM and Ki(broussochalcone A) = 4.7 μM.

Inhibition of [γ-^{32}P]8N_3-ATP photolabeling of LNBD2 with kaemferide and broussochalcone A was also investigated in the absence of $MgCl_2$ (Fig 7.7).

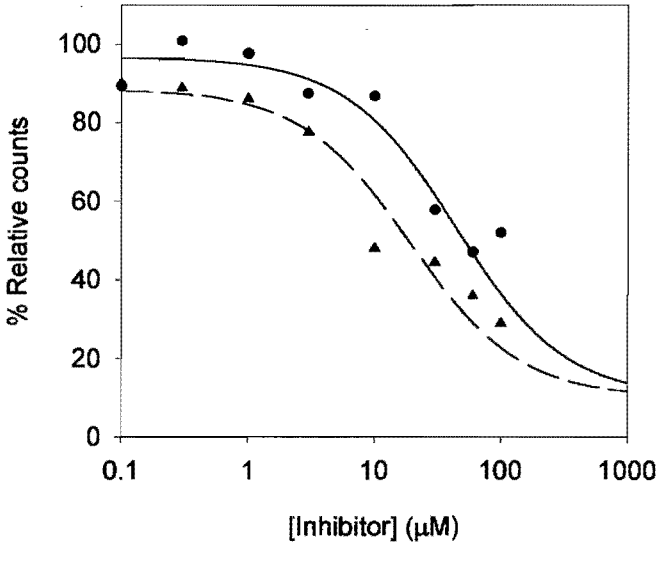

Figure 7.7. Effect of increasing concentrations of kaemferide (circles, solid line) and broussochalcone A (triangles, dashed line) on LNBD2 photolabeling with [γ-^{32}P]8N_3-ATP. Photolabeling was done in standard medium in 10 mM EDTA. The concentration of LNBD2 and [γ-^{32}P] 8N_3-ATP was 0.5 μM and 20 μM respectively.

Both broussochalcone A and kaemferide prevent labeling of LNBD2 with [γ-^{32}P]8N_3-ATP at increasing concentrations with a Ki(broussochalcone A) = 9 μM and Ki(kaemferide) = 20.5 μM. In summary, both kaemferide and broussochalcone A inhibit both TNP-8N_3-ATP and 8N_3-ATP photolabeling, the binding to the shorter domain being approximately 10-fold tighter than to the longer NBD (0.5 – 1 μM compared to 5 – 20 μM), assuming 1 mM Mg^{2+} does not have a large effect on the affinity (see Fig. 4.4 and 5.3).

Another series of flavonoids (kaemferides and galángines) were screened for interaction at the ATP binding site of mouse p-gp at 5 and 50 μM concentrations, using LNBD2 photolabeling with [γ-^{32}P]TNP-8N_3-ATP in 25 mM MES, pH 6.0, 20 % (v/v) glycerol and 0.01 % (v/v) Triton X-100 and 10mM EDTA as standard conditions. No prominent inhibitory effect of 8(1,1,-DMA)3-Me-kaemferide and 8(1.1-DMA)kaemferide (see Fig 7.3) on LNBD2 photolabeling at higher concentrations (5 and 50 μM) could be seen (data not shown). Elaborations on the 8 position of ring A of the kaemferides are evidently not tolerated in the ATP binding site.

Of three galangine derivatives (Fig 7.8), galangine, 6-prenyl-galangine and 8-prenyl-galangine, tested at 5 and 50 μM for their effect on LNBD2 photolabeling, only galangine itself showed significant inhibition (data not shown). For galangines, elaborations on the 6 or 8 position of ring A appear not to be tolerated in the ATP binding site.

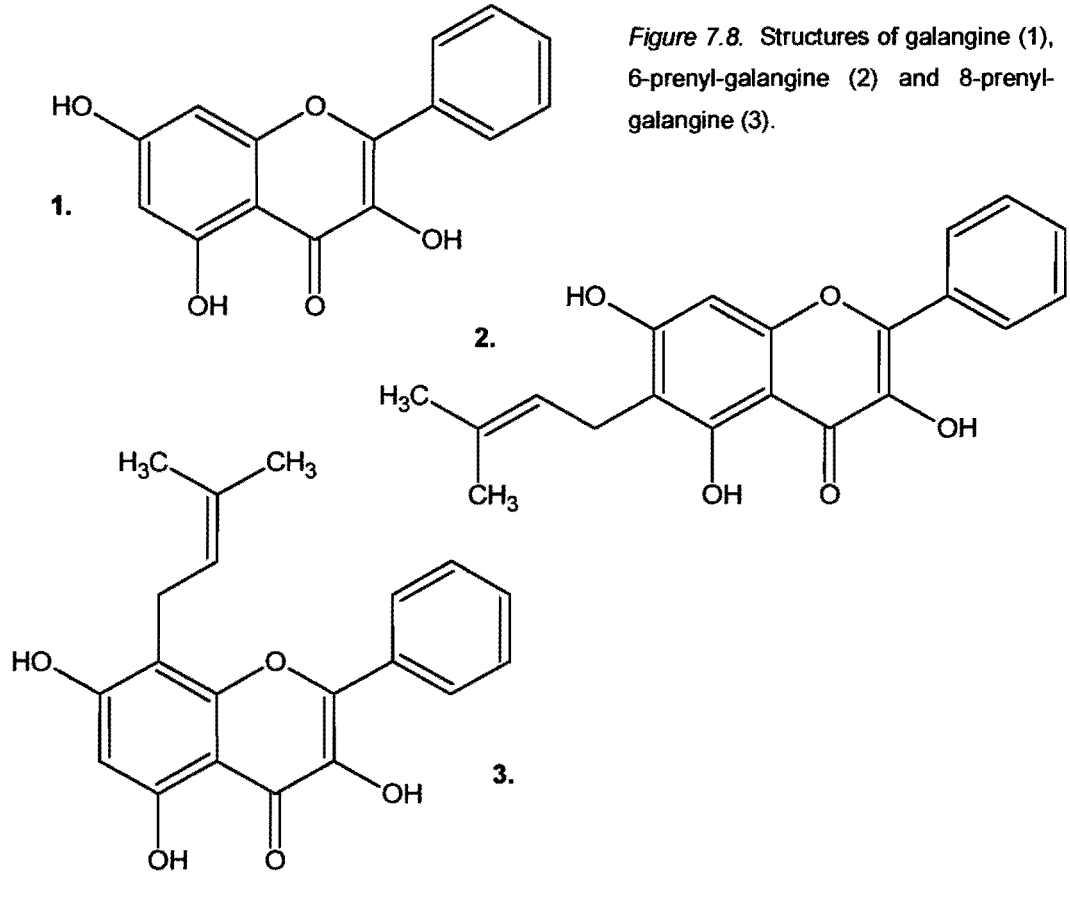

Figure 7.8. Structures of galangine (1), 6-prenyl-galangine (2) and 8-prenyl-galangine (3).

Using a more extensive concentration range of galangine and both [γ-^{32}P]TNP-8N$_3$-ATP and [γ-^{32}P]8N$_3$-ATP as photoprobes, the Ki(galangine) was calculated as 20 μM and 14 μM respectively (Fig 7.9).

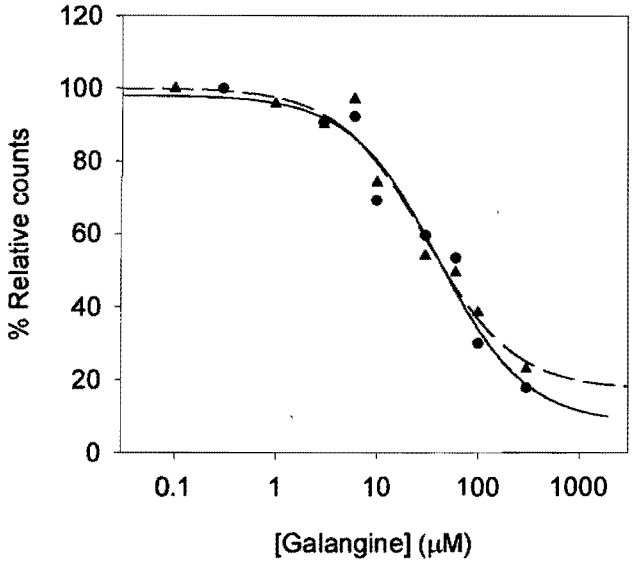

Figure 7.9. The effect of increasing concentrations of galangine on LNBD2 photolabeling with [γ-^{32}P]TNP-8N$_3$-ATP (circles, solid line) and [γ-^{32}P]8N$_3$-ATP (triangles, dashed line. Irradiation was done in standard medium in 10 mM EDTA. The concentration of LNBD2 and [γ-^{32}P]TNP-8N$_3$-ATP was 0.1 μM and 2.6 μM respectively, while LNBD2 concentrations was 0.5 μM for photolabeling with 20 μM [γ-^{32}P]8N$_3$-ATP.

Another group of flavonols, called silybins, were also screened at 5 and 50 μM concentrations for their effect on LNBD2 photolabeling with [γ-^{32}P]TNP-8N$_3$-ATP. These compounds were silybin, dehydrosilybin, 6-prenyl-dehydrosilybin and 8-prenyl-dehydrosilybin (Fig 7.10).

Figure 7.10. The structures of silybin (1), dehydrosilybin (2), 6-prenyl-dehydrosilybin (3) and 8-prenyl-dehydrosilybin (4).

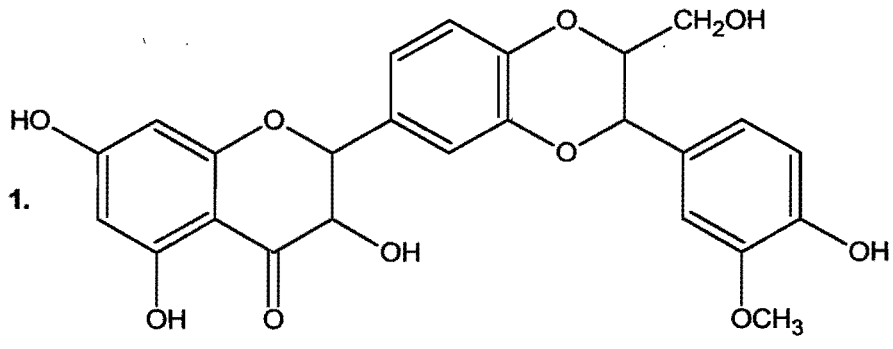

1.

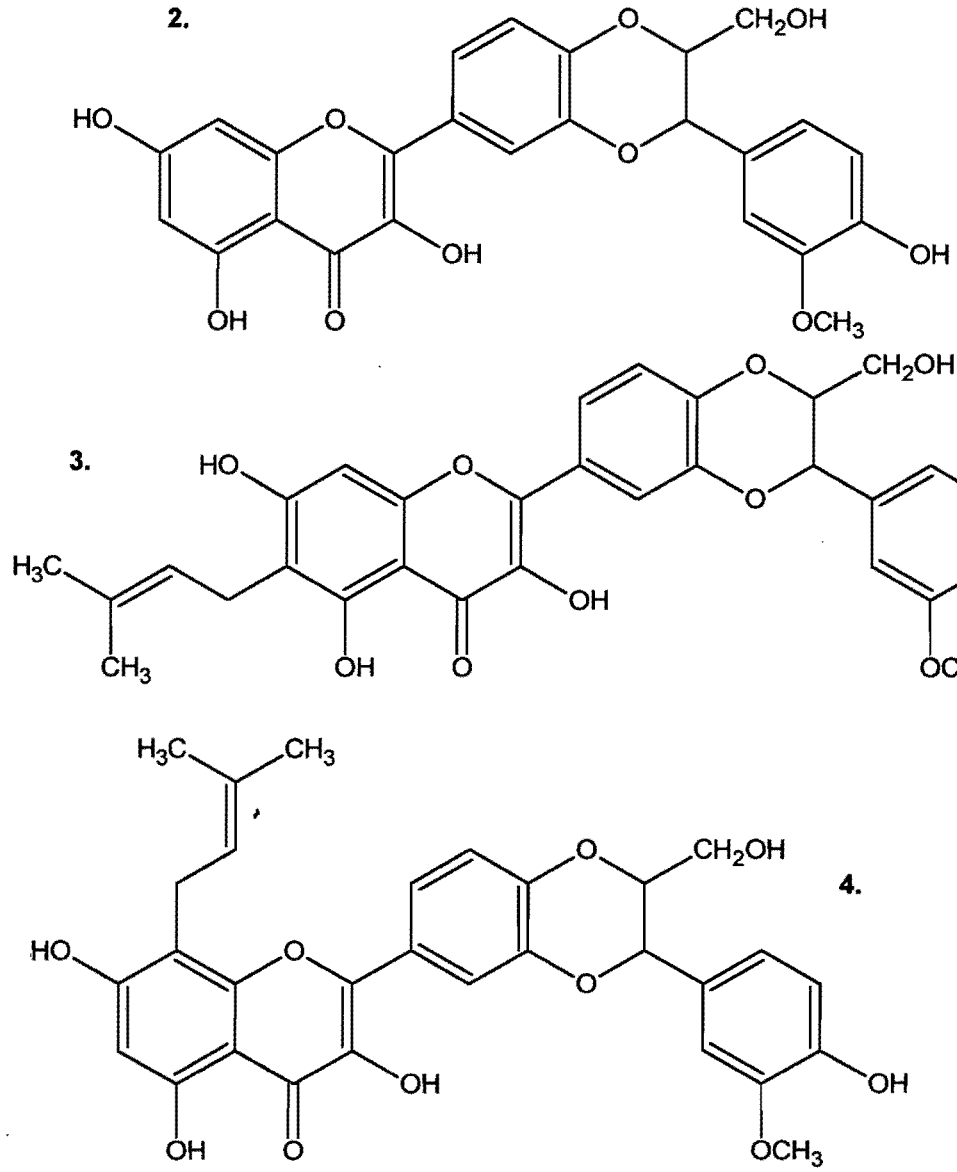

Dehydrosilybin inhibited photolabeling at high concentrations and a more extensive concentration range using both [γ-^{32}P]TNP-8N_3-ATP and [γ-^{32}P]8N_3-ATP yielded a Ki(dehydrosilybin) = 28 μM and 45 μM respectively, showing that elaboration on the B ring is tolerated in the ATP binding site (Fig 7.11). As for galangine, 6 and 8-prenyl-dehydrosilybin showed no inhibition of photolabeling at a concentration of 50 μM, convincingly demonstrating that elaboration on these positions are not tolerated in the ATP binding site.

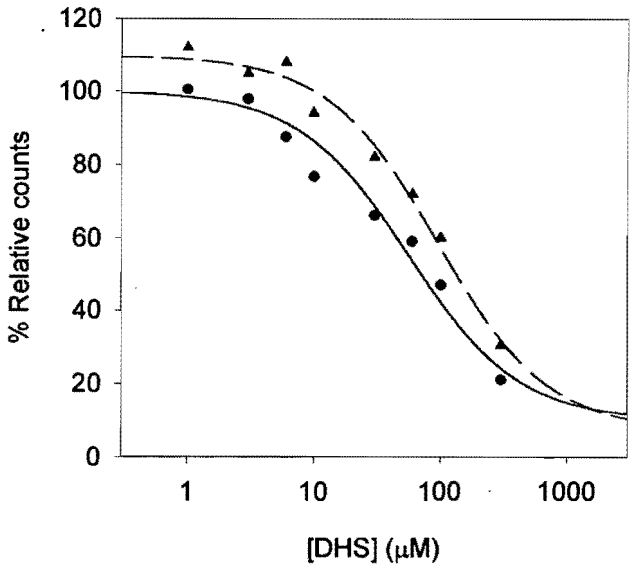

Figure 7.11. Effect of increasing concentrations of dehydrosilybin on photolabeling of LNBD2 with [γ-^{32}P]TNP-8N$_3$-ATP (circles, solid line) and [γ-^{32}P]8N$_3$-ATP (triangles, dashed line). Irradiation was done in standard medium in 10 mM EDTA. The concentration of LNBD2 and [γ-^{32}P]TNP-8N$_3$-ATP was 0.1 μM and 2.6 μM respectively, while LNBD2 concentrations was 0.5 μM for photolabeling with 20 μM [γ-^{32}P]8N$_3$-ATP.

Surprisingly, silybin itself did not prevent photolabeling, pointing to the importance of the double bond between position 2 and 3 on ring C for recognition by the ATP binding site.

An extensive group of chalcones (see Fig 7.1) was screened for inhibition of [γ-^{32}P]TNP-8N$_3$-ATP photolabeling in the 1 to 10 μM range: 4-F-chalcone, 4-I-chalcone, 4-C$_2$-chalcone, 4-C$_4$-chalcone, 4-C$_6$-chalcone, 4-C$_8$-chalcone, 2',4',4-triOH-3-prenyl-chalcone and 2',4',4-triOH-chalcone. Except for broussochalcone A (see Fig 7.2), investigated initially, no other chalcone was inhibitory. What is unique about broussochalcone is the presence of a 3-hydroxy group on ring B, absent from all the other chalcone derivatives, and presumably essential for recognition by the ATP binding site.

A group of 12 chrysins was also investigated – chrysin (see Fig 7.1), 6(3,3-DMA)chrysin, 7(3,3-DMA)chrysin, 8(1,1-DMA)chrysin, 8(3,3-DMA)chrysin, 6,8(di-DMA)chrysin, 6-geranyl-chrysin, 8-geranyl-chrysin, 6,8-di-geranyl-chrysin, 4'-F-chrysin and 4'-I-chrysin. None of these compounds prevented photolabeling of LNBD2 with [γ-^{32}P]TNP-8N$_3$-ATP. Comparing the structure of galangine (see Fig 7.7), that does inhibit photolabeling, and chrysin that does not, it seems to be the absence of the 3-hydroxy group from chrysin that prevents binding to the ATP binding site.

Of all 31 compounds tested for binding to the ATP binding site of mouse p-gp, 4 compounds successfully inhibited the binding of [γ-^{32}P]TNP-8N$_3$-ATP to LNBD2 in the μM concentration range. These were galangine, dehydrosilybin, kaemferide and broussochalcone A.

CHAPTER 8: ISOLATION AND PURIFICATION OF TNP-8N_3-ATP PHOTOLABELED PEPTIDES OF SNBD2 AND LNBD2

In order to identify the amino acid/s derivatised upon photolabeling with TNP-8N_3-ATP, the photolabeled protein must first be digested into sequence size peptides and the photolabeled peptides purified for sequencing. The TNP-8N_3-ATP photolabeled peptides are identified, in this case, by absorption at 408 nm – characteristic of the TNP moiety. The first step towards a pure photolabeled peptide, is to remove the excess of free and noncovalently bound TNP-8N_3-ATP and photolysis products from the irradiated sample. This step also includes the preparation of the photolabeled sample for digestion, which involves the removal of glycerol (a protease inhibitor) and a change of buffer, optimal for the enzyme of choice.

Previously, standard procedures for preparation of photolabeled protein for digestion in our laboratory involved removal of the noncovalently bound and free nucleotides by passage through an anion exchange column (resin: AG 1-X4) to which TNP-nucleotides bind irreversibly. Prior to digestion, the sample now containing only covalently attached TNP-nucleotide, was passed through a Sephadex G-25M PD-10 column in order to remove the glycerol. We found that for sNBD2, the protein was retained by both the AG1-X4 column and PD10 column and could not be eluted. These procedures were replaced by dialysis of labeled protein to remove the glycerol and precipitate the protein. The precipitated protein was repeatedly washed and collected by centrifugation. The protein was then re-dissolved in 8 M urea, diluted to 4 M and digested with the relevant enzyme. Alternatively, photolabeled LNBD2 samples (expressed with a His-tag) were denatured in 8 M urea following irradiation and applied to a nickel chelate column. Free TNP-8N_3-ATP and glycerol were washed away with 8 M urea and the sample eluted with 8 M urea and imidazole, followed by dilution and digestion. The digest was analysed by reverse phase HPLC.

sNBD2 and particularly LNBD2, are hydrophobic proteins that require special conditions in order to keep them soluble. Consequently, we reasoned that the peptides produced will also be hydrophobic and a C4 reverse phase column was chosen. In addition, the TNP-moiety tends to increase the hydrophobicity. Since several different enzymes and digestion conditions were investigated in order to optimize conditions for the processing and digestion of sNBD2 photolabeled with TNP-8N_3-ATP a rather short HPLC run time with a steep acetonitrile gradient was opted for.

sNBD2 digestion with Thermolysin

Thermolysin, an enzyme previously used in our laboratory to identify TNP-labeled amino acids (McIntosh *et al.*, 1992), is a proteolytic enzyme that cleaves peptide bonds on the N-terminal side of valine, leucine, isoleucine, phenylalanine, tyrosine or tryptophan residues and

does not interact with the TNP moiety of TNP-8N_3-ATP. The enzyme is stable at high temperatures and denaturing conditions and is active in 8 M urea, but the digestion temperature should be lowered to 25 °C under these conditions (Wilkinson, 1986). This was confirmed by comparing the digestion of a sample of sarcoplasmic reticulum Ca^{2+}-ATPase with 20 % (w/w) thermolysin, in the presence and absence of 6 M urea, at 28 °C for 3 h and 37 °C for 30 min respectively - showing comparable protein digestion under both conditions (data not shown). All irradiations were done under standard conditions - 25 mM MES, pH 6.0, 20 % (v/v) glycerol and 0.01 % (v/v) Triton X-100 and 1 mM $MgCl_2$ - with the TNP-8N_3-ATP concentration at 30 μM to compensate for higher protein concentrations (~ 20 μM). The irradiation time was 5 min. In the following series of experiments a) the digestion time and b) the proteolytic enzyme concentration were varied.

a) Digestion time: Fig 8.1 shows the HPLC profile of 0.5 mg sNBD2 digested with 4% (w/w) thermolysin for 30 min at 30 °C. The peptide profile is seen in blue (210 nm) and the TNP profile is seen in green (408 nm). The bulk of the peptides elute between 30 and 65 min, while most of the TNP-peptides elute in a broad peak at 50 – 65 min. As will be seen below, later eluting peptides tend to be less digested and this profile is indicative of a poorly digested sample.

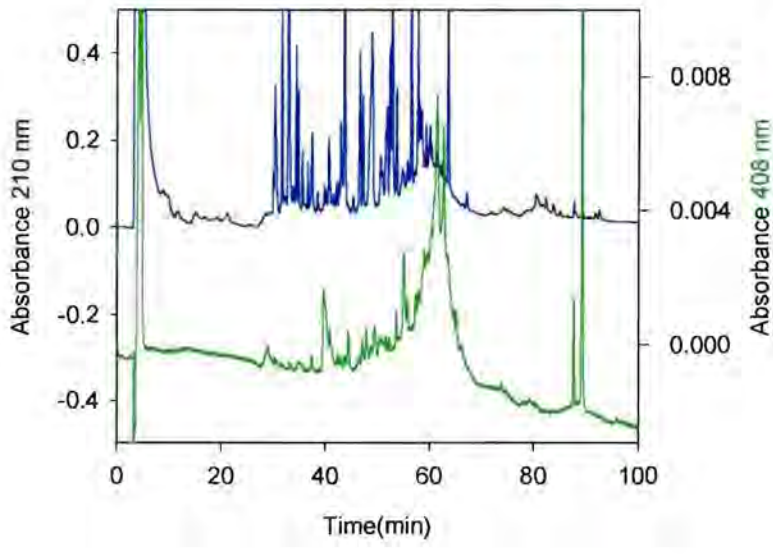

Figure 8.1 C4 HPLC elution profile of photolabeled sNBD2 (0.5 mg) digested with 4 % (w/w) thermolysin for **30 min** at 30 °C. Photolabeling was performed under standard conditions.

Fig 8.2 shows the HPLC profile of 1 mg sNBD2 digested with 4% (w/w) thermolysin for 3 h at 30 °C. The longer digestion time had the effect of shifting the bulk of the peptide profile (210 nm, blue) to the left. The TNP-peptide profile (408 nm, green) is spread from 35 min to 70 min with the majority of the TNP-peptides clustered in two groups at 40 min and 65 min. There is a disappointingly large number of TNP peaks.

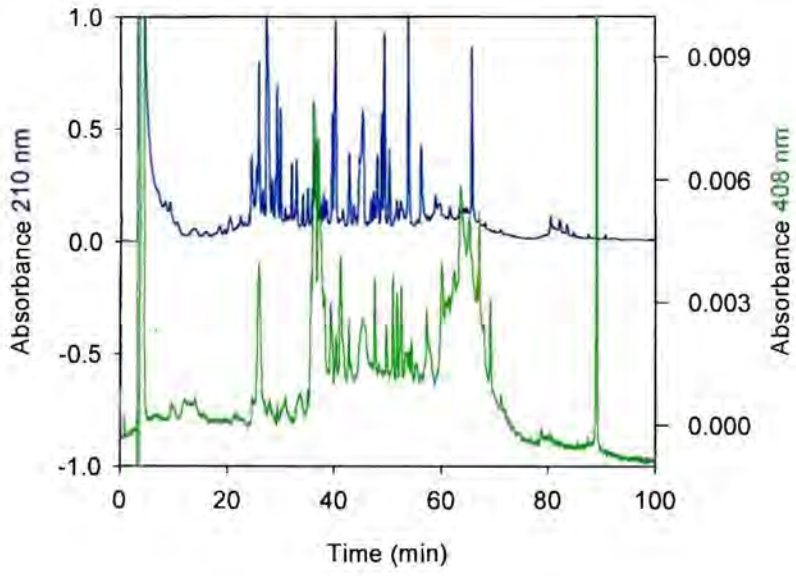

Figure 8.2 C4 HPLC elution profile of photolabeled sNBD2 (1.0 mg) digested with 4 % (w/w) thermolysin for **3 h** at 30 °C. Photolabeling was performed under standard conditions.

Fig 8.3 shows the HPLC profile of 0.5 mg NBD2 digested with 4% (w/w) thermolysin for 16 h at 30 °C. The very long digestion time shifted the peptide profile (210 nm) even further to the left. The TNP-peptide profile (408 nm) is spread from 25 min to 70 min but again no single major peak is evident. The TNP-peptide yield after a 16 h digestion is comparable with the TNP-peptide yield after a 30 min digestion (as reflected by the area under the 408 nm trace in fig 6.1 and 6.3), providing evidence that the TNP-peptide and TNP-ribose linkages are stable.

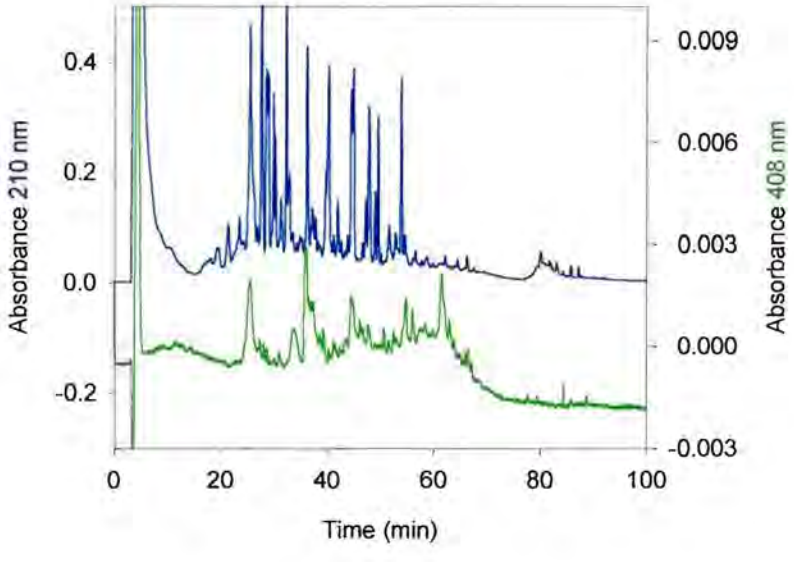

Figure 8.3 C4 HPLC elution profile of photolabeled sNBD2 (0.5 mg) digested with 4 % (w/w) thermolysin for **16 h** at 30 °C. Photolabeling was performed under standard conditions.

To determine the elution times of unphotolysed TNP-8N_3-ATP and photolysis products, samples of unphotolysed TNP-8N_3-ATP (Fig 8.4), the contents of the dialysis bag (Fig 8.5),

and the supernatant after the first wash of the pellet (Fig 8.6), were analyzed on HPLC. A sample of TNP-8N_3-ATP was also irradiated in standard medium and subjected to digestion conditions with 40% (w/w) thermolysin for 3 h at 37 °C and analyzed on HPLC to identify possible mono- and di- phosphate TNP adducts (Fig 8.7).

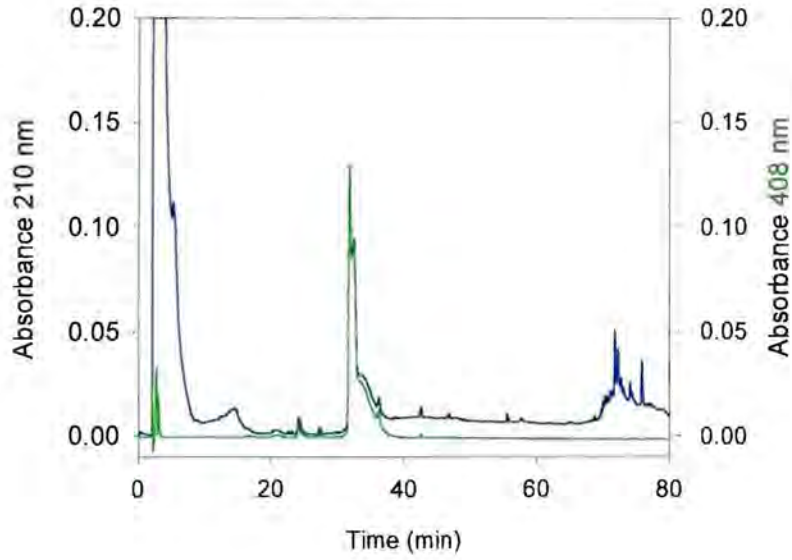

Figure 8.4 C4 HPLC profile of unphotolysed TNP-8N_3-ATP.

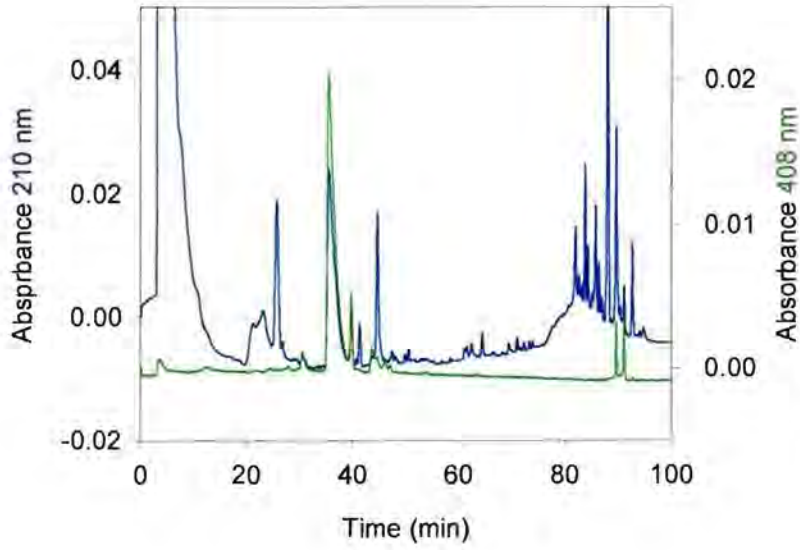

Figure 8.5 C4 HPLC profile of an aliquot of the dialysis bag contents after overnight dialysis – the majority of photolabeled sNBD2 was precipitated at the bottom of the dialysis bag.

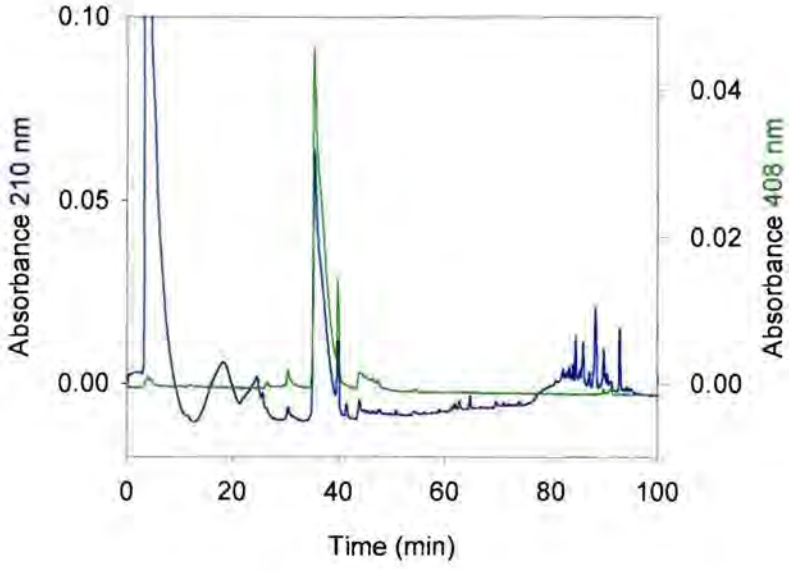

Figure 8.6 C4 HPLC profile of the supernatant after the first wash of the precipitated sNBD2 sample.

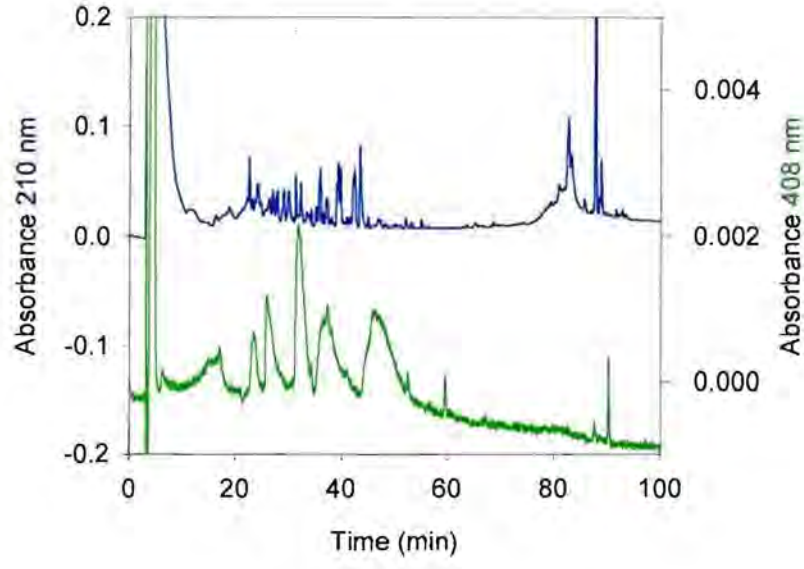

Figure 8.7 C4 HPLC profile of irradiated TNP-8N_3-ATP under standard conditions and subjected to thermolysin digestion conditions (40 % (w/w) thermolysin for 3 h at 37 °C).

unphotolysed TNP-8N_3-ATP eluted at 30 – 35 min (Fig 8.4). Analysis of the soluble portion of the contents of the dialysis bag (Fig 8.5) and the supernatant following washing of the precipitated sNBD2, indicates that one particular photolysis product was being selectively retained by the denatured protein – a species eluting at 37 min. Analysis of the photolysis products themselves (Fig 8.7) indicates that this species is one of about five, and not the most plentiful. Therefore, in appraising the TNP-profile of photolabeled and digested sNBD2 (Fig 8.1 to 8.3) peaks at 33 min (unphotolysed TNP-8N3-ATP) and 37 min (photolysis product) should be treated with suspicion. However, the washing procedure seems fairly good as these peaks are absent or small in all the HPCL profiles of digested sNBD2.

b) Proteolytic enzyme concentration: sNBD2 appeared to be well digested after 16 h with 4% (w/w) thermolysin. However, wishing to avoid long digestion times, the thermolysin concentration was raised to 40 % (w/w). Fig 8.8 shows 0.25 mg of NBD2 digested with 40% (w/w) thermolysin at 30 °C for 3.5 h. sNBD2 appears to be well digested, showing the peptide profile (210 nm) well shifted to the left, while the TNP profile (408 nm) is well separated from the bulk of the peptides and eluting rather later.

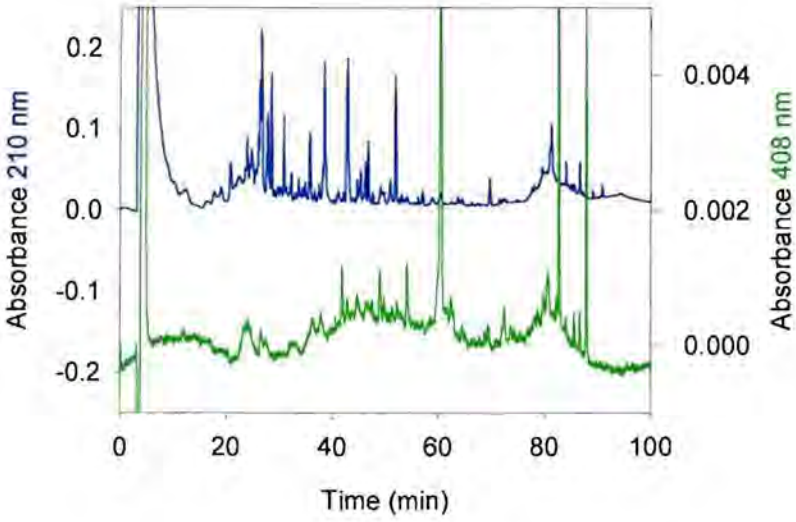

Figure 8.8 C4 HPLC profile of 0.25 mg sNBD2 digested with 40% (w/w) thermolysin for 3.5 h at 30 °C. Photolabeling was performed under standard conditions.

So far, the TNP (408 nm) HPLC profiles of sNBD2 digested under different conditions varied between experiments. To test reproducibility, a second experiment was done under exactly the same conditions as above. As shown in Fig 8.9, the peptide profile (210 nm) shows similarity to Fig 8.8 but the TNP profile is very different.

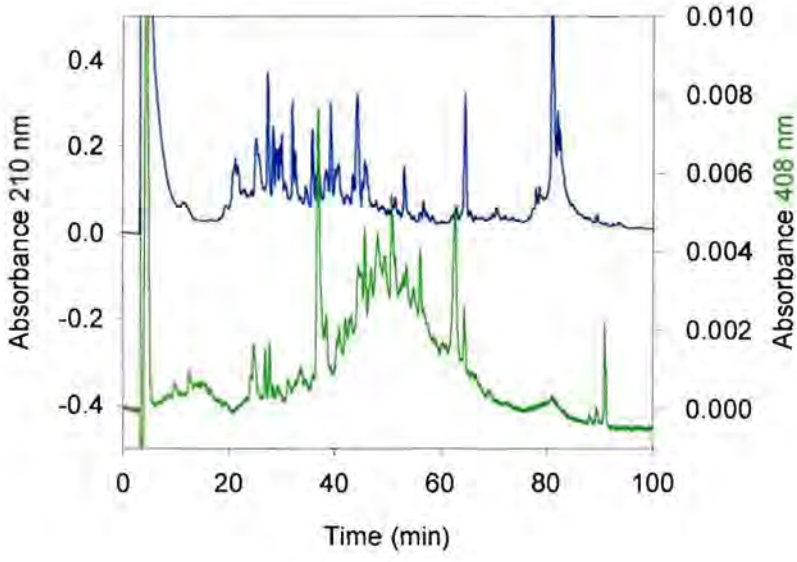

Figure 8.9 C4 HPLC profile of 0.25 mg sNBD2 digested with 40% (w/w) thermolysin for 3.5 h at 30 °C. Photolabeling was performed under standard conditions.

Again as a test of reproducibility, 0.5 mg of sNBD2 was photolabeled and digested as above. As shown in Fig 8.10, sNBD2 digestion was successful, with the peptide profile (210 nm) shifted to the left and the majority of the TNP profile associated with a peptide peak at 40 – 45 min. This experiment was repeated again as shown in Fig 8.11. Again a different TNP-profile was obtained.

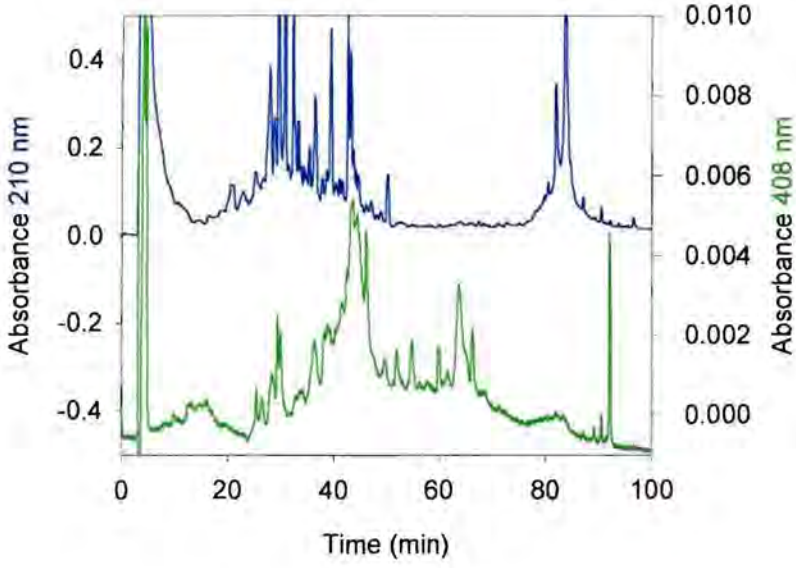

Figure 8.10 C4 HPLC profile of 0.5 mg sNBD2 digested with 40% (w/w) thermolysin for 3.5 h at 30 °C. Photolabeling was performed under standard conditions.

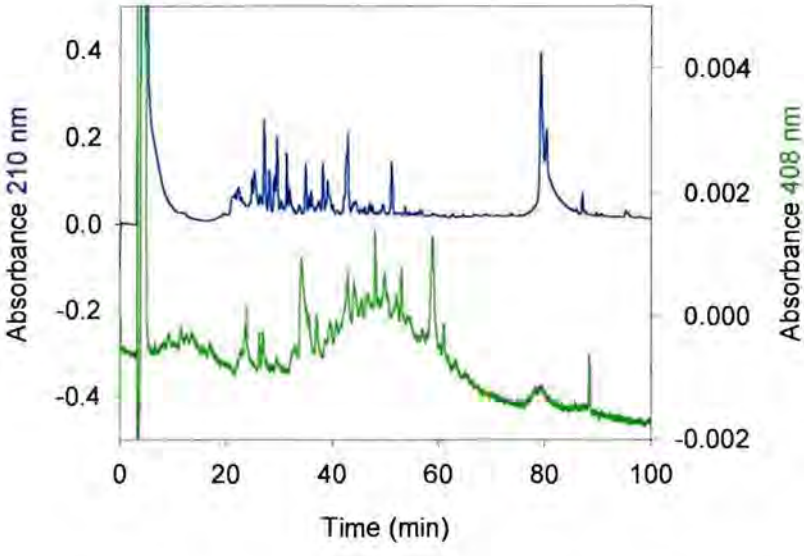

Figure 8.11 The HPLC profile of 0.5 mg sNBD2 digested with 40% (w/w) thermolysin for 3.5 h at 30 °C. Photolabeling was performed under standard conditions at pH 6.0.

In all seven experiments shown the TNP-peptide profile was extremely variable and no TNP peaks could be singled out as reproducibly dominating. We considered that perhaps the situation may be improved at pH 8.5 despite the fact that labeling is less at alkaline pH. Fig 8.12 shows 0.5 mg of sNBD2, photolabeled at alkaline pH under standard conditions (EPPS,

pH 8.5) and digested with 40% (w/w) thermolysin at 30 °C for 3 h. The peptide yield compared well with experiments done at pH 6.0, but, not unexpectedly, the TNP profile (408 nm) was significantly less than the experiments done at pH 6.0. There was no dominant TNP peak.

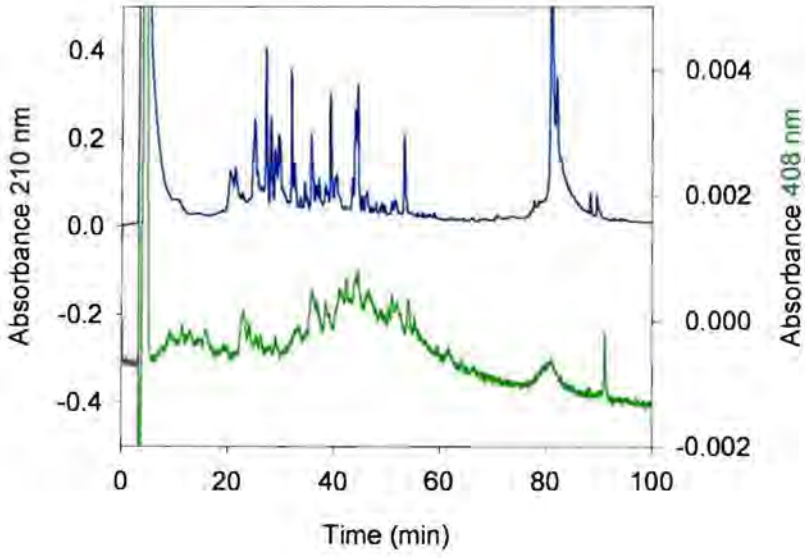

Figure 8.12 C4 HPLC profile of 0.5 mg sNBD2 digested with 40% (w/w) thermolysin for 3.5 h at 30 °C. Photolabeling was performed under standard conditions at **pH 8.5**. 25 mM EPPS was used a buffer.

In all of the above experiments efforts were made to purify and identify groups of TNP peptides or single TNP peaks by further HPLC and peptide sequence analysis. Individual TNP-peptides were difficult to purify as elution characteristics were very similar, possibly because of incomplete digestion, resulting in raggedy ends of essentially the same peptide. Sequence analysis consistently failed to yield PTH amino acids, probably because the concentration of TNP-adduct was too low. We have made an exploratory investigation into using MALDITOF mass spectroscopy to identify TNP-adducts and are hoping to utilize this method in identifying photolabeled peptides in the future.

A spike of [γ-^{32}P]TNP-8N_3-ATP was included in 7 of the above experiments in order to quantify sNBD2 photolabeling. The assays performed at pH 6.0 (total of 6) yielded a consistent ratio of 0.39 $\pm$ 0.07 nmol TNP-8N_3-ATP per nmol of sNBD2 (assuming 100 % protein recovery). The one assay performed at pH 8.5 gave a ratio of 0.2 nmol TNP-8N_3-ATP per nmol of sNBD2, consistent with less labeling observed at higher pH.

sNBD2 digestion with trypsin

Thermolysin cleaves at hydrophobic amino acids and in the case of a hydrophobic protein (like sNBD2 and LNBD2), may digest the protein into small peptides of 2 or 3 amino acid lengths, or even single amino acids, which may make identification of the labeled amino acid residue difficult. Therefore, trypsin was investigated as an enzyme for sNBD2 digestion.

Trypsin cleaves at the C-terminal side of lysine and arginine residues, bonds of the type –Lys-X- and –Arg-X- (Wilkinson, 1986). Previous experience with TNP-8N_3-ATP photolabeled Ca^{2+}-ATPase had shown that trypsin could not be used as it appeared to cleave the TNP moiety from the labeled peptide (McIntosh *et al.*, 1992). However, this may be related to the fact that two arginine residues are in close proximity to the labeled lysine. The situation could be different for sNBD2. sNBD2 (1 mg) was photolabeled under standard conditions at pH 6.0 and digested with 2% (w/w) trypsin at 37 °C for 4 h in 4 M urea. Digestion appeared to be poor as most of the digestion products eluted late. This may be because trypsin is sensitive to high concentrations of urea. Trypsin also proved to interact with the TNP moiety on the [γ-^{32}P]TNP-8N_3-ATP and the TNP profile (408 nm) was negligible in comparison with TNP profiles after thermolysin digestion (results not shown).

sNBD2 digestion with V8 protease

V8 protease was also investigated as an alternative to thermolysin. V8 protease is a proteolytic enzyme cleaving the C-terminal peptide bonds of glutamic acid residues (Wilkinson, 1986). The enzyme proved to be very sensitive to urea and exhibited significant auto-digestion at urea concentrations needed to solubilize precipitated sNBD2. sNBD2 digestion was poor or negligible.

sNBD2 digestion with clostripain

Clostripain is a sulfhydryl protease, cleaving the C-terminal peptide bonds of arginine residues, at bonds of the type –Arg-X- (Wilkinson, 1986). The presence of a sulfhydryl-reducing reagent is essential and the enzyme was activated for an hour before digestion in 2.5 mM DTT and 1 mM calcium acetate, pH 7.7. DTT, like trypsin, interacted with the TNP moiety on the [γ-^{32}P]TNP-8N_3-ATP and completely destroyed any TNP signal at 408 nm. When DTT was removed after activation, prior to digestion, by desalting with a Penefsky column (Penefsky, 1977), the enzyme appeared to become inactivated and sNBD2 digestion was poor in comparison with the experiment where DTT was included in the digestion medium.

LNBD2 digestion with thermolysin

TNP-8N_3-ATP photolabeling of LNBD2 followed by thermolysin digestion was also investigated. Digestion was routinely done with 20 % (w/w) thermolysin in 4 M urea at 30 °C for 2 h. In particular, preparative photolabeling was performed under similar conditions as was used for SDS-PAGE experiments where complete inhibition of photolabeling was achieved with increasing concentrations of ATP (i.e. low concentrations of protein).

For the first experiment, 0.5 mg of LNBD2 (0.8 μM) was photolabeled in 25 mM MES, pH 6.0, 20 % (v/v) glycerol, 0.01 % (v/v) Triton X-100 and 1mM $MgCl_2$, with 8 μM TNP-8N_3-ATP, the sample denatured in 8 M urea and applied to a nickel chelate column. The column was washed with buffer (including 8 M urea) to remove free TNP-8N_3-ATP and eluted. The sample was diluted to a final concentration of 4 M urea and 0.5 M imidazole, digested with 20 % (w/w) thermolysin at 30 °C for 2 h, and the digest analyzed by HPLC (Fig 8.13).

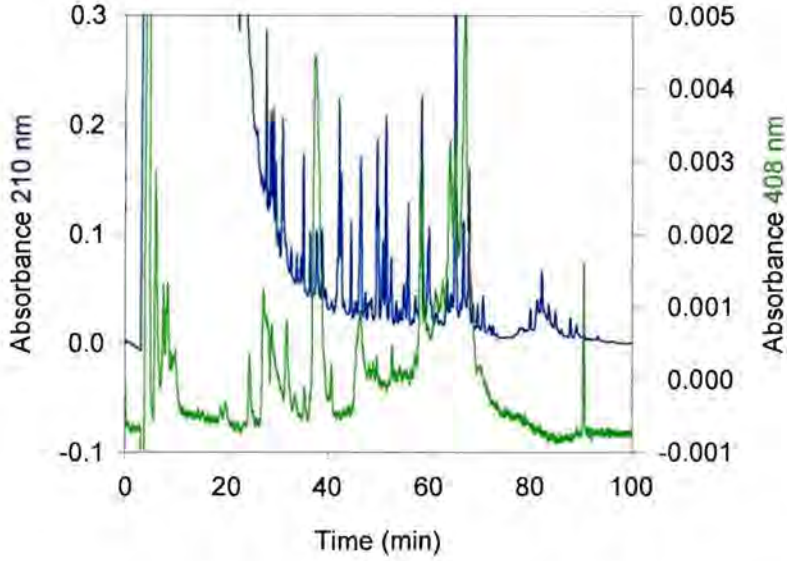

Figure 8.13. C4 HPLC profile of 0.5 mg LNBD2 photolabeled with 8 μM TNP-8N_3-ATP and digested with 20 % (w/w) thermolysin at 30 °C for 2 hours. Photolabeling was performed under standard conditions - 25 mM MES, pH 6.0, 20 % (v/v) glycerol, 0.01 % (v/v) Triton X-100 and 1mM $MgCl_2$,.

LNBD2 appears to be well digested under these conditions with the bulk of the peptides eluting in under 30 min. The majority of the TNP peptides eluted between 55 and 70 min. The TNP peak eluting between 35 and 40 minutes, previously identified as a tight binding photolysis product (Fig 8.5 and Fig 8.6) suggested that the washing step in this experiment was inadequate to remove all of the free TNP-species from the denatured protein. There appeared to be some interesting large TNP peaks eluting between 60 – 70 min. To determine whether these later eluting TNP peaks could be obtained reproducibly, the experiment was repeated under the same conditions - except that more rigorous washing of the protein adsorbed to the nickel chelate column was carried out (Fig 8.14).

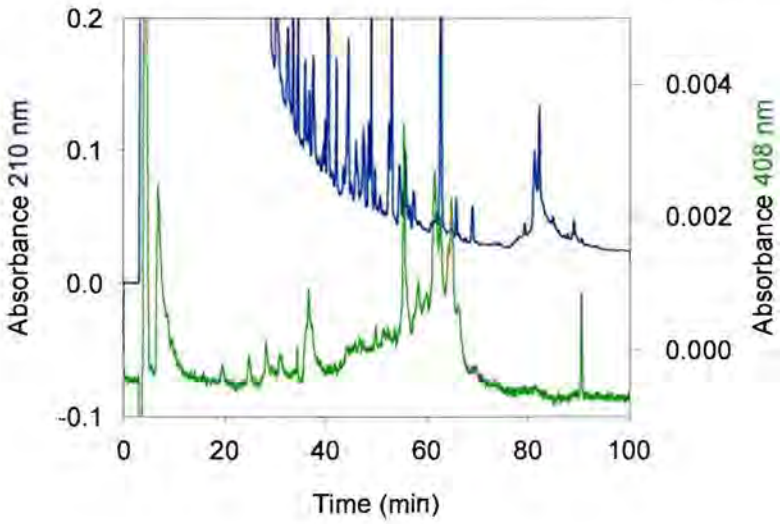

Figure 8.14. C4 HPLC profile of 0.5 mg LNBD2 photolabeled with 8 μM TNP-8N_3-ATP and digested with 20 % (w/w) thermolysin at 30 °C for 2 hours. Photolabeling was preformed under standard conditions.

Additional washing of the protein adsorbed to the nickel column markedly decreased the amount of TNP signal seen before 55 min, while the TNP cluster just after 60 min remained, suggesting that the latter are TNP peptides.

To confirm reproducibility again, a repeat of the previous experiment was performed (Fig 8.15). Again significant TNP peaks appeared after 60 min.

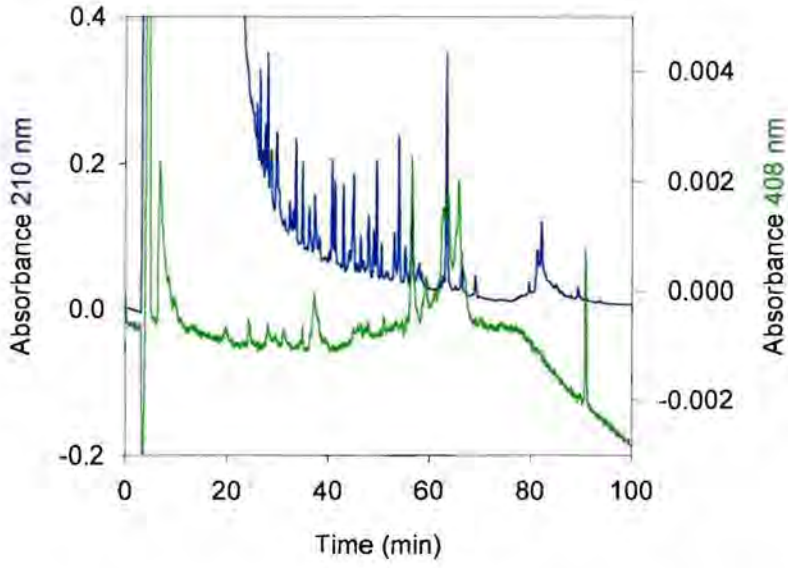

Figure 8.15. C4 HPLC profile of 0.5 mg LNBD2 photolabeled with 8 μM TNP-8N$_3$-ATP and digested with 20 % (w/w) thermolysin at 30 °C for 2 hours. Photolabeling was preformed under standard conditions.

A bulk experiment, using 2.6 mg of protein, was performed (using the above conditions) in an effort to isolate and purify larger amounts concentrations of TNP peptides for sequencing (Fig 8.16). This necessitated the irradiation of 112 ml of medium over a period of 3 h. This large volume was forced through the Nickel chelate column under mild pressure and washed, eluted and digested as before. The protein concentration was 5 times greater than before.

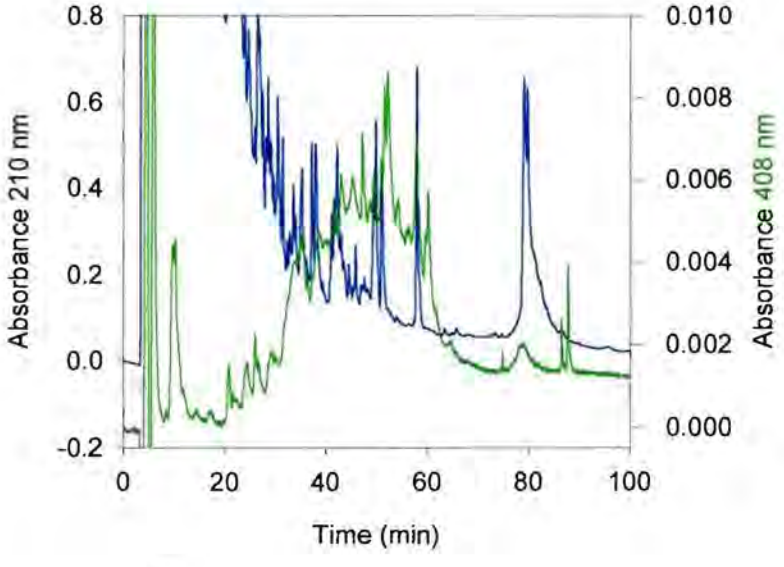

Figure 8.16. C4 HPLC profile of 2.6 mg LNBD2 photolabeled with 8 μM TNP-8N$_3$-ATP and digested with 20 % (w/w) thermolysin at 30 °C for 2 hours. Photolabeling was preformed under standard conditions.

Regrettably, the TNP peptide profile differed from the experiments performed with 0.5 mg of protein, and eluted as a large cluster from 30 to 64 min with no apparent prominent peaks. It appears that the only possible reason for this is that the high concentration of protein altered the course of digestion.

As for sNBD2, in all of the above experiments efforts were made to purify and identify promising peptides by further HPLC and peptide sequence analysis. In particular the major TNP-peak eluting at 62 min seen in Figs 8.8 – 8.9, was pooled, concentrated, subjected to C18 HPLC, the purified peak collected and sent for sequencing. Sequence analysis again consistently failed to yield PTH amino acids, either because the concentration of the TNP-adduct was too low, the amino terminal end blocked, or the TNP peptide was too short. Limited amounts of protein available for bulk preparative experiments and time constraints prevented further efforts to obtain larger amount of the 62 min species.

CHAPTER 9: SYNTHESIS AND CHARACTERISATION OF ANP-AMP AND ANP-TNP-AMP AS PHOTOAFFINITY PROBES FOR MOUSE LNBD2

Synthesis and Characterisation of ANP-AMP

The photoaffinity probe 4-azido-2-nitrophenyl phosphate (ANPP) has been used previously to probe the phosphate binding sites of the F1-ATPase, Ca^{2+}-ATPase and the Na^{+}/K^{+}-ATPase (Garin *et al.*, 1989., Lacapere and Garin, 1994., Tran and Farley, 1996). A disadvantage of ANPP is that irradiation tends to split off the phosphate and if the probe is ^{32}P labeled, it would be lost (Garin *et al.*, 1989). However, it appears that on covalent attachment to the protein the phosphate remains attached. (Garin *et al.*, 1989, Michel *et al.*, 1992). We considered that attaching ANP to AMP could yield a photoprobe where the azido group is almost exactly in the position of the end of the gamma phosphate of ATP, and make it a potentially powerful probe of the gamma phosphate binding region of ATP sites of enzymes. In general, there are few probes of this region, although adenosine triphosphopyrodoxal and 5'-(p-(fluorosulfonyl)benzoyl)-8-azidoadenosine have been used in the past (Dombrowski et al., 1992., Yamamoto et al., 1988., Yamamoto et al., 1989). In addition to introducing a single azido group there is the possibility of combining ANP with 8-azido ATP to make a bifunctional crosslinker. The addition of the TNP group could make the binding much tighter, especially in the case of p-gp.

ANP-AMP synthesis was followed by TLC and purification was carried out as described in the Methods section. ANP-AMP formation from AMP was apparent on TLC as the only other time dependent major species being formed after initiation of the reaction. ANP-AMP migrated just below AMP and roughly 80 % conversion of AMP to AMP-ANP was apparent after the reaction was continued overnight. After purification, analysis of the purified product yielded a species migrating similarly to that seen for the major species formed during synthesis. Irradiation of this product in 10 mM KPi, pH 7.0 for 2 min showed the formation of several species upon TLC analysis – an indication that this species is photoactive. A scan of ANP (Fig 9.1) shows two peaks, the main peak at 250 nm with a smaller second peak at 388 nm.

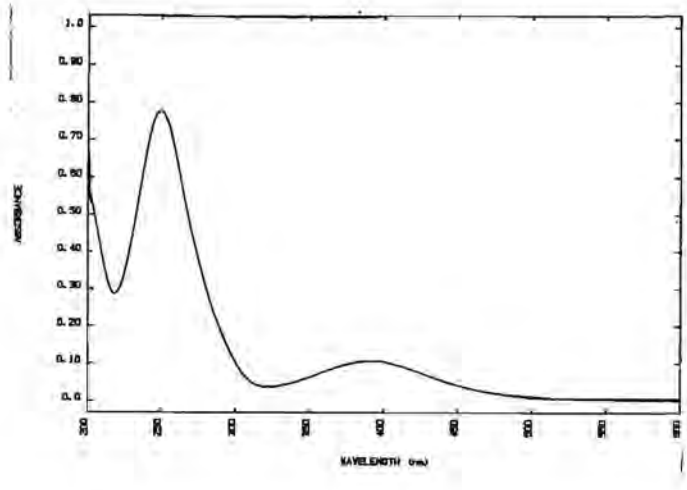

Figure 9.1. Absorption spectra of ANP in 10 mM KPi, pH 5.5

After the chemical addition of AMP to yield ANP-AMP, a shift in the maximal absorbance of the latter peak can be observed from 388 nm to 350 nm (Fig 9.2) – this scan can be correlated with the addition of ANP to AMP.

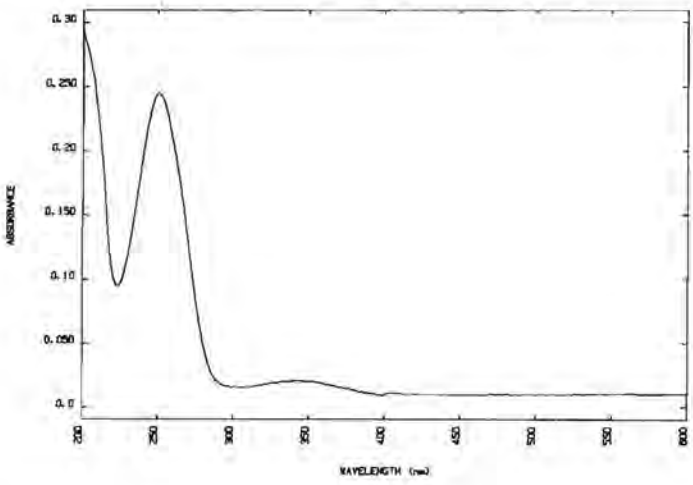

Figure 9.2. Absorption spectra of ANP-AMP in 10 mM KPi, pH 5.5

To confirm that the azido group was photoactive, a sample of purified ANP-AMP in 10 mM KPi, pH 5.5 was irradiated up to 120 s with no toluene filters (Fig 9.3). A decrease in the main absorbance of the peak is seen as well as a peak maximum shift from 250 nm to 263 nm. The second smaller peak shows an increase in absorbance and a significant red shift from 350 nm to 319 nm.

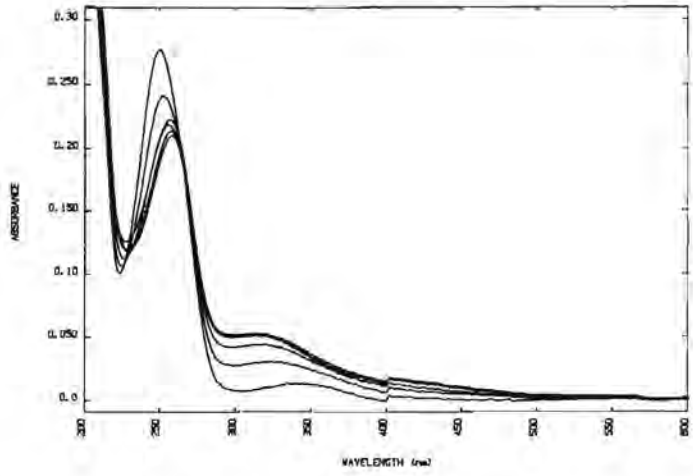

Figure 9.3. Absorption spectra of ANP-AMP irradiated for 0, 15, 30, 45, 60 and 120 s in 10 mM KPi, pH 5.5.

The irradiated sample was analysed on analytical HPLC on a C18 reverse phase column using standard solvents (Fig 9.4). Activation of the azido group led to the formation of several products and under these conditions, three major products were formed: peak 2.8'–3.6', peak 12.9'-14.2' and peak 16'-16.8'. Peak 16.8'-17.8' was identified as unphotolysed ANP-AMP from its scan and retention time.

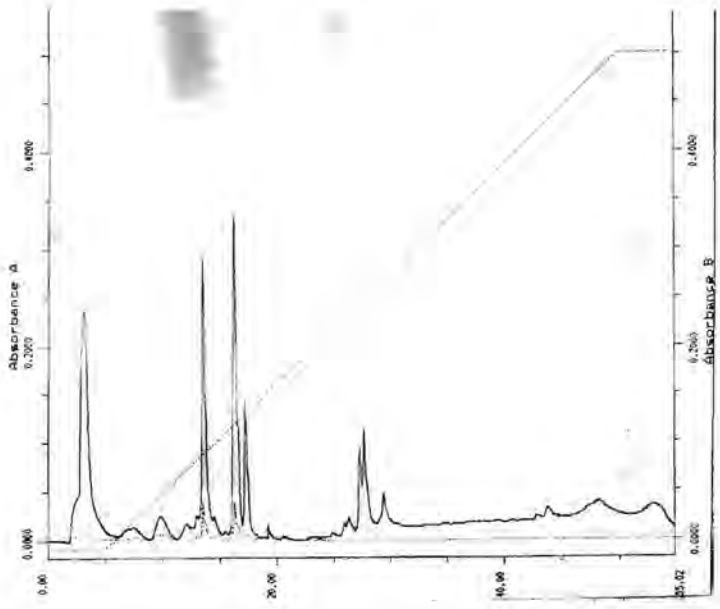

Figure 9.4. HPLC profile of ANP-AMP irradiated for 120 seconds in 10 mM KPi, pH 5.5, analysed on a C18 reverse phase column.

To determine whether ANP-AMP is interacting with the ATP binding site of mouse LNBD2, the effect of increasing concentrations of ANP-AMP on the photolabeling of LNBD2 with [γ-^{32}P]8N_3-ATP was assessed (Fig 9.5). Increasing concentrations of ANP-AMP inhibited the binding of [γ-^{32}P]8N_3-ATP to LNBD2 with Ki(ANP-AMP) = 550 μM.

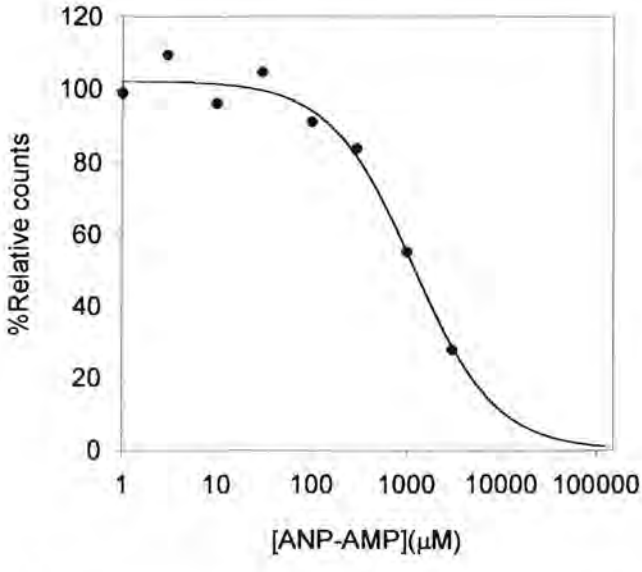

Figure 9.5. Effect of increasing concentrations of ANP-AMP on LNBD2 (0.5 μM) photolabeling with [γ-^{32}P]8N_3-ATP. The samples were irradiated under standard conditions – 25 mM MES, pH 6.0, 20 % (v/v) glycerol, 0.01 %(v/v) Triton X-100 in 10 mM EDTA

It can be concluded that ANP-AMP is photoactive and binds to the ATP binding site of LNBD2 with similar affinity as ATP.

Synthesis and Characterisation of ANP-TNP-AMP

4-Azido-2-nitrophenyl-2',3'-O-(2,4,6-trinitrophenyl) adenosine monophosphate (ANP-TNP-AMP) synthesis was carried out by reacting TNBS with ANP-AMP as described in the methods section. The reaction proceeded smoothly with a yield of about 30 %. The product was identified as being ANP-TNP-AMP from its scan, its light sensitivity and it being the major product with a typical Meisenheimer complex. A scan of purified ANP-TNP-AMP shows a major peak at 252 nm with a smaller doublet at 408 nm and 468 nm (Fig 9.6). The doublet of 408 nm and 468 nm is diagnostic of the TNP moiety.

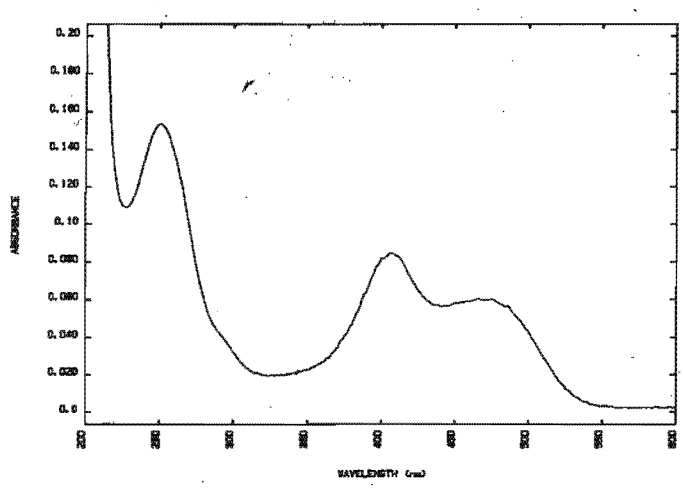

Figure 9.6. Absorption spectra of ANP-TNP-AMP in 10 mM KPi, pH

The photosensitivity of the azido group was verified by irradiating a pure sample of ANP-TNP-AMP with toluene filters in 10 mM KPi, pH 5.5 up to 12 min (Fig 9.7). Similar to ANP-AMP, ANP-TNP-AMP also displayed a decrease in maximal absorbance at the 252 nm major peak and a shift from 252 to 260 nm. The TNP-moiety remained unaffected.

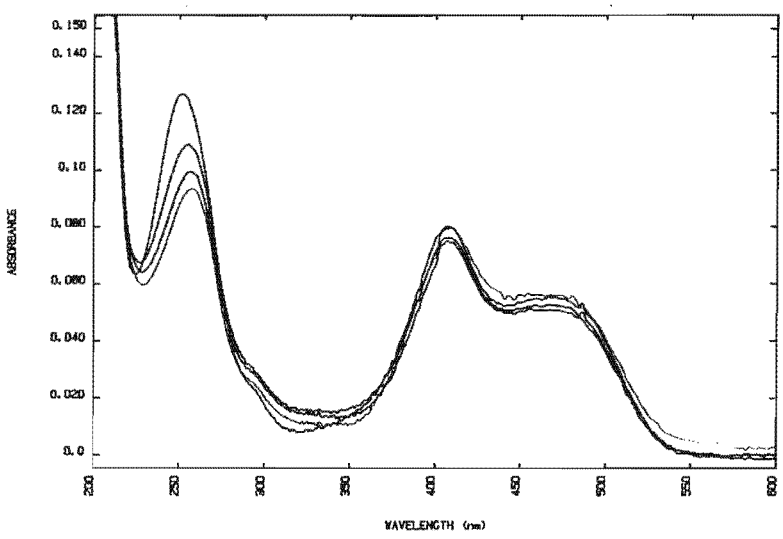

Figure 9.7. Absorption spectra of ANP-TNP-ANP irradiated with toluene filters in 10 mM KPi, pH 5.5 for 0, 4, 8 and 12 min.

When analysed on analytical HPLC on a C18 reverse phase column using standard solvents, one major photolysis product was observed, 20.6'-21.4', with two smaller peaks, 22.3'-23.3' and 25.5'-26' respectively (Fig 9.8). The 26'-26.8' peak is unphotolysed ANP-TNP-AMP.

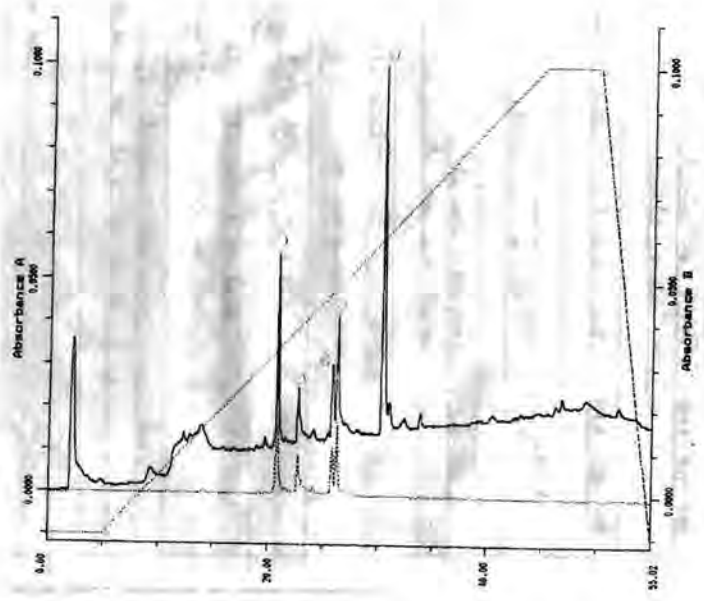

Figure 9.8. HPLC profile of ANP-TNP-AMP irradiated for 12 min with toluene filters in 10 mM KPi, pH5.5, analysed on a C18 reverse phase column.

When ANP-TNP-AMP was irradiated using a glass cuvette (cut off at 350 nm), 50 mM MOPS, pH 7.5 for up to 20 min, it resulted in a markedly different scan indicating different products (Fig 9.9). This is because the reaction of nitrenes is fairly indiscriminate and various irradiation products can be formed depending on reaction conditions such as type of buffer, medium composition, pH and possibly wavelength of irradiation. The HPLC profile obviously differed from the previous experiment (data not shown).

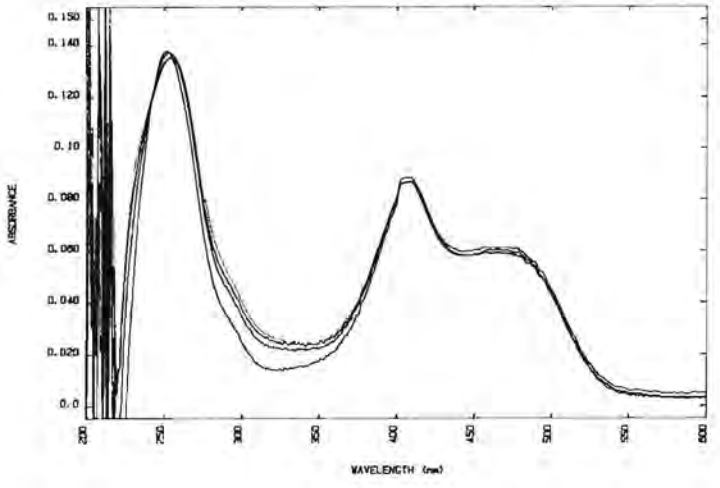

Figure 9.9. Absorption spectra of ANP-TNP-AMP irradiated in a glass cuvette for 0, 5, 10 and 20 min in 50 mM MOPS, pH 7.5

The binding of ANP-TNP-AMP to LNBD2 was determined as for ANP-AMP (Fig 9.10). ANP-TNP-AMP inhibited the binding of [γ-^{32}P]8N_3-ATP to LNBD2 with an affinity of 7.44 μM. This tighter binding correlates well with the fact that TNP-ATP interaction with LNBD2 is at least 10

X tighter than ATP binding (Baubichon-Cortay *et al.*, 1995) as well as our work with TNP-8N_3-ATP.

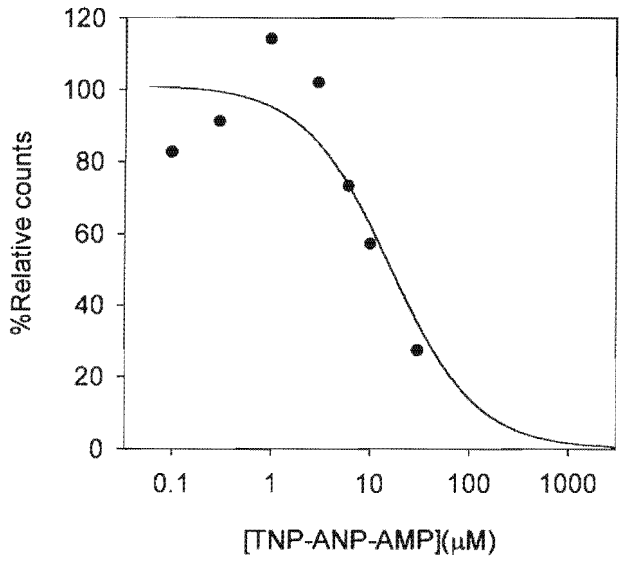

Figure 9.10. The effect of increasing concentrations of ANP-TNP-AMP on LNBD2 photolabeling with [γ-^{32}P]8N_3-ATP. The samples were irradiated under standard conditions in 10 mM EDTA

Binding of a photoactive probe to the binding site does not necessarily lead to the successful photoinsertion into an amino acid. To determine if ANP-TNP-AMP is not only binding to, but also capable of photolabeling an amino acid in the ATP binding site of LNBD2, prelabeling of LNBD2 with ANP-TNP-AMP was carried out before photolabeling with [γ-^{32}P]8N_3-ATP. Photolabeling with saturating concentrations of ANP-TNP-AMP followed by a large dilution should leave the majority of the ATP binding sites occupied with covalently attached ANP-TNP-AMP, blocking interaction and photolabeling with [γ-^{32}P]8N_3-ATP. Or, in the case of no favourable reactions with the binding site, a large dilution should leave the majority of the binding sites available for interaction with [γ-^{32}P]8N_3-ATP.

Samples of LNBD2 were irradiated under standard conditions in EDTA in the presence of 22.5 μM ANP-TNP-AMP (3X Kd). The sample was diluted 10-fold in standard medium and a second irradiation carried out in the presence of increasing concentrations of [γ-^{32}P]8N_3-ATP. Concurrently, a control was carried out to determine the amount of unreacted ANP-TNP-AMP interacting with the binding site after the dilution. In the control, no irradiation of ANP-TNP-AMP was done before dilution of the sample. As seen in Fig 9.11, preirradiation of LNBD2 with ANP-TNP-AMP (circles) had no effect on photolabeling with [γ-^{32}P]8N_3-ATP and appeared similar to the control (triangles).

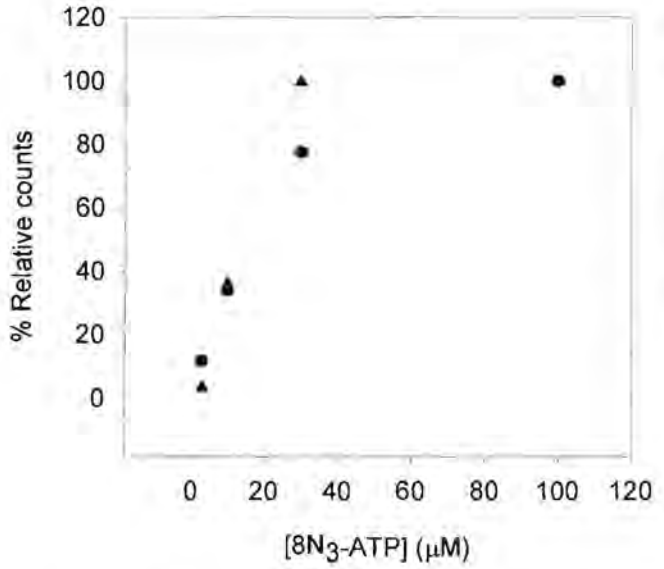

Figure 9.11. The effect of increasing concentrations of [γ-^{32}P]8N_3-ATP on 0.5 μM LNBD2 prelabeled with saturating concentrations of ANP-TNP-AMP (circles) under standard conditions in 10 mM EDTA; as compared to a control (triangles).

In conclusion, both ANP-AMP and ANP-TNP-AMP are photoactive and bind to the ATP site of LNBD2. Formation of a covalent bond between activated ANP-TNP-AMP and an amino acid in the ATP binding site of LNBD2, appears to be unsuccessful as prelabeling with ANP-TNP-AMP does not preclude [γ-^{32}P]8N_3-ATP photolabeling of LNBD2. Consequently, work on ANP-TNP-8N_3-AMP was not pursued.

CHAPTER 10: DISCUSSION

This study set out to explore the use of TNP-8N_3-ATP as a photoprobe of the ATP sites of p-gps in order to shed light on site architecture and function. We found that the yeast pumps Pdr5p and Yor1p are well photolabeled at acidic pH with a fairly modest affinity (Kd = 16 – 40 μM, and efficiency of labeling approximately 80 % for Pdr5p). Photolabeling is dependent on Mg^{2+} and is inhibited up to 90 % by ATP. Recombinant expression of mouse NBD2 allowed investigation of the photolabeling characteristics of the isolated domain. Interestingly, we find that the soluble domain is labeled extremely well even in the absence of Mg^{2+} (Kd = 2 μM, and efficiency of labeling approximately 80 %) and the specificity is excellent as judged from the complete inhibition of photolabeling by various nucleotides. It suggests that the isolated domain is largely folded correctly and yet there may be important differences in site architecture especially in relation to the Mg^{2+} site. An exciting possibility is that the differences reflect the lack of the trans membrane domain in the isolated NBD2. It could mean that the two fairly large extra membranous loops of the transmembrane domain are required for proper constitution of the ATP site. This study also demonstrates that certain flavonoids bind reasonably tightly to the ATP site and identifies ring C of the flavonoid nucleus as the only direction in which elaborations on the structure are tolerated. This is important for the future design of more powerful flavonoid reversers of multidrug resistance. Perhaps as important is the finding that hydrophobic flavonoids that previously have been shown to bind to the isolated NBDs and to reverse drug pumping do not bind at the ATP site and therefore must be binding at another site (Conseil *et al.*, 1998, Perez-Victoria *et al.*, 1999).

The yeast pumps

Photolabeling of the yeast p-gps, Pdr5p and Yor1p, by TNP-8N_3-ATP was characterised by fairly tight binding affinities (Kd = 16 - 40 μM, respectively), a strong pH dependence (pKa = 7.3 for Pdr5p) and a strong Mg^{2+} dependence. The photolabeling of both proteins was inhibited up to 90 % (in 20 % (v/v) glycerol) by millimolar concentrations of ATP (Ki = 0.4 and 0.3 mM, respectively) suggesting labeling at one or both ATP sites. The ten-fold increase in affinity for the TNP-nucleotide over ATP is compatible with the tight binding of TNP-ATP to CHO p-gp (Senior *et al.*, 1995) and the common finding that the TNP moiety increases binding affinity in many proteins (Seebregts and McIntosh, 1989, Baubichon-Cortay *et al.*, 1994).

The TNP grouping is fairly large and either there must be a convenient pocket adjacent to the ATP site for it to fit into or it significantly distorts the binding of the nucleotide. It should also be recalled that the bulky azido group causes the adenine moiety to adopt a *syn* rather than an *anti* conformation around the glycosidic bond, and hence the adenine position of TNP-8N_3-ATP may not be in the natural position in the binding site. The efficiencies of photolabeling of Yor1p could not be ascertained with accuracy because the preparations were not pure, but

judging from a comparison of PMA1 and Yor1p, at acidic pH, Yor1p was slightly better labelled than the proton pump and in a significantly lower concentration range. The labeling efficiency of purified Pdr5p at acidic pH was determined to be approximately 80 %.

The strong Mg^{2+} dependence suggests that either the nucleotide does not bind in the absence of Mg^{2+} (i.e. affinity for ATP is negligible) or Mg^{2+} is required for proper constitution of the site and positioning of the azido in proximity to a nucleophile. The correct answer may be a contribution from both quarters. The yeast pumps are rather nonspecific in their nucleotide requirements, with GTP, UTP and ATP being hydrolyzed at nearly equal rates in similar concentration ranges, suggesting that the base-protein interaction is not an important determinant of binding affinity and catalysis (Decottignies *et al.*, 1994, 1995, 1998). However, this lack of interaction is now probably offset by the favourable TNP-protein interaction which increases the affinity at least 10-fold. Also, as will be expanded on below, recombinant mouse NBD2 is well photolabeled and is strongly inhibited by ATP in the absence of Mg^{2+}, suggesting that nucleotide binding is not impaired in the absence of Mg^{2+}. This is borne out in recent work from Senior's laboratory where ATP was shown to bind to mouse Mdr3 p-gp in the absence of Mg^{2+}. The Kd(ATP) was similar in the presence and absence of Mg^{2+} (Lerner-Marmarosh *et al.*, 1999). Overall, it seems that Mg^{2+} may enhance the affinity to some extent but a more significant effect may be restructuring of the binding site and realigning the azido group in proximity to a nucleophile.

The strong pH dependence, with enhanced labeling at acidic pH was a surprise. The situation is exactly the opposite to that found for photolabeling of Lys^{492} of sarcoplasmic reticulum Ca^{2+}ATPase by TNP-8N_3-ATP (McIntosh *et al.*, 1992). In the latter case the labeling exhibits a pKa = 7.5 with stronger labeling at alkaline pH, and at pH 6.0 the small amount of labeling occurs outside of the ATP site and does not inactivate ATPase activity. The pH dependence may be explained by the greater nucleophilic nature of the neutral $-NH_2$ group compared with $-NH_3^+$. In the case of yeast, exactly the same pH dependence is found for PMA1 as for the p-gps, suggesting that the acidic optimum may be related to protonation of the nucleotide. However, there are no ionisable groups on TNP-8N_3-ATP in this range in the presence of Mg^{2+}. The hydroxyls of the phosphates have pKa's at 4.72 (Pecoraro *et al.*, 1984) and the 2' oxygen of the ribose is protonated with a pKa = 5.1, converting the spiro linkage of the Meissenheimer complex into a 3' trinitrophenyl grouping and 2' hydroxyl (Hiratsuka, 1982). An alternative explanation is that the yeast plasma membrane has a surface charge that is altered in this range and protonation permits easier access to the ATP site. However, as will be elaborated on below, soluble NBD2 exhibits a very similar pH dependence of photolabeling as the yeast pumps, suggesting that the H^+ concentration effect may be related to ionisable groups at the ATP site itself.

At the outset of the study of the two yeast p-gps, Pdr5p had been well characterized in terms of high nonspecific triphospho nucleotide hydrolysis and pleiotropic drug pumping (Decottignies *et al.*, 1994). This was not the case for Yor1p where no nucleotide hydrolysis could be detected. Our photolabeling results suggested that Yor1p did indeed possess intact ATP sites, compatible with its drug pumping activity. This prompted a re-investigation of the hydrolysis activity of Yor1p by the Goffeau laboratory and low activity (100 nmol/min/mg of protein) was eventually detected in the purified protein (Decottignies *et al.*, 1998). What is puzzling considering the 10-15 fold difference in hydrolysis activity is that the drug pumping activity of Yor1p in yeast cells, appears to be as good as Pdr5p. This might indicate that Yor1p is a much better coupled pump than Pdr5p, or else purification of the former has removed an effector protein or lipid.

Recombinant mouse NBD2

The modular structure of the ABC transporters suggests that the NBD's of p-gps may be able to be reconstituted as separate semi-functional entities from the transmembrane domains. Accordingly, the laboratory of Dr A.Di Pietro embarked on a programme to express the NBDs of mouse p-gp recombinantly in *E.coli* and to study the properties of the isolated soluble domains. This would have several advantages including an abundance of protein allowing standard physio-chemical studies to be performed, being able to determine unequivocally if reverser binding sites were located on these domains, and differences in ATP binding and function between the soluble domains and the whole protein may provide clues into the coupling mechanism.

Analysis of the amino acid sequence of the NBDs in terms of homology and secondary structure predictions suggested to Di Pietro's group that two lengths of NBD2 should be produced, namely sNBD2: Thr^{1044}-Thr^{1224} and LNBD2: Lys^{1025}-Ser^{1276} – both including the Walker A and Walker B ATP binding motifs, but the shorter excluding adjacent, nonconserved segments. Both proteins proved to be extremely difficult to maintain as soluble proteins but especially the longer one. Therefore, most of the earlier work was carried out on the shorter, more soluble protein. This turned out to be unfortunate as during our study Senior's group identified Tyr^{1041} of hamster CHO p-gp as a target of 8-azido ATP, and this residue is just outside of sNBD2 (Sankaran *et al.*, 1997b). Also, when the tertiary structure of bacterial HisP protein was elucidated (Hung *et al.*, 1998), it appeared that missing segments on both the N-terminal and C-terminal ends of sNBD2 formed central strands in the two β-sheets that flank the ATP site (see Fig 10.3). This necessitated repeating most of the work with the longer protein. At this stage of the programme, it was also deemed wise to compare the labeling characteristics of TNP-$8N_3$-ATP and $8N_3$-ATP largely because of Senior's work.

Photolabeling of both proteins was characterised by tight nucleotide binding (Kd(TNP-$8N_3$-ATP) = 0.8 – 2.6 μM and Kd($8N_3$-ATP) = 37 μM), with efficient derivatization (close to

mol/mol) at acidic pH (pKa = 6.8 and 7.8 for sNBD2 and LNBD2 respectively) in the absence of Mg^{2+}. The labeling of both proteins with both probes at acidic pH was completely inhibited by ATP. These characteristics strongly suggest that the isolated domains have a properly constituted ATP site and yet important differences between it and the whole protein – assuming the yeast pumps are suitable models - are apparent.

Unexpectedly, short and long NBD2s behaved very similarly. In order to appreciate why this is surprising, one needs to discuss it in the context of the structure of the ATP binding subunit of the bacterial HisP.

The crystal structure of the nucleotide binding subunit of the ABC transporter, histidine permease (HisP), became available in late 1998 (Hung *et al.*, 1998). The membrane-bound complex of the prokaryotic histidine permease is composed of two hydrophobic subunits, HisQ and HisM, and two identical, soluble ATP-binding subunits, HisP. Transport of histidine is energized by ATP hydrolysis. The soluble histidine binding protein, HisJ, in the periplasm binds to HisQ and HisM, inducing ATP hydrolysis by HisP and transport of histidine into the bacterium. Proteins of the ABC family demonstrate extraordinary redundancy, for example the bacterial antibiotic-resistance protein, LmrA, is completely functionally interchangeable with human p-gp MDR1. Therefore HisP could be a good model for mouse NBD2. An alignment of amino acid sequences of mouse NBD1 and NBD2 with HisP is shown in Fig 10.1 below.

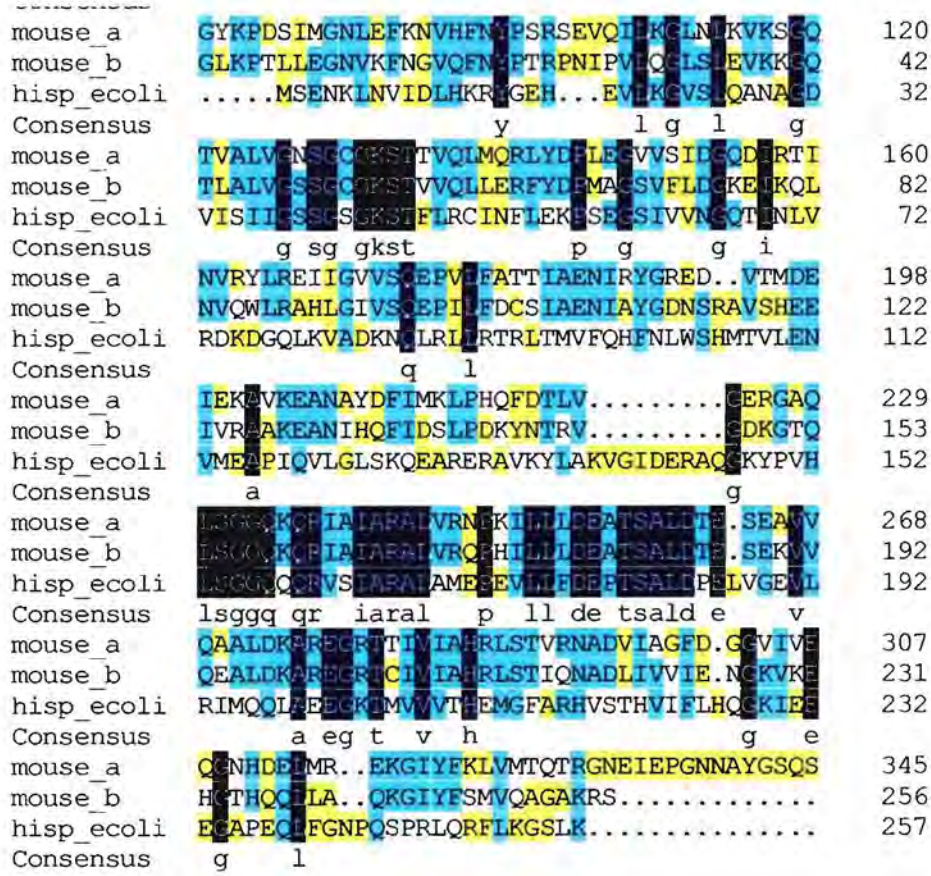

Figure 10.1. An alignment of amino acid sequences of mouse NBD1 and NBD2 with HisP.

The alignments were done with DNAMAN (ver 4.13, Lynnon BioSoft, USA), initially automatically but with some manual adjustments. This was guided by a similar alignment done by A. Di Pietro using Network Protein Sequence @nalysis (NPS@) in Lyon, France (personal communication). Several amino acids are highly conserved and most of the amino acid changes are conservative. Even outside of the Walker A and B motifs and the conserved linker peptide there are several completely conserved amino acids and only 3 or 4 small gaps. Many of the secondary structural elements of HisP can be found in mouse NBD2. An energy minimised structure of LNBD2 (coordinates from Di Pietro, Lyon, France and structure reproduced here with kind permission), using HisP as a template is shown in Fig 10.2a, alongside the HisP structure, Fig 10.2b. The conserved α-helices 1 (shown in yellow) have been orientated in similar positions for ease of comparison. It can be seen that most of the secondary elements are almost the same in both structures, however one can see differences in their overall positions resulting in a change from the L-shape of HisP to a V-shape of the energy minimised LNBD2 (compare distances between bottom loops).

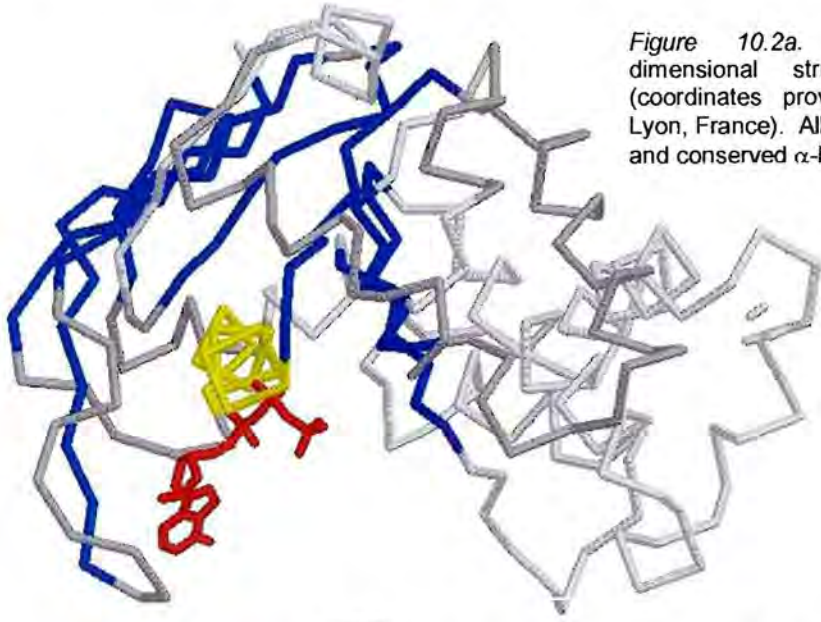

Figure 10.2a. Postulated 3-dimensional structure of LNBD2 (coordinates provided by Di Pietro, Lyon, France). All β-strands are in blue and conserved α-helix one in yellow.

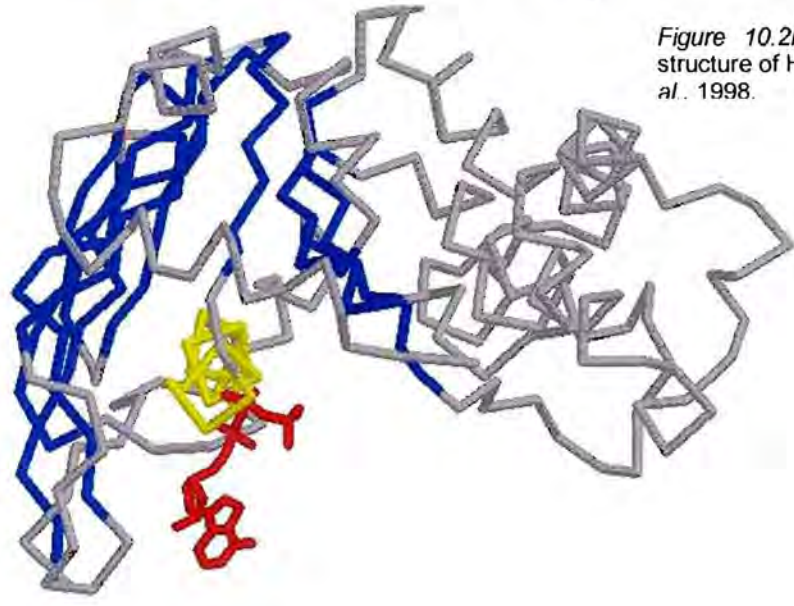

Figure 10.2b. Backbone 3-dimensional structure of HisP as determined by Hung *et al*. 1998.

The shorter NBD2 (sNBD2) had substantial sections missing from the HisP structure. This is shown in Fig 10.3, where the HisP structure (Fig1.14, p 24) is compared with a similar structure but with the missing sections of sNBD2 painted out.

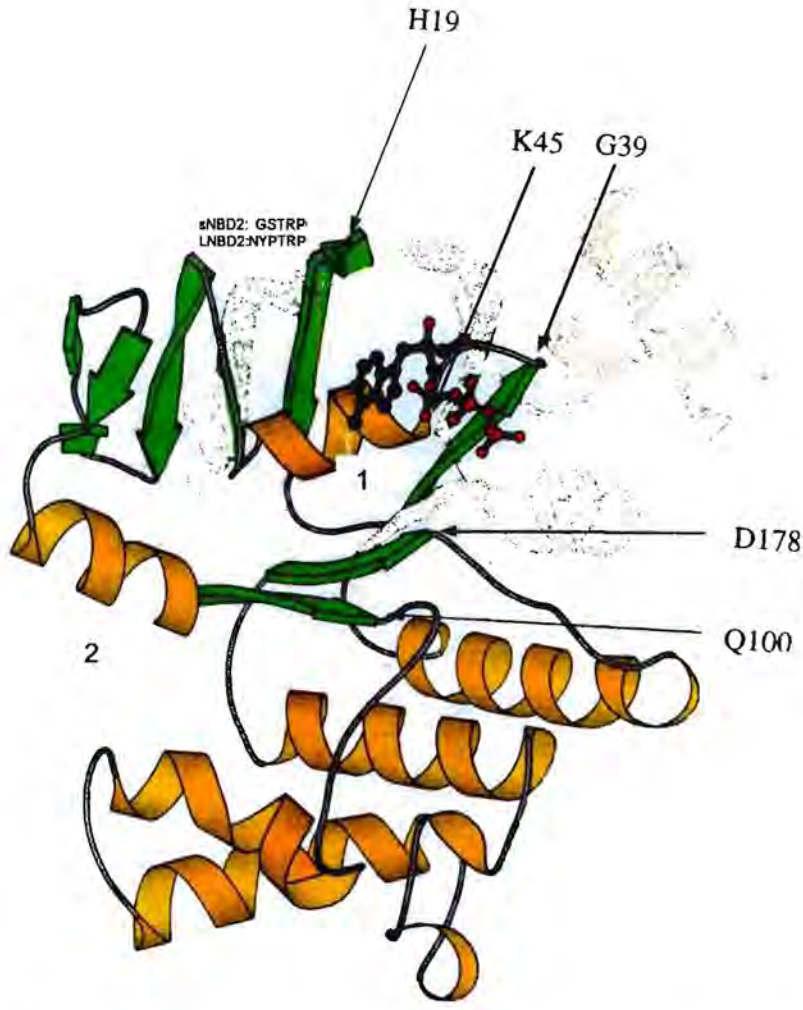

Figure 10.3. The 3-dimensional structure of HisP with the missing parts of mouse sNBD2 painted out (adapted from Hung *et al.*, 1998). Bridging α-helices 1 and 2 are labeled.

On the N-terminal end, β-strand 1 is missing. Note that the N-terminal end of sNBD2 consists of the residues GS whereas in the native structure of the mouse p-gp we have residues NYP (or RYG in HisP), where the tyrosine residue is that labeled by $8N_3$-ATP in CHO p-gp (Sankaran *et al.*, 1997b). On the C-terminal side, the cut is made just before β-strand 10, which removes 3 β-strands and 3 α-helices. The loss of the central two β-strands of both sheets could be expected to severely compromise the native structure. However, our photolabeling results indicate otherwise.

Both sNBD2 and LNBD2 showed identical or very similar pH dependencies for photolabeling with TNP-$8N_3$-ATP and $8N_3$-ATP. The affinity of sNBD2 for nucleotides appears to be higher

than for LNBD2 (Kd(TNP-8N_3-ATP) = 0.8 and 2.6 μM, Ki(ATP) = 1 and 2.7 mM, respectively). The Kd value for ATP binding to whole mouse p-gp (MDR3) is approximately 10 mM (Lerner-Marmarosh *et al.*, 1999), indicating that the binding to sNBD2 is significantly tighter. It is interesting that TNP-ATP binds with similar affinity to the whole mouse protein as TNP-8N_3-ATP to LNBD2 (Kd = 2.7 μM and 2.6 μM , respectively). However, again one needs to bear in mind that the conformation of the TNP nucleotides differs around the glycosidic bond. Another difference between sNBD2 and LNBD2 was the Triton X-100 sensitivity of the photolabeling of sNBD2. Low concentrations of Triton X-100 (< 0.01 %) enhance labeling of sNBD2 2-fold whereas LNBD2 was insensitive. This indicates that monomeric Triton X-100 (critical micelle concentration approximately 0.2 %) binds to the shorter protein and possibly increases the efficiency of labeling by stabilising the ATP site. This may come about by two detergent molecules fitting in the structure where the two central β-strands are missing, stabilising the flanking sheets. β-strands 11 and 12 may also be replaced by detergent. The extra labeling is not due to an affinity change by detergent, because a high concentration of 50 μM TNP-8N_3-ATP was used in the experiments and initial photolabeling data in the absence of Triton X-100 displayed a similar TNP-8N_3-ATP concentration dependence as with the detergent (latter data not shown). These results leave one no option but to conclude that the nucleotide binding site of sNBD2 is largely correctly constituted.

There seem to be two possibilities. The 3-dimensional structure of HisP indicates that α-helices 1 and 2 are "bridges" connecting the two β-sheets, with α-helix 1 assuming a central position between the two β-sheets and with α-helix 2 more peripheral. Both of these helices are present in sNBD2 (see Fig 10.3). The one end of α-helix 1 and the loop connecting it with β-strand 4 interacts with α-helix 2 and β-strands 8 and 9 (Fig 10.4).

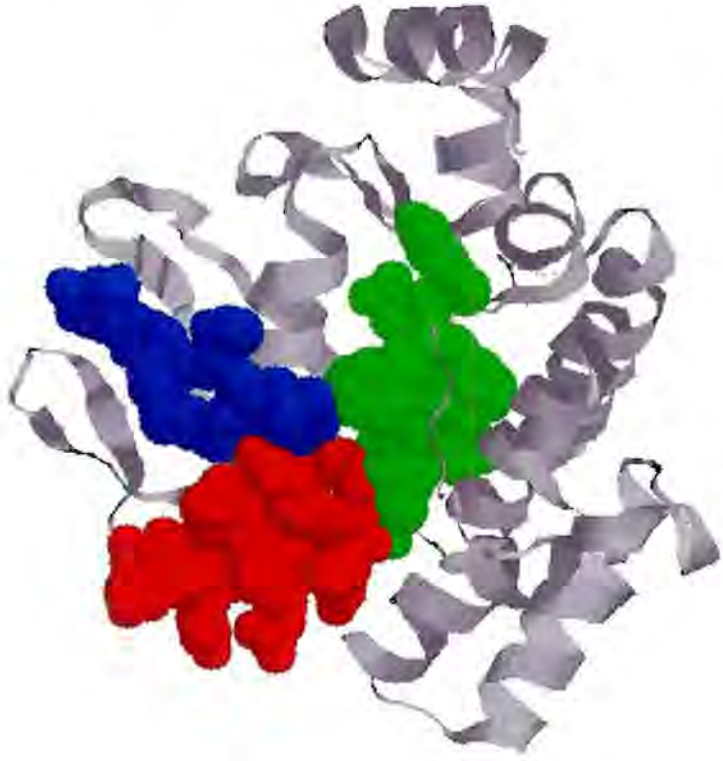

Figure 10.4. 3-dimensional structure of HisP, showing the loop connecting α-helix 1 with β-strand 4 in blue, α-helix 2 in red and β-strands 8 and 9 in green.

The interactions between the two α-helices and the rest of the protein may be sufficient to stabilise the correct abuttment of the C-terminal half of sNBD2 with the N-terminal half even in the absence of β-strand 2 and β-strands 10-12, such that the ATP site remains intact. The Mg^{2+} site may be disrupted by virtue of the fact that the membrane section of the whole protein is missing in the recombinant sNBD2. This will be enlarged upon later, especially with regard to LNBD2.

A second possibility is that the ATP site is constituted entirely from the N-terminal half and the C-terminal half is superfluous and indeed need not be properly folded. The lack of interaction of bound ATP with the C-terminal half of HisP is clearly seen in Fig 1.13 (p 23), where α-helices 3-9 are contained in the top half of the picture completely separate from the nucleotide. It is this top portion that is postulated to interact with the membrane section (Petronilli and Ames, 1991). In this second possibility it is not difficult to understand how the Mg^{2+} site is disrupted as this appears to be formed by residues from the end of β-strand 9.

Positioning of the nucleotide in sNBD2 and LNBD2

All the amino acids of HisP interacting with ATP as elucidated by Hung *et al.*, are shown in Fig 10.5. The adenine moiety is mostly complexed with water molecules, but does sit on a single amino acid, Tyr^{16} (green). The ribose 2'-oxygen is complexed with water, while the 3'-oxygen interacts with His^{19} (yellow). The phosphate tail of ATP interacs with the P-loop main chain amides, stretching from Ser^{41}-Thr^{47} (Ser^{41}, blue; Gly^{42}, orange; Ser^{43}, purple; Gly^{44}, green; Lys^{45}, yellow; Ser^{46}, purple; and Thr^{47}, blue). The putative amino acids important for Mg^{2+} complexation and ATP hydrolysis are also shown – Gln^{100} (green), Asp^{178} (orange), Glu^{179} (purple) and His^{211} (yellow).

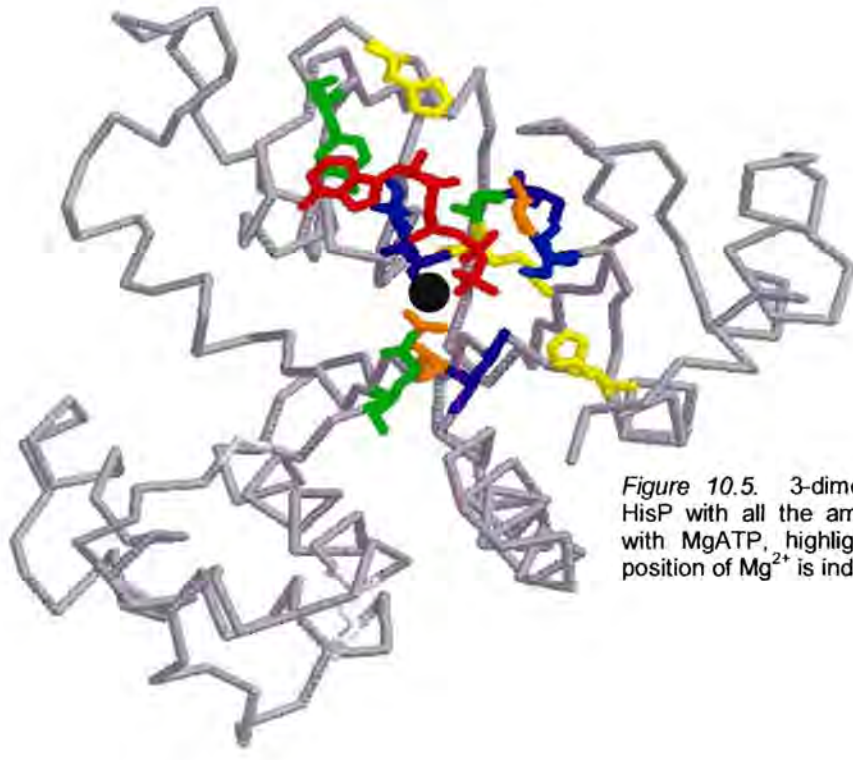

Figure 10.5. 3-dimensional structure of HisP with all the amino acids interacting with MgATP, highlighted. The putative position of Mg^{2+} is indicated as a black dot.

The position of Tyr^{16} in HisP (Tyr^{1042} in LNBD2), shown by Senior's group to be the main target for $8N_3$-ATP derivatisation in hamster p-gp, is in close proximity to the adenosine moiety (Fig 10.6, green). Flipping the adenine moiety into the expected *syn* conformation of $8N_3$ATP places the azido group in close proximity to the hydroxyl of the tyrosine. Mimura *et al.* photolabeled HisP with $8N_3$-ATP and identified His^{19} (blue) and Ser^{41} (yellow) as derivatized amino acids (Mimura *et al.*, 1990). Ser^{41} forms part of the Walker A consensus sequence in HisP while His^{19}, as indicated above, interacts with 3'-oxygen of the ribose and is located close to Tyr^{16} (Fig 10.6).

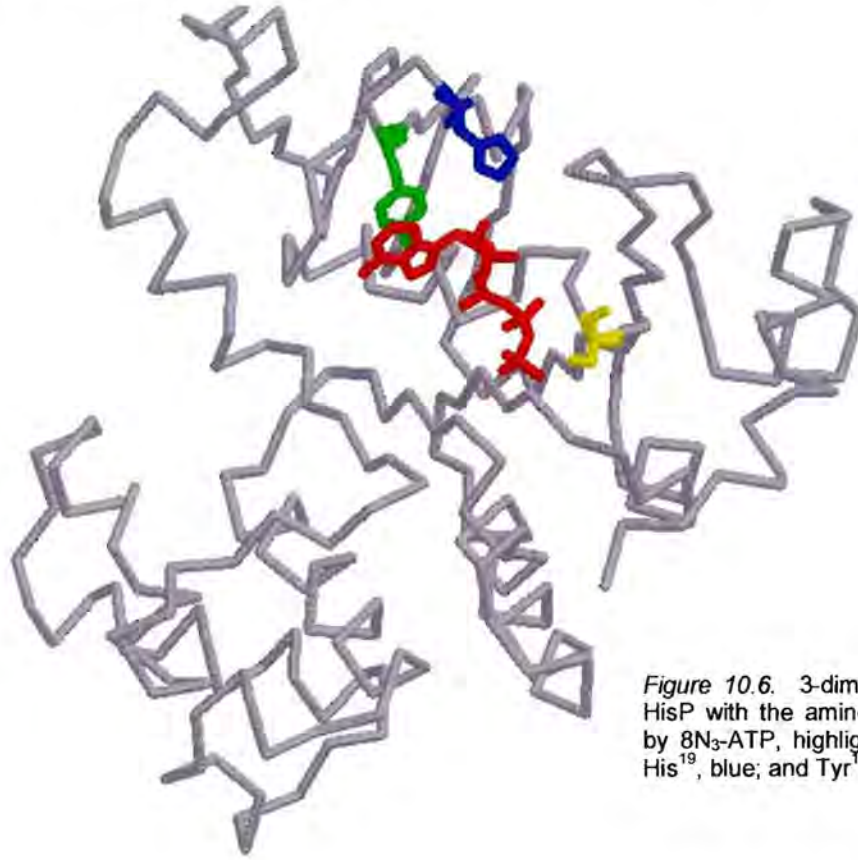

Figure 10.6. 3-dimensional structure of HisP with the amino acids photolabeled by $8N_3$-ATP, highlighted - Ser^{41}, yellow: His^{19}, blue; and Tyr^{16}, green.

Tyr^{16} and His^{19} are not highly conserved in p-gps – the tyrosine is absent from both NBDs of Pdr5p and NBD1 of Yor1p, while the histidine is absent from the mouse, Pdr5p and Yor1p NBDs (Fig 10.7).

```
mouse b     ....................................TE      2
mouse a     TFSIGHLAPNIEAFANARGAAFEIFKIIDNEPSIDSFSTK     80
yor1 b      ....................................MT      2
yor1 a      .....DYELNDAIEEAKGEAKDEGKKNKKKRKDTWGKPSA     35
pdr5 b      ..................SDRKMLQESSEEESDTYGE      19
pdr5 a      ................YNAEADVHLPHLTVFETLVTVAR      23
Consensus
```

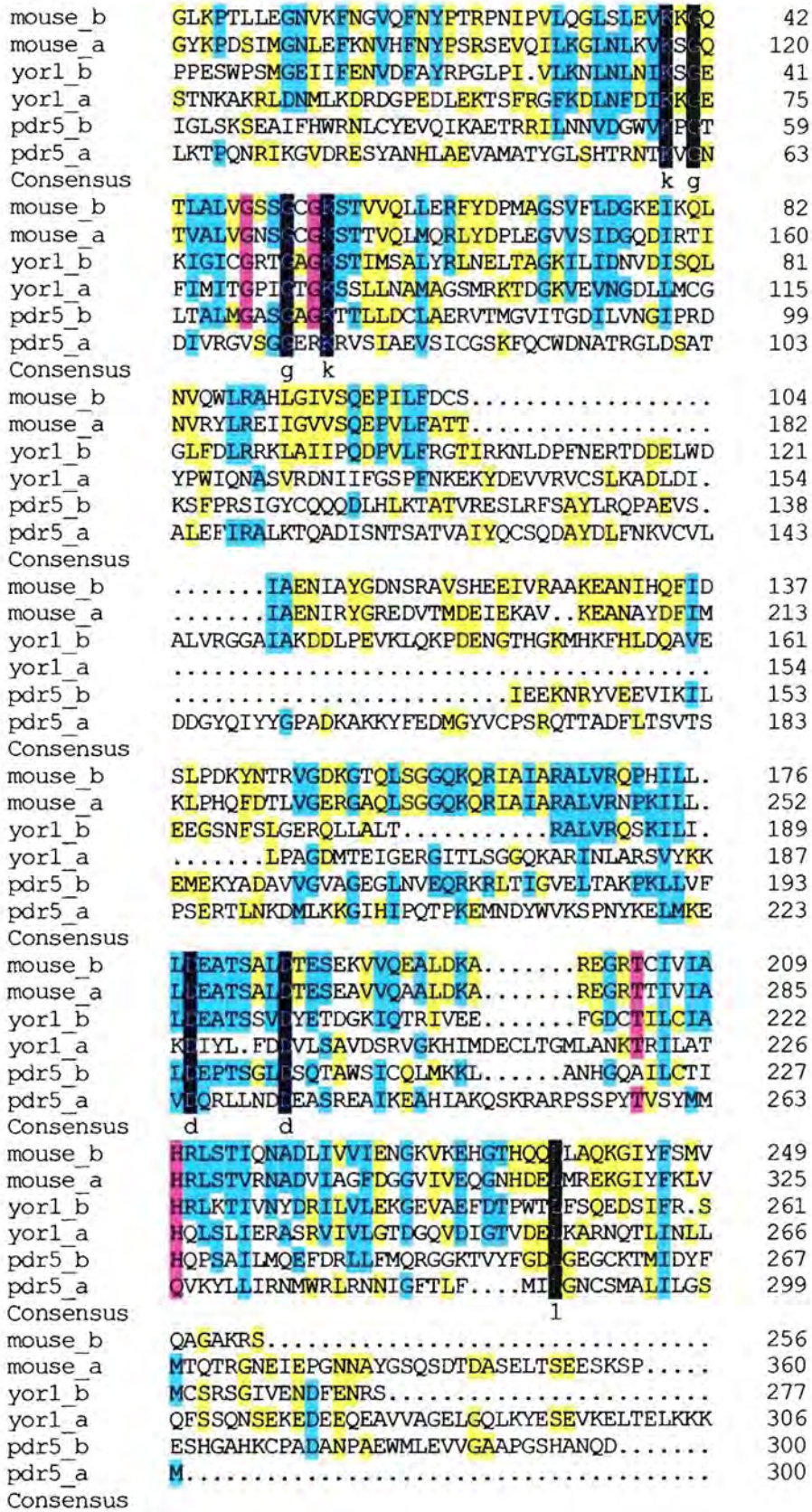

Figure 10.7. Amino acid sequence alignment of NBD1 and NBD2 of mouse p-gp MDR1, Yor1p and Pdr5p.

Photolabeling of Ser^{41} is unexpected, since there is a large distance between the adenosine moiety and this amino acid. It is possible that, since the affinity for ATP is so low for these proteins, the binding of the nucleotide is dominated by the phosphate tail, which allows the adenosine ring to move around fairly freely. Photolabeling of His^{19} is not unreasonable, if again some movement of the adenine is permitted.

The TNP moiety of TNP-$8N_3$-ATP is attached to the hydroxyls of the ribose via a spiro linkage which orientates the TNP ring at right angles to the plane of the furanyl ring. This creates a rigid Miessenheimer complex that is fluorescent. In the proposed crystal structure of NBD2, the ribose hydroxyls of ATP are orientated outwards from the structure pointing in the direction of a groove formed between the ends of the two β-sheets. This is well illustrated in Fig 10.8 where Ile^{18} (purple) and Asn^{216} (green) arising from β-sheet 1 and 2 respectively are highlighted. The ribose appears to be tilted towards β-sheet 1 rather than 2 and interactions with the former may dominate. This is borne out by the tighter binding of TNP-$8N_3$-ATP to sNBD2, which has the end of β-sheet 2 missing and hence Asn^{216}. One side of the groove may also arise from the P-loop (shown in turquoise), obviating the need for β-sheet 2.

Figure 10.8. The putative 3-dimensional structure of LNBD2, highlighting the amino acids that possibly flanks the TNP moiety; Ile^{18} in purple and Asn^{216} in green. The P-loop is shown in turquoise.

The amino acid(s) derivatized in mouse sNBD2 and LNBD2 by TNP-$8N_3$-ATP could not be identified during the course of this program. This can be attributed to several factors. Both

the recombinant proteins were very hydrophobic which made them difficult or impossible to manipulate using standard digestion and purification procedures formerly followed in our laboratory. Initially, the recombinant proteins were expressed as fusion proteins, without a His tail, that required precipitation of the protein after photolabeling to remove photolysis products. Precipitated protein needed to be re-dissolved in 8 M urea and the solubulized protein tended to come out of solution when the urea concentration was lowered below 4-6 M. The recombinant proteins containing His tails allowed affinity chromatography purification using a nickel chelate resin, but had to be denatured in 8 M urea prior to addition to the nickel column, otherwise the majority of the labeled protein bound irreversibly. Few proteolytic enzymes are active at high urea concentrations and thermolysin was the only enzyme of several that were tested, that showed significant activity in 4 M urea. Unfortunately, thermolysin is not very specific and mainly cleaves peptide bonds on the N-terminal side of hydrophobic residues. Nonspecific cleavage obviously tends to produce variable length peptide fragments, which is a serious disadvantage. Since none of the semi-preparative or preparative experiments done on the sNBD2, which did not contain a His tag, were reproducible, it was also considered that the concentration of protein during digestion could influence the outcome of digestion. Precipitation of sNBD2 by dialysis and repeated washing of the precipitate to remove the photolysis products, could lead to inconsistent yields of protein for each experiment, leading to different digestion products. Elution of LNBD2 from a nickel column appeared to be more quantitative as a series of experiments done with 0.5 mg protein/ml (protein concentration during photolabeling) yielded reproducible digestion products. To complicate matters further, the Ca^{2+}, that is mandatory for thermolysin activity, catalyses the hydrolysis of the phosphates of the attached TNP-$8N_3$-ATP derivative, causing the triphosphate to be converted into the di- or monophosphate – each of these having different elution characteristics. There is evidence of tight binding photolysis products, but these are mostly eliminated by repeated washing steps. All of the above could contribute to the complicated TNP profile seen after HPLC analysis of the digest.

In cases where some larger peaks were successfully carried through to a purified species, no amino acids were detected by standard sequencing (Edman degradation followed by HPLC analysis of PTH amino acid derivatives). This could be due to the small amount of TNP-peptide, a single amino acid or a very short peptide, or because the particular amino acids in the peptide do not have a high PTH yield (serines, threonines, lysines and arginines were sometimes problematical amino acids at the sequence facilities at UCT). In order to overcome these difficulties, MALDITOF analysis of purified peptides was attempted since much lower concentrations of peptide can potentially be detected and the peptide length is of less consequence. Analysis of TNP-ATP, TNP-$8N_3$-ATP, TNP-AMP and TNP-adenosine showed that each of these could be detected by MALDITOF, but several peaks were produced from the first three nucleotides whereas a single prominent peak was found for the TNP-adenosine. It seems that the presence of the phosphates lower the yield and

complicates the mass spectrum. It appears that a worthwhile protocol may be developed in the future in which the phosphates could be cleaved from the TNP-peptide using alkaline phosphatase, perhaps immediately before analysis of the digest by HPLC. This would also solve the problem of variable phosphate species (tri, di or mono-phosphates).

While the amino acids(s) photolabeled in Pdr5p, sNBD2 and LNBD2 could not be identified, some speculation is warranted. Considering the yeast pumps first, we find that Yor1p possesses the tyrosine in NBD2 labeled with $8N_3$-ATP in hamster p-gp by Senior's group, but not in NBD1. In the alignments shown before (Fig 10.7), Pdr5p does not appear to have a tyrosine in this position. However, there is a tyrosine three amino acids residues to the left in NBD2. A re-analysis in which this tyrosine is aligned with the labeled one in mouse NBD1, is shown as follows:

```
                *
Mouse NBD1:  G N L E F K N V H F N Y P
Pdr5p NBD2:  S E A I F H N R N L C Y E
```

This repositioning seems quite feasible since three amino acids align perfectly and three align conservatively, but it does mean that the loop following YE and preceding β-strand 2 would be larger. It is interesting that if this is the case both yeast pumps may only be photolabeled at the NBD2 and not NBD1, which may prove useful in future functional studies.

In HisP, His^{19} and Ser^{41} appear to be preferentially targeted by $8N_3$-ATP, rather than Tyr^{16} (Mimura *et al.*, 1990). As mentioned before, the equivalent histidine is missing in the yeast pumps, being replaced by glycine and lysine in Yor1p and glutamine and valine in Pdr5p. The hydrophobic residues (glycine and valine) are unlikely to be labeled because they are poor nucleophiles. The other two residues are possibilities but a lysyl-nitrene linkage is known to be unstable (McIntosh *et al.*, 1992) and we have found that the linkage in the case of p-gp is stable over several days at 4 °C. The other labeled residue in HisP, namely Ser^{41}, is present in Pdr5p and NBD2, and Yor1p has a threonine in this position in NBD2. However, while the adenosine in $8N_3$-ATP may be mobile in the binding pocket as discussed above, this is unlikely for TNP-$8N_3$-ATP because of the inflexible spiro linkage as well as the positive contribution the TNP moiety makes to the binding energy. Overall, the tyrosine may be the most likely candidate as the photolabeled target.

In the case of the mouse sNBD2, the equivalent residue to HisP Tyr^{16} and His^{19} are missing and are therefore not in contention. As can be seen from the putative structure of sNBD2 presented previously (Fig 10.3), the thrombin cleavage site introduced a glycine in this position. This is the last residue on the N-terminal end (GSTRP..) and is likely to be unstructured and mobile. HisP His^{19} is replaced by an arginine residue in mouse NBD2 and is a possible target, especially as it's length may bring it into proximity with the azido group.

HisP Ser^{41} is present in the mouse sequence, but for reasons given above it is an unlikely target for TNP-$8N_3$-ATP, but may be for $8N_3$-ATP.

Interestingly, the structure of RbsA, the ATP binding subunit of a bacterial ribose transporter, contains another tyrosine residue interacting with the adenine moiety of ATP (information supplied by A. Di Pietro from the work of C.S. Stauffacher). The equivalent residue in the mouse sequence is Tyr^{1085} and is positioned between α-helix 1 and β-strand 4, as shown in Fig 10.9 (shown in blue, the other tyrosine of LNBD2 is shown in green). It can be seen that this tyrosine is also well positioned to react with the azido group and could be a strong contender for nitrene interaction, at least for sNBD2. This tyrosine is missing from the yeast pumps.

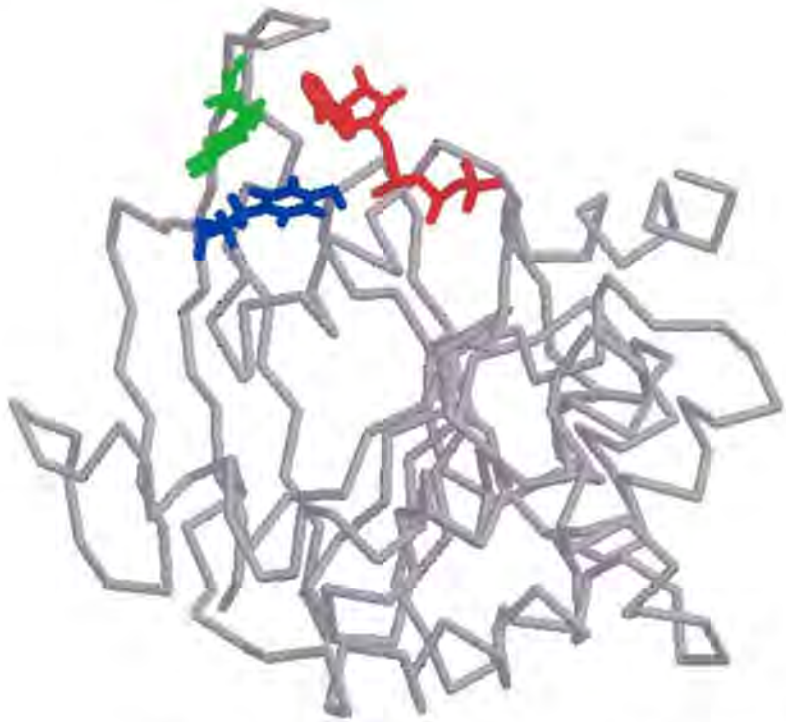

Figure 10.9. The putative 3-dimensional structure of LNBD2 with Tyr^{1042} (green) and Tyr^{1085} (blue) are highlighted.

pH effects

Photolabeling of mouse sNBD2 and LNBD2, as also seen for the yeast pumps, are maximal at acidic pH. As discussed before, this trend is unexpected because all ionised amino acids are better nucleophiles at alkaline pH (e.g. –OH → OH^-, His^+ → His, NH_3^+ → NH_2). And, as also elaborated on before, the dependence cannot be linked to protonation of the TNP-$8N_3$-ATP nucleotide in the presence of Mg^{2+}. This suggests that the pH dependence may be related to ionisable groups at the ATP site itself. Since the pH dependence is similar (in the presence of Mg^{2+}) for all the proteins used in this study, a conserved amino acid would be a likely candidate. Sequence alignments of mouse, Yor1p and Pdr5p NBD1 and NBD2 show two conserved lysine residues in and next to the Walker A motif and two conserved aspartic acids and a conserved histidine in and close to the Walker B motif (see Fig 10.7). The first

conserved lysine in the Walker A motif interacts with two oxygens on the β-phosphoryl group. The second is positioned just after β-strand 2 and could play a crucial role in positioning of α-helix 1 which forms the bed of the ATP site (Fig 10.10).

Protonation of either lysine could influence the interaction of the activated azido group with its

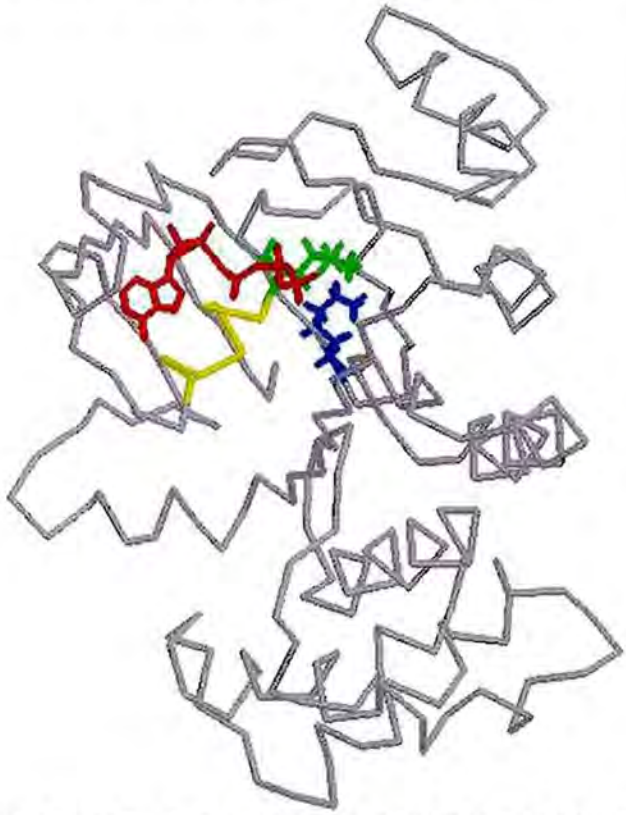

Figure 10.10. The two conserved lysines (Lys ^{1060}, blue; and Lys ^{1074}, green) may play a role in the pH dependent photolabeling of mouse NBD2, Yor1p and Pdr5p. α-Helix one is shown in yellow.

targeted residue. A pKa shift from pH 8.95 to pH 6.8 - 7.5, for an active site residue, is not unusual. The conserved aspartates seem less likely because they are further away from ATP, and perhaps are not correctly configured in sNBD2, and a pKa shift of 3 units from 3.86, to 6.8 - 7.5 is rather large. A conserved histidine is situated in close proximity to the phosphate tail of the ATP in the putative structure of LNBD2 (Fig 10.11).

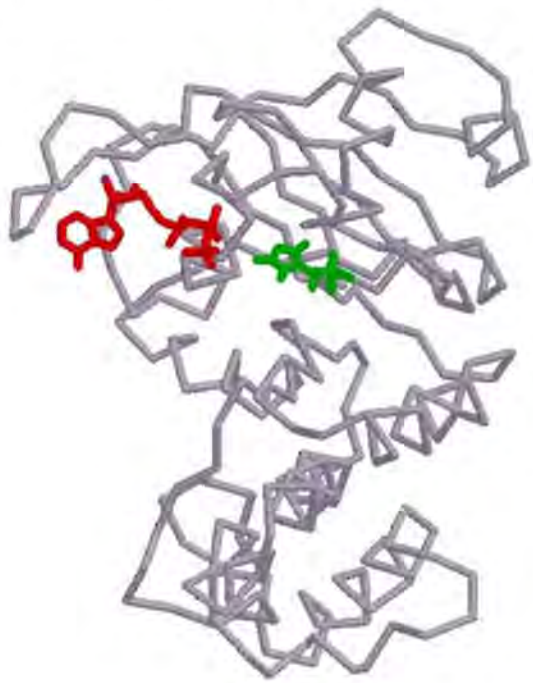

Figure 10.11. The conserved histidine, absent from sNBD2.

Protonation of this side chain could also promote binding of the negatively charged phosphate groups. However, sNBD2 does not contain His^{1230}, making a role for this histidine in the pH dependence less likely. We favour the possibility that the two conserve lysine residues are responsible for the pH dependent photolabeling of the p-gps and isolated NBDs.

NEM derivatisation

NEM derivatization of both sNBD2 and LNBD2 prior to photolabeling did not prevent photolabeling with either [γ-^{32}P]8N_3-ATP or [γ-^{32}P]TNP-8N_3-ATP, supporting previous findings that sulfhydryl modifying agents like NEM, NBD-Cl and MIANS do not compete with ATP for the same binding site on the NBD (Loo *et al.*, 1995, Liu *et al.*, 1996, Senior *et al.*, 1999). In the putative structure of LNBD2 (and HisP, not shown), a possible binding pocket/groove is located to the right of, and in close proximity to, the ATP binding site (Fig 10.12, shown with an arrow). Binding here of – SH reactive reagents need not interfere with ATP binding. However, it appears that the reverse is not true as ATP binding blocks NEM derivatisation (Al-Shawi *et al.*, 1994). A fact which can only be explained by ATP inducing a conformational change which covers the –SH group. In the case of sNBD2, which lacks the terminal 2 β-strands and α-helices, there may not be a binding pocket as such and the reaction may take place similar to a free sulphydryl.

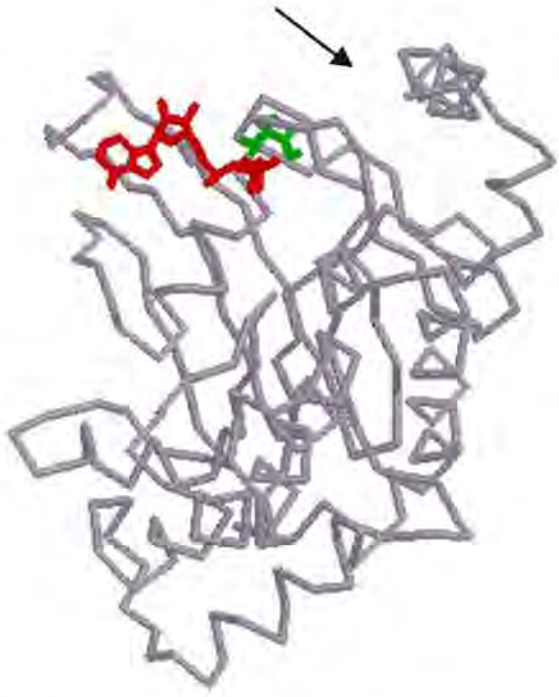

Figure 10.12. The putative 3-dimensional structure of LNBD2 showing the postulated NEM binding pocket (arrow) and the amino acids that interacts with NEM, Cys^{1072}.

An interesting outcome of the NEM labeling experiments, a procedure which involved lengthy incubation at pH 8.5 at 23 °C, was that the longer the incubation of control protein the less the photo labeling. This strongly suggests that denatured NBDs, which can be expected to arise

with increasing time of incubation, do not label efficiently and provides compelling evidence that the recombinant NBDs are, prior to incubation, properly folded.

Mg^{2+} effects

Full length yeast proteins Pdr5p and Yor1p – as well as human MDR1 p-gp (Hrycyna *et al.*, 1999) – are efficiently photolabeled by TNP-$8N_3$-ATP and/or $8N_3$-ATP only in the presence of Mg^{2+}. In contrast, photolabeling of the recombinant mouse proteins do not require Mg^{2+}, and in fact Mg^{2+}, at relative high concentrations, is inhibitory. The failure to label the whole pumps in the absence of Mg^{2+} is not due to poor nucleotide binding. ATP binding to mouse MDR3 is not Mg^{2+} dependent and Mg^{2+} actually lowers the affinity for TNP-ATP and TNP-ADP (Lerner-Marmarosh *et al.*, 1999). This latter negative effect of Mg^{2+} on the binding of TNP-nucleotides is similar to the lowering of affinity seen with the photolabeling of sNBD2 and LNBD2 with both TNP-$8N_3$-ATP and $8N_3$-ATP.

The fact that the recombinant proteins do not require Mg^{2+} for photolabeling indicates that the Mg^{2+} site is at least partially disrupted. This is not entirely unexpected for sNBD2, since the amino acids postulated to interact with bound Mg^{2+} in the HisP structure, either directly (Asp^{178}) or indirectly through water molecules (Glu^{179} and Gln^{100}), are located in the β-strands adjacent to the missing β-strand 10. However, another possibility is discussed below in relation to LNBD2.

In the case of LNBD2, all the amino acids of HisP are contained in this recombinant protein. Therefore, one could expect that the entire domain is folded correctly and this is substantiated by the complete inhibition of photolabeling by several nucleotides. However, the different Mg^{2+} effects from the whole protein suggest that something is disrupted at the Mg^{2+} site, a finding compatible with the inability of the recombinant protein to hydrolyse ATP (Baubichon-Cortay *et al.*, 1994). The reason for these differences may lie in the fact that the soluble recombinant NBDs are not linked to the membrane section. Coupling of drug transport to ATP hydrolysis must require linking of conformational changes in the NBDs, brought about by the binding/hydrolysis of ATP, to the translocation of the drug through or along the membrane helices in the TMD. This is well supported by findings that wild type HisP, in reconstituted proteoliposomes as $HisQMP_2$, displayed undetectable ATPase activity in the absence of histidine, indicating obsolete coupling of transport to hydrolysis, while mutations in the membrane interacting part of HisP (top part of protein in Fig 1.13), uncouples ATP hydrolysis from regulatory control by HisJ (Petronilli *et al.*, 1991 and Hung *et al.*, 1998). The modular structure of the bacterial ABC transporters suggest that the NBDs, such as HisP and RbsA, binds by means of simple association with the three fairly large cytoplasmic loops of the membrane section (between TM8 and 9, TM10 and 11 and following TM12 to the start of NBD2). Mutations in the long arm (C-terminal half) of HisP mentioned above, facilitate the dissociation of HisP from the other subunits, showing the interaction energy is less. It is worth

emphasising again that in the native protein, HisJ binding complexed with histidine is an absolute requirement for ATP hydrolysis and of histidine pumping. It is clear that these interactions play a pivotal role in energy transduction. It is not inconceivable that the proper constitution of the Mg^{2+} site is dependent on this interaction. This is an extremely exciting possibility as it would explain the abnormal Mg^{2+} effects of the recombinant protein and indicate a close tie between the Mg^{2+} site and interaction with the membrane section which harbour the drug binding site(s).

Flavonoid binding to the ATP binding site of sNBD2 and LNBD2

Flavonoids constitute a large and diverse pool of plant metabolites that are being intensely investigated because of their suitability as a scaffold to drug diversity and because some have been shown to interact with ATP sites. In this study, a group of 31 flavonoids, consisting of various flavonols (1), chalcones (2) and chrysins (3) (Fig 10.13), was screened for inhibition of photolabeling of the recombinant mouse NBDs with TNP-8N_3-ATP and 8N_3-ATP.

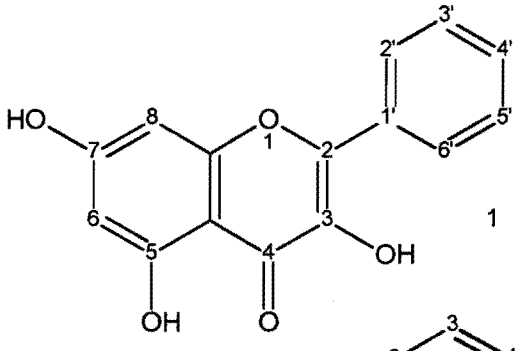

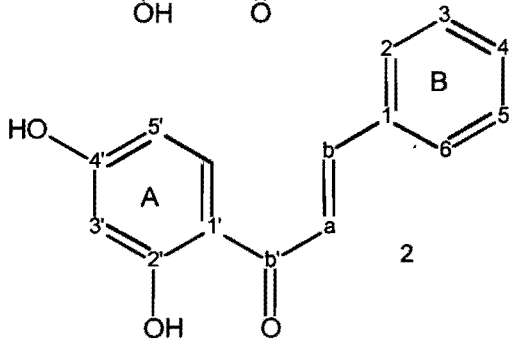

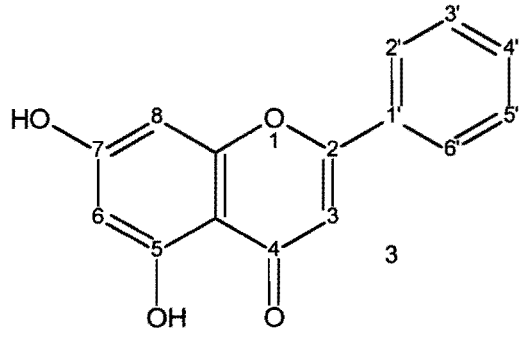

Figure 10.13. Structures of the different classes of flavonoids studied here: flavonols (1), chalcones (2) and chrysins (3)

Many elaborations on these basic structures were explored and found not to be tolerated, and out of these, four flavonoids prevented photolabeling in the micromolar range and may show some promise as reversers of multidrug resistance. This pattern with the same four, was repeated with both sNBD2 and LNBD2 and with both probes, at pH 6.0 and pH 8.5, in the presence and absence of Mg^{2+}. The four were kaempheride ($Ki_{(av)}$ = 2.4 μM), broussochalcone A ($Ki_{(av)}$ = 2 μM), galangine ($Ki_{(av)}$ = 17 μM) and dehydrosilybin ($Ki_{(av)}$ = 37 μM) (Fig 10.14).

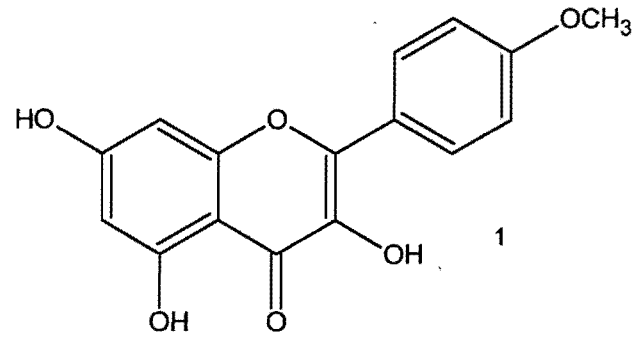

Figure 10.14. The chemical structures of kaempheride (1), broussochalcone A (2), galangine (3) and dehydrosilybin (4).

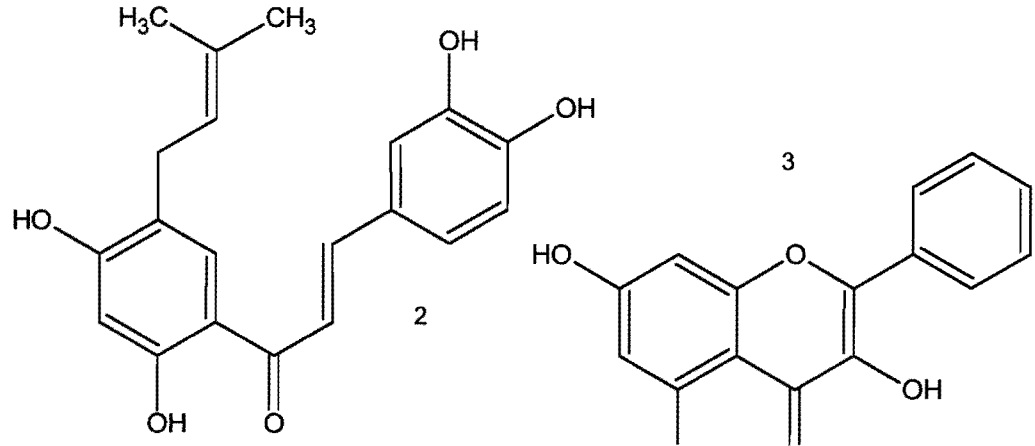

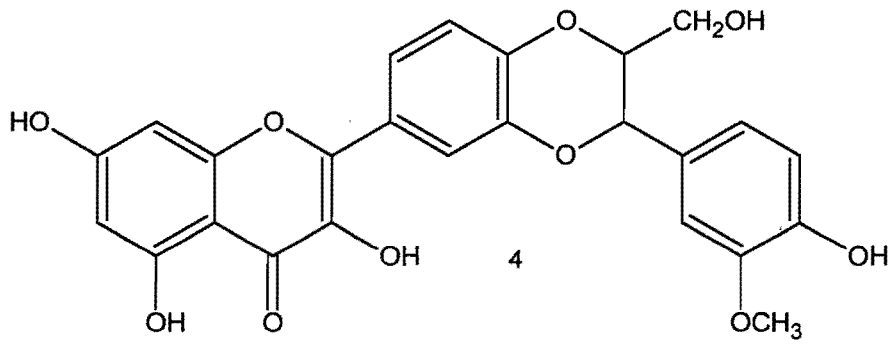

Interestingly, in the case of the two flavonoids that were studied more intensively, namely kaempheride and broussochalcone A, the binding to sNBD2 was approximately 10-fold tighter than to the LNBD2 which mimics what was found for TNP-8N_3-ATP and ATP binding to sNBD2 compared with LNBD2. In terms of the architecture of the ATP site and future drug development, knowledge of the flavonoids that did not bind to the ATP site may be as important as knowing those that did.

A discussion of these results may be facilitated by reference to Fig 10.15. Virtually all compounds tested here had hydroxyl groups at positions 5 and 7 of ring A. Compounds with (flavonols, e.g. galangine) or without (chrysins) the 3 hydroxyl on ring C, and some lacking this hydroxyl as well as the oxygen at position 1 (chalcones) were tested.

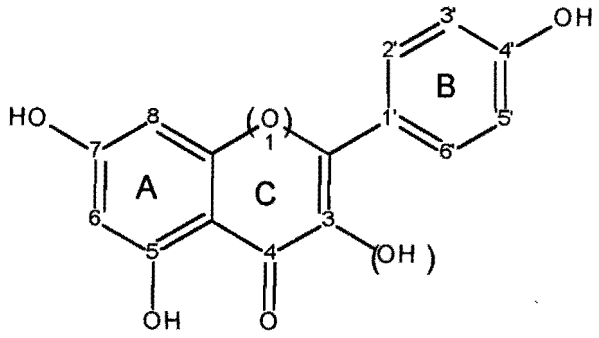

Figure 10.15. A general scaffold structure of compounds tested in this study.

None of the twelve chrysins had any effect on photolabeling indicating that they do not bind to the ATP site and highlighted the importance of the 3-OH for interaction with the ATP site. Chrysin itself binds to NBD2 of *Leishmania tropica* with Kd = 17.5 μM (Perez-Victoria *et al.*, 1999). Interestingly, many of the chrysin derivatives used in our study bind in the nanomolar range to mouse NBD2 (A. Di Pietro, personal communication). Therefore, importantly, there must be another flavonoid binding site, besides that of ATP, on the NBD.

In the case of the eight chalcones, which have an open ring C and lack the 3-OH, only broussochalcone A inhibited photolabeling. The lack of inhibition by the others again points to the importance of the 3-OH. The reason why broussochalcone A is the exception may be because it has a hydroxyl on ring B. Ring B may swivel such that the hydroxyl occupies the same position as the 3-OH of ring C in the ATP site. This may be possible because of the opening of ring C and increased flexibility around the carbonyl.

Galangine, with hydroxyl groups at positions 3,5, and 7 inhibited photolabeling. Elaborations at position 6 and 8 were not tolerated. An elaboration at the 4' position (OCH_3, kaempheride) was acceptable. A finding which prompted exploration of a group of compounds called dehydrosilybins which link to the 4' and 5' position of ring B. The dehydrosilybins have large extensions to the 4' and 5' positions including a cyclised ether and methoxy phenol. Excitingly, dehydrosilybin inhibited photolabeling, showing that these large extensions to the B ring were accommodated at the ATP site. Hydrophobic elaborations on the 6 and 8 positions of ring A, as for the galangines, were not tolerated. It is noteworthy that reducing the double bond between position 2 and 3 of ring C, producing silybin, destroys the ability to bind to the ATP site. A similar detrimental effect of such reduction has previously been found in the binding of naringenin versus apigenin (Conseil *et al.*, 1998). However, the latter binding may be at a site other than the ATP site as apigenin lack the 3-OH. The existence of a flavonoid binding site distinct from the ATP binding site on the NBDs of p-gps had been proposed and is supported by the evidence presented here.

The structure that emerges from these studies is fairly straightforward and illuminating. The basic structure of the flavonoid, epitomised by galangine, binds at the ATP site fairly tightly,

approximately 100 fold tighter than ATP. Hydroxyl groups at the 3,5 and 7 positions of ring A and C seem favourable. That at the 3 position is essential. No hydrophobic elaborations are tolerated on either of these rings. The double bond between C2 and 3 is also essential and this may relate to the electronegativity of the 3-OH, perhaps it is even required to be ionised. Ring B is the only direction in which extensions are possible, and they may be very large, (dehydrosilybins), pointing to the existence of a binding pocket/groove in this direction.

Considering the ATP binding site of HisP again the adenine mainly interacts with water molecules and a tyrosine, the ribose with a histidine and a water molecule, and the phosphates with five main chain amines (Ser41-Lys45) and water molecules. Positioning of the flavonoids is obviously guesswork, but there are two grooves emanating from the ATP site, one that we postulate to accommodate the TNP moiety and the other the maleimide moiety, either of which may accommodate the silybins extensions. In either case, the rest of the flavonoid nucleus is positioned approximately where the adenosine moiety lies. We considered that the all important 3-OH may then interact with one of the amides of the P-loop. Other hydroxyls may do the same and may provide the added binding energy.

A second flavonoid binding site

Of great significance is the finding that many hydrophobic flavonoids, in particular many prenylated chrysins, which have been shown to bind tightly to the isolated NBD2 (A. Di Pietro, personal communication), do not bind to the ATP site. This means that there is a second flavonoid binding site on the NBD. Several of these more hydrophobic flavonoids reverse multidrug resistance in Leishmania parasites (Perez-Victoria *et al.*, 1999). A steroid binding site has been found to overlap or be adjacent to the ATP site (Conseil et al., 1998). It seems an exciting possibility that such hydrophobic pocket neighbouring the ATP site may be utilised to design more efficacious nucleotide based inhibitors of human p-gp.

Characterization of ANP-AMP and ANP-TNP-AMP as photoaffinity probes for mouse LNBD2

The photoaffinity probe 4-azido-2-nitrophenyl phosphate (ANPP) has been used previously to probe the phosphate binding sites of the F1-ATPase, Ca^{2+}-ATPase and the Na^{+}/K^{+}-ATPase (Garin *et al.*, 1989., Lacapere and Garin, 1994., Tran and Farley, 1996). Attaching ANP to AMP could yield a photoprobe for the binding site of the phosphate tail of ATP, since the azido group is almost exactly in the position of the end of the gamma phosphate. Addition of the TNP group could also make the binding much tighter, especially in the case of p-gps.

Two new azido-ATP analogues – 4-azido-2-nitrophenyl adenosine monophosphate (ANP-AMP) and 4-azido-2-nitrophenyl-2',3'-O-(2,4,6-trinitrophenyl) adenosine monophosphate (ANP-TNP-AMP) – were synthesised. Increasing concentrations of ANP-AMP successfully

prevented photolabeling of LNBD2 with [γ-^{32}P]8N_3-ATP, yielding a Ki(ANP-AMP) = 0.55 mM, very similar to that seen for ATP. Similarly, [γ-^{32}P]8N_3-ATP photolabeling of LNBD2 was prevented by increasing concentration of ANP-TNP-AMP, yielding a Ki(ANP-TNP-AMP) = 7.44 μM, again comparable with the Kd(TNP-ATP).

Prelabeling of LNBD2 with ANP-TNP-AMP did, however, not prevent photolabeling with [γ-^{32}P]8N_3-ATP, indicating that although these two new probes do bind to the ATP binding site of LNBD2, the photolabeling reaction as such is not successful. As mentioned in the literature overview, binding of a photoprobe to the active site does not necessarily result in a favourable photolabeling reaction. The azido group on the phenyl ring could be facing away from the protein prohibiting a favourable reaction with a nucleophilic amino acid. These probes may find use in other ATP utilising enzyme systems.

BIBLIOGRAPHY

Al-Shawi, M.K., Urbatsch, I.L. and Senior, A.E. (1994). Covalent inhibitors of P-glycoprotein ATPase activity. *J.Biol.Chem.* **269**, 8986-8992.

Ambudkar, S.V., Cardarelli, C.O., Pashinsky, I. and Stein, W.D. (1997). Relation between the turnover number for vinblastine transport and for vinblastine-stimulated ATP hydrolysis by human p-glycoprotein. *J.Biol.Chem.* **272**, 21160-21166.

Ames, G.F.-L., Mimura, C.S., Holbrook, S.R. and Shyamala, V. (1992). Traffic ATPases: a superfamily of transport proteins operating from *Escherichia coli* to humans. *Adv Enzymol Relat Areas Mol Biol.* **65**, 1-47.

Ashfield, R., Gribble, F.M., Ashcroft, S.J. and Ashcroft, F.M. (1999). Identification of the high-affinity tolbutamide site on the SUR1 subunit of the K(ATP) channel. *Diabetes.* **48**, 1341-1347.

Babenko, A.P., Aguilar-Bryan, L. and Bryan, L. (1998). A view of sur/KIR6.X, K(ATP) channels. *Annu.Rev.Physiol.* **60**, 667-687.

Bakos, E., Evers, R., Szakacs, G., Tusnady, G.E., Wieker, E., Szabo, K., de Haas, M., van Deemter, L., Borst, P., Varadi, A. and Sarkadi, B. (1998). Functional multidrug resistance protein (MRP1) lacking the N-terminal transmembrane domain. *J.Biol.Chem.* **273**, 32167-32175.

Balzi, E., Wang, M., Leterme, S., Van Dyck, L. and Goffeau, A. (1994). PDR5, a Novel Yeast Multidrug Resistance Conferring Transporter Controlled by the Transcription Regulator PDR1. *J.Biol.Chem.* **269,** 2206-2214.

Barron, D. and Ibrahim, R.K. (1996). Isoprenylated flavonoids – a survey. *Phytochemistry.* **43**, 921-982.

Barnes, K.M., Dickstein, B., Cutler, G.B. Jr., Fojo, T. and Bates, S.E. (1996). Steriod transport, accumulation, and antagonism of p-glycoprotein in multidrug-resistant cells. *Biochemistry.* **35**, 4820-4827.

Baubichon-Cortay, H., Baggetto, L.G., Dayan, G. and Di Pietro, A. (1994). Overexpression and purification of the carboxyl-terminal nucleotide-binding domain form mouse P-glycoprotein. Strategic location of a tryptophan residue. (1994). *J.Biol.Chem.* **269**, 22983-22989.

Beaudet, L., Urbatsch, I.L. and Gros, P. (1998). Mutations in the nucleotide-binding sites of P-glycoprotein that affect substrate specificity modulate substrate-induced adenosine triphosphatase activity. *Biochemistry.* **37**, 9073-9082.

Berger, W., Hauptmann, E., Elbling, L., Vetterlein, M., Kokoschka, E.M. and Micksche, M. (1997). Possible Role of the Multidrug Resistance-Associated Protein (MRP) in chemoresistance of human melanoma cells. *Int.J.Cancer.* **71**, 108-115.

Berger, D., Citarell, R., Dutia, M., Greenberger, L., Hallett, W., Paul, R. and Powell, D. (1999). Novel multidrug resistance reversal agents. *J.Med.Chem.* **42**, 2145-2161.

Berkower, C. and Michaelis, S. (1991). Mutational analysis of the yeast a-factor transporter STE6, a member of the ATP binding cassette (ABC) protein superfamily. *EMBO Journal.* **10**, 3777-3785.

Berkower, C., Taglicht, D. and Michaelis, S. (1996). Functional and physical interactions between partial molecules of STE6, a yeast ATP-binding cassette protein. *J.Biol.Chem.* **271**, 22983-22989.

Boer, R., Dichtl, M., Borchers, C., Ulrich, W.R., Marecek, J.F., Prestwich, G.D., Glossmann, H. and Striessnig, J. (1996). Reversible labeling of a chemosensitizer binding domain of p-glycoprotein with a novel 1,4-dihydropyridine drug transport inhibitor. *Biochemistry.* **35**, 1387-1396.

Bois, F., Beney, C., Boumendjel, A., Mariotte, A.M., Conseil,G., Di Pietro, A. (1998). Halogenated chalcones with high-affinity binding to p-glycoprotein: potential modulators of multidrug resistance. *J.Med.Chem.* **41**, 4161-4164.

Bond, T.D., Higgins, C.F. and Valverde, M.A. (1998). P-glycoprotein and swelling-activated chloride channels. *Methods in Enzymology.* **292**, 359-370.

Bosch, I., Dunussi-Joannopoulos, K., Wu, R.-L., Furlong, S.T. and Croop, J. (1997). Phosphatidylcholine and phosphatidylethonolamine behave as substrates of the human MDR1 p-glycoprotein. *Biochemistry.* **36**, 5685-5694.

Bradford, M.M. (1976). A rapid and sensitive method for the quantitation of microgram quantities of protein utilzing the principle of protein-dye binding. *Anal.Biochem.* **72**, 248-254.

Bradshaw, D.M. and Arceci, R.J. (1998). Clinical relevance of transmembrane drug efflux as a mechanism of multidrug resistance. *Biology of Neoplasia.* **16,** 3674-3690.

Borst, P. (1997). Introduction: Multidrug resistant proteins. *Seminars in Cancer Biology.* **8**, 131-134.

Borst, P., Kool, M. and Evers, R. (1997). Do cMOAT (MRP2), other MRP homologues, and LRP, play a role in MDR ? *Seminars in Cancer Biology.* **8**, 205-213.

Borgnia M.J., Eytan, G.D. and Assaraf, Y.F. (1996). Competition of hydrophobic peptides, cytotoxic drugs, and chemosensitizers on a common p-glycoprotein pharmacophore as revealed by its ATPase acitivy. *J.Biol.Chem.* **271**, 3163-3171.

Bruggemann, E.P., Currier, S.J., Gottesman, M.M. and Pastan, I. (1992). Characterization of the azidopine and vinblastine binding site of P-plycoprotein. *J.Biol.Chem.* **267**, 21020-21026.

Bryan, J. and Afuilar-Bryan, L. (1997). The ABCs of ATP-sensitive potassium channels: more pieces of the puzzle. *Current Opinions in Cell Biology.* **9**, 553-559.

Callahan, H.L. and Beverley, S.M. (1991). Heavy metal resistance: A new role for P-glycoproteins in *Leishmania*. *J.Biol.Chem.* **266**, 18427-18430.

Callaghan, R. and Higgins, C.F. (1995). Interaction of tamoxifen with the multidrug resistance p-glycoprotein. *Br.J.Cancer.* **71**, 294-299.

Callaghan, R., Berridge, G., Ferry, D.R. and Higgins, D.F. (1997). The functional purification of p-glycoprotein is dependent on maintenance of a lipid-protein interface. *Biochim.Biophys.Acta.* **1328**, 109-124.

Chan, H.S.L., Haddad, G., Thorner, P.S., DeBoer, G., Yun Pin Lin, Ondrusek, N., Yeger, H. and Ling, V. (1991). P-glycoprotein expression as a predictor of the outcome of therapy for Neuroblastoma. *The New England Journal of Medicine.* **325**, 1608-1614.

Chen, C.-j., Chin, J.E., Clark, D.P., Pastan, I., Gottesman, M.M. and Roninson, I.B. (1986). Internal duplication and homology with bacterial transport proteins in the mdr1 (P-glycoprotein) gene from multidrug-resistant human cells. *Cell.* **47**, 381-389.

Chen, C.-j., Clark, D., Ueda, K., Pastan, I., Gottesman, M.M. and Roninson, I.B. (1990). Genomic organization of the human multidrug resistance (MDR1) gene and origin of P-glycoproteins. *J.Biol.Chem.* **265**, 506-514.

Cole, S.P., Bhardwaj, G., Gerlach, J.H., Macie, J.E., Grant, C.E., Almquist, K.C., Stewart, A.J., Kurz, E.U., Duncan, A.M. and Deeley, R.G. (1992). Overexpression of a transporter gene in a multidrug-resistant human lung cancer cell line. *Science.* **258**, 1650-1654.

Cole S.T., Brosch, R., Parkhill, J., Garnier, T., Churcher, C., Harris, D., Gordon, S.V., Eiglmeier, K., Gas, S., Barry III, C.E., Tekaia, F., Badcock, K., Basham, D., Brown, D., Chillingworth, T., Connor, R., Davies, R., Devlin, K., Feltwell, T., Gentles, S., Hamlin, N., Holroyd, S., Hornsby, T., Jagels, K., Krogh, A., McLean, J., Moule, S., Murphy, L., Oliver, K., Osborne, J., Quail, M.A., Rajandream, M.-A., Rogers, J., Rutter, S., Seeger, K., Skelton, J., Squares, R., Squares, S., Sulston, J.E., Taylor, K., Whitehead, S. and Barrell, B.G. (1998). Deciphering the biology of *Mycobacterium tuberculosis* from the complete genome sequence. *Nature.* **393**, 537-543.

Conseil, G., Baubichon-Cortay, H., Dayan, G., Jault, J.M., Barron, D. and Di Pietro, A. (1998). Flavonoids: a class of modulators with bifunctional interactions at vicinal ATP- and steroid-binding sites on mouse p-glycoprotein. *Proc.Natl.Acad.Sci.* **95**, 9831-9836.

Comwell, M.M., Safa, A.R., Felsted, R.L., Gottesman, M.M. and Pastan, I. (1986). Membrane vesicles from multidrug-resistant human cancer cells contain a specific 150 – to 170-kDa protein detected by photoaffinity labeling. *Proc.Natl.Acad.Sci.* **83**. 3847-3850.

Cornwell, M.M., Tsuruo, T., Gottesman, M.M. and Pastan, I. (1987). ATP-binding properties of P-plycoprotein from multidrug-resistant KB cells. *FASEB J.* **1**, 51-54.

Cotten, J.F. and Welsh, M.J. (1998). Covalent modification of the nucleotide binding domains of cystic fibrosis transmembrane conductance regulator. *J.Biol.Chem.* **273**. 31873-31879.

Critchfield, J.W., Welsh, C.J., Phang, J.M. and Yeh, G.C. (1994). Modulation of adriamycin accumulation and efflux by flavonoids in HCT-15 colon cells. Activation of p-glycoprotein as a putative mechanism. *Biochem.Pharmacol.* **48**, 1437-1445.

Cui, Z., Hirata, D., Txuchiya, E., Osada, H. and Miyakawa, T. (1996). The multidrug resistance-associated protein (MRP) subfamily (Yrs1/Yor1) of *Saccharomyces cerevisiae* is important for the tolerance to a broad range of organic anions. *J.Biol.Chem.* **271**, 14712-14716.

Czarnecki, J.J. (1994). Tautomerism of 2-azidoadenine nucleotides. Effects on enzyme kinetics and photoaffinity labeling. *Biochim.Biophys.Acta.* **800**, 41-51.

Dayan, G., Boubichon-Cortay, H., Jault, J.M., Cortay, J.C., Deleage, G. and Di Pietro, A. (1996). Recombinant N-terminal nucleotide-binding domain from mouse p-glycoprotein. Overexpression, purification, and role of cysteine 430 *J.Biol.Chem.* 271, 11652-11658.

Dayan, G., Jault, J.M., Baubichon-Cortay, H., Baggetto, L.G., Renoir, J.M., Baulieu, E.E., Gros, P. and Di Pietro A. (1997). Binding of steroid modulators to recombinant cytosolic domain from mouse p-glycoprotein in close proximity to the ATP site. *Biochemistry.* **36**, 15208-15215.

Decottignies, A., Kolaczkowski, M., Balzi, E. and Goffeau, A. (1994). Solubilization and characterization of the overexpressed PDR5 multidrug resistance nucleotide triphosphatase of yeast. *J.Biol.Chem.* **269**, 12797-12803.

Decottignies, A., Lambert, L., Catty, P., Gegand, H., Epping, E.A., Moye-Rowley, W.S., Balzi, E., and Goffeau, A. (1995). Identification and characterization of SNQ2, a new multidrug ATP binding cassette transporter of the yeast plasma membrane. *J.Biol.Chem.* **270**, 18150-18157.

Decottignies, A., Grant, A.M., Nichols, W.J., de Wet, H., McIntosh, D.B. and Goffeau, A. (1998). ATPase and multidrug transport activities of the overexpressed yeast ABC protein Yor1p. *J.Biol.Chem.* **273**, 12612-12622.

Deeley, G.D. and Cole, S.P.C. (1997). Function, evolution and structure of multidrug resistance protein (MRP). *Seminars in Cancer Biology.* **8**, 193-204.

Dekkers S.W., Comfurius, P., Schroit, A.J., Bevers, E.M and Zwaal, R.F. (1998). Transbilayer movement of NBD-labeled phospholipids in red blood cell membranse: outward-directed transport by the multidrug resistance protein 1 (MRP1). *Biochemistry.* **41**, 14833-14847.

Dey, S., Ramachandra, M., Pastan, I., Gottesman, M.M. and Ambudkar, S.V. (1997). Evidence for two nonidentical drug-interaction sites in the human P-glycoprotein. *Proc.Natl.Acac.Sci.* **94**, 10594-10599.

Demmer, A., Thole, H., Kubesch, P., Brandt,T., Raida, M., Fislage, R. and Tummler, B. (1997). Localization of the iodomycin binding site in hamster P-glycoprotein. *J.Biol.Chem.* **272**, 20913-20919.

Demeule, M., Laplante, A., Murphy, G.F., Wenger, R.M. and Beliveau, R. (1998). Identification of the cyclosporin-binding site in p-glycoprotein. *Biochemistry.* **37**, 18110-18118.

Dhainaut, A., Regnier, G., Tizot, A., Leonce, S., Guilbaud, N., Draus-Berthier, L. and Atassie, G. (1996). New purines and purine analogs as modulators of multidrug resistance. *J.Med.Chem.* **39**, 4099-4108.

Dombrowski, K.E., Huang, Y.C. and Colman, R.F. (1992) Identification of amino acids modified by the bifunctional affinity label 5'-(p-(fluorosulfonyl)benzoyl)-8-azidoadenosine in the reduced coenzyme regulatory site of bovine liver glutamate dehydrogenase. *Biochemistry.* **31**, 3785-3793.

Dorschner, H., Brekardin, E., Uhde, I., Schwanstecher, C. and Schwanstecher, M. (1999). Stoichiometry of sulfonylurea-iinduced ATP-sensitive potassium channel closure. *Mol.Pharmacol.* **55**, 1060-1066.

Eytan, G.D., Regev, R. and Assaraf, Y.G. (1996). Functional reconstitution of p-glycoprotein reveals an apparent near stoichiometric drug transport to ATP hydrolysis. *J.Biol.Chem.* **271**, 3172-3178.

Ferte, J., Kuhnel, J.M., Chapuis, G., Rolland, Y., Lewin, G. and Schwaller M.A. (1999). Flavonoid-related modulators of multidrug resistance:synthesis, pharmacological activity, and structure-activity relationships. *J.Med.Chem.* **42**, 478-489.

Foote, S.J., Thompson, J.K., Cowman, A.F. and Kemp, K.J. (1989). Amplification or the multidrug resistance gene in some chloroquine-resistant isolates of *P.falciparum. Cell.* **57**, 921-930.

Gadsby, D.C., Dousmanis, A.G. and Nairn, A. (1998). ATP hydrolysis cycles and the gating of CFTR Cl^- channels. *Acta.Physiol.Scand.* **163**, 247-256.

Gao, M., Loe, D.W., Grant, C.E., Cole, S.P.C. and Deeley, R.G. (1996). Reconstitution of ATP-dependent leukotriene C4 transport by co-expression of both half-molecules of human multidrug resistance protein in insect cells. *J.Biol.Chem.* **271**, 27782-27787.

Garin, J., Michel, L., Dupuis, A., Issartel, J.P., Lunardi, J., Hoppe, J. and Vignais, P. (1989). Photolabeling of the phosphate binding site of mitochondrial F1-ATPase by [32P]azidonitrophenyl phosphate. Identification of the photolabeled amino acid residues. *Biochemistry.* **28**, 1442-1448.

Garrigos, M., Mir, L.M. and Orlowski, S. (1997). Competitive and non-competitive inhibition of the multidrug-resistance-associated p-glycoprotein ATPases – futher experimental evidence for a multisite model. *Eur.J.Biochem.* **244**, 664-673.

Gerlach, J.H., Bell, D.R., Karakousis, C., Slocum, H.K., Kartner, N., Rustum, Y.M., Ling, V. and Baker, R.M. (1987). P-glycoprotein in human sarcoma: evidence for multidrug resistance. *Journal of Clinical Oncology.* **5**, 1452-1460.

Germann, U.A., Chambers, T.C., Ambudkar, S.V., Licht, T., Cardarelli, C.O., Pastan, I. and Gottesman, M.M. (1996). Characterization of phosphorylation-defective mutants of human p-glycoprotein expressed in mammalian cells. *J.Biol.Chem.* **271**, 1708-1716.

Glynn, I.M. and Chappell, J.B. (1964). A simple method for the preparation of 32-P-labelled adenosine triphosphate of high specific activity. *Biochem.J.* **90**, 147-149.

Goodfellow, H.R., Sardini, A., Ruetz, S., Callaghan, R., Gros, P., McNaughton, P.A. and Higgins, C.F. (1996). Protein kinase C-mediated phosphorylation does not regulate drug transport by the human multidrug resistance p-glycoprotein. *J.Biol.Chem.* **271**, 13668-13674.

Gottesman, M.M and Pastan, I. (1993). Biochemistry of multidrug resistance mediated by the multidrug transporter. *Annu.Rev.Biochem.* **62**, 385-427.

Grant. C.E., Valdimarsson, G., Hipfner, D.R., Almquist, K.C., Cole, S.P. and Deeley R.G. (1994). Overexpression of multidrug resistance-associated protein (MRP) increases resistance to natural products drugs. *Cancer Res.* **54**, 357-361.

Grant, C.E., Kurz, E.U., Cole, S.P. and Deeley R.G. (1997). Analysis of the intron-exon organization of the human multidrug-resistance protein gene (MRP) and alternative splicing of its mRNA. *Genomics.* **45**, 368-378.

Greenberger, L.M., Sisanti, C.J., Silva, J.T. and Horwitz, S.B. (1991). Domain mapping of the photoaffinity drug-binding sites in P-glycoprotein encoded by mouse mdr1b. *J.Biol.Chem.* **266**, 20744-20751.

Greenberger, L.M. (1993). Major photoaffinity drug labeling sites for iodoaryl azidoprazosin in P-glycoprotein are within, or immediately C-terminal to, transmembrane domains 6 and 12. *J.Biol.Chem.* **268**, 11417-11425.

Greenberger, L.M. (1998). Identification of drug interaction sites in p-glycoprotein. *Methods.Enzymol.* **292**, 307-317.

Gros, P., Croop, J. and Housman, D. (1986). Mammalian multidrug resistance gene: complete cDNA sequence indicates strong homology to bacterial transport proteins. *Cell.* **47**, 371-380.

Hamada, H. and Tsuruo, T. (1988). Purification of 170- to 180-kilodalton membrane glycoprotein associated with multidrug resistance. *J.Biol.Chem.* **263**, 1454-1458.

Hayes, J.D. and Wolf, C.R. (1990). Molecular mechanisms of drug resistance. *Biochemical Journal.* **272**, 281-295.

Higgins, C.F., Callaghan, R., Linton, K.J., Rosenberg, M.F. and Ford, R.C. (1997). Structure of the multidrug resistance p-glycoprotein. *Seminars in Cancer Biology.* **8**, 135-142.

Hiratsuka, T. (1982). Biological activities and spectroscopic properties of chromophoric and fluorescent analogs of adenine nucleoside and nucleotides, 2',3'-O-(2,4,6-trinitrocyclohexadienylidene) adenosine derivatives. *Biochim.Biophys.Acta.* **719**, 509-517.

Lerner-Marmarosh, N., Gimi, K., Urbatsch, I.L., Gros, P. and Senior, A.E. (1999). Large scale purification of detergent-soluble p-glycoprotein from *Pichia pastoris* cells and characterization of nucleotide binding properties of wild-type, Walker A and Walker B mutant proteins. *J.Biol.Chem.* **274**, 34711-34718.

Ling, V. (1992). Charles F. Kettering Prize. P-glycoprotein and resistance to anticancer drugs. *Cancer.* **69**, 2603-2609.

Litman, T., Zeuthen, T., Skovsgaard, T. and Stein, W.D. (1997). Structure-activity relationships of p-glycoprotein interacting drugs:kinetic characterization of their effects on ATPase activity. *Biochim.Biophys.Acta.* **1361**, 159-168.

Liu, R. and Sharom F.J. (1996). Site-directed fluorescence labeling of P-glycoprotein on cysteine residues in the nucleotide binding domians. *Biochemistry.* **35**, 11865-11873.

Liu, R. and Sharom, F.J. (1998). Proximity of the nucleotide binding domains of the p-glycoprotein multidrug transporter to the membrane surface: a resonance energy transfer study. *Biochemistry.* **37**, 6503-6512.

Loo, T.W. and Clarke, D.M. (1994). Mutations to amino acids located in predicted transmembrane segment 6 (TM6) modulate the activity and substrate specificity of human P-glycoprotein. *Biochemistry.* **33**, 14049-14057. (a)

Loo T.W. and Clarke, D.M. (1994). Reconstitution of drug-stimulated ATPase activity following co-expression of each half of human p-glycoprotein as separate polypeptides. *J.Biol.Chem.* **269**, 7750-7755. (b)

Loo, T.W. and Clarke, D.M. (1995). Membrane topology of a cysteine-less mutant of human p-glycoprotein. *J.Biol.Chem.* **270**, 843-848. (a)

Loo, T.W. and Clarke, D.M. (1995). Covalent modification of human P-glycoprotein mutants containing a single cysteine in either nucleotide-binding fold abolishes drug-stimulated ATPase activity. *J.Biol.Chem.* **270**, 22957-22961. (b)

Loo, T.W. and Clarke, D.M. (1996). The minimum functional unit of human p-glycoprotein appears to be a monomer. *J.Biol.Chem.* **271**, 27488-27492.

Loo, T.W. and Clarke, D.M. (1997). Drug-stimulated ATPase activity of human p-glycoprotein requires movement between transmembrane segments 6 and 12. *J.Biol.Chem.* **272**, 20986-20989. (a)

Loo, T.W and Clarke, D.M. (1997). Identification of residues in the drug-binding site of human p-glycoprotein using a thiol-reactive substrate. *J.Biol.Chem.* **272**, 31945-31948. (b)

Maring, C., Berridge, G., Higgins, C.F., Mistry, P., Charlton, P. and Callaghan, R. (2000). Communication between multiple drug binding sites on p-glycoprotein. Mol.Pharmacol. 58, 624-632.

McIntosh, D.B., Wooley, D.G. and Berman, M.C. (1992). 2'-3'-O-(2,4,6-trinitrophenyl)-8-azido-AMP and –ATP photolabel Lys^{492} at the active site of sarcoplasmic reticulum Ca^{2+}-ATPase. *J.Biol.Chem.* **267**, 5301-5309.

McIntosh, B.M., Woolley. D.G., MacLennan, D.H., Vilsen, B. and Andersen, J.P. (1999). Interaction of nucleotides with Asp^{351} and the conserved phosphorylation loop of sarcoplasmic reticulum Ca^{2+}-ATPase. *J.Biol.Chem.* **274**, 25227-25236.

Mechetner, E.B., Schott, B., Morse, B.S., Stein, W.D., Druley, T., Davis, D.A., Tsuruo, T. and Roninson, I.B. (1997). P-glycoprotein function involves conformational transitions detectable by differential immunoreactivity. *Proc.Natl.Acac.Sci.* **94**, 12908-12913.

Michel, L., Garin, J., Girault, G. and Vignais, P.V. (1992) Photolabeling of the phosphate binding site of chloroplast coupling factor 1 with [32P]azidonitrophenyl phosphate. *FEBS Lett.* **313**, 90-93.

Michelson, A.M. (1964). Synthesis of nucleotide anhydrides by anion exchange. *Biochim.biophys.Acta.* **91**, 1-13.

Nayfield, S.G. (1995). Tamoxifen's role in chemoprevention of breast cancer: an update. *J.Cell.Biochem.Suppl.* **22**, 42-50.

Nelson, K.E., Clayton, R.A., Gill, S.R., Gwinn, M.L., Dodson, R.J., Haft, D.H., Hickey, E.K., Peterson, J.D., Nelson, W.C., Ketchum, K.A., McDonald, L., Utterback, T.R., Malek, J.A., Linher, K.D., Garrett, M.M., Stewer, A.M., Cotton, M.D., Pratt, M.S., Phillips, C.A., Richardson, D., Heidelberg, J., Sutton, G.G., Fleischmann, R.D., Eisen, J.A., White, O., Salzberg, S.L., Smith, O.H., Venter, J.C. and Fraser, C.M. (1999). Evidence for lateral gene transfer between Archaea and bacteria from genome sequence of *Thermotoga maritima*. *Nature.* **399**, 323-329.

Newbald, C. (1990). The path of drug resistance. *Nature.* **245**, 202-203.

Norris, M.D., Bordow, S.B., Marshall, G.M., Haber, P.S., Cohn, S.L. and Haber, M. (1996). Expression of the gene for multidrug-resistance-associated protein and outcome in patients with neuroblastoma. *The New England Journal of Medicine.* **334**, 231-238.

Nue, C.H. (1992). The crisis in antibiotic resistance. *Science.* **257**, 1064-1072.

Orlowski, S., Mir, L.M., Belehradek, J.Jr. and Garrigos, M. (1996). Effects of steroids and verapamil on P-glycoprotein ATPase activity: progesterone, desoxycorticosterone, corticosterone and verapamil are mutually non-exclusive modulators. *Biochem.J.* **317**, 515-522.

Pajeva, I. and Wiese, M. (1998). Molecular modeling of phenothiazines and related drugs as multidrug resistance modifiers: a comparative molecular field analysis study. *J.Med.Chem.* **41**, 1815-1826.

Pascaud, C., Garrigos, M. and Orlowski, S. (1998). Multidrug resistance transporter P-glycoprotein has distinct but interacting binding sites for cytotoxic drugs and reversing agents. *Biochem.J.* **333**, 351-358.

Pastan, I., Gottesman, M.M., Ueda, K., Lovelace, E., Rutherford, A.V. and Willingham, M.C. (1988). A retrovirus carrying an MDR1 cDNA confers multidrug resistance and polarized expression of P-glycoprotein in MDCK cells. *Proc.Natl.Acad.Sci.* **85**, 4486-4490.

Pecoraro, V.L., Hermes, J.D. and Cleland, W.W. (1984). Stability constants of Mg^{2+} and Cd^{2+} complexes of adenine nucleotides and thionucleotides and relate constants for formation and dissociation of MgATP and MgADP. *Bochemistry.* **22**, 5262-5271.

Penefsky, H.S. (1977). Reversible binding of Pi by beef heart mitochondrial adensosine triphosphatase. *J.Biol.Chem.* **252**, 2891-2899.

Perez-Victoria, J.M., Chiquero, M.J., Conseil, G., Dayan, G., Di Pietro, A., Barron, D., Castanys, S. and Gamarro, F. (1999). Correlation between the affinity of flavonoids binding to the cytosolic site of Leishmania tropica multidrug transporter and their efficiency to revert parasite resistance to daunomycin. *Biochemistry.* **38**, 1736-1743.

Petronilli, V. and Ferro-Luzzi Ames, G. (1991). Binding protein-independent histidine prermease mutants. *J.Biol.Chem.* **266**, 16293-16296.

Prasad, R., de Wergifosse, P., Goffeau, A. and Balzi, E. (1995). Molecular cloning and characterization of a novel gene of *Candida albicans*, CDR1, conferring multiple resistance to drugs and antifungals. *Curr.Genet.* **27**, 320-329.

Qian, X.D. and Beck W.T. (1990). Progesterone photoaffinity labels p-glycoprotein in multidrug-resistant human leukemic lymphoblasts. *J.Biol.Chem.* **265**, 18753-18756.

Quang, D., and Gruol, D.J. (1999). Identification of p-glycoprotein mutations causing a loss of steroid recognition and transport. *J.Biol.Chem.* **274**, 20318-20327.

Ramachandra, M., Ambudkar, S.V., Chen, D., Hrycyna, C.A., Dey, S., Gottesman, M.M. and Pastan, I. (1998). Human p-glycoprotein exhibits reduced affinity for substrates during a catalytic transition state. *Biochemistry,* **37**, 5010-1519.

Ramjeesingh, M., Li, C., Garami, E., Haun, L., Galley, K., Wang, Y. and Bear, C.E. (1999). Walker mutations reveal loose relationship between catalytic and channel-gating activities of purified CFTR (cystic fibrosis transmembrane conductance regulator). *Biochemistry.* **38**. 1463-1468.

Rao, U.S. (1998). Drug binding and nucleotide hydrolyzability are essential requirements in the vanadate-induced inhibition of the human p-glycoprotein ATPase. *Biochemistry.* **37**,14981-14988.

Raviv, Y., Pollard, H.B., Bruggemann, E.P., Pastan, I. and Gottesman, M.M. (1990). Photosensitized labeling of a functional multidrug transporter in living drug-resistant tumor cells. *J.Biol.Chem.* **265**, 3975-3980.

Raymond, M., Gros, P., Whiteway, M. and Thomas, D.Y. (1992). Functional complementation of yeast ste6 by a mammalian multidrug resistance mdr gene. *Science.* **256**, 232-234.

Riordan, J.R., Rommens, J.M., Derem, B., Alon, N., Rozmahel, R., Grzelczak, Z., Zielenski, J., Lok, S., Plavsic, N., Chou J.L., Drum, M.L., iannuzzi, M.C., Collins, F.S. and Tsui, L.C. (1989). Identification of the cystic fibrosis gene: cloning and characterization of complementary DNA. *Science.* **245**, 1066-1073.

Rosenberg, M.F., Callaghan, R., Ford, R.F. and Higgins, C.F. (1997). Structure of the multidrug resistance p-glycoprotein to 2.5 nm resolution determined by electron microscopy and image analysis. *J.Biol.Chem.* **272**, 10685-10694.

Ruetz, S. and Gros, P. (1994). Phosphatidylcholine translocase: a physiological role for the mdr2 gene. *Cell.* **77**, 1071-1081.

Ruetz, S., Brault, M., Kast, C., Hemenway, C., Heitman, J., Grant, C.E., Cole, S.P., Deeley, R.G. and Gros, P. (1996). Functional expression of the multidrug resistance-associated protein in the yeast *Saccharomyces cerevisiae*. *J.Biol.Chem.* **271**, 4154-4160. (a)

Ruetz, S., Delling, U., Brault, M., Schurr, E. and Gros, P. (1996). The pfmdr1 gene of *Plasmodium falciparum* confers cellular resistance to antimalarial drugs in yeast cells. *Proc.Natl.Acac.Sci.* **93**, 9942-9947. (b)

Ruetz, S., Delling, U., Brault, M., Schurr, E. and Gros, P. (1999). The pfmdr1 gene of *Plasmodium falciparum* confers cellular resistance to antimalarial drugs in yeast cells. Retraction of publication. *Proc.Natl.Acac.Sci.* **96**, 1810.

Safa, A.R., Stern, R.K., Choi, K., Agresti, M., Tamai, I., Mehta, N.D. and Roninson I.B. (1990) Molecular basis of preferential resistance to colchicine in multidrug-resistant human cells conferred by Gly-185 – Val-185 substitution in P-glycoprotein. *Proc.Natl.Acad.Sci.* **87**, 7225-7229.

Safa, A.R. (1998). Photoaffinity labels for characterizing drug interaction sites of p-glycoprotein. *Methods.Enzymol.* **292**, 289-307.

Sankaran, B., Bhagat, S. and Senior, A.E. (1997). Inhibition of P-glycoprotein ATPase activity by beryllium fluoride. *Biochemistry.* **36**, 6847-6853. (a)

Sankaran, B., Bhagat, S. and Senior, A.E. (1997). Photoaffinity labelling of P-glycoprotein catalytic sites. *FEBS Lett.* **417**, 119-122. (b)

Scambia, G., Ranelletti, F.O., Panici, P.B., De Vincenzo, R., Bonanno, G., Ferrandina, G., Piantelli,M., Bussa, S., Rumi, C., and Cianfriglia, M. (1994). Quercetin potentiates the effect of adriamycin in a mutlidrug-resistanc MCF-6 human breast-cancer cell line: p-glycoprotein as a possible target. *Cancer.Chemother.Pharmacol.* **34**, 459-464.

Schwanstecher, M., Sieverding, C., Dorschner, H., Gross, I., Aguilar-Bryan, L., Schwanstecher, C. and Bryan, J. (1998). Potassium channel openers require ATP to bind to and act through sulfonylurea receptors. *EMBO.J.* **17**, 5529-5535.

Seebregts, C.J. and McIntosh, D.B. (1989). 2',3'-O-(2,4,6-trinitrophenyl)-8-azido-adenosine mono-, di-, and triphosphates as photoaffinity probes of the Ca2+-ATPase of sarcoplasmic reticulum. Regulatory/superfluorescent nucleotides label the catalytic site with high efficiency. *J.Biol.Chem.* **264**, 2043-2052.

Senior, A.E., al-Shawi, M.K. and Urbatsch, I.L. (1995). The catalytic cycle of p-glycoprotein. *FEBS lett.* **377**, 285-289.

Senior, A.E. and Gadsby, D.C. (1997). ATP hydrolysis cycles and mechanism in p-glycoprotein and CFTR. *Semin.Cancer.Biol.* **8**, 143-150.

Senior, A.C., Gros, P. and Urbatsch, I.L. (1998). Residues in p-glycoprotein catalytic sites that react with the inhibitor 7-chloro-4-nitrobenzo-2-oxa-1,3-diazole. *Arch.Biochem.Biophys.* **357**, 121-125.

Senior, A.E. and Bhagat, S. (1998). P-glycoprotein shows strong catalytic cooperativity between the two nucleotide sites. *Biochemistry.* **37**, 831-836.

Senior, A.E. (1998). Catalytic mechanism of p-glycoprotein. *Acta physiol.Scand.Suppl.* **643**, 213-218.

Shapiro, A.B. and Ling, V. (1997). Effect of quercetin on Hoechst 33342 transport by purified and reconstituted p-glycoprotein. *Biochem.Pharmacol.* **53**, 587-596. (a)

Shapiro, A.B. and Ling,V. (1997). Positively co-operative sites for drug transport by p-glycoprotein with distinct drug specificities. *Eur.J.Biochem.* **250**, 130-137. (b)

Shapiro, A.B. and Ling, V. (1998). Stoichiometry of coupling of rhodamine 123 transport to ATP hydrolysis by p-glycoprotein. *Eur.J.Biochem.* **254**, 189-193. (a)

Shapiro, A.B. and Ling, V. (1998). The mechanism of ATP-dependent multidrug transport by p-glycoprotein. *Acta. Physiol.Scand.* **643**, 227-234. (b)

Slater, L.M., Sweet, P., Stupecky, M. and Gupta, S. (1986). Cyclosporin A reverses vincristine and daunorubicin resistance in acute lymphatic leukemia in vitro. *J.Clin.Invest.* **77**, 1405-1408.

Smith, A.J., de Vree, J.M., Ottenhoff, R., Oude Elferink, R.P., Schinkel A.H. and Borst, P. (1998). Hepatocyte-specific expression of the human MDR3 p-glycoprotein gene restores the biliary phosphatidylcholine excretion absent in MDR2 (-/-) mice. *Hepatology.* **28**, 530-536.

Solary, E., Velay, I., Chauffert, B., Bidan,J.M., Caillot, D., Dumas, M. and Guy, H. (1991). Sufficient levels of quinine in the serum circumvent the multidrug resistance of the human leukemic cell line K562/ADM. *Cancer.* **68**, 1714-1719.

Sonveaux, N., Vigano, C., Shapiro, A.B., Ling, V. and Ruysschaert, J.M. (1999). Ligand-mediated tertiary structure changes of reconstituted p-glycoprotein. A tryptophan fluorescence quenching analysis. *J.Biol.Chem.* **274**, 17649-17654.

Stein, W.D. (1997). Kinetics of the multidrug transporter (p-glycoprotein) and its reversal. *Physiological reviews.* **77**, 545-590.

Suhadolnik, R.J., Kariko, K., Sobol, R.W., Li, S.W., Reichenbach, N.L. and Haley, B.E. (1998). 2- and 8-azido photoaffinity probes. 1. Enzymatic synthesis, characterization, and biological properties of 2- and 8-azido photoprobes of 2-5A and photolabeling of 2-5A binding proteins. *Biochemistry.* **27**, 8840-8846.

Szabo, K., Bakos, E., Welker, E., Muller, M., Goodfellow, H.R., Higgins, C.F. Varadi, A. and Sarkadi, B. (1997). Phosphorylation site mutations in the human multidrug transporter modulates its drug-stimulated ATPase activity. *J.Biol.Chem.* **37**, 23165-23171.

Szabo, K., Welker, E., Bakos, B., Muller, M., Roninson, I., Varadi, A. and Sarkadi, B. (1998). Drug-stimulated nucleotide trapping in the human multidrug transporter MDR1. Cooperation of the nucleotide binding domains. *J.Biol.Chem.* **273**, 10132-10138.

Szabo, K., Szakacs, G., Hegeds, T. and Sarkadi, B. (1999). Nucleotide occlusion in the human cystic fibrosis transmembrane conductance regulator. Different patterns in the two nucleotide binding domains. *J.Biol.Chem.* **274**, 12209-12212.

Szczypka, M.S., Wemmie, J.A., Moye-Rowley, W.S. and Thiele, D.J. (1994). A yeast metal resistance protein similar to human cystic fibrosis transmembrane conductance regulator (CFTR) and multidrug resistance-associated protein. *J.Biol.Chem.* **269**, 22853-22857.

Takada, Y., Yamada, K., Taguchi, Y., Kino, K., Matsuo, M., Tucher, S., Komano, T., Amachi, T. and Ueda, K. (1998). Non-equivalent cooperation between the two nucleotide-binding folds of P-glycoprotein. *Biochem. et Biophys. Acta.* **1374,** 131-136.

Taguchi, Y., Kino, K., Morishima, M., Komano, T., Kane, S.E. and Ueda, K. (1997). Alteration of substrate specificity by mutations at the His61 position in predicted transmembrane domain 1 of human MDR1-P-glycoprotein. *Biochemistry.* **36**, 8883-8889.

Tavale, S.S. and Sobell, H.M. (1970). Crystal and molecular structure of 8-bromoguanosine and 8-bromoadensoine, two purine nucleosides in the syn conformation. *J.Mol.Biol.* **28**, 109-123.

Tommasins, R., Evers, R., Vogt, E., Mornet, C., Zaman, G.J., Schinkel, A.H., Borst, P. and Martinoia, E. (1996). The human multidrug resistance-associated protein functionally complements the yeast cadmium resistance factor 1. *Proc.Natl.Acad.Sci.* **93**, 6743-6748.

Tran, C.M. and Farley, F.A. (1996). Photoaffinity labeling of the active site of the Na^+/K^+-ATPase with 4-azido-2-nitrophenyl phosphate. *Biochemistry.* **35**, 47-55.

Tsuruo, T., Iida, H., Tsukagoshi, S. and Sakurai, Y. (1981). Overcoming of vincristine resistance in P388 leukemia in vivo and in vitro through enhanced cytotoxicity of vincristine and vinblastine by verapamil. *Cancer Res.* **41**, 1967-1972.

Tunsnady, G.E., Bakos, E., Varadi, A. and Sarkadi, B. (1997). Membrane topology distinguishes a subfamily of the ATP-binding cassette (ABC) transporters. *FEBS letters.* **402**, 1-3.

Urbatsch, I.L., Sankaran, B., Weber, J. and Senior, A.E. (1995). P-glycoprotein is stably inhibited by vanadate-induced trapping of nucleotide at a single catalytic site. *J.Biol.Chem.* **270**, 19383-19390.

Urbatsch, I.L., Sankaran, B., Ghagat, S. and Senior, A.E. (1995). Both P-glycoprotein nucleotide-binding sites are catalytically active. *J.Biol.Chem.* **270**, 26956-26961.

Urbatsch, I.L., Beaudet, L., Carrier, I. and Gros, P. (1998). Mutations in either nucleotide-binding site of P-glycoprotein (Mdr3) prevent vanadate trapping of nucleotide at both sites. *Biochemistry.* **37**, 4592-4602.

van Veen, H.W. and Konings, W.N. (1998). The ABC family of multidrug transporters in microorganisms. *Biochimica et Biophysica Acta.* **1365**, 31-36.

van Veen, H.W., Callaghan, R., Soceneantu, L., Sardini, A., Konings, W.N. and Higgins, C.F. (1998). A bacterial antibiotic-resistance gene that complements the human multidrug-resistance p-glycoprotein gene. *Nature.* **391**, 291-295.

Volkman, S.K., Cowman, A.F. and Wirth, D.F. (1995). Functional complementation of the ste6 gene of *Saccharomyces cerevisiae* with the pfmdr1 gene of *Plasmodium falciparum*. *Proc.Natl.Acad.Sci.* **92**, 8921-8925.

Walker, J.E., Saraste, M., Runswich, M.J. and Gay, J.J. (1982). Distantly related sequences in the α and β-subunits of ATP-synthase, myosin, kinases and other ATP-requiring enzymes and a common nucleotide binding fold.

Wang, G., Pincheira, R., Zhang, M. and Zhang, J.T. (1997). Conformational changes of p-glycoprotein by nucleotide binding. *Biochem.J.* **328**, 897-904.

Wang, G., Pincheira, R. and Zhang, J.T. (1998). Dissection of drug-binding-induced conformational changes in p-glycoprotein. *Eur.J.Biochem.* **255**, 383-390.

Wilkinson, J.M. (1986). Fragmentation of polypeptides by enzymatic methods. As in *Practical protein chemistry - a handbook.* Edited Darbre, A. 122-148. Published by John Wiley and Sons.

Wilson, C.M., Serrano, A.E., Wasley, A., Bogen Schutz, M.P., Shankar, A.H. and Wirth, D.F. (1989). *Science.* **244**, 1184-1186.

Wu, Q., Bounaud, P.Y., Duduk, S.D., Yang, C.P., Ojima, I., Horwitz, S.B. and Orr, G.A. (1998). Identification of the domains of photoincorportaion of the 3'-and 7-benzophenone analogues of taxol in the carboxyl-terminal half of murine mdr1b p-glycoprotein. *Biochemistry.* **37**, 11272-11279.

Yamamoto, H., Tagaya, M., Fukui, T. and Kawakita, M. (1988). Affiiniity labeling of the ATP-bindiing site of Ca^{2+}-transportiing ATPase of sarcoplasmic retiiculum by adenosine triphosphopyridoxal: identifiication of the reactive lysyl residue. *J.Biochem.* **103**, 452-457.

Yamamoto, H., Imamura, Y., Tagaya, M., Fukui, T. and Kawakita, M. (1989) Ca^{2+}-dependent conformational change of the ATP-binding site of Ca2+-transporting ATPase of sarcoplasmic reticulum as revealed by an alteration of the target-site specificity of adenosine triphosphopyridoxal. *J.Biochem.* **106**, 1121-1125.

Zamora, J.M., Pearce, H.L. and Beck, W.T. (1988). Physical-chemical properties shared by compounds that modulate multidrug resistance in human leukemic cells. *Mol.Pharmacol.* **33**, 454-462.

Zhang, X., Collings,K.I. and Greenberger, L.M. (1995). Functional evidence that transmembrane 12 and the loop between transmembrane 11 and 12 form part of the drug-binding domain in P-glycoprotein encoded by MDR1. *J.Biol.Chem.* **270**, 5441-5448.

Zhou, Y., Gottesman, M.M. and Pastan, I. (1999). Studies of human MDR1-MDR2 chimeras demonstrate the functional exchangeability of a major transmembrane segment of the multidrug transporter and phosphatidylcholine flippase. *Mol.Cell.Biol.* **19**, 1450-1459.